Influence of the Hot Rolling Process on the Mechanical Behavior of Dual Phase Steels

Dissertation

Zur Erlangung des Grades eines Doktors
der Ingenieurwissenschaften

vorgelegt von

Mehdi Asadi

aus Teheran / Iran

genehmigt von der
Fakultät für Natur- und Materialwissenschaftlichen
der Technischen Universität Clausthal

Tag der mündlichen Prüfung:

21.10.2010

Bibliografische Information Der Deutschen Nationalbibliothek
Die Deutsche Nationalbibliothek verzeichnet diese Publikation in der Deutschen Nationalbibliografie; detaillierte bibliografische Daten sind im Internet über http://dnb.d-nb.de abrufbar.

Vorsitzender der Prüfungskommission:	Prof. Dr.-Ing. Albrecht Wolter
Hauptberichterstatter:	Prof. Dr.-Ing. Heinz Palkowski
Berichterstatter:	Prof. Dr.-Ing. Bruno De Cooman

D 104

1. Auflage, 2011

ISBN 978-3-86948-148-7

Acknowledgements

I would like to express my sincere thanks to my supervisor Prof. Dr.-Ing. Heinz Palkowski for his strong support, guidance and giving me the opportunity to pursue my Ph.D. degree at TU Clausthal. Furthermore, my deep gratitude is given to Prof. Dr.-Ing. Bruno De Cooman for his scientific support during my stay at GIFT in Pohang and for agreeing to be on my thesis committee despite his extremely busy schedules and the long travelling-distance. Moreover, the author is indebted to Prof. Dr.-Ing. Georg Frommeyer. The achievement of this work was a result of his wide ranging knowledge and support.

This thesis would not be what it is without the support and cooperation of the members of the department of “Werkstoffumformung” as well as the technical staff of the Institute of Metallurgy. I would like to express my thanks to the past and present scientific colleagues of the department for their continuous help, friendship and kindness: Thank you Kai-Michael Rudolph, Mohamed Soliman, Nicole Schlosser, Olga Sokolova, Hanaa Mostafa, Lu Yu, Mithat Akdesir and Marcus Kühn.

Moreover, I would like to acknowledge Salzgitter Flachstahl GmbH as well as Salzgitter Mannesmann Forschung GmbH, here especially Dr.-Ing. Thomas Evertz and Dr.-Ing. Markus Krieger, regarding to scientific supports and provision of the materials.

Thank is owed to my friend Dr.-Ing. Ali Aghajani at Ruhr-Universität Bochum for providing the facilities of TEM tests as well as to my students, especially Reza Kaboli and Oliver Steinbis, who supported me during my activities.

Special thanks are given to my family and to my parents. Without their wisdom and guidance, I would not have been able to reach the goals I have to strive and be the best to reach my dreams.

Finally, I wish to record my deep sense of appreciation for my lovely wife for relentlessly supporting me during the entire period, in spite of all the hardship. This work is dedicated to my wife, BEHNAZ, a loyal friend and compassionate critic.

Table of Contents

Nomenclature

Abbreviations

A	Interaction parameter defining the strength of the atmosphere
Ae_1	Lower limit temperature of $\alpha+\gamma$ phase field under equilibrium [°C]
Ae_3	Upper limit temperature of $\alpha+\gamma$ phase field under equilibrium [°C]
AHSS	Advanced high strength steels
APT	Atom probe tomography
Ar_1	Temperature at which conversion of austenite to ferrite is completed [°C]
Ar_3	Temperature at which austenite begins to convert to ferrite [°C]
b	Burgers vector [m]
b_{BH}	Bake hardening coefficient
bcc	Body centered cubic
bct	Body centered tetragonal
BH	Bake hardening [MPa]
C	Carbon
CDRX	Continuous dynamic recrystallization
Cr	Chromium
CRA	Cold rolled annealed
D	Diffusion coefficient for carbon [$m^2 \cdot s^{-1}$]
DP	Dual phase steel
DRX	Dynamic recrystallization
$d_{\alpha,\ \alpha',\gamma}$	Grain size (ferrite, martensite, prior austenite) [m]
f_α	Ferrite fraction [%]
f_γ	Austenite fraction [%]
F/F	Ferrite/ferrite
F/M	Ferrite/martensite
FEG	Field emission gun

F_T	Finishing temperature [°C]
G	Shear modulus [GPa]
GIFT	Graduate Institute of Ferrous Technology
HAADF	High angle annular dark field
HDG	Hot dip galvanized
HSLA	High strength low alloy
K	Strength coefficient [MPa]
k_B	Boltzmann's constant [$1.38 \cdot 10^{-23}$ $J \cdot K^{-1}$]
K_d	Numerical constant [-]
k_y	Hall-Petch coefficient [MPa $\cdot m^{1/2}$]
l	Actual length of the sample measured during the transformation [m]
LAGB	Low angle grain boundaries
LC	Low carbon
LOM	Light optical microscopy
m	Taylor factor [-]
MDRX	Metadynamic recrystallization
MFS	Mean flow stress [MPa]
Mn	Manganese
Mo	Molybdenum
M_S	Martensite start temperature [°C]
MVF	Martensite volume fraction [%]
n	Work hardening coefficient [-]
N	Nitrogen
N_s	Initial dislocation density [m^{-2}]
N(t)	Number of C atoms, diffusing to dislocations in a unit volume in time t
n_0	Concentration of C in solution [ppm]
Nb	Niobium
NoRX	Non-recrystallization

P	Phosphorus
PS	Prestrain [%]
Q_{def}	Activation energy for deformation [$J \cdot mol^{-1}$]
R	Gas constant [8.314 $J \cdot mol^{-1} \cdot K^{-1}$]
R_e	Lower yield strength [MPa]
R_m	Tensile strength [MPa]
$R_{p0.2}$	Yield strength [MPa]
RT	Room temperature [°C]
RTT	Recrystallization time temperature
RUB	Ruhr-Universität Bochum
RX	Recrystallization
$RXST$	Recrystallization stop temperature
S	Numerical constant [-]
Si	Silicon
SM	Saturation magnetization
$STEM$	Scanning transmission electron microscopy
$SZFG$	Salzgitter Flachstahl GmbH
T	Temperature [°C]
T_A	Austenitization temperature [°C]
T_{abs}	Absolute temperature [K]
T_{HJ}	Holloman-Jaffe temperature [K]
T_z	Zener-Hollomon temperatur [K]
t_A	Austenitization time [s]
TEl	Total elongation [%]
TEM	Transmission electron microscopy
T^{FC}	Fast cooling start temperature [°C]
$TMCP$	Thermomechanical controlled processing
T_{nRX}	Non-recrystallization temperature [°C]

T_R	Reheating temperature [°C]
TRIP	Transformation induced plasticity
ULC	Ultra low carbon
UTS	Universal testing machine
V	Vanadium
WH	Work hardening [MPa]
X	Transformed austenite fraction [-]
Z	Zener-Hollomon parameter [-]

Greek Symbols

α	Ferrite
α'	Martensite
β	Proportionality constant [-]
γ	Austenite
ε	Engineering strain, deformation [%]
θ	Angle [°]
λ	Slip distance of the dislocation [m]
ρ	Dislocation density [m^{-2}]
ρ_{gen}	Generated dislocation density [m^{-2}]
ρ_{ann}	Annihilated dislocation density [m^{-2}]
σ	True stress [MPa]
σ_0	Friction stress [MPa]
$\sigma_{2.0}$	Corresponding stress for 2 % plastic strain [MPa]
σ_y	Yiled stress [MPa]
φ	True strain [-]
φ_c	Critical true strain [-]
φ_t	Total true strain [-]
$\dot{\varphi}$	Strain rate [s^{-1}]

1 Introduction

To combine fuel saving with increased safety of vehicles, the automotive industry was led to develop Advanced High Strength Steels (AHSS). Their high yield and tensile strengths enable a decrease in sheet thickness (weight saving) and, at the same time, maintaining or even improving crash behavior (safety) [Hil09, Pan09]. This is achieved by microalloying [Ste04] and a thermo-mechanical treatment [Wu08]. The group of promising AHSS includes various steel grades such as dual phase (DP), transformation induced plasticity (TRIP) and complex phase (CP) steels. Their microstructures consist of different phases, including ferrite, martensite, bainite and retained austenite, making up "multiphase" steels. Among the different multiphase steels, DP steels actually have the biggest share [Tsi06].

DP steels are characterized by a good formability, high strength and a good compromise between strength and ductility [Dav78a, Fur84]. Moreover, the DP steels exhibit a continuous yielding behavior, low yield point and a high strain-hardening coefficient [Col09, Das09]. This has been attributed to an increase in the work hardening (WH) limits through forming mobile dislocations due to the martensite transformation during heat treatment and martensite twinning during forming [Tim07, Spe81a].

Furthermore, the DP steels often show a large potential for bake hardening (BH). BH refers to the increase in yield strength that occurs as a result of the paint baking treatment of the formed auto-body parts. The primary mechanism that causes the additional strengthening is the immobilization of dislocations by the segregation of interstitial atoms, known as classical static strain aging [Cot49a-b]. The increase of strength thus achieved allows a further reduction of sheet thickness and improves the crash safety and the dent resistance. The BH of special steel qualities is technically used in DP, where e.g. the increase in strength is realized in the final heat treatment [Jeo98, Sam08]. Previous own investigations [Asa08a-b, Pal08a] stated that the BH effect of DP is much stronger than that one for conventional BH steels.

The production of hot rolled DP sheet steels is possible using either conventional or thermomechanical controlled processing (TMCP) way. TMCP means control of the reheating temperature, the rolling schedule and the cooling rate, i.e. control of the entire processing sequence. TMCP is a microstructural

control technique combining controlled rolling and controlled cooling and eliminates the need for further heat treatments. TMCP is used to obtain excellent properties for steel sheets and strips, such as high strength, excellent toughness and excellent weldability. In steels with the presence of martensite in the microstructure, the other aim of TMCP is to refine the martensite by the deformation in the non-recrystallized austenite region [Tim03].

In TMCP, the structure of steels is refined by a suitable combination of controlled rolling and subsequent controlled cooling and accelerated cooling. To increase the nucleation sites of ferrite during cooling, controlled rolling is used to refine the grains and strain the austenite. The microstructural evolution during TMCP involves accumulation, annihilation and rearrangement of dislocations, recrystallization and grain growth. For controlled rolling, the microstructural evolution that occurs in the material is dependent on the alloying elements, the amount of the reductions, the strain rate, the temperature and the length of the holding times between reductions [Bäc09].

It is well known that varying processing parameters during hot strip rolling and the chemical composition has a major influence on the microstructure of steels and consequently on their properties. However, the study of the influence of those parameters on the microstructure development, mechanical properties and BH behavior of DP steels has not been sufficiently investigated and is not available in the literature. Thus, the aim of this study is to develop hot rolled DP steels indicating improved mechanical properties and bake hardenability by employing the optimized compositions and microstructural constituents together with the feasible processing schedules. For this purpose, the influence of processing parameters, microstructural constituents and chemical composition on the mechanical properties and the BH behavior in hot rolled DP steels is investigated. Furthermore, this study is intended to contribute to the understanding of the microstructural evolution and transformation behavior during TMCP.

The hot rolled DP steels are typically produced on a hot strip mill, where the level of roughing and finishing rolling depend on the mill configuration and the starting and final thicknesses of the strips. This work is done on hot strip products of Salzgitter Flachstahl GmbH (SZFG), starting with material after

roughing. The simulation of controlled rolling is primarily intended for the hot strip mill process at SZFG. The outline of the present thesis is as follows:

- Simulating finishing rolling for the last stands and studying the influence of applied strains and temperatures during hot deformation on the phase transformation behavior, microstructure development, mechanical properties and BH behavior of DP steels (chapter 4).
- Simulating finishing rolling and studying the effect of cooling rate and structural constituent (amounts of martensite and ferrite) on the phase transformation behavior, microstructure development, mechanical properties and BH behavior of DP steels (chapter 5).
- Studying the influence of chemical composition on the phase transformation behavior, microstructure development, mechanical properties and BH behavior of DP steels (chapter 6).
- Investigation on the influence of reheating temperature during simulation of roughing on the microstructure and the final mechanical properties of Nb microalloyed DP steels (chapter 6).

2 Theoretical Background

2.1 Dual Phase (DP) High Strength Steels

One of the first commercial DP products was marketed in the USA [Mat79]. It was based on a pearlite-reduced vanadium microalloyed steel, commonly encountered in the 1970's, plus an intercritical annealing process. DP steels are low carbon (~0.05 to 0.2 %) AHSS grades, which usually contain manganese (Mn), silicon (Si) and microalloying elements as additions. The amount of martensite usually varies within 5 - 30 % [Ang06], but in practice also larger amounts are possible. Small amount of bainite, retained austenite or acicular ferrite may be present in microstructure as well [Kim87, Mur06, Smi93, Spe02].
DP steels quickly became one of the most popular and versatile materials in today's automotive industry. Currently these steels are most commonly used in structural applications where they have replaced more conventional high strength low alloy (HSLA) steels [DeC04]. They offer a great potential for part weight reduction. DP steels have both, high tensile strengths and moderate total elongations, excellent for auto applications, such as cold-pressed wheel rims [Dav78a, Mat87]. In addition to the high strength, the DP steels often show a large potential for BH. However, the BH mechanism in multi phase steels is not fully understood yet.
In general, the production of DP sheet steels is possible using different process routes. In the conventional route DP steels are produced by intercritical annealing (producing an $\alpha + \gamma$ microstructure) followed by severe cooling/quenching, resulting in a soft ferrite matrix containing hard martensite particles [Hua04]. The intercritical anneal can be followed either by finishing rolling for hot strip product or cold rolling for cold rolled annealed (CRA) or hot dip galvanized (HDG) products. In thermomechanical process routes the strips are finished rolled in the two phase fields of austenite and ferrite and then cooled down towards low temperatures. Due to the higher cooling rate in that scheme lower amounts of alloying elements are needed [Hel05].

2.1.1 Alloying Elements in DP steels

DP steels belong to the low alloyed steels, with C, Mn and Si being the main alloying elements. C shifts the formation of martensite and bainite towards

longer times [Sol10]. It has the greatest impact on the hardness of the martensite in AHSS [Mai86]. Mn is foremost an austenite stabilizing element. Mn increases C solubility in austenite [Mur06] and lowers the pearlite reaction, which allows for a wider range of cooling rates. However, excessive levels of Mn can promote carbide precipitation in the austenite [Ble02]. Si is not an austenite stabilizing element. In fact, it raises the ferrite-austenite eutectoid temperature and significantly reduces the activity of C in ferrite [Smi93]. Si decreases the precipitation of carbides, especially cementite [Ray81, Ray82]. Si has a very low solubility in cementite; thus, high Si-steel would be an inhospitable environment to cementite [Bha92a, Les78]. However, high Si contents tend to form very adherent oxides on the surface during rolling or continuous annealing that are very difficult to remove [Kim00]. Mahieu et al. [Mah02] noted that this effect is due to the segregation of Si to the surface and the formation of complex Mn-Si-oxides that resist wetting by the zinc bath.

Phosphorus, like Si, inhibits the formation of carbides, leaving more C in solution for segregation to austenite. Less carbide was observed in the phosphorus-alloyed steels than in the non-phosphorus alloyed steels [Che89a].

Chromium effectively extends the austenite field and shifts the pearlite and bainite phase fields towards longer times [Pic99a]. Cr tends to increase strength, but decreases elongation and austenite retention [Kim00]. This may be helpful if it is desired to produce AHSS that require ductility superior to DP material, but the extraordinary elongations found in TRIP steels (at their lower strengths) are not required. Cr (or Mo, Co, W, V, etc.) poisoning of TRIP steel to produce a compromise between DP and TRIP properties is an important field for future research. Mintz [Min01] noted that Cr can have an effect on carbide precipitation similar to that of Al, Si and P, but that > 0.5 % Cr can lead to poor galvanizing.

2.1.2 Martensite in DP Steels

The influence of the martensite volume fraction (MVF) in DP steels, as a hard phase, was investigated by a number of authors [Ajm09, Dav78a, Mar82a, She84]. The growth of the MVF results in increased yield point, tensile strength and impact strength of DP steels. According to [Bag99, Tav99], this effect could only be observed up to MVF of about 55 %. At higher MVF values, the authors

observed a decrease of strength properties, which they explain by a decreased carbon concentration in martensite.

The martensitic transformation in steel is just one example of a more general phenomenon of martensitic transformations described as shear-dominant, lattice-distortive and diffusionless transformations, occurring by nucleation and growth [Bha92a]. Martensite can form at very low temperatures, where diffusion, even of interstitial atoms, is not conceivable over the time period of the experiment. The martensite transformation in steels is generally considered to be a time-independent, athermal process, which begins at the martensite-start (M_S) temperature and proceeds upon cooling below this temperature. The kinetics of the martensite transformation in steels is nucleation controlled as the growth rate of the martensite is extremely rapid [Wan00].

There are two types of martensite: lath and plate. Lath martensite is normally found in steels with lower concentrations of C (up to 0.5 wt. %) [Mor03]. The structure units are laths, mostly separated by low angle boundaries, grouped into packets. The substructure consists of a high density of dislocations arranged in cells. The martensite in DP steels is usually of lath type. Each martensite lath is composed of many dislocation cells with an average width of 2500 A [Mar69, Spe65]. Typical dislocation densities are estimated to be 0.3 to $0.9 \cdot 10^{12}$ cm^{-2} [Gho94]. The substructure is superficially similar to that developed in iron by heavy cold work [Emb66].

Plate martensite is characteristic for high carbon steels (more than 1.3 wt. %) [Bha92b]. The structure is made of lenticular plates of martensite units, each consisting of fine twins about 5 nm apart [Mil85]. These twins gradually merge into an array of dislocations near the periphery of the plate. The microstructure of steels containing C in the range 0.5 to 0.8 wt. % is generally complicated, with lath martensite, plate martensite and residual, non-transformed austenite coexisting together [Spe72].

Martensite is a metastable structure, and as such it can undergo structural changes even at low temperature. Historically, the term tempering is used for a process of heating martensitic steels to elevated temperatures so that they become more ductile. The term aging is referring to the processes that occur during the storage of martensite at room temperature (RT). The aging and tempering behavior of iron-carbon martensite has been the subject of intensive

investigation for more than 60 years and a large amount of literature exists covering the subject [Cha86, Che88, Han01, Ino78, Ohm92, Ols83]. Research has shown that the decomposition processes are complex and involve many overlapping phenomena. The temperature ranges at which they occur are dependent on heating rate, composition and structural details. They can be summarized as follows [Dec78, Mit91, She83]:

a) Transformation of a part of the retained austenite into martensite between 115 and 215 K.

b) Redistribution of C atoms (precipitation processes) around and slightly above RT, ascribed to:

i) Segregation of C atoms to lattice defects (~0.2 wt. % C).

ii) Transfer of C atoms at a/b octahedral interstices to c octahedral interstices.

iii) Formation of C enrichments in the matrix for the predominant part of the C atoms.

c) First stage of tempering between 355 and 455 K: precipitation of transition carbides.

d) Second stage of tempering between 475 to 625 K: decomposition of retained austenite into ferrite and cementite.

e) Third stage of tempering between 525 and 625 K: precipitation of the stable carbide, cementite.

f) Recovery of dislocation substructure, grain growth and sphereoidization of cementite between 600 and 900 K.

2.1.3 Properties of DP Steels

There is broad consensus that the low elastic limit (defined as the first deviation from Hooke's law in the stress-strain curve), the continuous yielding and the high strain hardening rate are a consequence of the austenite to martensite transformation which involves a volume expansion [Cal10, Col09, Tim04]. The strains produced by the transformation result in residual stresses in the surrounding ferrite [Che85, Sak83]. The volume change induces plastic deformation of adjacent ferrite grains and therefore, creates a high density of unpinned dislocations in the vicinity of martensite [Dav79, Rig79] as was qualitatively studied by transmission electron microscopy (TEM) [Kor84, Mat79].

In order to avoid decohesion at the ferrite/martensite (F/M) interfaces this expansion must be accommodated by microplastic deformation of the surrounding ferrite grains. This leads to the generation of mobile dislocations, i.e. there is a higher dislocation density next to the F/M interfaces than in the interior of the ferrite grains [Lid01, Mat79]. The dislocation density in the interior of ferrite grains is about $6 \cdot 10^{12}$ m^{-2} and at the F/M interface about $30 \cdot 10^{12}$ m^{-2} [Fan94].

Several theoretical models have been proposed to explain the deformation behavior of DP steels [Mil69, Tom76]. Most of these models treat each constituent of the microstructure as a continuum, and the mechanical properties of each constituent are assumed to be independent of the other elements in the microstructure. Another assumption of many of these models is that the martensite deforms to approximately the same extent as the ferrite. However, the results of several studies indicate that the deformation of a DP steel is inhomogeneous, with the strain in the ferrite much greater than the strain in the martensite [Bal81, Kar74, Kor80, Mar81]. A mechanism which is based on the accumulation of dislocations in a material which deforms inhomogeneously has been proposed by Ashby [Ash71] and Ballinger [Bal81] as responsible for the high WH rates typical of DP steels. Some deformation models of DP steels assume both martensite and ferrite phases are ductile and obey the Ludwig relationship (Eq. 2.1), with equal strain in both phases [Hup99, Ume00]:

$$\sigma = k.\varphi^n \qquad \text{(Eq. 2.1)}$$

where n [-] is a work hardening coefficient, k [MPa] is the strength coefficient, σ [MPa] is true stress and φ [-] true strain. Unlike most steels, the stress-strain behavior of DP steels frequently cannot be approximated by a simple parabolic function over the entire strain range, i.e. DP steels do not exhibit single n values [Mat79]. Analysis with constitutive equations has indicated that the stress-strain curve of a DP steel may be divided into as many as three strain regions, each described by a different parabolic function or n value [Law81]. The character and number of regions or stages observed depend on microstructural parameters such as grain size and MVF [Mat79]. The existence of more than one stage indicates that a single WH mechanism may not describe the WH behavior at all strains.

2.2 Thermomechanical Controlled Processing (TMCP)

To achieve the desired final mechanical properties of the strip such as a good combination of strength, fracture toughness and weldability, thermomechanical controlled processing (TMCP) is utilized [DeA88]. TMCP means control of the reheating temperature, the rolling schedule and the cooling rate. The purpose of TMCP is to obtain optimum grain refinement and it is therefore necessary to maximize the area of austenite grain boundary per unit volume at the onset of phase transformation.

The stored energy due to the accumulated dislocations during hot rolling is generally lowered by three processes: recovery, recrystallization and grain growth [Bra77, Dja72]. Recovery and recrystallization can take place during and after deformation and to distinguish them they are called dynamic and static, respectively. The flow curve is dependent on the conditions of the deformation, such as temperature (T_z) [K] and strain rate ($\dot{\varphi}$) [s^{-1}], which can be expressed by the Zener-Hollomon parameter (Z) [DeA88]:

$$Z = \dot{\varphi}.\exp\left(\frac{Q_{def}}{RT_z}\right) \qquad \text{(Eq. 2.2)}$$

where Q_{def} [J mol^{-1}] is the activation energy for deformation and the gas constant, R = 8.314 J mol^{-1} K^{-1}.

During hot strip rolling, the material generally stops recrystallizing below a certain temperature. This temperature is often called the recrystallization stop temperature (RXST) or the non-recrystallization temperature (T_{nRX}). The T_{nRX} denotes the temperature above which static recrystallization (SRX) occurs between the passes [Yue97]. It depends on the deformation, the cooling rate and the inter-pass times in the rolling process. Below this temperature recrystallization is retarded due to strain-induced precipitation of second-phase particles.

For the controlled hot rolling a setup (rolling schedule) determines the temperature and reduction that has to be met in each pass in order to obtain the desired final product. The setup is determined on the basis of the desired final mechanical and geometrical properties of the strip. Several studies of the effects of TMCP parameters on the final properties of AHSS have been performed, and will be reviewed in the following.

2.2.1 Effect of Deformation, Temperature and Strain Rate

Calcagnotto et al. [Cal08] investigated the effect of large strain warm deformation on the microstructure of DP steels. Using deformation dilatometry they produced ultrafine grained DP steel by a large strain warm deformation and subsequent intercritical annealing. The authors found that the final microstructure consisted of martensite islands embedded in an ultrafine grained polygonal ferrite matrix. The average grain size was 1-2 µm. The strain hardenability was drastically improved by the introduction of martensite as a second phase. Small amounts of retained austenite might further enhance strain hardenability. Small amounts of retained austenite (< 1 µm) were finely dispersed. Similar results were reported in [Par05].

Hanzaki et al. [Han95a-b, Han97] studied the effects of different TMCP paths on the final properties of TRIP steels. The steels were processed by soaking in the austenite regime and then deforming to various degrees, intercritical annealing, isothermal bainitic transformation and cooling to RT. The hot deformation was done in one step with $\varphi = 0.3$ or a double reduction with two passes, each $\varphi = 0.3$. This resulted in materials of varying austenite grain sizes, where the materials that received more deformation had a finer austenite grain structure.

Godet et al. [God02] have shown that larger hot deformations in the intercritical region of a hot band TRIP steel resulted in greater mechanical properties. Samples given a deformation pass of $\varphi = 0.7$ in the intercritical regime reached a strain hardening parameter (n) of 0.28 during subsequent tensile tests, whereas samples without deformation below the austenite non-recrystallization temperature only reached n = 0.20. Additionally, the heavily deformed material had a higher tensile strength in addition to its better strain hardening and a longer total elongation.

Hanzaki et al. [Han97] studied the influence of the deformation finishing temperature on the mechanical properties of TRIP steels. The steels were deformed at temperatures of 1000 °C and 1050 °C. The steel showed a slightly larger ductility and decreased strength at 1050 °C. The same authors [Han95a] varied the strain rate ($\dot{\varphi}$) to obtain both, statically and dynamically recrystallized samples. Samples were deformed at two temperatures (1000 and 1050 °C) and the second hit of the double hit tests were performed at $\dot{\varphi} = 0.1\ s^{-1}$ (still static recrystallization, SRX) and at $\dot{\varphi} = 0.001\ s^{-1}$, resulting in dynamic recrystalliza-

tion (DRX). The lower deformation temperature for both strain rates produced a lower fraction of retained austenite. At 1050 °C, both strain rates gave the same fraction of retained austenite, and the dynamic process gave slightly higher fraction of retained austenite at 1000 °C. They suggest that the dynamically recrystallized dislocation substructure will be more prone to the retention of austenite, without giving an argument. This is likely due to a lower magnitude of precipitation.

2.2.2 Effect of Cooling Rate

The cooling rate from the intercritical area to the ferrite, bainite or martensite formation region strongly affects the final properties of the steel. Sakuma et al. [Sak91] noted that increasing cooling rate resulted in greater values for yield strength and total elongation in bainitic steels although increasing to the highest rates (≥ 100 K/s) steadily reduced these values. Minote et al. [Min96] stated that a slow cooling rate of 3 K/s produced a high volume fraction of epitaxial ferrite in TRIP steels as compared to faster cooling rates. This resulted in stronger carbon partitioning to the austenite which is beneficial for mechanical properties.
The study of Speer and Matlock [Spe02] demonstrated the effect of cooling rate on the formation of epitaxial ferrite in DP steels. At about 1000 K/s quenching, relatively little epitaxial ferrite can be formed. At 12 K/s, almost all of the intercritically formed austenite is lost to epitaxial ferrite, leading to a tiny volume fraction of martensite. As the nucleation barrier for epitaxial ferrite should be minor or zero, only reducing its growth time or growth rate will suppress it. However, epitaxial ferrite is not necessarily detrimental. It will, after all, reject C into the remaining austenite. Excessively fast cooling resulted in growth of ferrite supersaturated in C or transformation to martensite. Thus, a compromise value of cooling rate seems to give optimum final properties.
Sakuma et al. [Sak91] noted almost no effect of cooling rate at values of 20 - 60 K/s in bainitic steels. At 80 K/s they found a slight decrease in uniform elongation. They did not discuss the mechanism behind this result, but it seems likely the loss of C rejection from epitaxial ferrite may be to blame. Pichler et al. [Pic01] and Traint et al. [Tra02] independently noted constant mechanical properties with cooling rate except at the slowest values. Pichler and Stiaszny [Pic99b] found only negligible effects of cooling rate on mechanical properties of

TRIP steels. However, all of these studies varied cooling rate by less than one order of magnitude, rather than over multiple orders.

2.2.3 Effect of Microalloying Elements

Microalloying elements (Ti, Nb or V) can also be used in the production of DP [Dav79, Spe83]. They retard recrystallization by adding small amounts of them [DeA84]. Cuddy [Cud82] investigated the effect of microalloying elements on recrystallization behavior in a 0.07 C - 1.40 Mn - 0.25 Si (wt. %) steel and reported that Nb provides the most effective raise of the recrystallization temperature. Also, recrystallization is impeded at higher temperatures with small additions of Nb. In Cuddy's investigation multi-pass deformation was conducted with a total reduction of about $\varphi = 0.5$.

In [Muk96], the temperature during reheating the slabs is chosen in that way that the microalloying elements are in solution. For rolling, the temperature is reduced, so Nb forms nitrides, carbides and/or carbo-nitrides which effectively retards recovery and recrystallization leading to finer austenite grains. The highly work hardened (pancaked) austenite provides numerous nucleation sites for the ferrite during the subsequent transformation which give very fine ferrite grains [Ouc77]. The effect of Nb in solution on the dynamic recrystallization time temperature (RTT) curves was investigated by Bäcke [Bäc09]. RTT curves were constructed from the recrystallization start time at a certain temperature taken as the peak strain through the strain rate. The values were obtained from the flow stress curves at a strain rate of $0.1\ s^{-1}$ and a temperature between 1000 - 1200 °C. The author reported that recrystallization is much faster in the plain C-Mn steel compared to the Nb microalloyed steels. The effect is enhanced at lower temperatures.

Yamamoto et al. [Yam82] investigated the effect on recrystallization of Nb in solution and as precipitated carbides and nitrides. The softening in the material was studied by double compression tests and the fraction softening between deformations was determined by an offset-method. The fraction softening was compared to the fraction recrystallized determined for a quenched steel with high hardenability (0.04 C - 2.0 Mn - 0.3 Mo - 0.1 Nb; in wt. %) by microscopic observations. The microscopic observation compared to the softening curves indicated that recrystallization starts at the softening ratio around 20 %. The

authors found that the retarding effect of Nb in solution is very significant in the region below 20 % softening, i.e. before the start of recrystallization. Above 20 % softening the effect is smaller which indicates that solute Nb retards recovery and the onset of recrystallization.

2.3 Microstructure Evolution after TMCP

For several decades the microstructural evolution of austenite during hot deformation of steels has been investigated [Cud82, Ouc77, Sic00]. In the last few years, more and more attention has been paid to the development of mathematical models that can predict the microstructural evolution during hot rolling [Sic96, Wan03]. The goal is usually to be able to predict the microstructure of the materials and to optimize the different process conditions to obtain the best combination of strength, ductility and weldability in the as-hot-rolled product. To be able to practice controlled hot rolling and thereby get the desired final mechanical properties of the product, knowledge of the microstructural evolution of the austenite during rolling is essential [Gar81, Goe87, Sug92]. Some important parameters describing the microstructural evolution will be reviewed as follows:

2.3.1 Grain Structure

The kinetics of recrystallization and grain growth depend on the migration of grain boundaries. Grain boundaries are regions of considerable atomic misfit and act as strong barriers to dislocation motion [Hul84]. A grain boundary is a boundary that separates regions of different crystallographic orientations and the misorientation between two crystals (grains) is an angle (θ) which is the smallest rotation required to make the two crystals coincide [Hum04]. A schematic picture of a grain boundary is shown in Fig. 2.1. Five macroscopic degrees of freedom are needed to define the geometry of a boundary. In Fig. 2.1, AB represents a boundary plane and the overall geometry of the boundary is defined by the orientation of this plane with respect to one of the two crystals (two degrees of freedom) and by the angle θ (three degrees of freedom).

Grain boundaries are usually separated into the categories of low and high angle grain boundaries which are dependent on the size of the misorientation [Hum04]. Low angle grain boundaries (LAGB) or subgrain boundaries are

boundaries misoriented by an angle less than 10 - 15°. Above that high angle grain boundaries (HAGB) are defined.

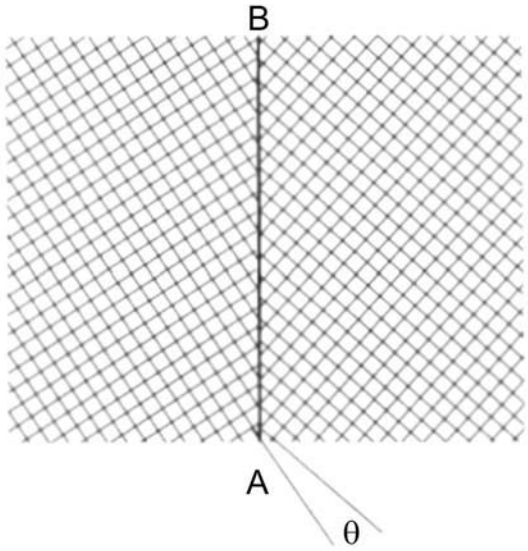

Fig. 2.1 Grain boundary between two crystals, misorientation described by the angle θ [Hum04].

2.3.2 Dislocation Generation and Recovery

Most of the applied deformation work during rolling turns into heat and only a small part remains as stored energy (~1 %) [Bäc09]. The increase in stored energy is mainly due to the accumulation of dislocations which is caused by both, tangling of existing dislocations and the generation of new ones. The energy is also raised by the increase of grain boundary areas. The stored energy in the material is the driving force for recovery and recrystallization.

Recovery of the material is a process that occurs prior to recrystallization and is primarily due to changes in the dislocation structure. During recovery, the dislocations rearrange in configurations of lower energy. Recovery is actually a series of events: formation of cells, annihilation of dislocations within cells, formation of low-angle subgrains and, finally, subgrain growth as sketched in Fig. 2.2.

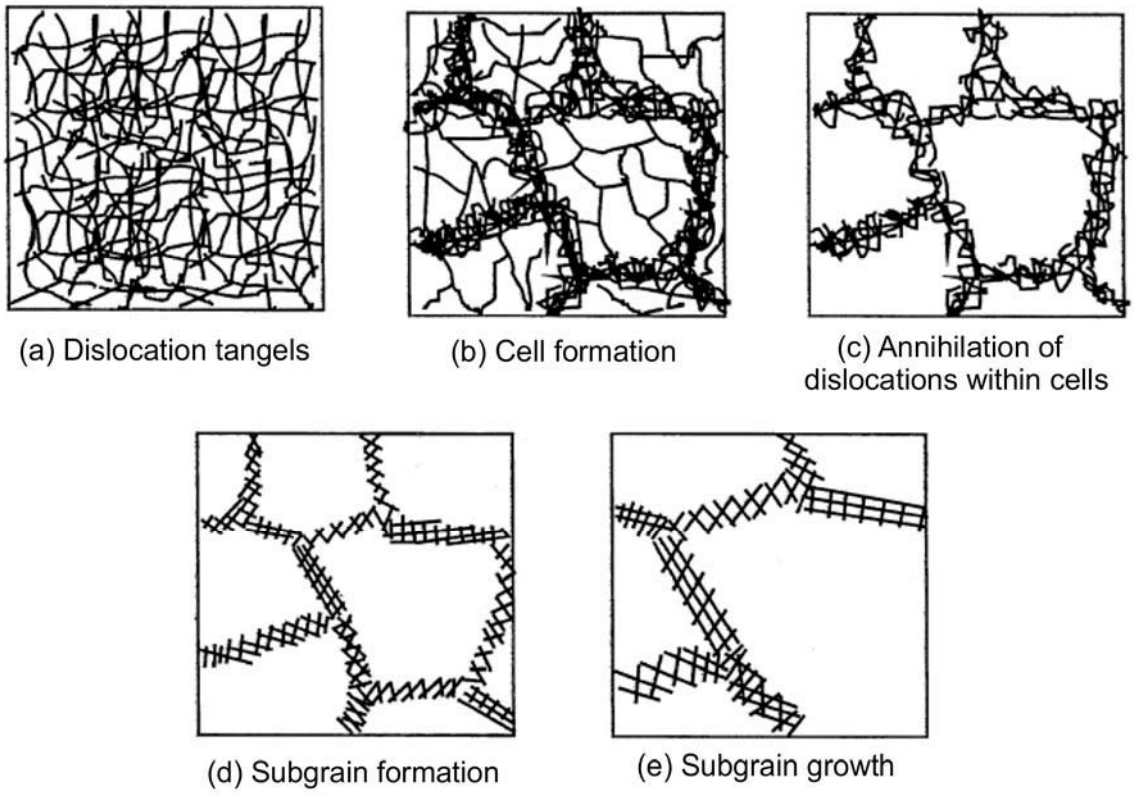

Fig. 2.2 The stages of recovery where first cells are formed due to the rearrangement of dislocations and then subgrains are formed and grow due to annihilation of dislocations [Bäc09].

During hot deformation, dislocation accumulation due to deformation and annihilation and rearrangement of dislocations due to dynamic recovery occur simultaneously. The evolution of dislocations during hot deformation can be separated in two parts: dislocation generation and dislocation annihilation

$$\frac{d\rho}{dt} = \frac{d\rho_{gen}}{dt} - \frac{d\rho_{ann}}{dt} \qquad \text{(Eq. 2.3)}$$

where ρ [m^{-2}] is dislocation density, ρ_{gen} [m^{-2}] is the generated dislocation density and ρ_{ann} [m^{-2}] is the annihilated dislocation density. If dynamic recovery is the only form of restoration that occurs in the material, the flow-stress in a stress-strain curve reaches a plateau and then holds a steady-state flow-stress. This depends on the fact that the rate of recovery and work hardening reaches a dynamic equilibrium. The flow stress (σ) [MPa] during deformation is dependent on the dislocation density (ρ) [m^{-2}] and is usually described by:

$$\sigma = \sigma_0 + m.\beta.G.b.\sqrt{\rho} \qquad \text{(Eq. 2.4)}$$

where σ_0 [MPa] is the friction stress, mainly due to the strengthening contribution of precipitation, m [-] is the Taylor factor which is dependent on the

deformation due to the development of a deformation texture [Siw97], β [-] is a proportionality constant (~0.15), G [GPa] is the shear modulus and b [m] is the Burgers vector. Eq. 2.4 gives a good description of the flow stress, see for example the work by Bergström [Ber83].

2.4 Mechanisms of Bake Hardening

The term “bake hardening” generally denotes an artificial and controlled ageing of steels and stands for a time dependent, often undesirable, mutation in the properties of materials and organisms. Concerning low carbon (LC) steels, BH results in an increase of yield strength, tensile strength and hardness with a corresponding decrease in ductility and the appearance of discontinuous yielding. The process depends on time and temperature and results from segregation, clustering and precipitation of supersaturated interstitial atoms such as carbon and nitrogen [Bak02a, Chr98].

Determining BH is based on a conventional tensile test (Fig. 2.3). According to DIN EN 10325 [Eur06, Sta87] the BH_0 [MPa] value is defined as the stress difference between the 0.2 % offset yield strength ($R_{p0.2}$) [MPa] of a non-heat treated specimen and the lower yield strength (R_e) [MPa] of a second specimen which has been heat treated (“baked”) at 170 °C (± 5 K) for 20 min (± 1 min). These parameters are chosen to simulate the paint baking process.

$$BH_0 = R_{e170°C/20\,\mathrm{min}} - R_{p0.2initial} \qquad \text{(Eq. 2.5)}$$

By contrast, in order to determine the BH_2 value a single specimen is used. First it is strained to a total elongation of 2 % and the corresponding flow stress $\sigma_{2.0}$ is measured. Next, it is baked for 20 min at 170 °C, and finally this specimen is subjected to a tensile test again, yet with new specimen dimensions after prestraining (PS) and baking. The stress difference between R_e [MPa] after baking and $\sigma_{2.0}$ [MPa] before baking yields the BH_2 [MPa] value:

$$BH_2 = R_{e170°C/20\,\mathrm{min}} - \sigma_{2.0} \qquad \text{(Eq. 2.6)}$$

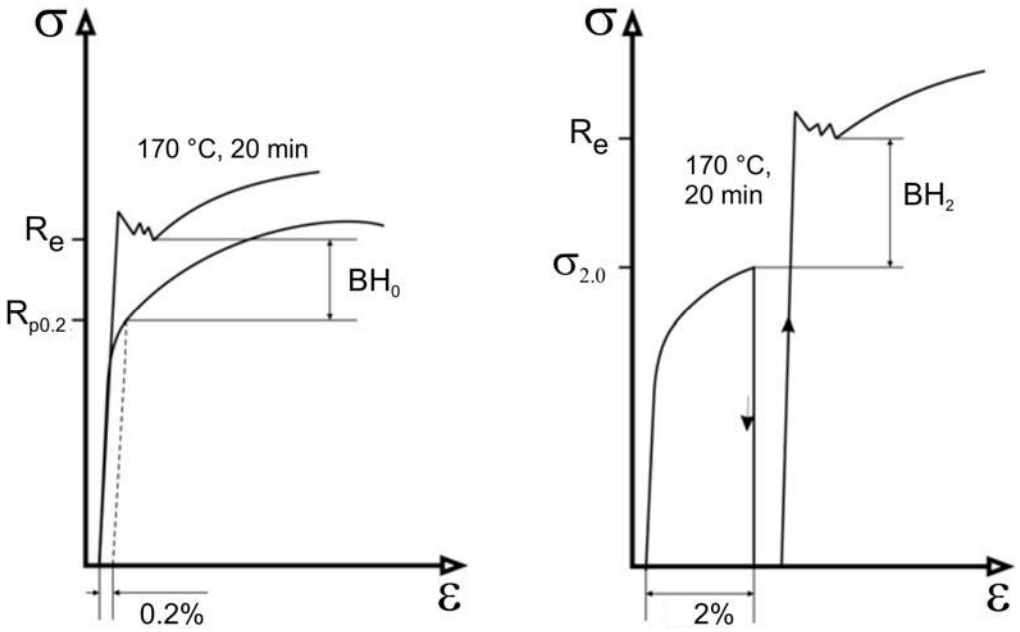

Fig. 2.3 Definition of BH_0 and BH_2 indices according to [Sta87].

From physical metallurgy point of view the mechanism of BH is static strain aging, which can be observed in other metals like aluminium, too [Bir05, Dan68]. BH of steel is supposed to be controlled by the same mechanism responsible for static strain aging, but for multiphase steels other mechanisms may contribute to BH as well (section 2.6). In order to occur measurable static strain aging, several criteria must be simultaneously met [De99]: sufficient mobile dislocations, concentrations of solute C or N atoms and sufficient sluggish of dislocation recovery processes to avoid significant softening. In this mechanism, solute N and C diffuse and interact with the strain fields of mobile dislocations and hence form atmospheres around them [Bak02a, Koz97, Rat00, Sha01]. These atmospheres are known as Cottrell atmosphere, which has been named after Alan Cottrell, who proposed his famous theory in 1948 [Cot49a]. These atmospheres would constitute regions in which the elastic strain field of the dislocation was partially relaxed, and hence its energy reduced, so that the solutes would effectively lock the dislocations. Hence they work either to increase the stress required for unlocking and subsequent dislocation movement or immobilize the dislocations [De00]. This will either increase the stress required to unlock and move dislocations, or immobilize dislocations and thus require generation of new dislocations for subsequent plastic flow. Either mechanism results in an increase in strength and a return of discontinuous yielding. The latter mechanism is thought to be more likely. This results in the

return of discontinuous yielding behavior during the tensile test [Cot49b, De00]. The static strain aging as well as BH process may be more accurately characterized as occurring in three stages as follows:

2.4.1 Snoek Rearrangement or Ordering

The first stage of static strain aging, attributed to Snoek rearrangement of interstitials in the stress field of dislocation [Wat03a]. This is a short time process. In fact it is too fast to be measured. Snoek rearrangement is a form of local rearrangement or short-range migration of interstitial solute atoms to favored octahedral sites under stress. The activation energy for this process is reported to be 59 ± 9.6 to 62.4 ± 2.1 KJ/mole [Exe01]. It is reported that this stage is complete in about the time required for a single jump between two interstitial sites in the stress field of a dislocation and thus occurs very rapidly at normal paint baking temperature. This step causes an increase in yield strength, but not the ultimate tensile strength, by pinning the dislocations.

Initially, there is a random distribution of interstitials in the matrix. After an applied deformation, the interstitials in the stress field of a dislocation attempt to minimize the strain energy in the region of the dislocation by moving from random to minimum energy site positions [Ast80]. Only a minute amount of interstitials takes part in the Snoek rearrangement process and the time required is less than the time required for a normal interstitial jump [Mat98].

2.4.2 Cottrell Atmosphere Formation

The second and slower stage follows $t^{2/3}$ kinetics [Ber04, Zha00]. This stage based on the formation of Cottrell atmospheres by long-range diffusion of interstitial solutes from outside the strained region. It is a form of long-range diffusion of interstitial solute atoms to dislocation cores, which immobilize the dislocation, and results in increase in both the yield strength and ultimate tensile strength [Sam08].

Hence, a solute atmosphere is formed which modifies the dislocation stress fields. The consequent decrease in strain energy increases the stress required for subsequent dislocation movement. This movement requires separation of the dislocations from their solute atmospheres under applied stress. The activation

energy for the second stage is 87.1 ± 10 KJ/mole, in agreement with the activation energy for bulk diffusion of C [Exe01].

Free interstitial atoms diffuse to dislocations because the strain energy of a crystal is lowered thereby. Dislocations therefore in general will be surrounded by a cloud of interstitial atoms which prevent or hinder their motion. In order to pull a dislocation away from its atmosphere, an increased stress is needed [Bak02a, Zha01].

By neglecting the effect of saturation of dislocations and the variation of C concentration during aging they obtained the expression for the degree of formation of the atmosphere at time t,

$$\frac{N(t)}{N_S} = 3 n_0 \lambda \left(\frac{\pi}{2}\right)^{\frac{1}{3}} \left(\frac{A D t}{k_B T_{abs}}\right)^{\frac{2}{3}} \qquad \text{(Eq. 2.7)}$$

where *N(t)* [-] is the number of C atoms diffusing to dislocations in a unit volume in time *t* [s] at absolute temperature T_{abs} [K], N_s [m^{-2}] is the initial dislocation density, λ [m] is the slip distance of the dislocation, n_0 is the initial concentration of C in solution [ppm], D [$m^2\ s^{-1}$] is the diffusion coefficient of carbon, A is an interaction parameter defining the strength of the atmosphere and k_B [$J\ K^{-1}$] is the Boltzmann's constant [Wat03a].

The formation of Cottrell atmosphere has been investigated by various authors with respect to the determination of the strength of binding of an atom to a dislocation, determination of the migration rate of an atom in the stress field of a dislocation [Cot49b, Mei67], and determination of the relation between atmosphere formation and observed yield stress [Har66, Lou56]. Since approaches mentioned above are valid only for dilute solid solutions, Sakamoto [Sak89] proposed the theory for obtaining Cottrell atmosphere and it's dragging stress on dislocation for high concentration solid solutions.

Cottrell also mentioned that the first atoms, which arrive at a dislocation, ought to be more effective in anchoring it than those that arrive later. Thereby, it is obvious that for the later stages of aging, the direct proportionality between the numbers of C atoms around a dislocation and the yield stress cannot be valid. Hence, a new equation, considering the back diffusion, needs to be properly formulated [Sak89, Soe04].

Zhao et al. [Zha01] developed a model which takes into account the variation of free C concentration, the saturation of dislocations and the segregation of C

atoms to grain boundaries and to pre-existing cementite particles to describe the formation of the Cottrell atmosphere during aging of ultra low carbon (ULC) steels [Zha00]. As expected, it was found that for small grain sizes (< 16 μm) the influence of segregation of C to grain boundaries on the formation of Cottrell atmosphere is increasing with decreasing grain size and is negligible for the larger grain sizes (> 16 μm). Their model also revealed that saturation level of dislocations increases exponentially with time and that changing the dislocation density within the range of typical application of bake hardening steels does not affect the formation of Cottrell atmosphere. This model can be used for prediction of the C redistribution in a continuously annealed ULC steels.

2.4.3 Precipitation of Coherent Carbides

The last stage of the bake hardening process is the precipitation of ε-carbides. It is established that within a temperature range of 100 – 250 °C, the carbide that precipitates from a supersaturated solid solution of C in bcc iron is hexagonal ε-carbide [De01]. It forms as platelets or needles growing along $\langle 100 \rangle_\alpha$ directions [Abe84, Les81]. In other aging studies in low C steels some authors demonstrated that prior to the precipitation of ε-carbides a low temperature carbide forms at temperatures below the aging temperature of 75 °C [Bak02a, Nei94, Zhu96].

The precipitation of ε-carbides is supposed to occur at dislocation regions. This will cause an increase in yield strength and ultimate tensile strength. However, with continued solute segregation to dislocation cores, the increased local solute concentration leads to the formation of clusters, which can eventually saturate the dislocation sites. When the aging time is too long, a decrease is observed due to coarsening of the carbides [Kem90, Wat96, Yam76].

Flat homogeneous clusters of C atoms, which are not connected with lattice defects, are formed at temperatures below 100 °C. Their formation is due to considerable displacements of iron atoms and the appearance of elastic distortions. As the tempering temperature increases, the clusters become larger and their composition is close to Fe_4C [De01]. This process depends on C diffusion. Metastable ε-carbide (Fe_2C) is formed above 100 °C. It possesses a hexagonal lattice and appears directly from C clusters when the C concentration is increased. Metastable ε-carbide can also precipitate directly from α solution.

At low temperatures ε-carbide precipitates as very fine (10 – 100 nm) plates or rods. With an increase in tempering temperature or time, ε-carbide particles become coarser. This carbide precipitates in steels containing a minimum of 0.2 % C [Abe84].

2.5 Metallurgical Factors of Bake Hardening Mechanisms

The main factors of microstructure influencing the bake hardening effect are the solute C content, grain size, alloying element, dislocation density and the degree of prestrain. A discussion of these factors is presented below.

2.5.1 Effect of Solute Carbon

The amount of C obviously controls the possibility for pinning mobile dislocations. Consequently, with more solute C, more dislocations can be pinned and a higher hardening effect can be obtained [Nab05, Yam88].

As mentioned earlier, strain aging and subsequently BH effect, are very sensitive to the amount of dissolved interstitial atoms, primarily C and N. Modern automotive steel sheets are aluminium-killed, which means that the N atoms are combined as aluminium -nitrides. Hence, the bake hardenability in low C steels is exclusively caused by dissolved C [Oka89]. To maximize the strength increase associated with BH, it is necessary to have as much free C as possible [Che98]. However, as the amount of solute C increases, the resistance to room temperature aging decreases. RT aging prior to forming is not acceptable for exposed automobile panels because it can result in stretcher strain markings on formed panels. To determine the amount of free C that may be used in bake hardenable steel, it is necessary to examine RT aging resistance. It is generally considered that if yield point elongation is 0.2 % or less in a uniaxial tensile test, stretcher strain problems will not arise during panel forming. The times and temperatures of RT aging depend on the time and temperature at which the steel is stored between production and forming [Lie03]. Resistance to aging at 30 °C for 90 days is commonly used as a guideline for the upper limit of RT aging [De01].

The amount of free C requisite for the desired BH effect is evaluated differently by different researchers. By the data of [Miz90] ferrite should contain 15 – 25 ppm free C for a BH effect of 30 – 60 MPa. According to [Sti98], for a

BH effect of 40 MPa it is sufficient that the amount of free C in ferrite be about 6 ppm. The amount of solute C in the ferrite can be measured using the Snoek effect [Sno41], which is caused by movement of interstitial C atoms [Bag01, Fu09]. The term Snoek relaxation refers to the anelastic relaxation in bcc metals produced by interstitial solutes in the process of strain-induced ordering [Now72]. It was first observed by Snoek [Sno39] in α-iron loaded with N and C. The prerequisite for an anelastic relaxation by point defects is the existence of several defect positions.

2.5.2 Effect of Grain Size

The stable processing of BH steels requires proper grain size control as grain boundaries provide low energy sites for interstitial species. Contradictory information about the effect of ferrite grain size on the bake hardenability is reported in the literature [Han84, Van98]. Some authors do not find any correlation between grain sizes and bake hardening [Pra90]. Others found an increase in the bake hardening effect with a decrease in grain sizes [Kwo03, Miz94].

A variation of the grain size influences the distribution of C between the grain interior and the grain boundary by changing the number of segregation sites at the grain boundary. With an increase in grain size the grain boundary area decreases and the total amount of C that can be stored in the grain boundary decreases compared to that in a fine grain structure. In the case of a fine grain size, interstitials from the grain boundaries can move faster to dislocations in the middle of a grain due to the shorter distances [Kwo03].

The effect of ferrite grain refinement on increase of bake hardenability is associated with the location of solute C. It is assumed that during cooling, the C atoms diffuse to the grain boundaries. The smaller the grains are, the more C should be in the grain boundaries because of shorter diffusion paths. Thus, although the same overall solute C content can be measured, the contributed C content as well as bake hardenability can be higher in case of fine grains as the hidden C is more in finer grains [De04, Mes89, Van98].

Ferrite grain size controls the diffusion distance between intragranular solute C and the grain boundary area with higher density of mobile dislocations [Sto00]. In the case of low solute C, the difference in gain size contributes only a little to

the hardening effect because the diffusion distances for C atoms are practically equal for the large and small grains. Since bake hardenability is higher in steels with fine grains for the same solute C content, the efficacy of solute C content has to be higher the finer the grain size. The explanation seems to be not in the activity of C located at the grain boundaries, but in the shorter diffusion distances between intragranular solute C and the grain boundary area. During straining, grain boundaries are the major sources of mobile dislocations and with a smaller grain size, the intragranular solute C is more readily available to block these mobile dislocations, thus producing a higher BH effect [Han84, Van98].

In the recent researches, Ballarin et al. [Bal09a-b] developed a physically based model for bake hardenable steels which is suitable to predict the BH behavior of steels. To take the effect of grain size into account in the model, this effect is introduced in the definition of coefficient b_{BH}. This coefficient is responsible for the initial slope of the softening branch of the material behavior law and allows indirect representation of the grain size and strain rate effects on band propagation. The following equation is introduced to determine b_{BH}:

$$b_{BH} = K_d . d^{0.8} - S . \left(\frac{\dot{\varphi}}{\dot{\varphi}_0} \right) \qquad \text{(Eq. 2.8)}$$

where d [m] is the grain size, $\dot{\varphi}$ [s^{-1}] is the strain rate K_d, S and $\dot{\varphi}_0$ are constants. The effect of grain size appears with $d^{0.8}$ in order to give a linear relation between the lower yield stress and $d^{-1/2}$ when considering BH steel standard behaviors.

2.5.3 Effect of Alloying Elements

Advanced high strength steels commonly contain small amounts of solid solution strengthening elements, such as Mn, Si, and P. A straightforward way to increase the strength in these steels would be to increase the amounts of these solid solution elements. However, each of these elements has characteristics, which limit their additions. The influences of some relevant elements on BH are described as follows:

Manganese is reported to have an affinity for C and forms a dipole with C [Abe84, Miz94, Wat99]. It is, however, not clear whether the Mn-C dipole decreases BH. In [Wat99], it is reported that the formation of Mn-C clusters reduces the amount of C available to move to dislocations. As a disadvantage

Mn reduces plastic strain ratio. Dissolving of Mn into cementite accelerates the precipitation of cementites, which reduces dissolved C content resulting in lower bake hardenability [Han84, Sai89].

But on the other hand, proper control of Mn can enhance aging index and BH index. In [Miz90] this is validated by the fact that manganese-sulfides (MnS) that segregate instead of titanium-sulfides (TiS) serve as a substrate for the segregation of TiC thus removing C from the solid solution. Without Mn, only Ti (C, N) and $Ti_4C_2S_2$ were observed. On LC steels Mizui et al. [Miz98] noted that with Mn at the 1.0 wt. % levels, MnS and TiS replace $Ti_4C_2S_2$ as the precipitates, which combine with S and C. As a result, less C is combined as $Ti_4C_2S_2$, and more C is available to go into solution and contribute to aging and BH.

The effect of Mn is connected not only with the formation of sulfides. It is shown in [Miz98] that in Ti-free steel alloyed with Nb alone the BH effect enhances from 40 to 60 MPa as the Mn content is increased from 0.5 to 2 %. The authors associate this with the appearance of the temperature of phase transformation, which causes segregation of niobium-carbides at a lower temperature and, consequently, causes their disintegration and higher solubility.

Silicon is reported to repel C in steel and thus enhances the bake hardenability [Miz94]. Si delays the precipitation of cementites because it enhances the activity of C around the cementites [Les81]. Therefore, higher bake hardenability is obtained with increasing Si content. But Si causes higher yield point elongation as compared to its strengthening capability. Si is not used for bake hardenable steels as long as the BH steels can be strengthened by other elements [Sea03].

However, no more than 0.5 % of Si should be added to have the highest bake hardenability and to avoid poor surface quality due to SiO_2 formation. Si also contributes to the increase in bake hardenability by reducing grain size. Hanai et al. [Han84] reported that the BH quickly reached the highest value, as Si content was increased up to 0.5 %. A further increase of Si content (above 0.5 %) led to the grain coarsening. Similar results on LC steels were obtained by [Yam88]. The authors found, that Si retarded the precipitation of carbides because Si enhances the activity of C around the carbides. This result was reported before by Keh and Leslie [Keh63]. Watershoot et al. [Wat99] noted that Si suppressed

the aging at RT in a Ti-ULC steel. They observed no significant effect of Si on bake hardenability of this steel.

Phosphorus increases BH. It is reported that this is due to the fact that P segregates to the grain boundaries, which are favorable sites for C to precipitate [Sea03, Sha01]. Less C segregation to grain boundaries results in greater intragranular solute C and therefore greater bake hardenability [Ble04a]. Furthermore, P has grain refining effect [Pra90, Yam88]. In [Sai91] was reported, that P increases the solubility of C in ferrite grain. Drewes and Engl [Dre90] observed an increase in the BH values at an aging temperature of 180 °C on a P-alloyed steel. Moreover, the authors pointed out [Dre90] that the maximum BH value is achieved without prestrain. In another study no significant influence of P content on the bake hardenability of Ti-ULC steels was observed [Wat99].

P has the advantage that it does not deteriorate the plastic strain ratio. Hence, it is used mainly as the strengthening element of bake hardenable high strength steel of drawing quality [Met09]. Although P is the most effective solid solution strengthening element, not more than 0.1 % P causes strain induced brittleness and welding problems [Yam88].

Molybdenum (Mo): Bleck [Ble02] noted that Mo thermodynamically favors the formation of carbides, but that kinetically, it is found to slow carbide precipitation. Jiao et al. [Jia01] added Mo to slow the formation of Nb(C, N) in their steel. Mintz [Min01] reported that Mo allows the use of slower cooling rates, as Mo decreases the critical cooling rate for the bainite transformation and it suppresses the formation of pearlite. There are no studies about the effect of Mo on the BH behavior.

Niobium is present in the form of carbonitride. Nb binds C into NbC carbides and forms segregations on the boundaries of ferrite grains. The presence of Nb in the solid solution and on grain boundaries improves the texture of the steel and the adhesion of hot zinc-bearing coatings [Mey94]. The authors of [Sti98] assumed that microalloying by Nb alone was favorable for the production of steels with hot zinc-bearing coatings.

Vanadium is a weaker carbide former than Ti or Nb [Dav78b]. Hence, it is expected to dissolve easily during annealing and, as a result, increases the amount of solute C, thus enhancing bake hardenability of the LC steels [Eng96].

VC carbides dissolve well at a relatively low temperature and vanadium-alloyed steels are highly resistant to natural aging and poorly sensitive to changes in the process parameters [Sto01].

2.5.4 Effect of Temper Rolling and Prestraining

Strains introduced into bake hardenable steels come from two sources: temper rolling and tension deforming. These strains produce different dislocation structures and affect BH behavior differently [Cha84].

During sheet metal forming, the material undergoes complex strain-paths up to large accumulated plastic strains. Therefore, good ductility and high strength are required, which can be partly controlled by solid solution strengthening [Lui09]. However, non-uniform plastic deformation patterns due to strain aging, like Lüders bands or “stretcher-strains marks” on the surfaces of sheets during stamping operations, have to be avoided [Pep07]. This is usually done in industry by temper rolling, which produces a thickness reduction of only a few percent in a final rolling process. For thin sheets, temper rolling is also used to improve the material strength through higher reductions. Mechanical loading after temper rolling induces a strain-path change, which may promote specific effects on the material hardening. In LC steels, such effects have already been observed in tension after cold rolling [Wil94] and during strain-path changes combining tensile and shear testing [Bou06, Rau89].

Aging of temper rolled steels is more sluggish than for tension-deformed steels. The reason is the difference in the aging behavior because of two folds. First, the dislocation density of the temper-rolled steel is less than that of the tension-deformed material. Therefore, the average distance between dislocations is greater for the temper-rolled steel than for the tension-deformed steel. Hence, the distance of C atoms diffusing to dislocations to promote aging is greater for the temper-rolled steels. Second, a strain aging suppression effect peculiar to temper rolling has been observed. Temper rolling produces regions of high and low strains in the sheet. The inhomogeneous strain distribution is believed to be the cause of the strain aging suppression effect associated with temper rolling [Bai94, Les81].

It is reported that after the temper rolling (without PS), ferrite grains exhibit a heterogeneous dislocation structure in such a way, that the areas near the grain

boundary contain some mobile dislocations but their density decreases sharply with the increasing distance from the boundary [But63]. PS of 2 % generates a considerably higher mobile dislocation density but the heterogeneity of dislocation structure remains [Fan02].

A number of papers give profound insight into the prestraining effect on the BH behavior [Ble04a, Brü10, Jeo98, Kri07, Wat03c]. Stiaszny et al. [Sti90] reported a generally BH increment with increasing PS for a BH steel (ALFORM 260 BH). Krieger [Kri07] conducted studies into the effects of PS on the BH behavior of cold rolled DP steels. He reported large BH values in the prestrained condition up to prestrains below 0.5 %. A decrease of BH values was observed when the degrees of PS further increased. Drewes and Engl [Dre90] found the same behavior for ZStE 180 BH and ZStE 220 BH steels. Both grades show relatively low BH_0 indices and peak values at low prestrains, followed by a continuous decrease of the BH levels. Similar results on ZStE 220 BH steel were obtained by Van Snick et al. [Van98]. Elsen et al. [Els93] explained the BH mechanism of the ZStE 180 BH steel in the following way: A first contribution to BH comes from the forming of Cottrell atmospheres around dislocations. In the first mechanism step they found no correlation between PS and BH. A second contribution is given by the formation of coherent carbide precipitates, where the authors found decreased BH values with increased PS. A similar behavior was reported by Baker at el. [Bak02b] for ULC steels microalloyed with Nb and Ti. They noted that in the first step (100 °C / 100 min) there is no depending from PS and relates to $t^{2/3}$ low, while in the second step (200 °C / 100 min) increased BH values with increasing PS appears. Contrary to these findings, De at al. [De99] reported that the PS does not affect the BH of LC steels.

2.6 Bake Hardening in Multiphase Steels

Unlike the ULC steels, where aging phenomena are principally guided by the amount of interstitial C and dislocation density, the aging in multiphase steels is much more complex, as a result of its multiphase microstructure and strain partitioning. It was argued that the aging mechanism in the ferritic phase is influenced by the interstitial C, the C in the grain boundaries and the specific distribution of dislocations and residual stresses [Dre99]. In multiphase steels, additional mechanisms must be taken into account. Waterschoot et al. [Wat06]

reported an increase of the BH values in DP steels by C released from the martensite as a result of tempering. The mechanism of strain aging in TRIP steels is expected to be more complex and has not yet been studied in a fundamental manner. The BH value of TRIP steels is known to be considerable. The intrinsic BH response of the different phases in multiphase steels must be investigated to understand the various aging mechanisms in each phase [Ble04a].

The BH effect of TRIP steels was investigated by Pereloma et al. [Per08a-b]. Using the atom probe tomography (APT) they observed the presence of fine C-rich clusters in the martensite phase. After BH treatment, the formation of iron carbides, containing 25 to 90 at. % C was found. The evolution of iron carbide compositions was independent of steel composition and was a function of carbide size.

In DP steels, high BH values have been shown to be related to the relaxation of internal stresses [Wat03a-b]. The multiphase microstructure formed in DP steels controls the combination of strength and ductility. Grain boundaries could act as low energy sites for C, and in this case, the C could remain there, which would decrease the BH response. It is possible for C to diffuse from the grain boundaries to the grain interiors during treatment, which would increase the BH response [Gün08].

Aging causes martensite tempering and a decrease in the internal stresses, increasing tensile stress needed to initiate plastic flow. This results in the increased static strain aging behavior exhibited by DP steels [Tim07, Wat03c]. In DP steels, therefore, several stages must be considered in both the ferrite and martensite, namely the Cottrell atmosphere formation stage, the C clustering and precipitation stage in ferrite, as well as the effects of volume contraction and changes in strength of the martensite due to tempering of the martensite. Furthermore, the additional C clustering or precipitation near the F/M interfaces has to be taken into account [De01].

The aging behavior of DP steels with a composition characteristic for the martensite phase was recently studied by neutron diffraction [Wat03b]. On tempering martensite at 170 °C and 350 °C the authors observed the sequential precipitation of η- and θ-carbides, as well as the loss of tetragonality. The large increase of yield stress in DP steels was explained by the relaxation of

compressive stresses originating from the transformation of austenite to martensite.

In [Wat03a] the strain aging of DP steels had been studied with specific reference to the contribution of particular phases to overall strengthening. The authors proposed a technique for determination of BH effect, which allowed the observation of different aging stages in DP steels more accurately.

The different phenomena observed during the aging of DP steels are schematically shown in Fig. 2.4, in which the data of the investigated steel is plotted using the Holloman-Jaffe parameter [Hol45], which combines temperature and time in one parameter $T_{HJ}(\log t + 14)$ (T_{HJ}: temperature [K] and t: time [s]) to obtain a master aging curve. They observed three different stages of BH: the Cottrell atmosphere formation stage, precipitation stage and the strengthening stage due to contribution from the martensite phase (Fig. 2.4). It was concluded that the magnitude of the second stage depends on the interstitial C content of the initial matrix and that internal stresses in the ferrite is reduced by the martensite volume decrease due to the formation of C clusters or transition carbides which consequently, in combination with the presence of pinned dislocations, results in a strong BH effect. By using dilatometric tests, the same authors [Wat06] had been able to distinguish five different stages of structural changes during tempering of martensite similar to the martensite phase present in DP steels, namely the segregation of C to lattice defects, precipitation of η- and Hägg- carbides, transformation of retained austenite and martensite transformation to cementite.

Timokhina et al. [Tim07, Tim08, Tim09] studied the BH behavior of intercritically annealed DP steels using X-ray diffraction, TEM and three-dimensional atom probe tomography (APT). They found an increase in the yield strength and the appearance of the upper and lower yield points after a single BH treatment as compared to the as-received condition. This effect appeared because of the formation of plastic deformation zones with high dislocation density around the as-quenched martensite in the DP steel, which allows C to pin these dislocations, which, in turn, increases the yield strength. Furthermore it was found for the DP steel that the BH behavior depends on the dislocation rearrangement in ferrite with the formation of cell, micro-bands and shear band structures after prestraining. Moreover, APT showed a high C content of ferrite

in the DP steel after the BH treatment. The C atom map of the DP steel after BH treatment also revealed the formation of Fe_3C carbides within the martensite crystal.

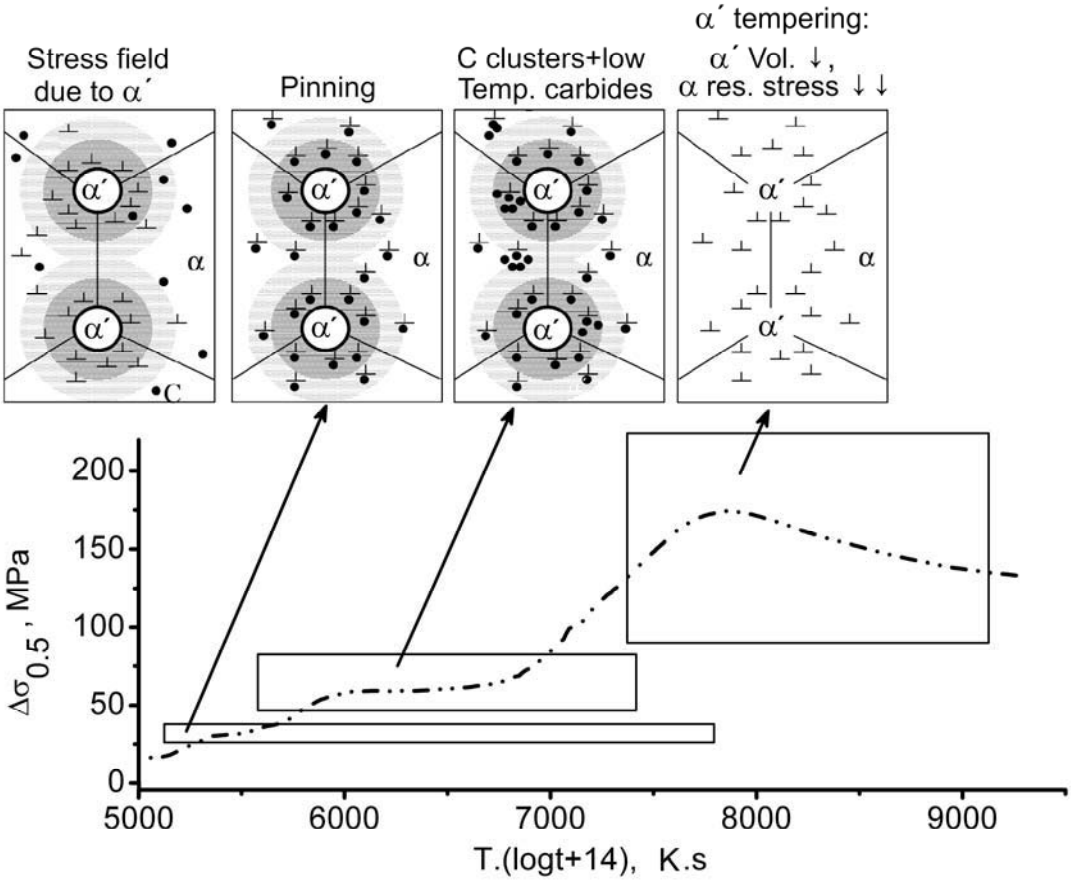

Fig. 2.4 Schematic overview of the processes involved in the aging process of DP steels as a function of Holloman-Jaffe parameter: the pinning of dislocations by interstitial C, C clusters, or low-temperature carbide formation in the ferrite, and stress relaxation due to tempering of the martensite [Wat03a].

Krieger [Kri07] studied the effect of continuous galvanising line processes (CGL) on the BH behavior of cold rolled DP steels. The author reported a clear influence of the different stages of the CGL process. The martensite volume fraction is largest for steels directly quenched from the intercritical temperature regime in the ferrite plus austenite two phase field. Intermediate fractions were obtained for steels processed up to the overaging stage, while lowest amounts were found after including the final galvanising stage. Those steels which did not undergo the zinc bath stage showed large BH values on non-prestrained samples. The steels subjected to full CGL cycles showed low BH values without prestraining. With respect to PS, the author found the highest BH values at low strains of about 0.5 % due to a large number of mobile dislocations in the ferrite

grains and the diffusion of solute C atoms from the energetically favored sites near the F/M interfaces into the ferrite grains as soon as PS is applied, making a most effective pinning of dislocations possible. He reported further BH increase especially at temperatures above 200 °C due to an additional contribution from the tempering of martensite.

The same author studied the BH behavior of different cold rolled DP steel grades [Kri03, Kri06]. He found only very little BH effect without PS. With increasing PS up to 1 %, the BH values quickly reached more than 60 MPa and stayed at a constant level up to a PS of about 5 %. At even larger strains, a further increase of BH values could be measured. The BH effect of cold rolled DP steels was investigated additionally by [Doe07, Far06, Ste04].

Brühl et al. [Brü05, Brü10] conducted studies into the effects of PS, temperature and holding time on the BH behavior of DP steels. The prestrains used were from 0 % up to 10 % in uniaxial tension. At low temperatures and without PS, they did not observe an increase of yield strength in case of hot rolled DP steels indicating a good stability against RT aging. Maximum BH values (up to 100 MPa) are reported at a PS of 2 % and at the highest temperature of 250 °C. At elevated baking times a decrease of BH values is observed attributing to overaging phenomena.

Strain paths effects on the BH behavior of hot rolled DP, TRIP, CP and MS steels were investigated by Anke et al. [Ank05, Pal06]. The influence of both, uniaxial and biaxial prestrained specimens, was studied for different degrees of prestrain. The prestrains used were between > 0 % and the strain corresponding to uniform elongation in both, uniaxial tension and biaxial stretch. Additionally, the effect of temperature (130 to 240 °C) as well as holding time (15 to 27 min) was investigated. No distinct influence of holding time on BH properties could be stated. An increase of BH values at higher temperatures (above 170 °C) was observed for the investigated steels. A significant effect on BH could be seen for variation of the strain paths. The biaxial prestrained specimens revealed larger BH values than uniaxial prestrained specimens.

Recent studies by Müller [Mül07] regarding DP steels have shown that an increase of the PS in biaxial state can result in substantial decrease to the BH effect. For DP steels, an increase in the PS from 0.04 to 0.4 results in a decrease of the BH values well under 40 MPa. The BH values of the biaxial

state with the same principal strain were higher than the values investigated in the uniaxial tensile test. The effect of strain paths on the BH behavior was studied for hot rolled CP, DP [Asa10a-b] and LC steels [Bal09a-b].

Asadi et al. [Asa09a-b, Asa10a-b, Pal08a-b] investigated the local aging effect in multiphase steels, mainly DP steel. For this purpose, two methods were applied to achieve local strengthening, namely local deformation and local heat treatment. Samples were locally deformed by bending to total strain φ_t = 0 to 0.3 and embossing to total strain φ_t = 0 to 0.15. A local deformation with defined prestrains results in enhanced hardness and strengthening in DP steels. A subsequent BH treatment in the temperature range of 100 – 240 °C for 20 min leads to a further increase of strengths. Local heat treatment was applied using a laser and an electron beam. Before the local heat treating the DP sheet samples were globally cold rolled with defined deformations (ε = 0 to 10 %). It could be stated that with partial heat treatment, local high strengthening can be produced. The authors concluded that at lower heat treating temperatures, strengthening effect can be attributed to BH. The large increase of the strength with increased heat treating temperature was because of affecting the initial microstructure near the surface. They also studied the influence of the overaging in locally strengthen regions. A good resistance against RT aging is observed for local strengthen DP steels. The good resistance against RT aging were also reported for non-deformed steels in [Ste04], which is attributed to the presence of martensite and larger activation energies for aging [Ble07].

3 Experimental Methods and Details

3.1 Materials

DP steel used in this study was delivered by SZFG as roughing rolled plates (including melting, casting and roughing rolling) with a thickness of 50 mm. The chemical composition of the steel is listed in Tab. 3.1. This steel is used as basic alloy for the investigation of chemical composition being cast in laboratory. The chemical composition and the method of preparation of alloys are introduced at the beginning of chapter 6.

Tab. 3.1 Chemical composition of the steels (wt. %)

Steel	DIN 10336	C	Si	Mn	Cr	Mo	Nb	P	N	Al
DP 600	HDT580X	0.06	0.10	1.30	0.60	0.005	0.002	0.04	0.006	0.035

3.2 Simulation of Roughing Rolling Process

Hot rolling tests were carried out on a 12”-2-high laboratory rolling mill (Fig. 3.1). The maximum rolling width is 350 mm. The maximum roll gap is 60 mm and the gap displacement speed is 1 mm/s. The maximum rolling force is 1800 kN. The rolling conditions are introduced at the beginning of chapter 6.

The mill data were recorded during the rolling process. This included: pass reduction (%), temperature (°C), true thickness (mm), strain rate (s^{-1}), true strain (-), rolling forces (kN), rolling gap width (mm) and rolling speed (m/min).

Fig. 3.1 Laboratory reversing mill for hot rolling simulation (a picture of plates during roughing rolling simulation is inserted in the upper right corner).

3.3 Simulation of Finishing Rolling Process

For studying the kinetics of phase transformation which takes place in the steels investigated during their TMCP as well as for simulation of last three deformation steps of hot rolling process a “Bähr TTS820” type deformation simulator was used. Using this deformation simulator it is possible to simulate different thermomechanical schedules by changing the applied strain, the number of temperature of individual deformation and the subsequent cooling condition. The experiments were preformed using a flat compression setup mounted on the deformation simulator. With this equipment the simulations of combination of selected technological steps under controlled laboratory conditions had been carried out.

Fig. 3.2(a) shows the flat compression setup on the deformation simulator. The Bähr deformation simulator consists of a chamber which can be closed and evacuated. In the experimental setup, the flat compression specimen is placed on two pedestals and is only fixed in place with the aid of a clamping device during the punch return. The specimen is inductively heated by an U-shaped induction coil. Two deformation stamps, right and left on the specimen, are provided for deforming the flat compression specimen. Four gas coils with drill holes faced to the middle of specimen side are located symmetric left and right on the specimen to quench the specimen (Fig. 3.2(b)). Helium gas was used for cooling. The equipment has a laser extensometer, which measures dilation across the sample width during experiment. The laser extensometer has a resolution of 0.05 μm. The test specimens had been degreased using an acetone solvent. Sheathed type S “Pt/Pt-10 % Rh” thermocouple wires with a nominal diameter of 0.1 mm have to be individually spot welded to the specimen’s surface in central position using a welding jig. After placing the sample on the pedestals, the insulating sheaths on the thermocouple wires had been moved along the thermocouple wires until they contacted the specimen’s surface. This step is essential to prevent undesirable heat loss and to avoid contact between the two thermocouple wires [AST04]. The thermal cycles had been performed under vacuum of 5×10^{-5} mbar. The dilatometric curves had been recorded along the thermal cycle with the help of a computer-data acquisition system.

T_{nRX} can be determined by the method proposed by the group of Jonas [Bai93] which is based on multi-stage torsion test. This method intrinsically takes into account thermo-mechanical processing parameters. In order to determine T_{nRX}, the torsion test was also conducted using the Bähr deformation simulator. The deformation simulator has additionally a setup for torsion test (Fig. 3.3(a)-(b)). The main principle of the torsion setup is similar to flat compression setup. In Fig. 3.3(b) a picture of a torsion sample during hot torsion test is inserted inside the induction coil. Relevant technical characteristics of the deformation simulator for flat compression and torsion setup are listed in Tab. 3.2.

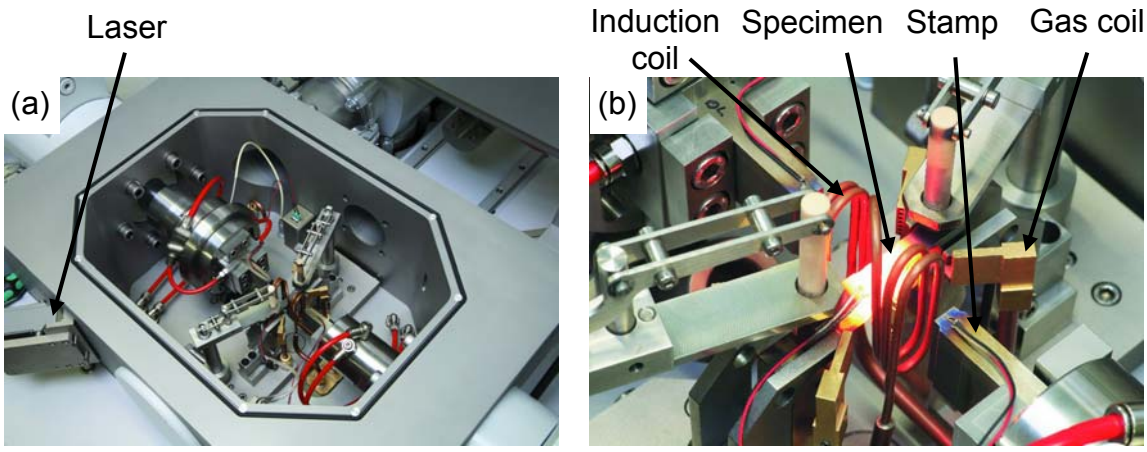

Fig. 3.2 (a) Experimental flat compression setup and (b) position of the flat compression sample in the chamber inside the induction coil of the deformation simulator.

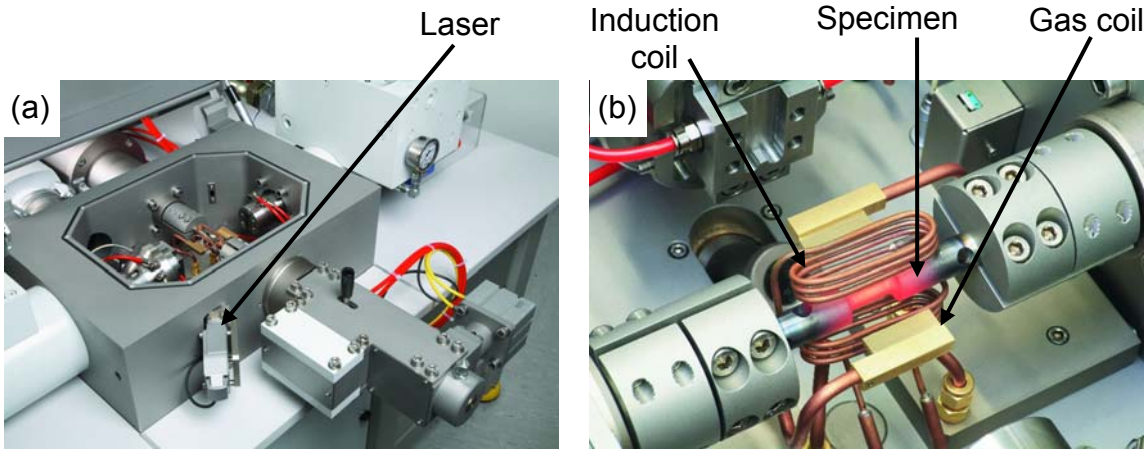

Fig. 3.3 (a) Experimental setup of torsion test and (b) position of the torsion sample in the chamber inside the induction coil of the deformation simulator.

Flat compression specimens as well as torsion specimens were taken out from the hot rolled plates with the longitudinal axis parallel to the original rolling direction. Fig. 3.4 indicates the dimension of the flat compression sample. Heat

transfer of the flat compression specimen was reduced by two holes with a diameter of 8 mm.

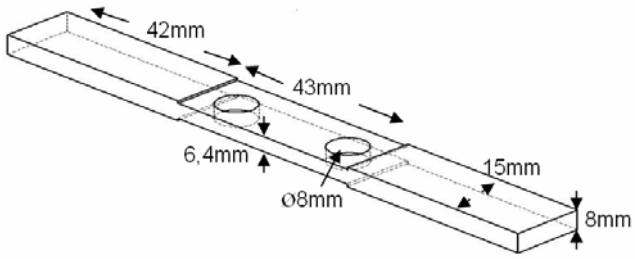

Fig. 3.4 Specimen's dimension for flat compression test.

Tab. 3.2 Technical specification of the deformation simulator Bähr TTS820

Specification		Flat compression	Torsion
min. - max. deformation rate	[mm/s]	1 - 1000	---
min. - max. torsion rate	[rpm]	---	6 - 1400
min. - max. strain rate	[s^{-1}]	0.1 - 100	0.04 - 8.5
min. - max. true strain	[-]	0.1 - 2	0.04 - 10.8
min. pause between deformation steps	[ms]	50	10
max. force	[kN]	100	78
max. heating rate	[K/s]	50	50
max. cooling rate	[K/s]	100	100

The procedure of T_{nRX} determination consists of calculating the mean flow stress (MFS) that corresponds to each deformation step. MFS [MPa] is defined as the area under the given stress-strain curve for selected interval divided by this interval:

$$MFS = (\varphi_2 - \varphi_1)^{-1} \int_{\varphi_1}^{\varphi_2} \sigma(\varphi) d\varphi \qquad \text{(Eq. 3.1)}$$

3.4 Characterisation of Microstructure

3.4.1 Light Optical Microscopy

Light optical microscopy (LOM) analysis of the as-received samples as well as samples from various processing and conditions was performed by sectioning the samples parallel to the deformation direction, and mounting them in bakelite. The samples were then rough polished using standard metallographic abrasive grinding papers ranging from course (180) to fine (1200). The final polishing was done using 1.0 µm and 0.05 µm alumina, respectively. The microstructure was developed for LOM by etching with 2 % Nital. Etching time was between 10 to

15 s. After etching, the samples were rinsed with ethyl alcohol and dried under a warm air drier. Nital etchant stains bainite brown and martensite grey to back, while ferrite remains white [Mar82b, De03]. Quantitative analysis of the photomicrographs was performed using image analysis software “Analysis Five”®. The grain sizes were obtained using a line interception method [DIN85].

3.4.2 Thermal Etching

The method of thermal etching consists in revealing the austenite grain boundaries in a pre-polished sample by the formation of grooves at the intersections of austenite grain boundaries with the polished surface when the steel is exposed to a high temperature in an inert atmosphere. These grooves decorate the austenite grain boundaries and make them visible at RT in the light optical microscope [Gar02].

Cylindrical samples of 5 mm in diameter and 10 mm in length were used to reveal grain boundary by the thermal etching method. For that purpose, a 2 mm wide surface was generated along the longitudinal axis of samples by polishing and finishing with 1 μm diamond paste. Later, those samples were heat treated in a dilatometer Bähr 805 (Fig. 3.5) at a heating rate of 5 K/s to an austenitization temperature of 950 °C. A vacuum pressure higher than 5×10^{-5} mbar is advised to avoid oxidation on the polished surface. Subsequently, samples were cooled down to RT by argon gas at a cooling rate of 1 K/s.

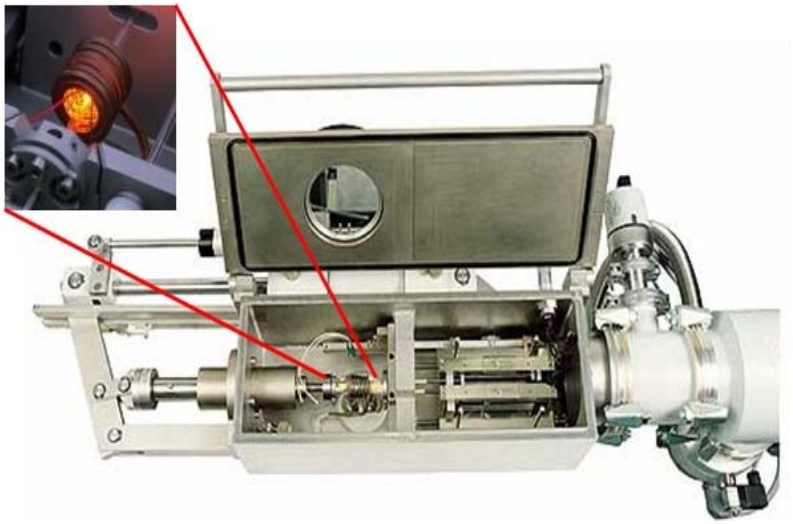

Fig. 3.5 Dilatometer setup of the Bähr 805 A/D for thermal etching tests.

3.4.3 Transmission Electron Microscopy (TEM)

TEM microscopy was performed to do the fine detailed analysis of the microstructure, including the measurement of the dislocation density present in the materials. It was also used to try to reveal the existence of Cottrell atmospheres or barriers. Thin foils were prepared by manual grinding until a thickness of 100 µm. Small disks with a diameter of 3 mm were punched out and prepared by rough grinding to 40 µm to reduce the magnetic mass of the specimens [Agh09] and then immersed in a solution of 5 % perchloric acid ($HClO_4$) in methanol (CH_3OH) at -30 °C at an operating voltage of 50 V using a Struers TENUPOL 5 double jet polishing device.

TEM examination of materials was conducted in various TEM instruments. Most of the examination was conducted in a Tecnai F20 G^2 field emission gun (FEG) TEM operating at 300 kV at Ruhr-Universität Bochum (RUB). For taking bright field micrographs as well as diffraction pattern a CCD camera (Gatan US 1000) was installed. In addition, a high angle annular dark field (HAADF) was used in scanning transmission electron microscopy (STEM). STEM operates on the same principles as TEM, but, like in SEM, the electron optics focuses the beam into a narrow spot which is scanned over the sample. Unlike normal dark field imaging where the signal comes from elastic scattering of electrons typically at smaller angles, the HAADF signal is the result of inelastic scattering of electrons typically to larger angles. In a high resolution HAADF image, brighter spots represent the heavier atomic elements while the less intense spots indicate the lighter atomic elements [Bro93].

Some of the examinations were also done using a JEM-200CX TEM operating at 200 kV at Graduate Institute of Ferrous Technology (GIFT) in Pohang. Analysis from JEM-200CX TEM included bright field, dark field and diffraction pattern.

3.4.4 Saturation Magnetization Measurements

To measure the retained austenite volume fraction of samples after TMCP saturation magnetization (SM) measurements were carried out at SZFG. The equipment (Fig. 3.6) consists of a magnetic yoke, which produces a high and homogeneous magnetic field between its poles. A magnetic flux sensing coil mounted in the center of this magnetic field is used as the measurement coil.

The specimen to be measured is pushed trough the measurement coil along its axis. The integral of the voltage pulse, which is induced in the coil, is measured. From this signal, the amount of the retained austenite in the specimen can be calculated. Specimen dimensions were 7.5 mm x 5 mm x thickness.

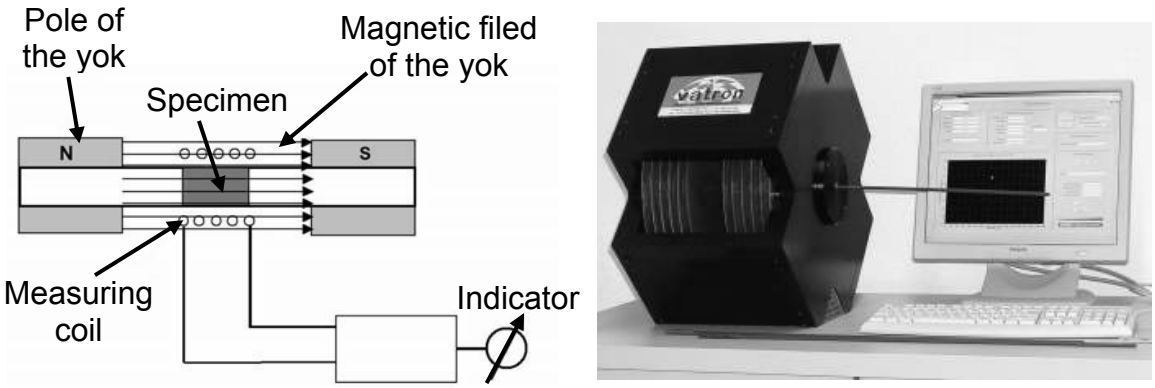

Fig. 3.6 Experimental setup for the SM measurements.

3.5 Tensile Testing

To determine the mechanical properties tensile specimens with special geometry (see Fig. 3.4) were machined out of flat compression specimens. Fig. 3.7 shows flat compression specimens before and after hot deformation as well as after machining. Three specimens were tested for each condition and the results were averaged.

The tensile tests were conducted in a computerised universal testing machine (UTS) with a 250 kN load cell using a crosshead speed of 5 mm/min. The traverse sensor on the sample was set at a gauge length of 15 mm. The following properties were evaluated:

- $R_{p0.2}$ 0.2 % offset yield strength (proof stress), [MPa]
- R_e lower yield strength (after PS and BH), [MPa]
- R_m tensile strength, [MPa]
- TEl total elongation, [%]

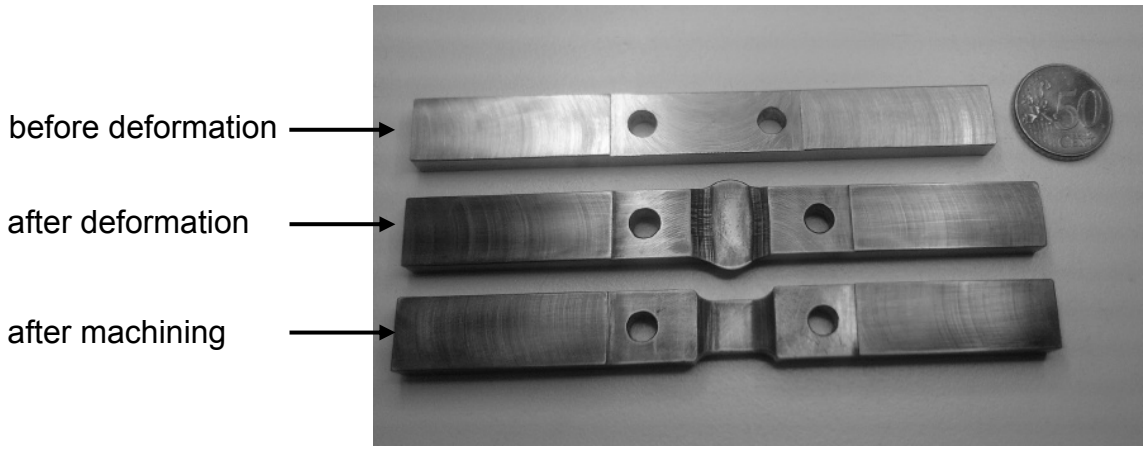

Fig. 3.7 Flat compression specimens before and after hot rolling simulation and after machining.

3.6 Bake Hardening Experiments

The test method used for the BH experiments is based on SEW 094 as described in section 2.4. In accordance with the standard procedure the test was extended by variation of prestrain and temperature of the BH. For all conditions the holding time of BH treatment was kept to 20 min. For the samples without PS the difference between $R_{P0.2}$ of the tensile sample and lower yield strength (R_e) of the respective BH sample was taken as a measure of BH. Prestraining as well as tensile testing after BH treatment was done on the universal testing machine with a crosshead speed of 3 mm/min, too. A Heraeus recirculating air furnace with temperature control to the accuracy of ± 2 K was used for BH heat treatment. Finally, the changes of yield stresses due to BH effect were calculated.

The method proposed by Waterschoot et al. [Wat03c], which enables more accurate distinguishing between contributions to the increase of yield stress due to BH and WH effect, is not applicable in this study, since it relies on the sample geometry. Therefore, in the present study BH effect was measured according to the common practice using the same specimen in both, PS and tensile testing step, respectively. For each condition at least two to three tests were conducted and then the results were averaged.

4 Hot Deformation Parameters: Results and Discussion

4.1 Introduction

Traditionally, the main objective in conventional thermomechanical controlled processing (TMCP) of multiphase steels has been to refine the ferrite grain size through (1) refining prior austenite grains, (2) increasing grain boundary area per unit volume by changing the grain shape, e.g., pancaking, and (3) increasing boundaries [Pic78]. Moreover, it has also been observed that the morphology of ferrite is related to the prior austenite [Oga10, Tor03]. In DP steels with the presence of ferrite and martensite in the microstructure, the other aim of TMCP is to refine the microstructure by the deformation in the non-recrystallized austenite region. It has been reported that the bainite can be significantly refined by more than 50 % deformation in the non-recrystallized region [Fuj98]. Furthermore, the TMCP schedule also influences the transformation behavior, leading to different morphologies of the ferrite and martensite.
For hot strip rolling of steels it is the desired final mechanical and geometrical properties of the strip that determines the rolling schedule, which is the setup for the rolling process, i.e. the amount of reduction, the rolling velocity and the temperature [Bäc09]. The hot rolled DP steels are typically produced on a hot strip mill, where the level of roughing rolling and finishing rolling depends on the mill configuration and the starting and final thicknesses of the plates [Hod97, Tim03].

4.1.1 Aim of the Study

Prior to finishing, the austenite grain size will vary, depending upon the amount of reduction and the finishing temperatures. Hence, in the current work, a wide range of finishing strains and temperatures are used to clarify the effect of different TMCP schedules on the phase transformation kinetics, microstructure development, mechanical properties and BH behavior of the DP steel. The optimized TMCP schedules are discussed in relation to the microstructure evolution and mechanical properties as well as the BH behavior.

4.2 Thermomechanical Controlled Processing

DP steels can be produced in different ways. The most common methods are cold rolling followed by continuous annealing or processed directly by hot rolling and defined cooling on the run-out table. The first consist of reheating steel with ferrite-pearlite microstructure to the austenite-ferrite temperature range, which is then followed by cooling the material below M_S. The second way, which had been used in this study, allows the formation of prescribed amount of ferrite after the hot deformation step and then accelerated cooling below M_S. In this study the last three deformation steps of hot strip finishing rolling process were simulated according to different schedules. The simulation was carried out on the deformation simulator using flat compression test, as described in section 3.3.

4.2.1 Estimation of T_{nRX}

When dynamic recrystallization (DRX) takes place during deforming a material, e.g. by rolling, grain size is determined by the steady state flow stress. Whenever the critical strain (φ_c) for the onset of DRX is reached and exceeded during hot deformation, a metadynamic recrystallization (MDRX) takes place after interruption of straining, consequently coarsening austenite grains. If deformation is interrupted before reaching the strain φ_c and if temperature is high enough, then static recrystallization (SRX) takes place [Rob78]. By deforming the material in the recrystallization region the austenite grains are being refined. This is important because the grain size of the austenite strongly affects both, the kinetic of subsequent $\gamma \rightarrow \alpha$ transformation and the ferrite grain size, namely smaller austenite grains consequently lead to the refinement of ferrite grains [Ye02]. When deformations are applied at temperatures below T_{nRX} the austenite grains elongate and deformation bands are introduced within the grains. As the amount of deformation in this region increases, the number of nucleation sites at the austenite grain boundaries and within austenite grains increases, too. Because of that, $\gamma \rightarrow \alpha$ transformation from deformed austenite yields in much finer ferrite grains than that from recrystallized, strain-free austenite. Therefore, T_{nRX} is a very important parameter and its determination represents a crucial step in designing rolling schedules. Accordingly, the present schedules have been selected according to this temperature. T_{nRX} for the given

chemical composition can be calculated from the empirical equation proposed by Samuel et al. [Sam88]:

$$T_{nRX} = 887C + 4645Nb - 644\sqrt{Nb} + 732V - 230\sqrt{V} + 890Ti + 363Al - 357Si \quad \text{(Eq. 4.1)}$$

here alloy contents are in [wt. %] and T_{nRX} is in [°C]. It yields for the chemical composition of the DP steel, used (see Tab. 3.1), T_{nRX} = 865 °C. The equation does not take into account the influence of thermomechanical parameters on this temperature and sometimes predicts too high values.

Alternatively, T_{nRX} can be determined by the method proposed by Jonas and co-workers [Bai93] which is based on a multistage torsion test. In the present work the torsion test was conducted on the deformation simulator using torsion setup (section 3.3). Twenty strain steps were selected each one of them φ = 0.3 at a strain rate $\dot{\varphi}$ = 10 s^{-1}. The stress-strain curves obtained are shown in Fig. 4.1 and indicate that the level of stress - as known - depends on the deformation temperatures. Stress increases as temperature decreases, but this increment is higher at the last four deformation steps. On the other hand, there is a higher work hardening rate observed on this curve.

As described in section 3.3, the mean flow stress (MFS) is the area under the given stress-strain curve for selected interval divided by pass strain. The mean flow stresses for all the torsion steps have been calculated by numerical integration (see Eq. 3.1) and the results are plotted as a function of inverse absolute temperature on Fig. 4.2. From this graph the value of T_{nRX} can be determined by finding the intersection between the regression lines of the points that corresponds to each part of the curve with two different slopes. In our case the estimated value is T_{nRX} = 855 °C.

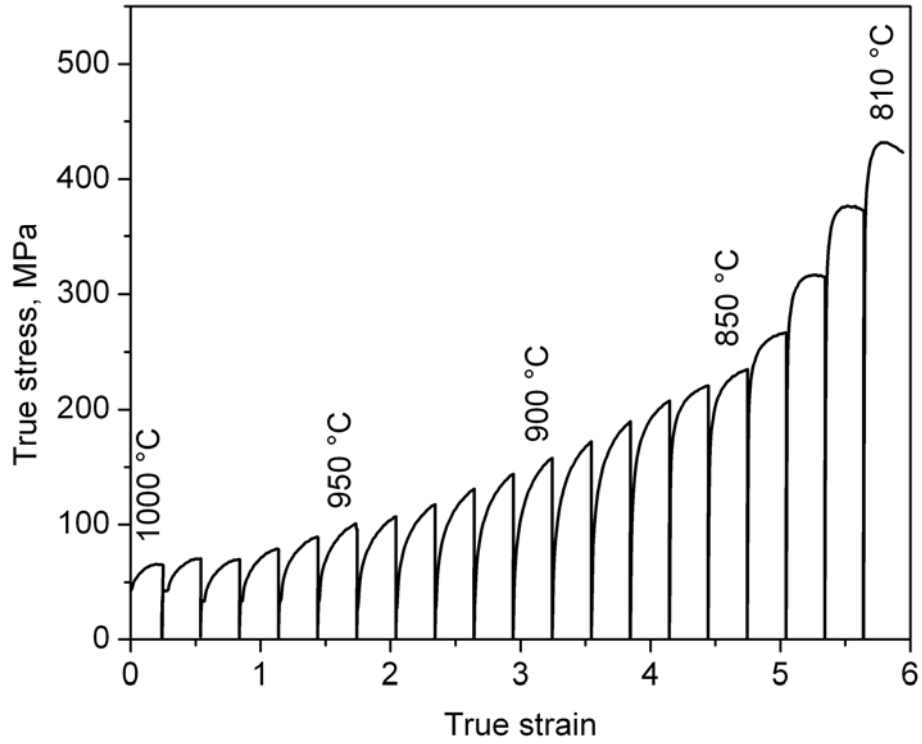

Fig. 4.1 The true strain-true stress curves obtained in twenty-stage torsion test for determination of the T_{nRX} temperature at a strain rate of 10 s^{-1}; temperature sequence denoted on the graph.

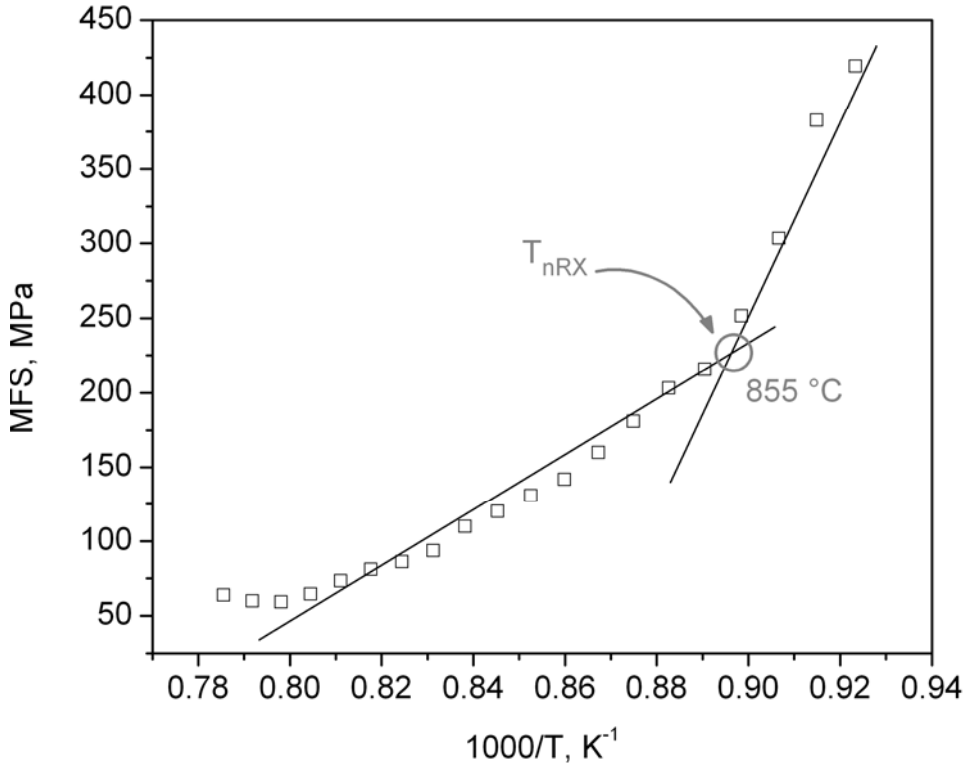

Fig. 4.2 Dependence of the MFS on the inverse absolute temperature.

4.2.2 Simulation of Finishing Rolling

In order to influence the shape and the size of the austenite grains before $\gamma \rightarrow \alpha$ transformation, austenite conditionings were conducted using three different deformation schedules. With the estimated T_{nRX} temperature, the deformation part for the schedules was determined in such a way that all the three possibilities were covered, namely all deformations conducted above T_{nRX}, deformations below T_{nRX} and deformations mixtures of above and then below T_{nRX} (named above-below T_{nRX}).

For the first schedule the condition of the austenite before $\gamma \rightarrow \alpha$ transformation were controlled by recrystallization, which means that all deformations have been conducted in the recrystallization region. The third schedule was aimed at obtaining elongated austenite grains and at introducing deformation bands within grains. For this schedule all the deformation steps were conducted in the non-recrystallization region. In this way, it was expected to obtain austenitic microstructure which was topologically completely different from those obtained by applying the first schedule, where the grains were equiaxial. The purpose of the second schedule was to reduce the austenite grain size to obtain smaller equiaxial grains, and afterwards to deform obtained microstructure in the non-recrystallization region, additionally. By applying this schedule we obtained a deformed austenitic structure, but with smaller and less deformed grains than those that had been obtained with the third schedule. These schedules enabled us to produce three topologically different austenitic microstructures before $\gamma \rightarrow \alpha$ transformation. Samples having those three different microstructures consequently indicated different $\gamma \rightarrow \alpha$ transformation kinetics and subsequently yielded different ferritic microstructures. Fig. 4.3 illustrates schematically different schedules applied in this work. The data corresponding to the numbers denoted on this figure are collected in the Tab. 4.1.

The upper and the lower limits of technological influencing parameters have been selected according to industrial processes. The finishing temperatures (T_f) in large scale production of hot rolled DP steels are between 780 and 900 °C. Therefore, the deformation temperatures and the amounts of strain varied close to this interval. Tab. 4.2 represents deformation temperatures and amounts of strain for the last three deformation steps of hot deformation.

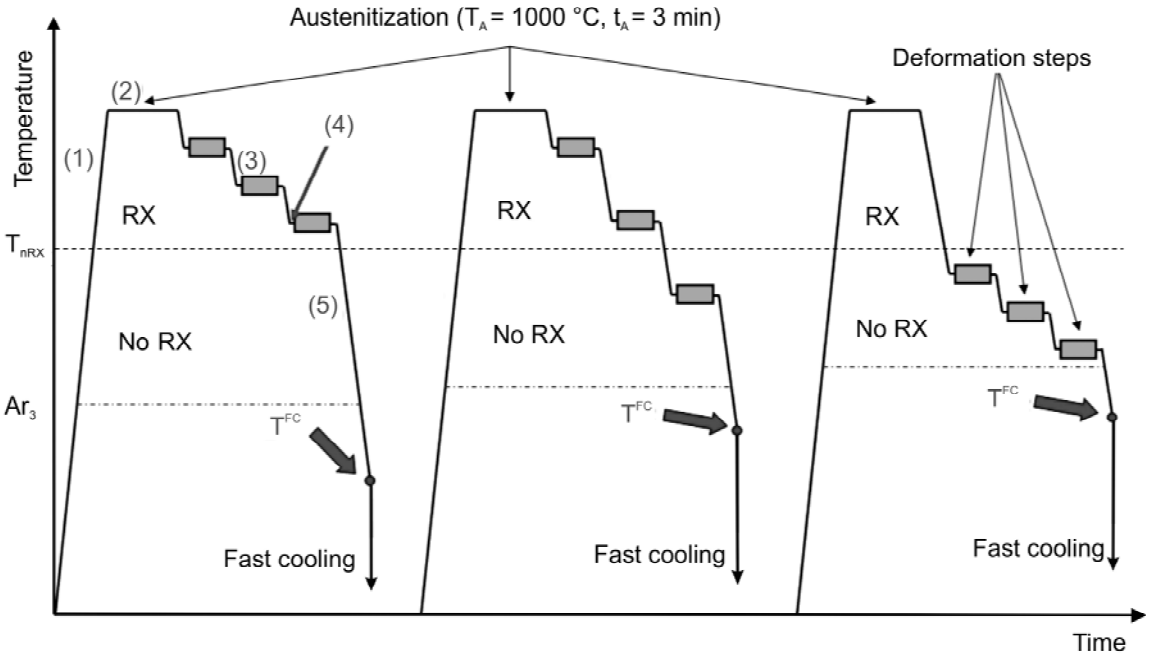

Fig. 4.3 The schedules used for simulation of the final steps of finishing hot rolling process; RX: recrystallization region and No RX: non-recrystallization region. (1) - (5) see Table 4.1.

Tab 4.1 Data corresponding to Fig. 4.3

Denotation	Specification		Corresponding data
(1)	Heating rate	[K/s]	10
(2)	Austenitization time	[s]	120
(3)	Cooling rate before each deformation	[K/s]	10
(4)	Break time before each deformation	[s]	5
(5)	Cooling rate	[K/s]	10
	Strain rate of each deformation step	[s^{-1}]	10
T^{FC}	Start of fast cooling	[°C]	Section 4.3.1

After austenitizing at 1000 °C for 3 min, flat compression specimens were subjected to three defined deformations in three different temperature intervals. Strain rate of each deformation step was $\dot{\varphi}$ = 10. Two cooling stages took place during TMCP. First, the specimens were cooled after the last deformation step to fast cooling start temperature (T^{FC}) with 10 K/s until required fraction of ferrite was obtained ($\gamma \rightarrow \alpha$ transformation). Second, specimens were accelerated cooled below M_S with a high cooling rate of ~100 K/s to achieve martensite from retained austenite ($\gamma \rightarrow \alpha$' transformation). The determining T^{FC} is described in section 4.3.1. As the amount of martensite in industrially produced DP steels is typically between 10 – 30 %, martensite volume fraction MVF = 20 % was

chosen in this research. Minimum three DP samples with prescribed amount of ferrite (80 %) and martensite (20 %) were prepared for each schedule.

Tab. 4.2 Variation of deformation temperatures (T_1, T_2, T_3) and strains (φ_1, φ_2, φ_3) for the last three deformation steps

Parameter		Corresponding data
T_1	[°C]	930, 900, 855
T_2	[°C]	900, 855, 830
T_3	[°C]	855, 830, 800
φ_1	[-]	0.45, 0.40, 0.35
φ_2	[-]	0.30, 0.25, 0.20
φ_3	[-]	0.20, 0.15, 0.10

The approach of schedule considers six influencing parameters, namely three temperatures and three strains. If each of them would be varied in the manner parameter $\pm$ *x* %, than by using the one factor at a time method, we would have had to perform $3^6 = 729$ experiments. Because of time and costs a limited number of experiments were selected. Tab. 4.3 illustrates the selected schedules for TMCP simulation.

Tab. 4.3 Hot deformation schedules and values of influencing parameters for each schedule; φ_t is the amount of total strain

Number of schedule	T_1 [°C]	T_2 [°C]	T_3 [°C]	φ_1 [-]	φ_2 [-]	φ_3 [-]	φ_t [-]
Sch. 1				0.45	0.30	0.20	0.95
Sch. 2				0.45	0.25	0.15	0.85
Sch. 3	930	900	855	0.40	0.25	0.15	0.80
Sch. 4				0.35	0.20	0.20	0.75
Sch. 5				0.35	0.20	0.10	0.65
Sch. 6				0.45	0.30	0.20	0.95
Sch. 7				0.45	0.25	0.15	0.85
Sch. 8	900	855	830	0.40	0.25	0.15	0.80
Sch. 9				0.35	0.20	0.20	0.75
Sch. 10				0.35	0.20	0.10	0.65
Sch. 11				0.45	0.30	0.20	0.95
Sch. 12				0.45	0.25	0.15	0.85
Sch. 13	855	830	800	0.40	0.25	0.15	0.80
Sch. 14				0.35	0.20	0.20	0.75
Sch. 15				0.35	0.20	0.10	0.65

4.3 Results

4.3.1 Phase Transformation Behavior and Defining T^{FC}

In order to obtain DP steels with defined amount of phases the $\gamma \rightarrow \alpha$ transformation kinetic must be known. Then the appropriate T^{FC} can be found from which the specimens have to quench below M_S. In order to determine T^{FC} temperatures, depending on applied schedules, the deformation / dilatometric tests had been performed using the deformation simulator. The specimens were prior subjected to the same deformation schedules as TMCP (Tab. 4.3) and subsequently cooled from the last deformation step to RT at a cooling rate of 10 K/s, which is the same as the first cooling stage of TMCP. The results of dilatometric measurements are shown on Fig. 4.4(a) where change in length is plotted vs. temperature during cooling. For better discrimination, the dilatation curves of three schedules (1, 6 and 11) are plotted in this figure to show the shifting of the $\gamma \rightarrow \alpha$ transformation nose towards shorter incubation times and higher transformation temperatures for deformations at lower finishing temperatures.

From the variation of the change in length as a function of temperature the transformed austenite fraction (f_γ) was calculated employing the lever rule. The progresses of $\gamma \rightarrow \alpha$ phase transformation had been determined by measuring length change of samples as a function of temperature. From those measurements the transformed fraction X [-] was calculated according to the following equation:

$$X = \frac{l_0 - l}{l_0 - l_1} \qquad \text{(Eq. 4.2)}$$

where l [m] is the length of the sample measured during the transformation and l_0 and l_1 [m] are linear functions of temperature for the non-isothermal cooling experiments conducted at constant cooling rate.

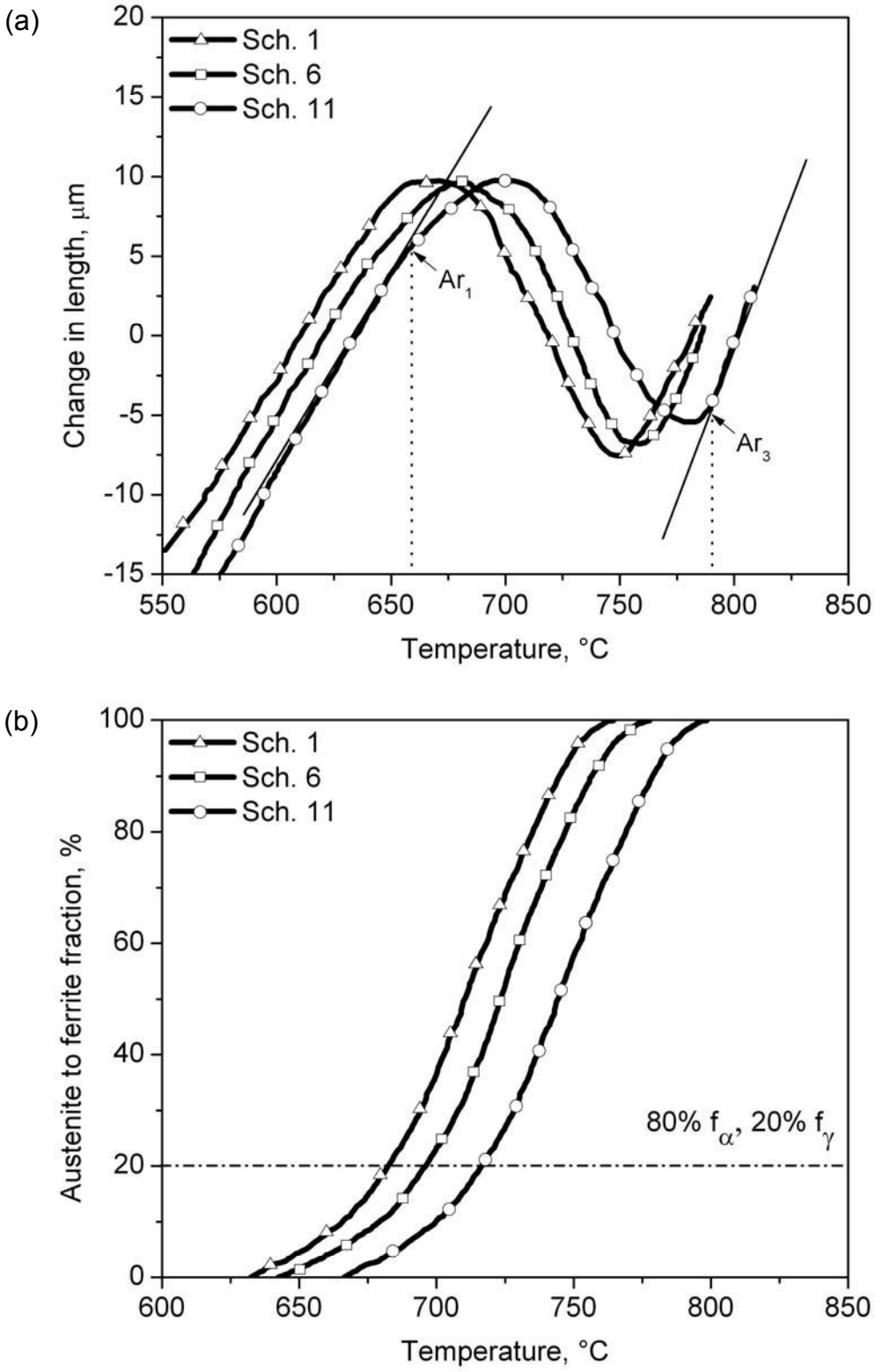

Fig. 4.4 Influence of the hot deformation schedule on the phase transformation behavior; (a) dependences of the change in length on the temperature at $\gamma \rightarrow \alpha$ phase transformation during cooling stage at 10 K/s and (b) calculated fraction of $\gamma \rightarrow \alpha$ as a function of temperature for specimens applied different hot deformation schedules.

The results of calculation are given in Fig. 4.4(b) showing transformed austenite to ferrite fraction as a function of temperature. From this figure, T^{FC} temperatures for different schedules can be found. Tab. 4.4 represents Ar_3 and Ar_1 as well as determined T^{FC} and M_S (after accelerated cooling) temperatures of the individual schedules. The data of Fig. 4.4 and Tab. 4.4 indicate that the hot deformation temperatures exert a stronger influence on the Ar_3 and Ar_1. The highest Ar_3 and Ar_1 temperatures are achieved for schedules applied below T_{nRX}. It can be also seen that increasing total amount of strain for each temperature interval results in increasing $\gamma \rightarrow \alpha$ transformation temperatures (Ar_3 and Ar_1) and T^{FC}. M_S decreases when deformations applied in non-recrystallization region, i.e., higher total strains lead to lower M_S (Tab. 4.4).

Tab. 4.4 Determined Ar_3, Ar_1, appropriate T^{FC} for f_α = 80 %, f_γ = 20 % and M_S obtained during accelerated cooling for different schedules

Number of schedule	Ar_3 [°C]	Ar_1 [°C]	T^{FC} [°C]	M_S [°C]
Sch. 1	762	632	682	403
Sch. 2	758	630	680	411
Sch. 3	750	627	675	414
Sch. 4	750	627	674	415
Sch. 5	748	623	670	420
Sch. 6	775	642	695	395
Sch. 7	770	642	694	404
Sch. 8	767	637	688	409
Sch. 9	763	735	687	411
Sch. 10	760	735	687	413
Sch. 11	796	666	716	353
Sch. 12	792	664	711	361
Sch. 13	790	663	709	364
Sch. 14	790	662	709	366
Sch. 15	788	655	703	370

4.3.2 Microstructure Evolution

Microstructural evolution of thermomechanically produced DP specimens with defined f_α and $f_{\alpha'}$ was studied. Fig. 4.5 displays exemplary the microstructure of two DP steels subjected to sch. 1 (deformed above T_{nRX}) and sch. 11 (deformed below T_{nRX}). The Nital etchant reveals the martensite dark while the ferrite remains white. During the first cooling stage after the last deformation step austenite progressively transforms to ferrite, whereas the remaining part transforms to martensite. All images show a classical DP microstructure with

relatively globular martensite islands embedded in the ferrite matrix phase. The ferrite grains are equiaxed with average sizes depending on the applied hot deformation schedule. The MVF determined by the line intercept method is ~20 % for all samples. Small amounts of retained austenite between 1 - 2 % were found by saturation magnetization measurements for all conditions. Martensite islands can be clearly observed in the microstructure. They often display dark substructures either within or in their immediate surroundings. In addition, such a dark phase can also be observed at the boundaries between two neighboring ferrite grains.

The influence of hot deformation schedule on the microstructure is very significant. It can be seen from Fig. 4.5 that deformation of the steel in the non-recrystallization region results in a finer grained structure, which is the expected result. Tab. 4.5 lists the grain sizes of ferrite (d_{α}) and the sizes of martensite block ($d_{\alpha'}$) being observed due to the different hot deformation schedules for the DP steel. From this table it can be noted that deformation of the steel below the T_{nRX} and/or at a higher amount of total strain results in finer grained material.

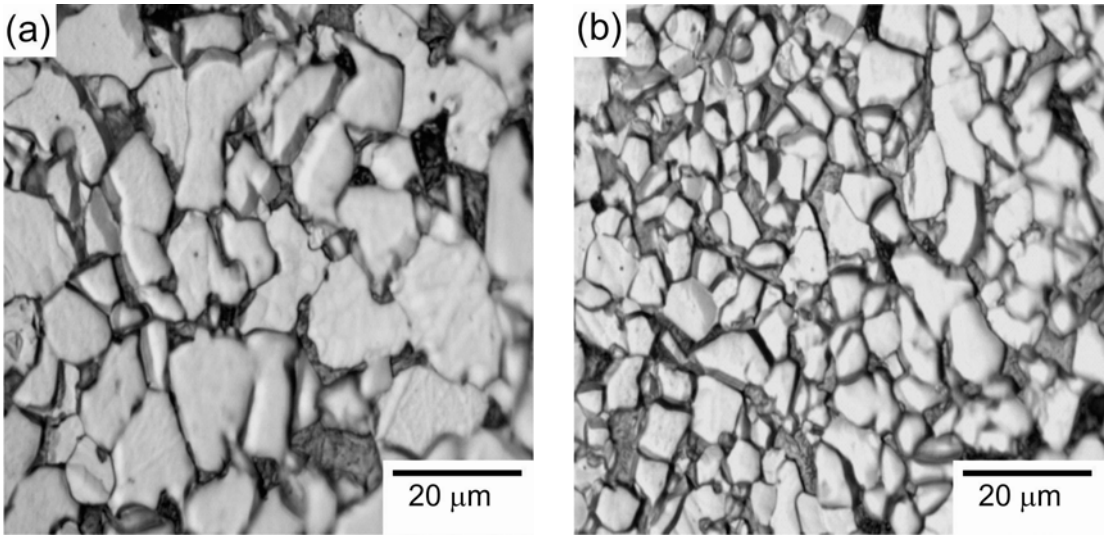

Fig. 4.5 Microstructure of DP steels showing different ferrite grain sizes and martensite blocks obtained after TMCP when all the deformation steps were conducted: (a) above T_{nRX} (sch. 1) and (b) below T_{nRX} (sch. 11); cooling rate of all samples in first cooling stage = 10 K/s and in second cooling stage = 100 K/s.

Tab. 4.5 Effect of the hot deformation schedule on the grain size of ferrite (d_α) and martensite ($d_{\alpha'}$)

Schedules	d_α [μm]	$d_{\alpha'}$ [μm]
Sch. 1	15.1 ± 5	12.0 ± 5
Sch. 2	16.2 ± 4	11.3 ± 3
Sch. 3	18.6 ± 6	12.8 ± 3
Sch. 4	15.7 ± 4	13.7 ± 4
Sch. 5	18.2 ± 3	14.6 ± 4
Sch. 6	12.4 ± 3	10.3 ± 5
Sch. 7	13.7 ± 5	11.0 ± 3
Sch. 8	14.5 ± 7	11.8 ± 3
Sch. 9	13.5 ± 3	11.5 ± 4
Sch. 10	14.7 ± 4	12.8 ± 5
Sch. 11	6.3 ± 2	3.8 ± 1
Sch. 12	6.9 ± 2	4.5 ± 1
Sch. 13	8.8 ± 3	6.3 ± 2
Sch. 14	7.3 ± 4	6.8 ± 1
Sch. 15	6.9 ± 3	6.3 ± 2

Further information about the microstructure of the steels could be collected from transmission electron microscopy (TEM). TEM microscopy was performed to do the fine detailed analysis of the ferritic, martensitic microstructure present in various processing conditions. Fig. 4.6 provides overviews on the thermomechanically produced DP steels obtained from sch. 1 (Fig. 4.6(a)), and sch. 11 (Fig. 4.6(b)). The bright ferrite grains can be clearly identified, while the dark grains are attributed to the martensite phase. The dominant martensite morphology of low carbon steel grades like DP steels is of lath type, which is characterised by a high dislocation density [Kim81, Roc05], leading to a strong contrast in the TEM.

TEM observations confirm the evidence from the LOM investigation that the processing parameters of hot deformation schedule affect the grain size of ferrite significantly. It can be observed that deformation of specimens below T_{nRx} reduces d_α. It is interesting to note that deformation the specimens in non-recrystallization region generate more dislocations within the ferrite grains.

In general, the subgrain boundaries are developed inside of micrograins and also the heterogeneity of dislocations is observed. Such dislocation structures were found to be non-homogeneous, referred to as dislocation cell structures. These cells have a high dislocation density in the walls, while it is low in the interior of the cells. In Fig. 4.6 (a)-(b) cell with broad and diffuse walls is visible.

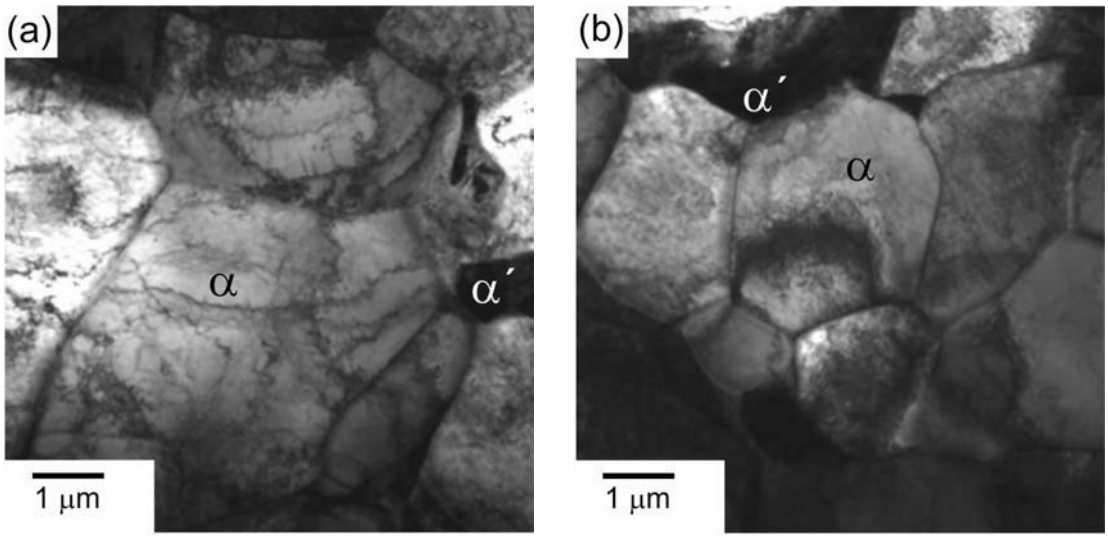

Fig. 4.6 TEM images of DP steels showing different ferrite grain sizes and localized dislocations obtained from: (a) sch. 1 applied above T_{nRX} and (b) sch. 11 applied below T_{nRX}.

Further investigations in the microstructure show that varying TMCP parameters influence not only the grain size but also the morphology of ferrite and martensite. Fig. 4.7 compares the development of dislocation distributions of two DP steels following schedules 1 (deformed above T_{nRX}) and 11 (deformed below T_{nRX}) obtained by HAADF STEM. It can clearly be seen that the dislocation density significantly increases with deformation in the non-recrystallization region. An evidence of low dislocation density is observed for sch. 1 when the sample is deformed above T_{nRX} at the highest amount of total strain (Fig. 4.7(a)), while for sch. 11 dislocation density is seen to be increased (Fig. 4.7(b)). Additionally, strongly heterogeneous structure with tangles can be seen in the ferrite matrix, though the density of the tangles increases in and around the grain boundary region. For both conditions dislocations inside the ferrite grains are distributed irregularly. While in the interior of the grains usually a relatively low dislocation density is observed, at the F/M interfaces a strongly increased number of dislocations can be observed. This is due to the volumetric expansion from austenite to martensite by accelerated cooling during TMCP [Jac01, Man93].

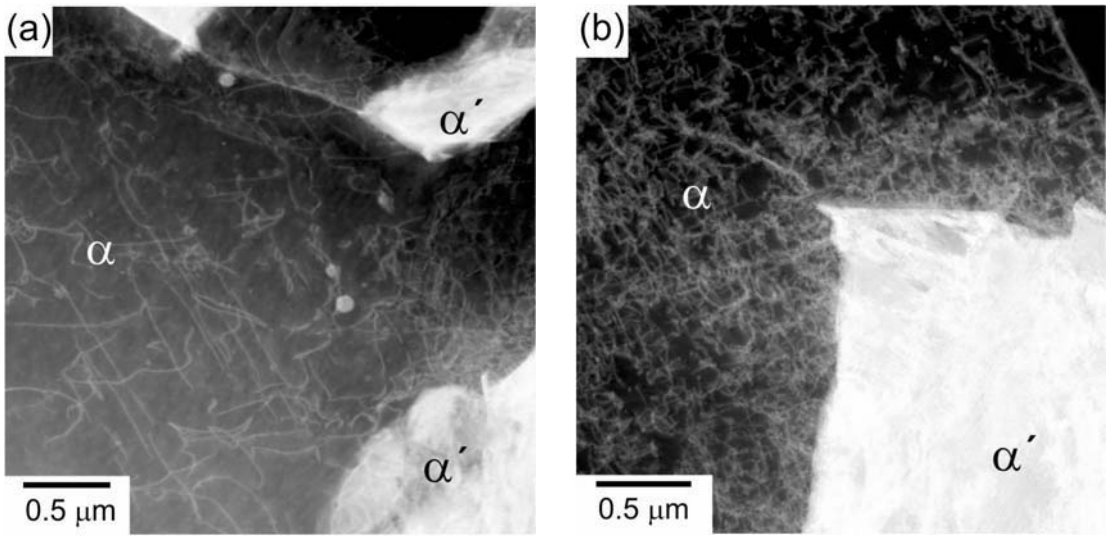

Fig. 4.7 HAADF STEM images of DP steels showing a good view of dislocation density within the ferrite grains obtained from: (a) sch. 1 applied above T_{nRX} and (b) sch. 11 applied below T_{nRX}. All schedules deformed at the highest amount of total strain (φ_t = 0.95).

4.3.3 Mechanical Properties

The results of the basic tensile tests of all DP steels, containing 80 % ferrite and 20 % martensite, produced by TMCP are displayed in Fig. 4.8. This figure demonstrates the effect of hot deformation parameters on the R_m, $R_{p0.2}$ and TEl with their accompanying standard deviations for all specimens. Evaluating the different conditions of DP steels, a pronounced influence of the hot deformation schedule is obvious. The largest strength (676 ± 9) MPa, but lowest ductility (18.5 ± 3) % can be observed for sch. 11, when the samples were deformed below T_{nRX} at the highest amount of total strain (φ_t = 0.95). For sch. 6, in which the samples are deformed above-below T_{nRX} at the same total strain as before, still quite high strength (656 ± 14) MPa is achieved. At the same time TEl increases to more than 20 %. Compared to sch. 11 a slightly lower $R_{p0.2}$ is observed for sch. 6 (432 ± 11 vs. 448 ± 9) MPa. The mechanical properties of sch. 1 show smaller values of R_m, $R_{p0.2}$ for this condition. R_m with (642 ± 12) MPa is found, being slightly reduced when the amount of total strain is decreased (sch. 2). Comparing sch. 1 with sch. 11 it can be seen that a larger strength level combined with a lower ductility is found for sch. 11 deformed in the non-recrystallized austenite region. sch. 5 subjected to the lowest amount of total strain indicates the lowest values of R_m and $R_{p0.2}$.

Comparing schedules 11 to 15 followed hot deformations below T_{nRX} the lowest value of R_m (637 ± 8) MPa and $R_{p0.2}$ (415 ± 3) MPa but the largest value of

Tel (22.3 ± 4) % is found for sch. 15 having the lowest amount of total strain. A slightly higher level of R_m, $R_{p0.2}$ is observed for schedules 13 and 14 at higher total strain.

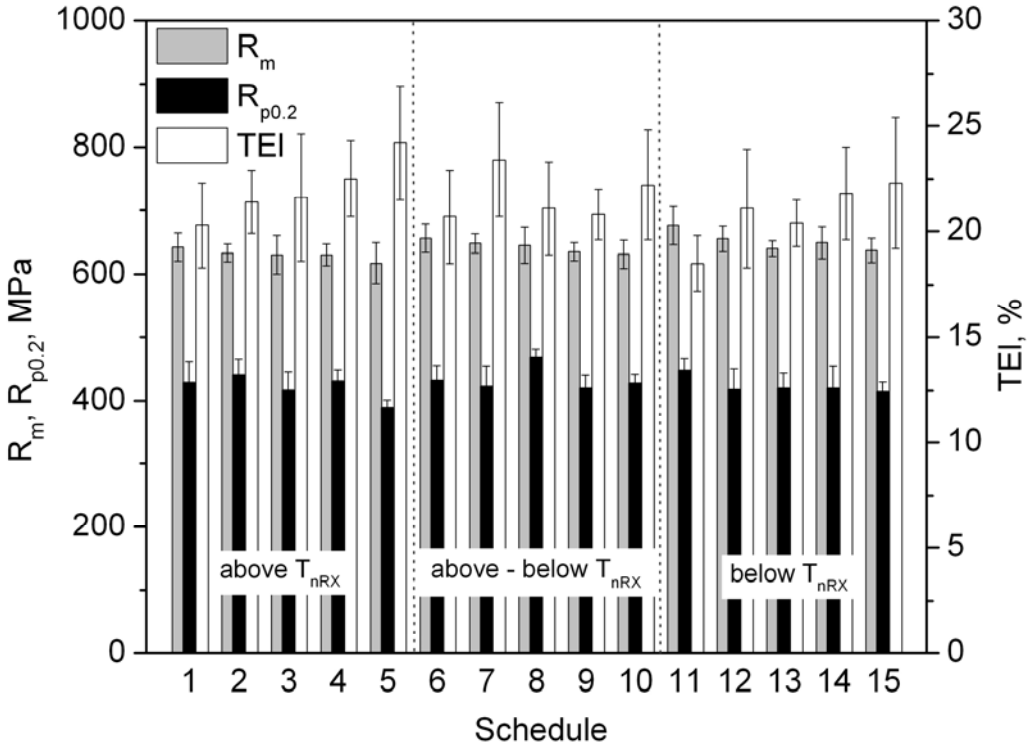

Fig. 4.8 Tensile strength (R_m), yield strength ($R_{p0.2}$) and total elongation (TEl) dependence on the hot deformation schedules after TMCP.

4.3.4 Bake Hardening Behavior

According to the prescribed schedules the DP specimens containing 80 % of ferrite and 20 % of martensite had been thermomechanically produced for the subsequent examination of their BH effect. For each condition three samples had been prepared for prestraining and simulation of paint baking process. The parameters were selected according to the standard conditions of PS = 0 and 2 % at T = 170 °C for t = 20 min.

Results are shown in Fig. 4.9 and Fig. 4.10 from which it can be clearly seen that varying processing parameters influencing mechanical properties and bake hardenability of DP steel is given. Fig. 4.9(a)-(b) shows the influence of different schedules on mechanical properties of DP steels with PS = 0 % and 2 % after baking simulation at 170 °C for 20 min. For the samples without PS the difference between $R_{P0.2}$ of the tensile sample and lower yield strength (R_e) of the respective BH sample was taken as a measure of BH. In general, it can be noted that the values of strength (R_m, R_e) increase after BH treatment for all

applied schedules, combined with a negligible decrease of TEl. The increasing in strength level is more remarkable after 2 % PS as compared to PS = 0 %. Schedules 11 to 15, applied below T_{nRX}, reveal the highest R_m and R_e after baking, while for schedules 1 to 5 (applied above T_{nRX}) and 6 to 10 (applied above-below T_{nRX}) the R_m and R_e show lower levels. Evaluating the graphs with respect to the total strains indicates that the highest strength is achieved at the highest amount of total strain. Comparing schedules 1 to 5 the lowest strength levels are obtained for sch. 5, in which the amount of total strain is the lowest, while schedules 1 and 2 reveal the highest strength due to the higher total strains. Despite a low total strain, sch. 4 indicates a higher level of strength. This could be due to higher amount of strain at the last deformation step which has the most effectiveness on the grain size of prior austenite among the applied deformation steps. This result is also valid for schedules 9 and 14. On the other hand, the samples processed to higher amount of total strain have recorded lower TEL values. For this case, ferrite grain size is small, as explained before.

(a)

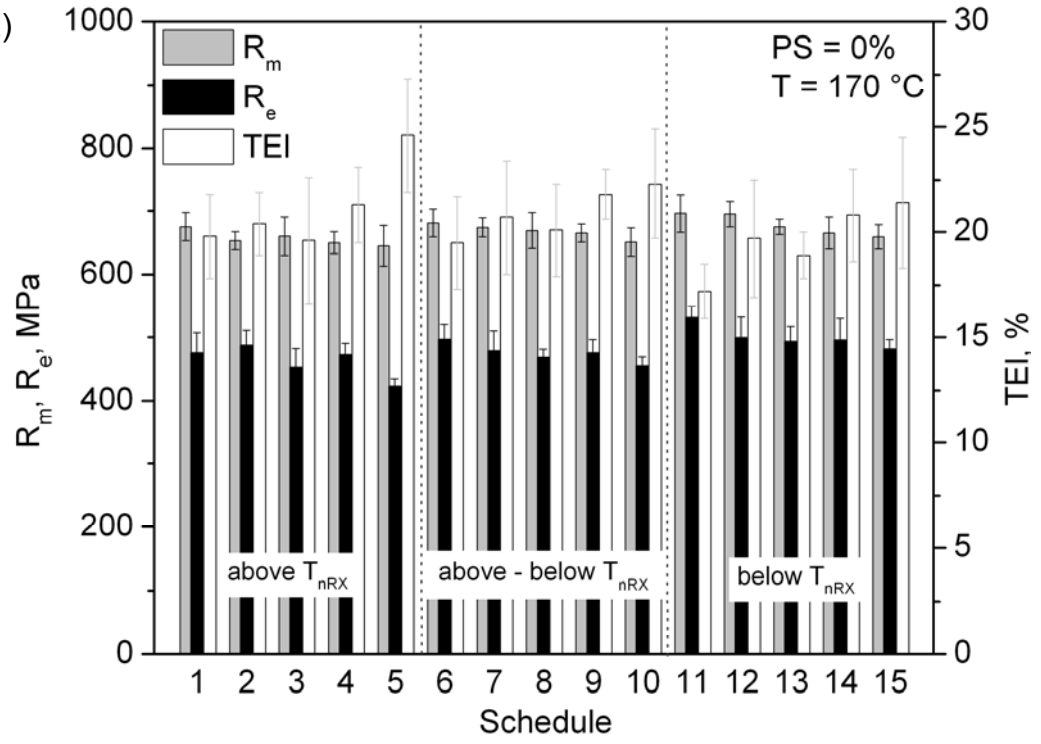

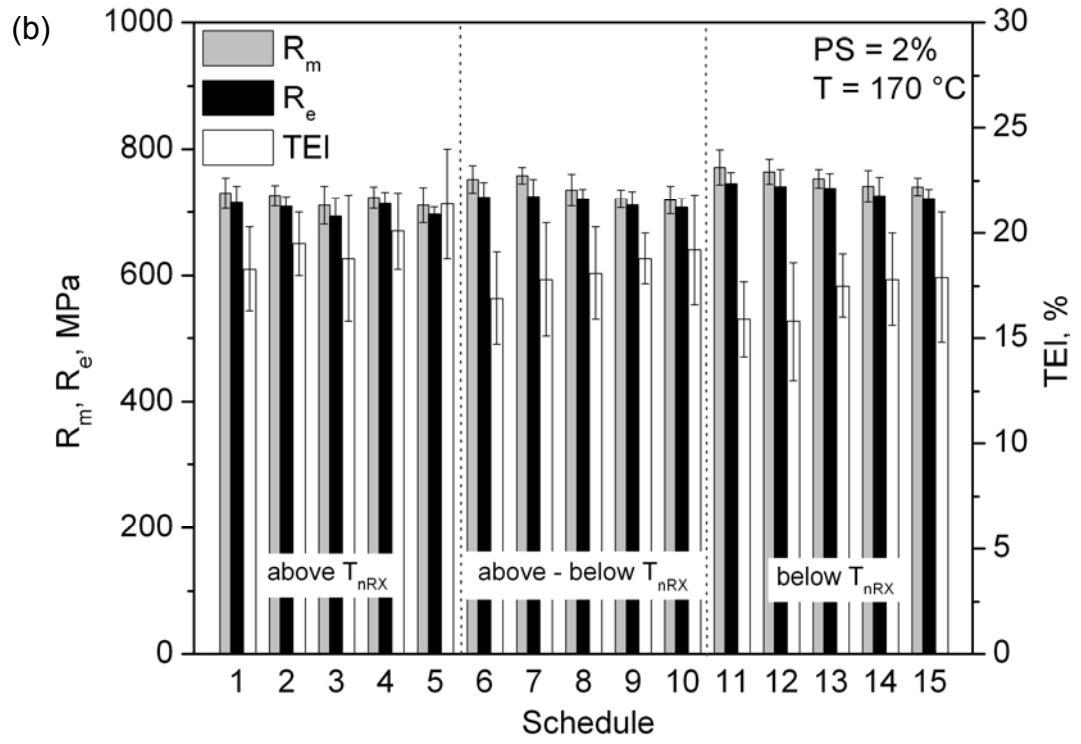

Fig. 4.9 Influence of the prestraining and baking process on the mechanical properties of different schedules with T = 170 °C, t = 20 min; (a) PS = 0 % and (b) PS = 2 %.

Fig. 4.10 displays BH_0 and BH_2 of DP samples for different TMCP schedules. This is best revealed in this figure, which shows the comparative results of BH_x (BH increment after PS at 0 or 2 % and BH at 170 °C for 20 min) increments. Referring to the graphs on Fig. 4.10, it can be concluded that prestraining the samples to 2 % and paint baking simulation result in relatively high BH values. Furthermore, on average the higher increase of the BH is obtained for samples subjected to deformations in non-recrystallized austenite region at larger amounts of total strain. Schedules followed deformations above-below T_{nRx} exhibit intermediate values.

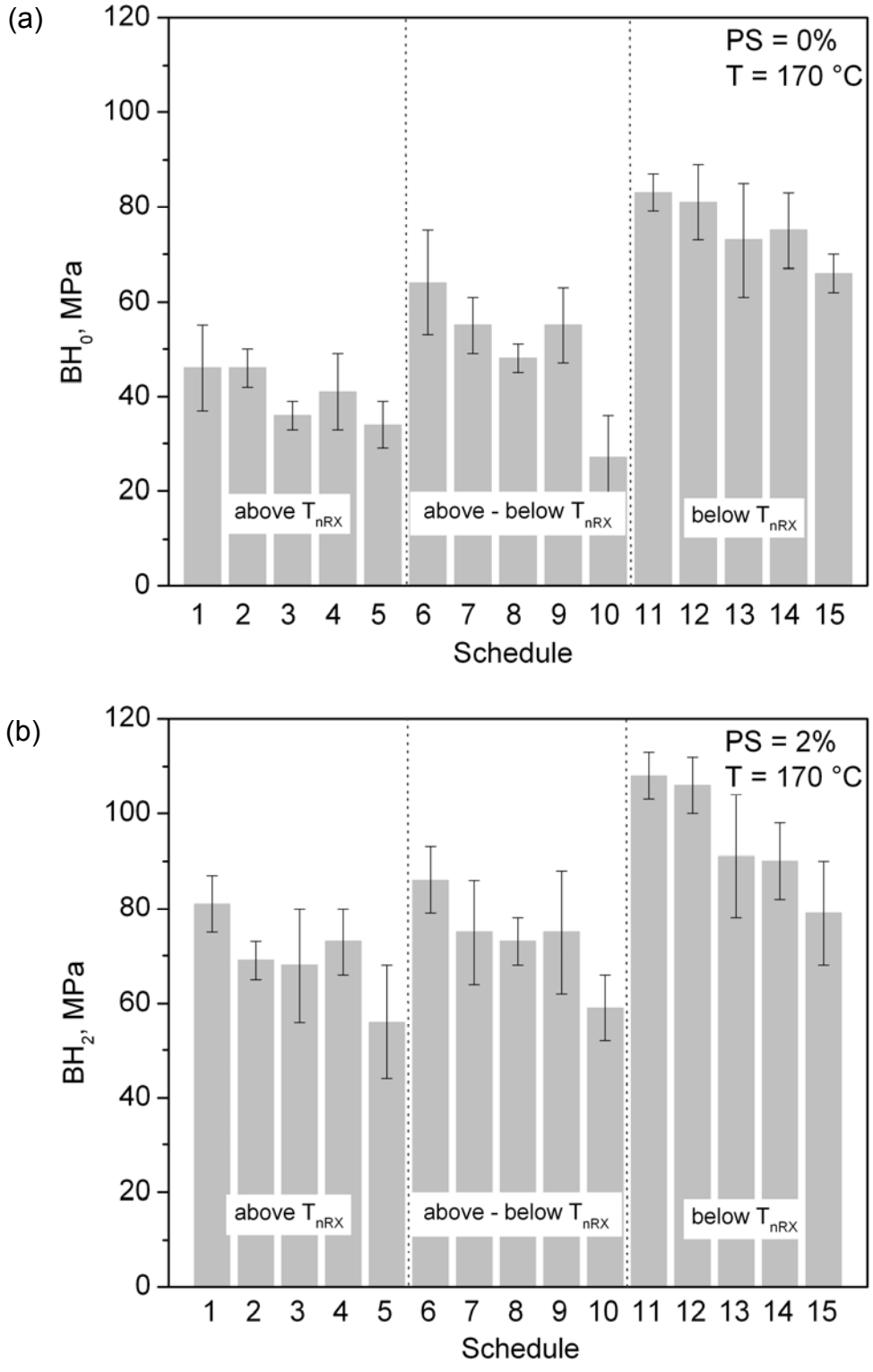

Fig. 4.10 (a) Dependence of BH_0 on the hot deformation schedules, calculated from difference between $R_{P0.2}$ of the tensile sample and R_e of the respective BH sample and (b) dependence of BH_2 on the hot deformation schedules.

Fig. 4.11 demonstrates exemplary TEM micrographs of DP steels followed sch. 11 before PS and BH (Fig. 4.11(a)) and after PS = 2 % and baking at 170 °C for 20 min (Fig. 4.11(b)). In Fig. 4.11(a) the dislocation structure within a typical ferrite grain is inhomogeneous, generally with a higher dislocation density or finer cell size adjacent to martensite. This inhomogeneity is observed in a large majority of the grains examined and is interpreted as resulting from plastic incompatibility between martensite and the adjacent ferrite. It was impossible to measure the dislocation density due to the heavy tangles and cell structures. After PS and BH the dislocation density increases both in the matrix and at grain boundaries of ferrite, leading to the development of a homogeneous dislocation substructure (Fig. 4.11(b)). A subdivision of grains into regions characterized by a relatively homogeneous dislocation density is also observed for the condition after PS and BH. Such regions are seen to be separated by rather narrow transition (deformation) bands, which may extend in length over a significant part of the grain and may carry a cumulative misorientation across them. The dislocation density is seen to be high and fairly homogeneous in nature, both in the boundary region as well as inside the grain.

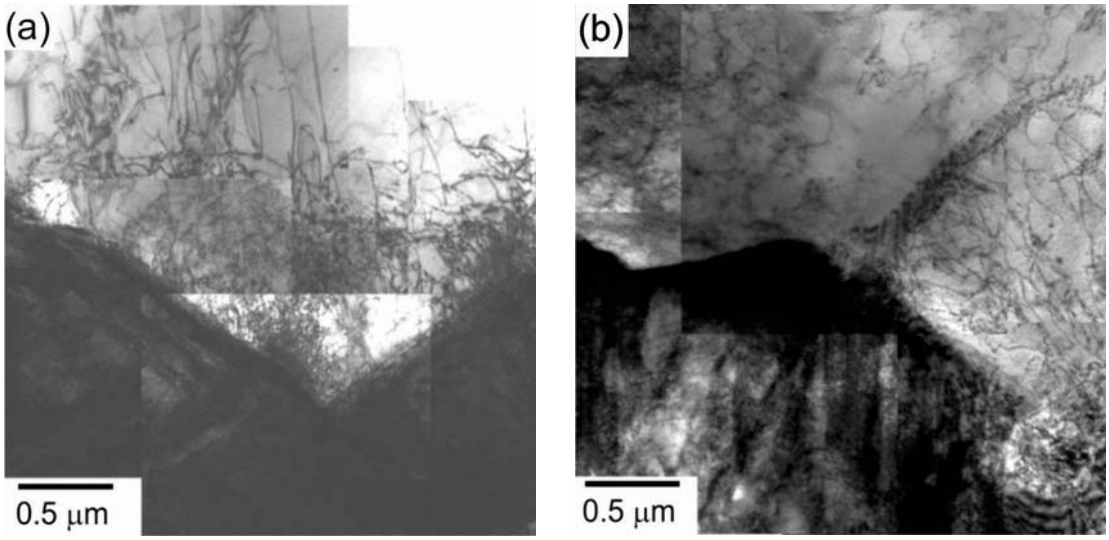

Fig. 4.11 TEM micrographs of the DP steel subjected to sch. 11 showing dislocation distributions of DP steels; (a) after TMCP and (b) after prestraining to PS = 2 % and baking at T = 170 °C for t = 20 min.

Fig. 4.12(a) shows a typical dislocation distribution of ferrite after 2 % PS and BH at 170 °C / 20 min. This structure consists primarily of randomly distributed straight dislocations. The dislocations are oriented predominantly in ‹111›

directions, as indicated by the oriented diffraction pattern, and on this basis are identified as screw dislocations. Large jogs are visible on many dislocation lines and may have resulted from an accumulation of vacancies, dislocation intersection, or cross slip. The area of the sample shown in Fig. 4.12(a) was examined in more detail. The white square in Fig. 4.12(a) indicates the position of Fig. 4.12(b). From this figure the development of dislocation substructures in the ferrite grains can be seen. The dislocations are pinned by nanometer sized carbides.

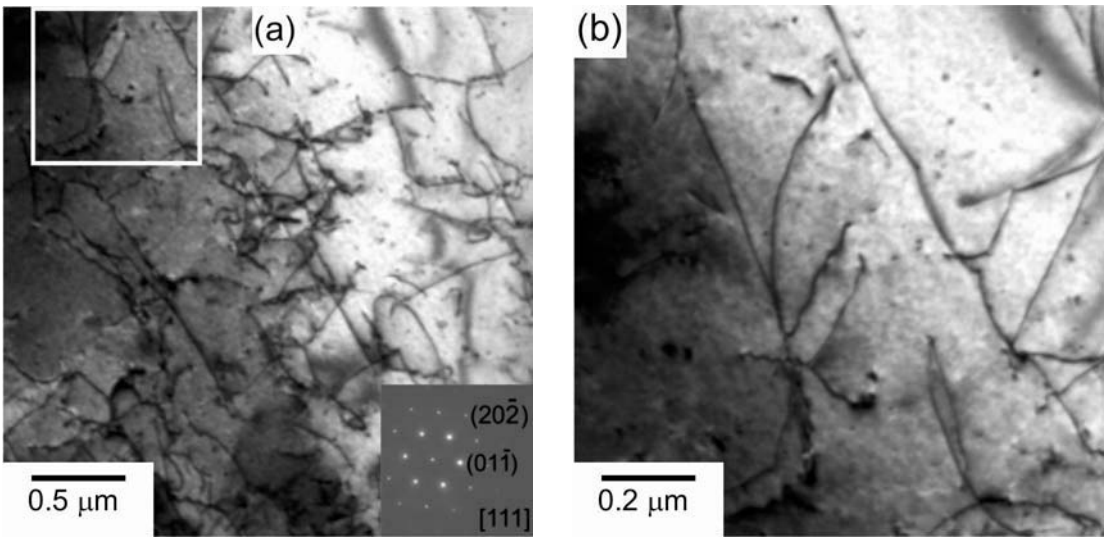

Fig. 4.12 TEM images of the DP steel showing dislocation distributions and pinning of dislocations by carbide particles after PS = 2 % and BH at T = 170 °C for t = 20 min; (a) 0.5 μm and (b) 0.2 μm.

4.4 Discussion

4.4.1 Influence of the Hot Deformation Schedules on the Phase Transformation Behavior

The factors that accelerate ferrite transformation under static condition are large ferrite nucleation site distribution such as austenite grain boundary area, density of deformation bands and high strain rate as well as large amount of strain before $\gamma \rightarrow \alpha$ transformation. From the results of Fig. 4.4 and Tab. 4.4 it can be observed that the Ar_3 and Ar_1 temperatures increase when deformations are applied in non-recrystallization region or/and at larger strains. This is due to the increase of austenite grain boundary which leads to increase of nucleation site and thus grain refinement. Kozasu et al. [Koz75] have shown that the effective interfacial areas per unit volume of austenite and the nucleation rate are

increased by austenite grain refinement and deformation below T_{nRX}. It is thus expected that deformations in this region accelerate the $\gamma \rightarrow \alpha$ transformation and raise the Ar_3 temperature as reported by other groups [Man96, Man98, Zha03].

During straining of austenite in the non-recrystallization region deformation bands and twinning boundaries form and the dislocation density inside austenite grains is strongly increased, providing favorable nucleation sites and enhancing nucleation rate. Therefore, the grain refinement effect of deformation in the non-recrystallization region is stronger than that in the recrystallization region [Qu02, Egh07a]. Eghbali [Egh06] noted two effects, causing austenite transformation to ferrite at a faster rate in the non-recrystallization region than in recrystallization region: a) the higher internal energy of the deformed and thus less stable austenite and b) larger number of nucleation sites provided by defects.

There are many reports in which the effect of plastic deformation on the austenite to ferrite transformation is considered [Bha04, Han01]. In this case, as the stored energy of deformation increases, both the start and finish temperatures of the austenite to ferrite transformation were found to increase, and the temperature range of the austenite to ferrite transformation was reduced.

It is obvious from Tab. 4.4 that hot deformation schedules influence the M_S temperature during the $\gamma \rightarrow \alpha$' transformation. A clear decrease of the M_S temperature is observed when deformation temperatures are increased or amounts of strain are decreased. In agreement with our results, Salehi et al. [Sal06] have reported that decreasing applied strain increases the M_S of DP steels.

This can be explained by the C enrichment in austenite during the $\gamma \rightarrow \alpha$ transformation. It is well known that the amount of ferrite determines the C content in the intercritical austenite of the DP steels where higher fraction of ferritic phase results in greater C enrichment of the austenite [Spe03]. The thermodynamic calculations using the Thermo-Calc TCW3 software shows that maximal solubility of C in the ferritic phase for DP steel is 0.0063 wt. % (Fig. 4.13).

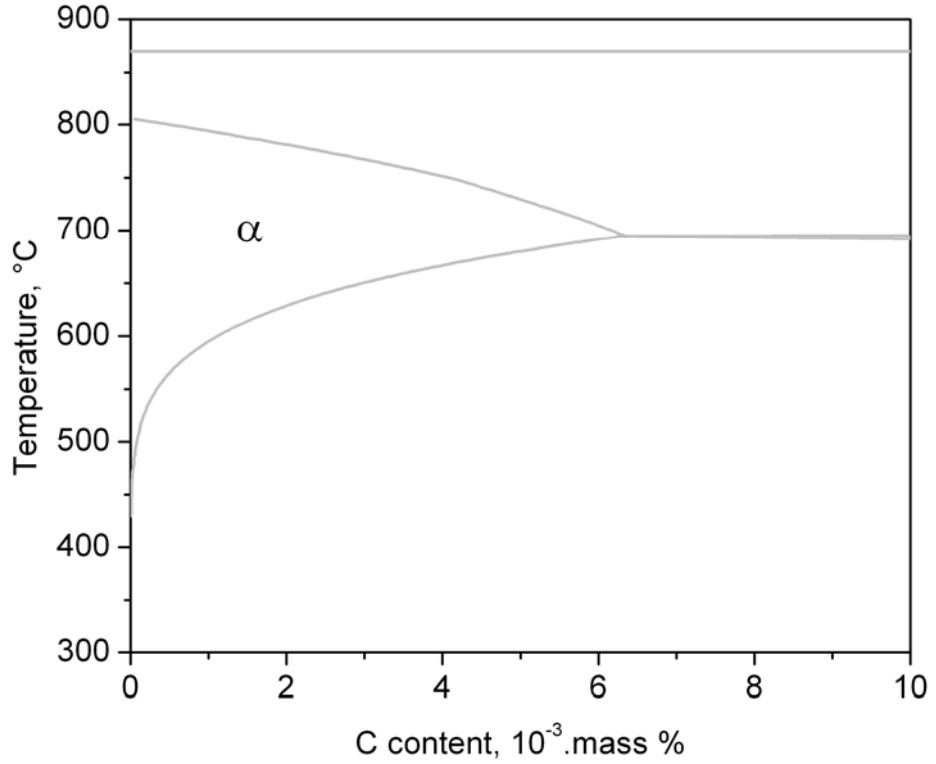

Fig. 4.13 Part of the equilibrium phase diagram for DP steel with chemical composition given in Tab. 3.1 showing maximal solubility of C in the ferritic phase.

With this value it is possible to estimate the dependence of C concentration in the austenite on ferrite fraction (f_α) by neglecting the partitioning of other elements and concentration profiles using the lever rule. The calculated dependence is given in Fig. 4.13. On the other hand, M_S can be estimated using empirical equation proposed by Andrews [And65] which is valid for low alloyed steels with a C content less than 0.6 %:

$$M_S = 539 - 423 \cdot C - 30.4 \cdot Mn - 17.7 \cdot Ni - 12.1 \cdot Cr - 11.0 \cdot Si - 7.0 \cdot Mo \qquad \text{(Eq. 4.3)}$$

where alloy contents are in [wt. %] and M_S temperature is in [°C]. By combining this equation with estimated dependence C (f_α) it is possible to obtain the dependence of the M_S on the f_α which is shown in Fig. 4.14.

As mentioned before, deformation of austenite below the non-recrystallization region or/and to high strains results in faster ferrite transformation. Consequently, C becomes faster enriched in the remaining austenite. Hence, more driving force for the martensitic transformation is required which can be provided at lower temperatures. Therefore, remaining austenite transforms into martensite during the $\gamma \rightarrow \alpha$' transformation at somewhat lower temperatures.

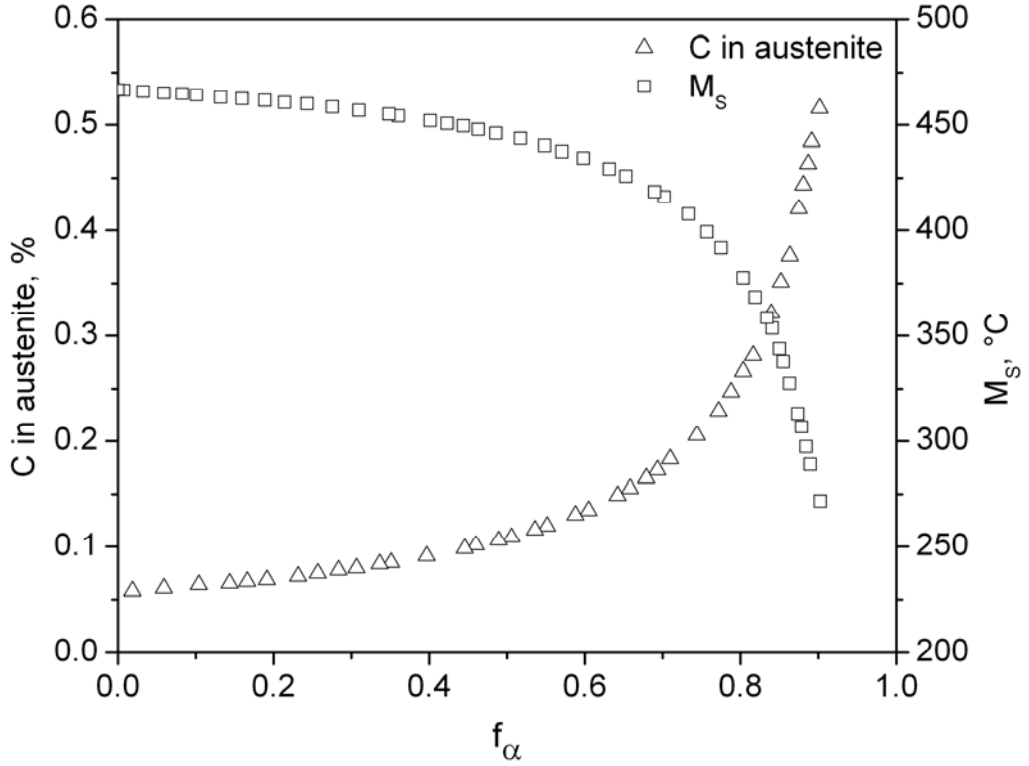

Fig. 4.14 Dependence of the C content in the retained austenite as a function of f_α determined using the lever rule and M_S as a function of f_α formed during $\gamma \rightarrow \alpha'$ transformation.

4.4.2 Influence of the Hot Deformation Schedules on the Microstructure

As can be seen in Tab. 4.5 during the TMCP as the total strain increases the average grain size of ferrite and martensite decreases noticeably. It is reported that a heavy deformation of about 80 % per pass at just above the Ar_3 temperature, resulting in deformation induced ferrite transformation, increases much more nucleation rate in austenite matrix as well as at grain boundary being associated with ferrite grain refining [Li07]. Some authors reported that deformation to a high strain produces equiaxed and homogeneous ultrafine ferrite grains [Bel98, Bel03, Gou03].

It is well known that the change in the ferrite grain size with varying hot deformation schedule is due to the difference in the morphology of the austenite grains from which the ferrite is formed [Han01]. The possible mechanisms for the refinement of ferrite and martensite grains, during warm deformation of DP steels, may be suggested fine-grained austenite [Kor84]. In the fine-grained austenite, fine grains occur much more readily due to increase of austenite grain boundaries that can store the strain energy. Therefore, making a lot of lattice

defects in austenite such as austenite grain boundary, dislocation, vacancy, twin boundary, interstitial atom and stacking fault may be important factors that encourage the formation of fine-grained ferrite at high strains. For example, applying a complex strain mode such as multi-axial deformation could obtain fine grain of submicron [Val91]. It might operate new slip system resulting in more effects.

Chan Hong et al. [Cha02] have reported that at least reduction of 50 % per pass above Ar_3 as a finishing temperature is required to form fine ferrite grains. They argued that deformation to a high strain is effective for increase of austenite free energy. Therefore, the critical amount of strain is required to raise the austenite free energy.

On the other hand, it is suggested that the formation of equiaxed fine ferrite grains due to high applied strain is mainly the result of a kind of continuous dynamic recrystallization (CDRX) of austenite during warm deformation [Son05, Song05]. It can be concluded that through CDRX, a kind of grain fragmentation takes place by development of deformation-induced low angle dislocation boundaries followed by a gradual increase in their misorientation, finally leading to their transformation into usual grain boundaries. The high angle boundary fine ferrite grains produced through CDRX do not contain any substructure and are relatively equiaxed. Furthermore, CDRX is obviously different from the conventional dynamic recrystallization, i.e. there is no evidence of nucleation and growth of new grains within the original grains through the bulging of grain boundaries [Egh07b].

It can be observed from Fig. 4.5 to Fig. 4.7 and Tab. 4.5, that deformations below T_{nRX} result in smaller d_α and $d_{\alpha'}$ and higher dislocation density in ferrite. For example, for sch. 11 the grains are produced from work hardened (pancaked) austenite through austenite to ferrite transformation. The sizes of these ferrite grains are smaller and the dislocation densities of them are higher than those produced from the recovered and recrystallized austenite grains.

The austenite microstructure is completely recrystallized above T_{nRX}. Multipass hot deformation sequences which end in this region and where there is a pre-existing pinning force to suppress grain coarsening are entitled recrystallization controlled rolling (RCR) practices. Hence, the distinguishing feature of RCR processing is having a pre-existing pinning force (precipitate or solute) that is

small enough to allow the accruement of static recrystallization but large enough to suppress grain coarsening. As the deformation temperature is decreased (above-below T_{nRX}) so that the progress of recrystallization becomes increasingly difficult, a partially recrystallized microstructure is observed. This microstructure is often referred to as being duplex because of a non-uniform grain size. Finally, a completely non-recrystallized microstructure is present when deformation occurs below T_{nRX}. Multipass hot deformation sequences which occur largely in this region are entitled conventional controlled rolling (CCR) practices. For a fixed rolling schedule which includes a specific number of roughing and finishing passes, the higher the T_{nRX}, the larger will be the amount of rolling strain imparted in the non-recrystallization region. It is reported that the density of the near-planar crystalline defects (i.e. grain boundaries, deformation bands, and twin boundaries) increases with increasing deformation in the non-recrystallization region [Haw79]. Since these defects act as nucleation sites for proeutectoid ferrite during subsequent cooling, there is a strong relationship between the final ferrite grain sizes and processing conditions [Kya98].

It is also seen from Tab. 4.5 that the lowest grain sizes are achieved for schedules subjected to the highest total strain below T_{nRX}. As mentioned before, the deformation temperature has an influence on the ferrite nucleation sites and a decrease of the deformation temperature will enhance intragranular nucleation. A larger strain could lead to more deformation bands within austenite grains and more ferrite fragments. The deformation bands produced by large amounts of strain in non-recrystallization temperature region of austenite act as nucleation sites for ferrite formation and finally refine the ferrite grains [Naj92].

4.4.3 Influence of the Hot Deformation Schedules on the Mechanical Properties

The microstructure of DP steels could be characterized in terms of a number of morphological features such as the size and morphology of the martensite packets, the volume fraction and distribution of martensite within the microstructure and the volume fraction and morphology of ferrite. These features should be related to the mechanical properties of DP steels. In the present study, the volume fraction of martensite is kept similar for all steels of about 20 %. Thus, it can be deduced that volume fraction of ferrite and martensite is not an operating mechanism. Thus, this mechanism is ruled out. Therefore, the

main contribution of ferrite and martensite to the mechanical properties is related to the grain size. Grain size has an influence on the velocity of the Lüders band front. Grain boundaries act as obstacles to the front propagation, so that they control the Lüders band velocity. Thus, a small grain size will make the band propagation more difficult and lead to a higher value of lower yield stress and yield point elongation [Fuj78]. A decrease in the grain size generally leads to an increase in the ultimate tensile strength and the yield strength through the Hall-Petch relationship:

$$\sigma_y = \sigma_0 + k_y d^{-1/2} \quad \text{(Eq. 4.4)}$$

where σ_y [MPa] is the lower yield stress, σ_0 [MPa] is friction stress, k_y [MPa·m] is the Hall-Petch coefficient and d [m] is the grain size [Tak10].

However, it was found, that the yield strength of multi phase steels is not only a function of the grain size [Tim03]. The ferrite grain size does contribute to the yield strength, but there are other factors affecting the yield strength, as ferrite is only one component of the microstructure. The morphology and distribution of the martensite play an important role in the structure-property relationship. According to [Tim03, Tim07] and [Edm90] it is possible to account for the strength of the martensite structure in terms of four major contributions:

1. A term relating to slip-band length, which includes both colony (packet) and lath size.
2. A term due to the dislocation substructure within the laths.
3. A term including solid solution hardening from substitutional elements, such as Si, Mn, Ni, etc., but additional interstitial hardening from C.
4. A term which arises from the dispersion hardening effect of the carbide particles.

The microstructures resulting from various deformation tests have been described previously (Fig. 4.5 to Fig. 4.7). In general, it can be noted that the R_m increases when specimens are deformed below T_{nRX} and/or to high strains (Fig. 4.8). On the other hand, deformations in the non-recrystallization austenite region to a large amount of total strain result in smaller ferrite grain size. Therefore, higher strength level of these conditions can be attributed to the finer ferrite and martensite grain size.

It is seen from Fig. 4.8 that $R_{p0.2}$ of specimens deformed below T_{nRX} at low amounts of total strain (less than 0.8) is lower than in the case when specimens

are deformed above or above-below T_{nRX} at high amounts of total strains (more than 0.8) or when the amount of the strain of the last deformation step is in its highest value (φ_3 = 0.2). This reduction could be related to the distribution of martensite before straining. As mentioned before, deformation below T_{nRX} lead to finer martensite blocks within ferrite matrix. The blocks of martensite formed between the ferrite enhance the reduction of $R_{p0.2}$ by the generation of the new mobile dislocations in the parent ferrite matrix prior to straining. The movement of these unobstructed dislocations results in the yield strength reduction, as commonly observed in the DP steel [Mat84].

In Fig. 4.8 it can be also observed that for schedules subjected to hot deformations below T_{nRX} at high strains a low ductility was obtained. In this case the morphology (size of blocks) and location of martensite within the soft ferrite matrix are more significant in determining the structure-property dependence. The distribution of different phases within the microstructure is important, because when a large fraction of a harder phase such as martensite, is included in a soft matrix, plastic deformation at first occurs in the softer phase. On the other hand, the hard phase only begins to deform when the softer phase has strain hardened sufficiently to transfer load. The hard martensite phase under straining can stimulate the formation of new mobile dislocations in a soft ferrite matrix and, by means of this, decrease the ductility. Furthermore, the martensite is not uniformly distributed within the ferrite, so giving rise to a gradual deviation from elastic deformation. Hence, it is proposed that all these features decrease the ductility [Mat84].

4.4.4 Influence of the Hot Deformation Schedules on the Bake Hardening Behavior

The average values of BH_0 and BH_2 have been calculated from the values recorded at each combination of hot deformation condition. A comparison among these averages is shown in the histogram of Fig. 4.10. From this figure it is clear that a high BH level is obtained when steels deformed at high amounts of total strains (φ_t more than 0.8) or at the highest amount of the strain of the last deformation step (φ_3 = 0.2) or below T_{nRX}. The highest BH_0 and BH_2 values are recorded for schedules followed hot deformations in the non-recrystallization region to the highest amount of total strain. This result is in association with the

strength increase recorded at these conditions (Fig. 4.9). As discussed earlier, the hot deformation schedule has a pronounced effect on the grain size [Ahm08, Tim03]. A deformation below T_{nRX} or at high amounts of total strain results in distinct refinement of the final DP steel microstructure (Tab. 4.5). Thus, the improvement in BH behavior for these schedules seems entirely to be due to microstructural refinement. In addition to the effect of grain refinement on the improvement of the bake hardenability, the higher dislocation density of the finer grains has a further improving effect. A poorer BH level for the schedules deformed above T_{nRX} to low amounts of total strain could be related to lower dislocation density and coarser grains after TMCP. For schedules with lower deformation temperatures (below or above-below T_{nRX}) and smaller amounts of total strain, increasing trend in BH effect with decreasing mean grain size can be identified. This can be probably attributed to the influence of grain sizes on the concentration profiles of dislocation in the interior of the grains and in the grain boundaries. It is expected that there will be relative high dislocation present in the matrix for a smaller grain size, as a consequence of more intensive dislocation pinning by free C atoms. Therefore, the BH effect should increase with decreasing grain size because the distance, which the free C atoms move to the grain boundaries, is less [Bal09a, But62, Han84, Wil68].

Furthermore, it is shown in Fig. 4.7 that small grain sizes (i.e. deformed below T_{nRX}) contain increased dislocation densities after deformation due to the high number of obstacles in form of grain boundaries (discussed in section 4.4.2). Probably a large part of the solute C is present near the F/M interfaces or in the grain boundaries of the ferrite, which may contribute to the process of BH [Kri07]. On the other hand, the diffusion of C atoms towards the energetically favored positions on the dislocation lines is a rather fast process for the given conditions. In the case of a fine grain size, solute C atoms from the grain boundaries can move faster to dislocations in the middle of a grain due to the shorter distances. Baker et al. [Bak02a] found that the solute C atoms nearly completely migrate to the dislocation lines in the first stage of BH, while the C atoms involved in cluster and carbide formation become available from those sites after the Cottrell atmospheres have formed.

Moreover, precipitation in the DP microstructure must also be mentioned as an additional point which contributes to the BH effect. As can be observed in

Fig 4.12, after prestraining and baking in the steel dislocations are pinned by nanometer sized carbides, following sch. 11 (deformed below T_{nRX} at the highest amount of total strain). It is well known, that hot deformation conditions affect the formation of precipitations. Weiss and Jonas noted that deformation accelerates the precipitation kinetics [Wat77, Wei79]. They found that after a deformation of 5 % during hot compression test the rate of precipitation is about ten times faster than in a material without deformation. Watanabe et al. [Wat77] also found that the deformation increases precipitation kinetics by a factor of more than ten in terms of isothermal holding time. On the other hand it is reported, that precipitation kinetic is reduced due to few nucleation sites, if recrystallization is completed before the onset of precipitation [Bäc09]. Therefore, deformations below T_{nRX} lead to increased precipitation kinetics which could contribute to the bake hardenability of DP steels.

4.4.5 Influence of the Prestraining and Baking Condition on the Bake Hardening Behavior

From Fig. 4.9 and Fig. 4.10 it can be noted that BH values after PS = 2 % are significantly higher compared to the conditions without PS, where the binding between dislocations and the C atoms is strong. Thus, it is more difficult for the C atoms to diffuse into the ferrite for dislocation pinning. For the C atoms present in the ferrite in a low concentration, it takes a long diffusion path to reach the few dislocations being present. At the same time there are ample dislocations at the F/M interface to maintain smooth yielding without distinct increase of yield strength, although part of them may be anchored by carbon atoms. As soon as the material is prestrained, the dislocations start to move, releasing C atoms, which now reach the increased number of dislocation lines inside the ferrite more easily resulting in a higher increase of yield strength. When the prestrained samples were baked, it is generally noticed that the microstructural developments from the tangled array of dislocations to cells occur. Dislocations start to cluster inside individual grains, and these clusters eventually join together to form a cell structure after the baking treatment.
As shown in Fig. 4.11 (a), before the baking treatment the density of dislocations is mostly heterogeneous, being more in the vicinity of the grain boundary and long, straight widely spaced dislocations within the matrix. The dislocations tend

to be more structured when PS and BH are applied Fig. 4.11 (b) and Fig. 4.12. This is clearly understood as follows: the total energy of any dislocation is the sum of the energy stored in the long-range strain field and the energy of the dislocation core [Sre07]. The dislocation structure of minimum energy (the equilibrium core diameter) follows from the condition that the total energy of the long-range strain field (decreasing with growing core size) and the core energy (increasing with growing core size) is a minimum [Fau01, Gle82]. Though evidence of atmospheres is yet to be seen, these dislocation solute interactions are seen to be the driving force that causes huge BH increments seen in this research.

Fig. 4.15 represents the HAADF STEM micrographs of the DP steel subjected to sch. 11 after PS = 2 % and BH at T = 170 °C for t = 20 min. The microstructure after this treatment seems to be strongly dislocated, resulting in the homogeneous structure with dislocations relatively uniformly distributed in the ferrite matrix as well as within the grains. The ferrite grains are subdivided into well-defined cells whose walls consist of a tangled network of dislocations (Fig. 4.15(a)). The cell walls become more sharply defined and tend to align themselves in certain crystallographic directions. A complex array of dislocations is seen consisting of two sets of parallel dislocations, which have formed short lengths of dislocations in a third direction at their point of intersection (Fig. 4.15(b)). These dislocation arrays are generally favored over a quasi uniform three-dimensional distribution since for a given total dislocation density, the dislocation spacing is smaller in the arrays.

This network will probably keep them immobile, giving stability to the whole system. Hence, the pinning effect or the BH increment by the interstitial species after their diffusion to these mobile dislocations during the baking treatment is seen to be very strong.

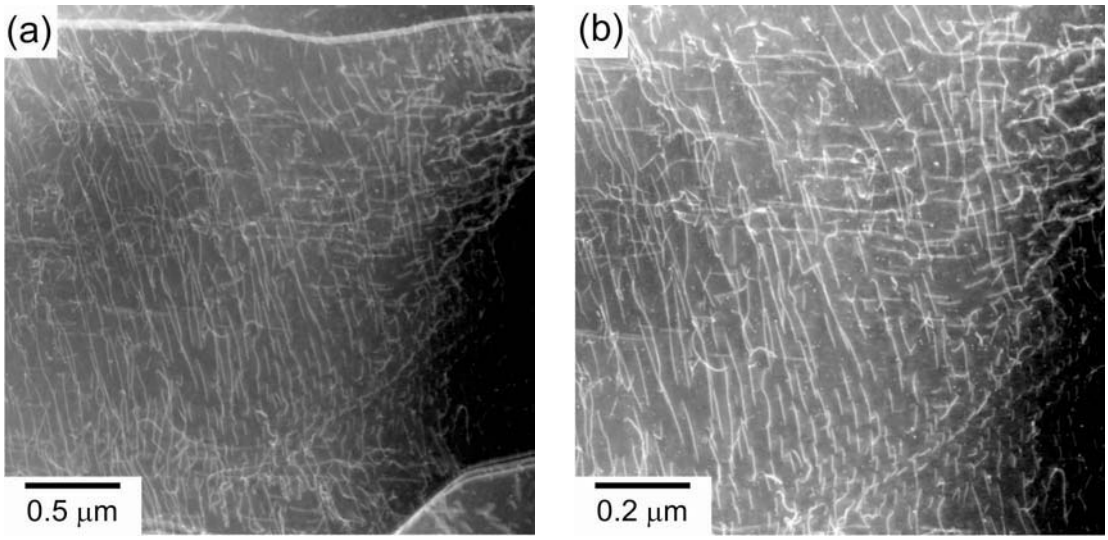

Fig. 4.15 HAADF STEM micrographs showing distribution of dislocation density for the DP steel obtained from sch. 11 applied below T_{nRX} at the highest amount of total strain after prestaining at PS = 2 % and baking at T = 170 °C for t = 20 min; (a) 0.5 μm and (c) 0.2 μm.

4.5 Conclusions

This chapter provided an investigation of the microstructure formation and mechanical properties obtained after TMCP simulation of DP 600 steels. The samples followed different hot deformation schedules on the deformation simulator. The microstructure evaluation, mechanical properties and BH behavior were also studied after TMCP and after prestraining and paint baking simulation. From the present investigation the following conclusions can be drawn:

1- Varying hot deformation parameters has a significant influence on the phase transformation behavior. Decreasing hot deformations or/and increasing strains shift the Ar_3 and Ar_1 temperatures to higher levels and the M_S towards lower temperatures.

2- By making use of the beneficial effect of the hot deformation below T_{nRX} and/or to high amounts of total strain, pronounced finer ferrite grains and finer martensite blocks in DP steels had been produced. This results in improvement of mechanical properties and BH behavior of the steels.

3- For the given alloying composition, the most promising microstructures with respect to the mechanical properties are those processed below T_{nRX} at higher amounts of total strain. The microstructures of this steel seem to be strongly dislocated, resulting in a heterogeneous structure with dislocations irregularly distributed in the ferrite matrix. A higher dislocation density is

observed for the samples applied at higher amount of total strain. This results in improved strength after TMCP as well as after baking process.

4- A noticeable higher strength increment is observed after prestraining at 2 % and baking at 170 °C for 20 min as compared to that one without PS. This increment is significantly higher for conditions conducted below T_{nRX} at high amounts of total strain.

5- TEM and HAADF STEM observations reveal a slightly increased dislocation density after PS and BH. For DP steel cell walls and uniform distributed structures are different ways to minimize the energy per unit dislocation line. Additionally, the formation of fine iron carbides in ferrite, pinned by dislocations, is detected in the ferrite after BH.

6- By controlling the deformation temperatures and the amounts of strain during the TMCP, it is possible to achieve the optimized microstructure and hence, to improve the mechanical properties and bake hardenability of the DP steel.

5 Martensite Content and Cooling Rate: Results and Discussion

5.1 Introduction

Hot rolled DP steels are referred to the steels with microstructures consisting largely of ferrite and martensite. The amount of both phases is engineered through alloy design and processing to induce extra strengthening in phases either through grain refinement, dislocation hardening and precipitate strengthening or by solid solution strengthening [Mat84].
Since ferrite is the major microstructural constituent in hot rolled DP steels, it is expected that during martensite transformation, most of the plastic strain will be accommodated by the ferrite phase itself [Bha93, Lan82]. Cooling rate after the last finishing rolling will therefore be largely dictated by the ferrite properties. The martensite phase blocks may exert significant influence on the ferrite properties and therefore modify the microstructure in total.

5.1.1 Aim of the Study

In this chapter the present study was aimed at designing microstructural variations in DP steels and assessing the cooling rate influenced by such microstructural variations. The elements of microstructural control through TMCP in DP steels along with a consideration of microstructural effects on mechanical properties, with emphasis on cooling rate during $\gamma \rightarrow \alpha$ transformation, will be discussed in detail. The following variations in the microstructure were sought in the DP materials for the present study:
a) Vary the volume fraction of martensite
b) Vary the cooling rate during $\gamma \rightarrow \alpha$ transformation

5.2 Simulation of Finishing Rolling

Analogous to chapter 4 the simulation of the last three steps of finishing rolling was conducted on the deformation simulator using flat compression setup. Fig. 5.1 illustrates schematically the employed TMCP schedule for simulation the final steps of the finishing rolling. All flat compression specimens had been austenitized at a temperature of T_A = 1000 °C for t_A = 3 min. The heating rate was 10 K/s. The hot deformation parameters of the last three deformation steps had been selected according to industrial conditions and kept fixed (Tab. 5.1).

As can be seen in Tab. 5.1, hot deformation parameters are the same as schedule 7 (chapter 4) where the first and second deformation steps took place in the recrystallization region (above T_{nRX}) followed by a further step in the non-recrystallization region. The strain rate of each deformation step was $\dot{\varphi}$ = 10 s^{-1}. The break time between the deformation steps was 5 s. After the last deformation step the specimens were cooled below M_S in two stages. First, they were cooled at different cooling rates to fast cooling start temperature (T^{FC}) in $\gamma \rightarrow \alpha$ transformation region, until required fraction of ferrite and austenite was obtained and then accelerated cooled below M_S at a high cooling rate of ~100 K/s (Fig. 5.1).

In order to obtain DP steels with prescribed amounts of ferrite and martensite the appropriate T^{FC} temperatures must be determined from which the specimens have to be fast cooled. As discussed in previous chapter, varying TMCP parameters affects this temperature. Determining T^{FC} is described in following section. The accelerated cooling of the specimen from T^{FC} below M_S results in transformation of prescribed remaining austenite to martensite. Therefore, adjustment of MVF is possible by variation of T^{FC}. Variation of the cooling rate during the $\gamma \rightarrow \alpha$ transformation and volume fraction of martensite in the DP 600 steel are shown in Tab. 5.2.

Tab. 5.1 Parameters of hot deformation process during the simulation of controlled rolling selected according to the industrial condition

Steel	T_1 [°C]	T_2 [°C]	T_3 [°C]	φ_1 [-]	φ_2 [-]	φ_3 [-]	φ_t [-]
DP 600	900	855	830	0.45	0.25	0.15	0.85

Tab. 5.2 Variation of cooling rate during simulation of controlled cooling after the last deformation to T^{FC} and variation of MVF

Steel	Cooling rate after last deformation to T^{FC} [K/s]	MVF [%]
DP 600	1, 10, 20, 30, 40	10, 20, 30

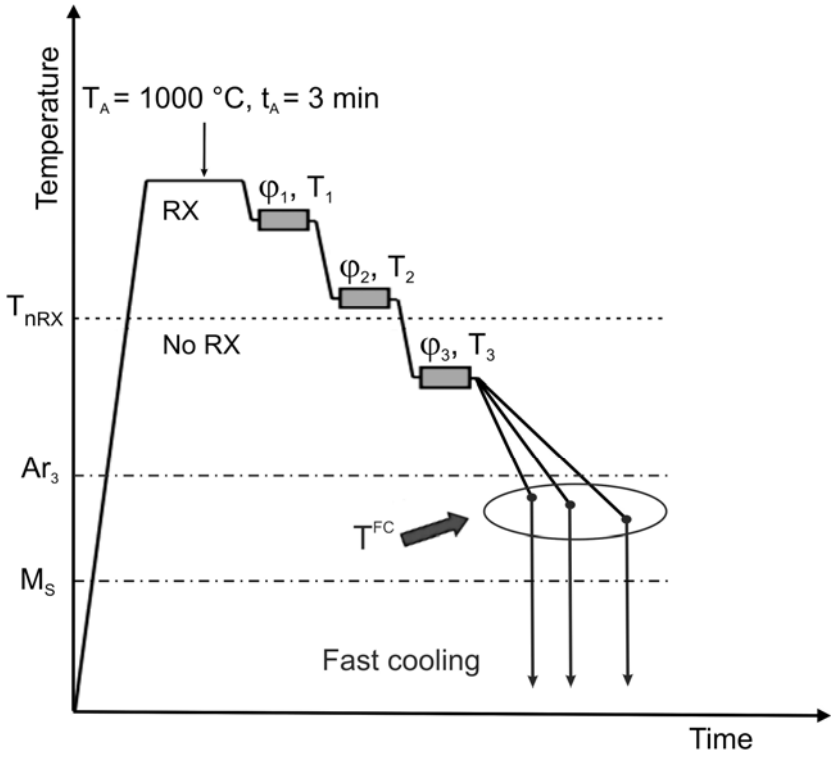

Fig. 5.1 TMCP schedule applied for simulation of the final steps of finishing rolling process following schedule 7.

5.3 Results

5.3.1 Phase Transformation Behavior and Defining T^{FC}

To define T^{FC} depending on the cooling rate the dilatometric measurements had been performed, as described in section 4.3.1. As mentioned earlier, processing parameters (deformation, temperature, cooling rate and etc.) influence the $\gamma \rightarrow \alpha$ transformation kinetic. Therefore, the dilatometric tests were preformed according to applied conditions. Fig. 5.2 shows schematically thermomechanical schedule of the deformation / dilatometric tests. Specimens were prior subjected to the deformation parameters as controlled rolling (Tab. 5.1) and subsequently cooled from the last deformation step to RT at different cooling rates, listed in Tab. 5.2.

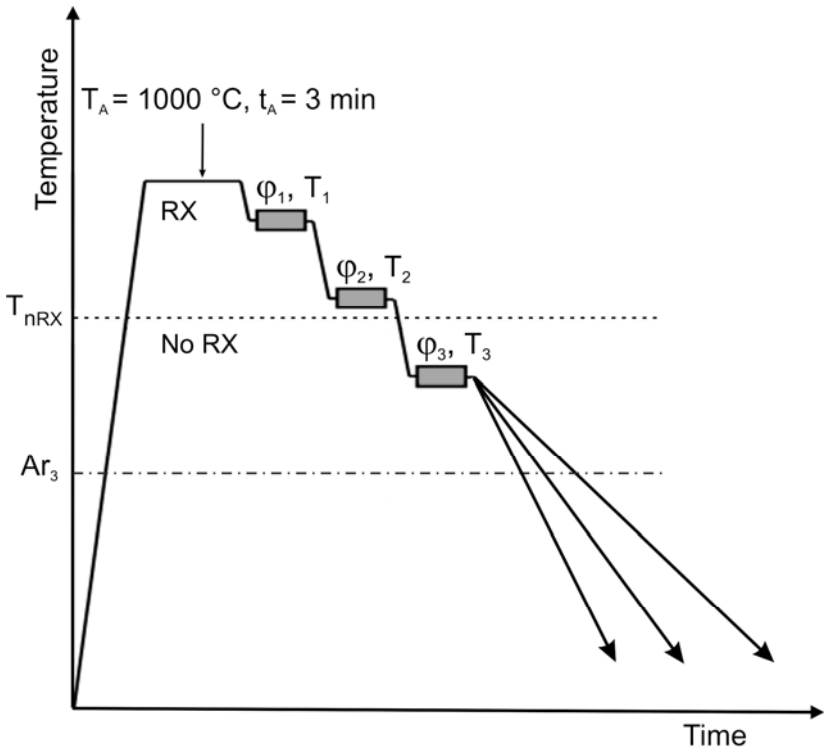

Fig. 5.2 Schematic representation of the employed schedule for deformation / dilatometric test (same as Fig. 5.1) with different cooling rates to RT after deformation.

The change in the length (dilatation) during the cooling was measured by the laser. The transformation behavior depending on cooling rate was determined by means of length change as a function of temperature. Fig. 5.3(a) illustrates dilatation curves corresponding to different cooling rates. On this graph the change in lengths of specimens cooled to RT at different cooling rates are plotted as a function of temperature.

From Fig. 5.3(a) the transformed fraction of austenite to ferrite can be determined for different conditions, as described in section 4.3.1. Fig. 5.3(b) displays the transformed f_γ to f_α as a function of temperature during cooling at different cooling rates. It can be seen that with a higher cooling rate the $\gamma \rightarrow \alpha$ transformation nose is shifted towards lower transformation temperatures.

For this study, amounts of martensite for DP steel were defined to MVF = 10, 20 and 30 %. From transformed volume fraction curves (Fig. 5.3(b)) T^{FC} temperatures, corresponding to different MVFs at different cooling rates, can be determined, presented in Tab. 5.3. For example, at a cooling rate of 1 K/s 10 % of remaining austenite and 90 % of ferrite are formed at a temperature of about

687 °C (Fig. 5.3(b)). In addition, Tab. 5.3 lists Ar_3, Ar_1 and M_S temperatures corresponding samples with different cooling rates.

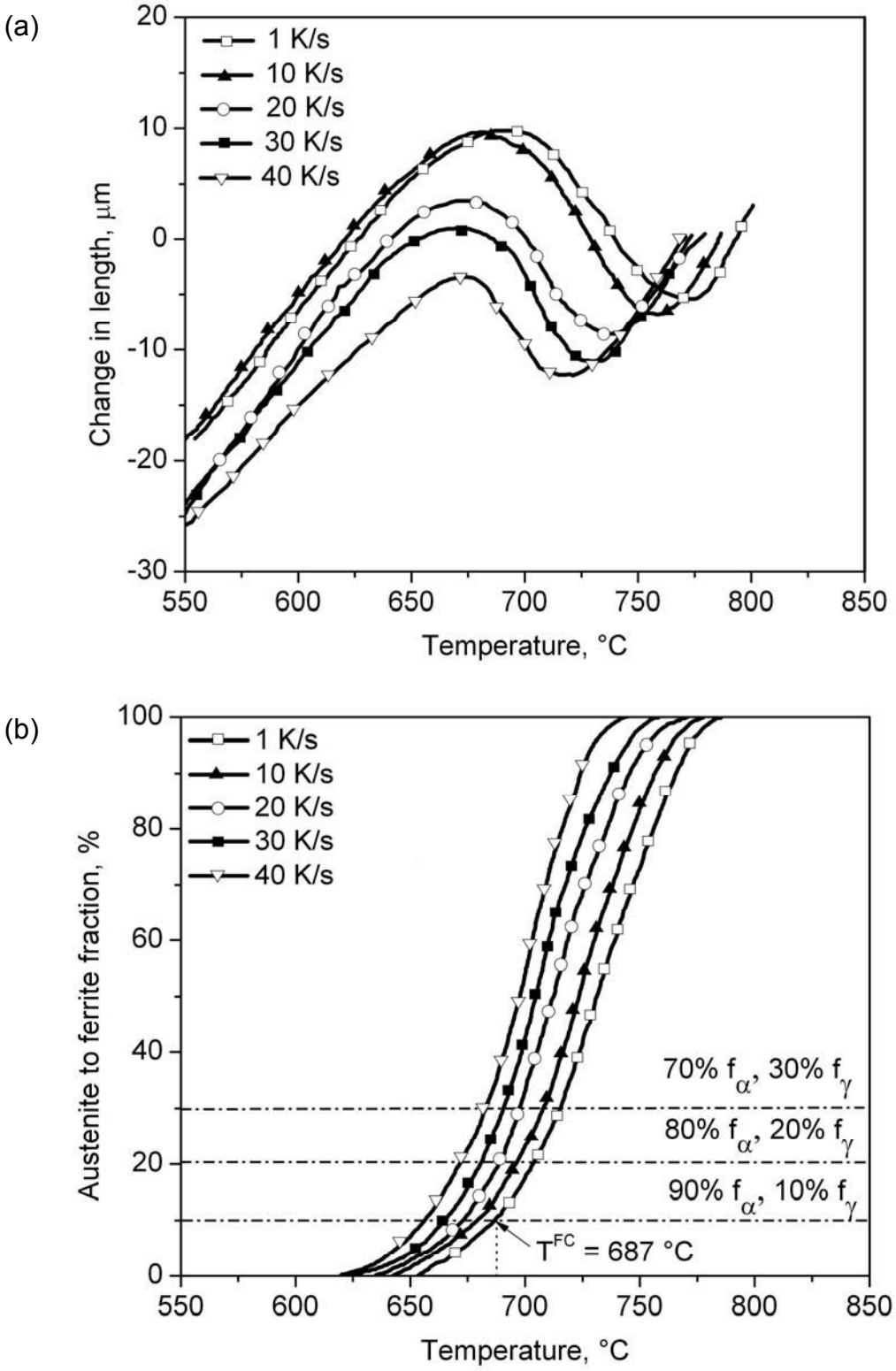

Fig. 5.3 Influence of the cooling rate on the phase transformation behavior; (a) dependences of the change in length on the temperature at $\gamma \rightarrow \alpha$ phase transformation during cooling stage at 10 K/s and (b) calculated fraction of $\gamma \rightarrow \alpha$ as a function of temperature for specimens cooled at different cooling rates.

The data from Fig. 5.3 and Tab. 5.3 indicate that the cooling rate reveals a strong influence on Ar_3 and Ar_1 during the $\gamma \rightarrow \alpha$ transformation as well as on M_S during the $\gamma \rightarrow \alpha$' transformation. It can be concluded that higher cooling rate results in lower Ar_3, Ar_1, T^{FC} and M_S. With increasing cooling rate from 1 to 10 K/s the Ar_3 and Ar_1 decrease by about 10 and 8 K, respectively. The specimen having lowest cooling rate of 1 K/s shows the highest Ar_3, Ar_1 and M_S while the lowest Ar_3, Ar_1 and M_S are obtained for the specimen with highest cooling rate of 40 K/s. A comparison of the lowest cooling rate at 1 K/s to the highest cooling rate at 40 K/s shows a difference of about 43 K for Ar_3 and about 30 K for Ar_1.

Tab. 5.3 Determined Ar_3, Ar_1, appropriate T^{FC} for f_α = 70, 80 and 90 %, f_γ = 10, 20 and 30 % and M_S obtained during accelerated cooling for different schedules

Cooling rate [K/s]	Ar_3 [°C]	Ar_1 [°C]	$T^{FC,90\ \%\ \alpha}$ [°C]	$T^{FC,80\ \%\ \alpha}$ [°C]	$T^{FC,70\ \%\ \alpha}$ [°C]	M_S [°C]
1	785	651	687	704	714	427
10	775	643	679	697	705	420
20	769	635	672	688	696	414
30	756	626	663	681	690	408
40	742	623	656	671	682	403

5.3.2 Microstructure Evolution

Flat compression samples were cooled after the last deformation step to different T^{FC} temperatures at different cooling rates and then accelerated cooled below M_S. The TMCP was designed to produce DP microstructures with different MVFs. LOM investigations were performed to study the microstructure evolution after TMCP. Fig. 5.4 displays exemplary LOM images corresponding to samples containing 10, 20 and 30% of MVF with a cooling rate of 10 K/s. It is revealed that three DP microstructures are characterized by similar cooling rate (10 K/s) but exhibit different MVFs. The estimated MVFs in the final microstructure based on dilatation curves are in good agreement with the quantitative analysis. All images show a classical DP microstructure with relatively globular martensite islands embedded in the ferrite matrix phase. Large martensite islands can clearly be observed, but they often show dark substructures either within or in their direct surroundings. In addition, such a dark phase can also be observed at the boundaries between two neighbors. Some bainitic phases could also be detected in the microstructure. Diffusion of

C from the enriched martensite to the ferrite zones facilitates bainite formation in these regions [Bha92a]. The amount of retained austenite was investigated and measured by SM. Small amounts of retained austenite between 1 - 2 % could be detected for all conditions.

For samples, cooled during the $\gamma \rightarrow \alpha$ transformation with different cooling rates and the same MVFs, no significant differences with regard to the morphology, phase distribution and grain size could be found.

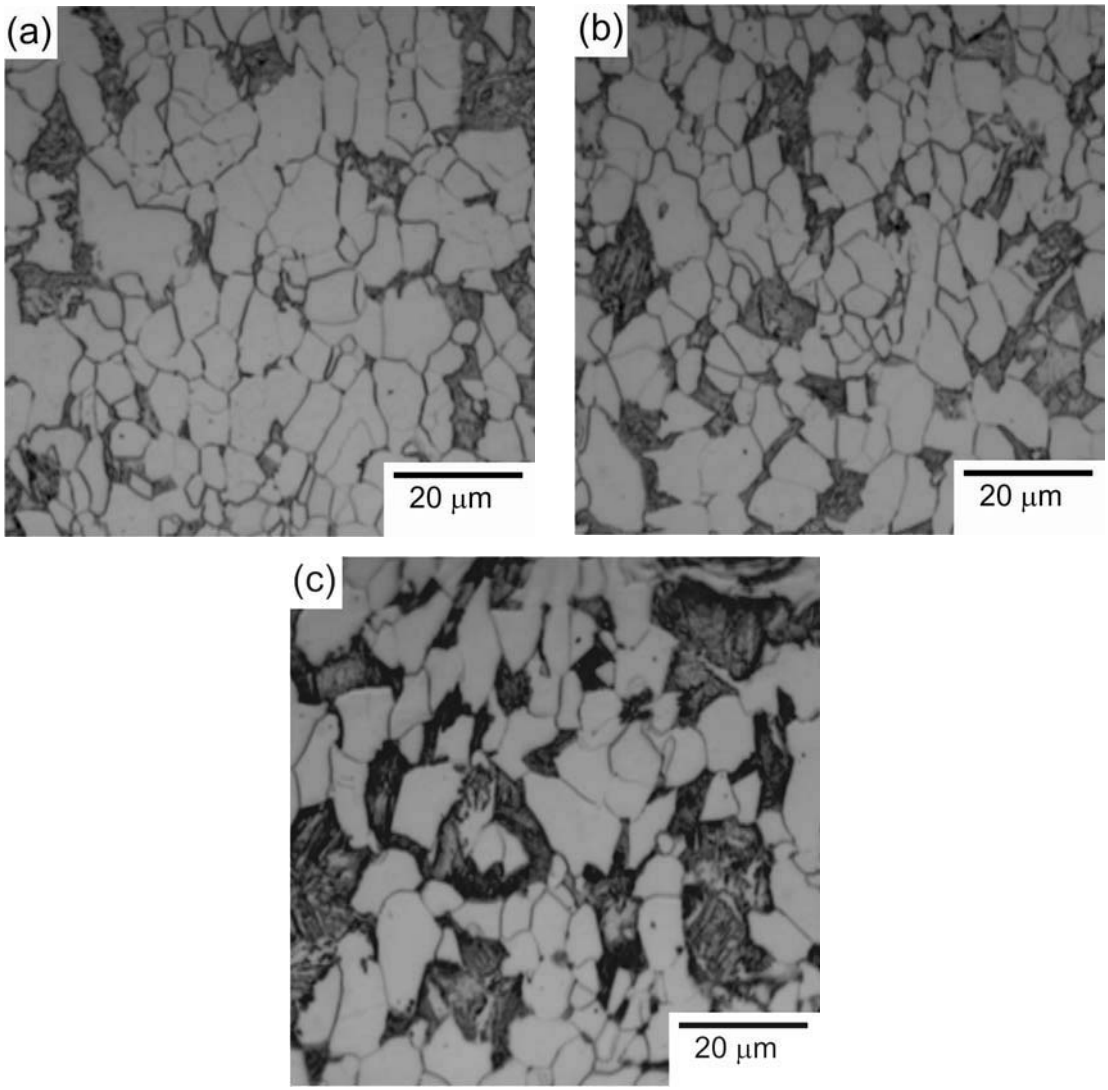

Fig. 5.4 Microstructure of DP steels showing different volume fractions of martensite obtained after TMCP: (a) $f_{\alpha} = 90$ %, $f_{\alpha'} = 10$ %; (b) $f_{\alpha} = 80$ %, $f_{\alpha'} = 20$ % and (a) $f_{\alpha} = 70$ %, $f_{\alpha'} = 30$ %; cooling rate of samples in the first cooling stage was 10 K/s.

5.3.3 Mechanical Properties

The engineering stress-strain curves of DP steels with MVFs of 10, 20 and 30 %, and cooling rate of 10 K/s are plotted in Fig. 5.5. All three steels show a

continuous yielding behavior. Rigsbee et al. [Rig79] have stated that at least 4 % of martensite in DP steels is necessary to achieve a continuous yielding behavior. Ultimate tensile strength, yield strength and total elongation of the specimens with different MVFs after TMCP at different cooling rates are compared to that ones after PS and BH treatment and illustrated in the next section. As expected, Fig. 5.5 shows that both, the yield and tensile stress increase with increasing volume fraction of martensite. At the same time, the elongation behavior decreases. This behavior is commonly interpreted in terms of local dislocation accumulation [Bal81] introduced by the martensitic transformation. Yet, as the plastic strain of the martensite phase is negligible, the total elongation to fracture is reduced with increasing martensite fraction.

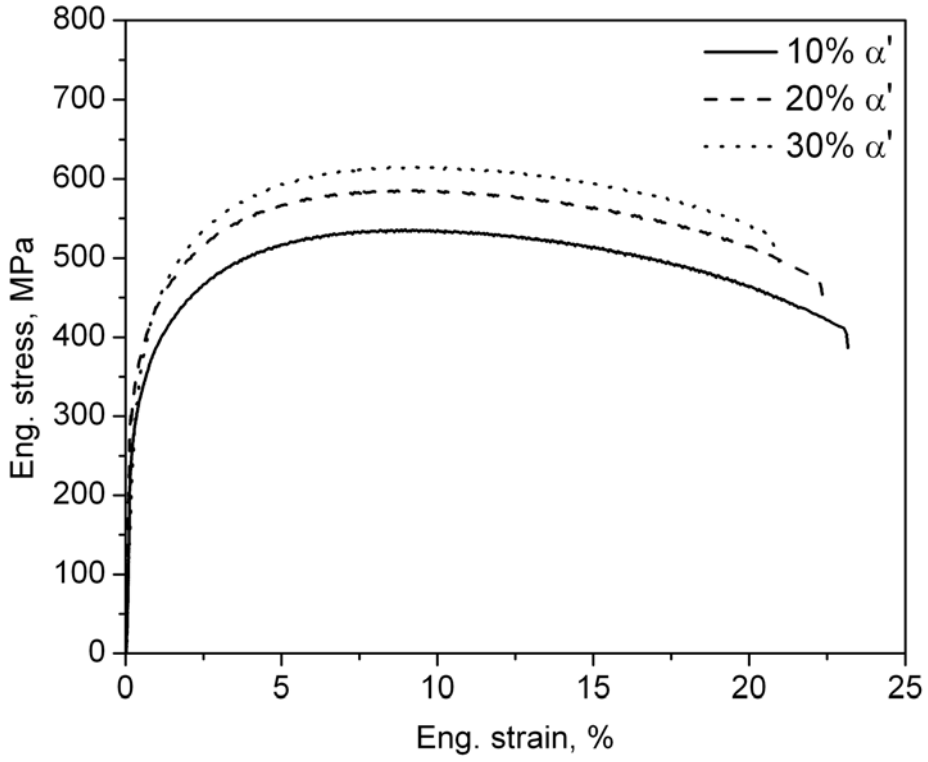

Fig. 5.5 Stress-strain curves for three DP steels with MVF = 10 %, 20 % and 30 %.

5.3.4 Bake Hardening Behavior

Mechanical properties of thermomechanically processed samples before and after PS and BH were determined using tensile testing. In this part of the study the parameters varied one at a time with respect to the standard condition of PS = 0 and 2 %, T = 170 °C and t = 20 min. The results of the experiments are presented a) in term of changes in the strength and elongation and b) in term of BH_0 and BH_2 values.

The mechanical behavior of thermomechanically produced samples before and after PS and BH with respect to cooling rate and MVF is sketched in Fig. 5.6. As a result, higher cooling rates after the last deformation step to fast cooling start temperature during the $\gamma \rightarrow \alpha$ transformation yield higher strength level. This is more demonstrative for the condition after TMCP. As the MVF increases the strength values increase steeply to higher strength level (Fig. 5.6(a)-(b)). Total elongation decreases by increasing cooling rate from 1 to 40 K/s as shown in Fig. 5.6(c).

Fig. 5.6(a)-(b) shows a constant increase of R_m and R_e for any value of MVF and cooling rate after 2 % PS and baking at T = 170 °C, t = 20 min. The cooling rate sensitivity of prestrained and baked DP steels is less than the condition before PS and BH. Fig. 5.6(c) compares values of total elongation before and after PS and BH. Lower TEl level of the DP steel can be found on this figure after a paint baking treatment (2 % of PS and at 170 °C / 20 min) as a function of cooling rate. Further decrease of TEl is found by increasing MVF.

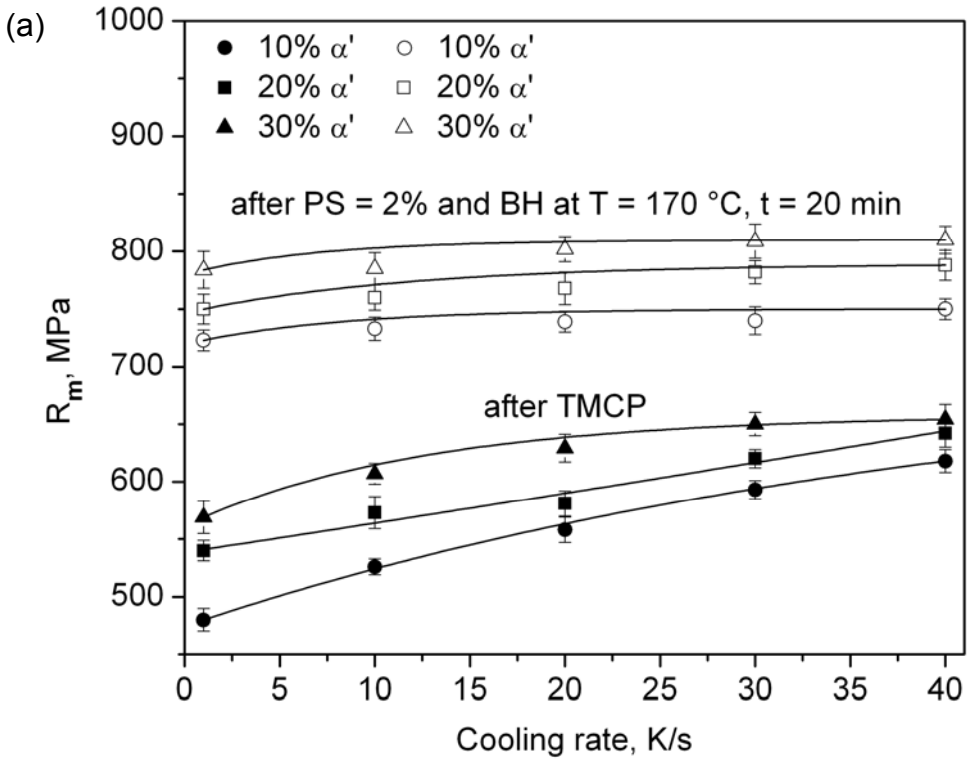

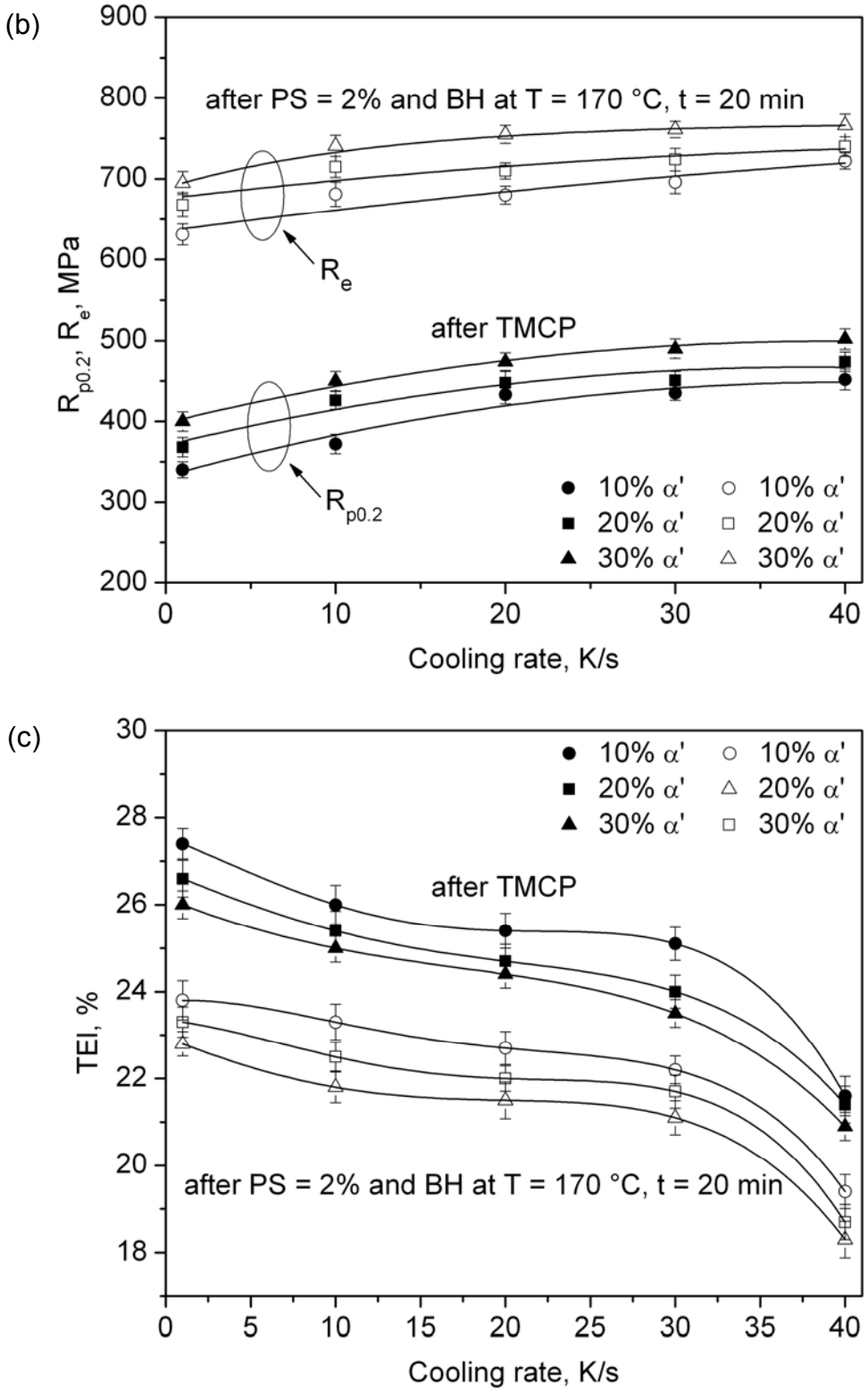

Fig. 5.6 Influence of MVF and cooling rate on the mechanical properties of DP steels after TMCP and after prestraining and baking process with PS = 2 %, T = 170 °C, t = 20 min; (a) tensile strength (R_m); (b) yield strength ($R_{p0.2}$) and lower yield strength (R_e) and (c) total elongation (TEl).

Fig. 5.7 compares the effects of cooling rate and MVF on the strength increase after PS and BH in term of BH_0, BH_2 values. At each cooling rate, this figure plots the difference between the yield strength after PS and BH (R_e) and the yield strength of the samples after TMCP ($R_{p0.2}$). As shown in this figure, both BH_0 and BH_2 values increase with increasing MVF at all cooling rates. Without PS the samples indicate a lower BH level than with PS = 2 % (BH_2). DP steels with 10 % MVF reveal no significant increase in BH_0 values at all cooling rates. For DP steels with 30 % MVF, BH_0 increases steeply with increasing cooling rate. For steels having 20 % MVF, BH_0 increment is found after a cooling rate of 20 K/s (Fig. 5.7(a)).

The lowest BH_2 value of about 73 MPa is reached for the steel with 10 % MVF at the lowest cooling rate of 1 K/s, while the highest BH_2 value of about 120 MPa could be obtained with 30 % MVF and a cooling rate of 40 K/s (Fig. 5.7(b)). DP steels containing 10 % MVF appear no distinct BH_2 increment at low cooling rates (less than 10 K/s), while BH_2 values at high cooling rates show an increased level.

Three major observations from these data on the response to BH are:

(a) Pre-strained DP steels to 2 % indicate a remarkable higher BH level compared to non-prestrained steels.

(b) At high cooling rates (above 20 K/s), there is a significant increase in strength due to aging and a return of a well defined yield point on loading, i.e. the cooling rate sensitivity of the baked materials at the low cooling rates is much lower than the high cooling rates.

(c) The contribution of BH increases with an increase in MVF at all cooling rates.

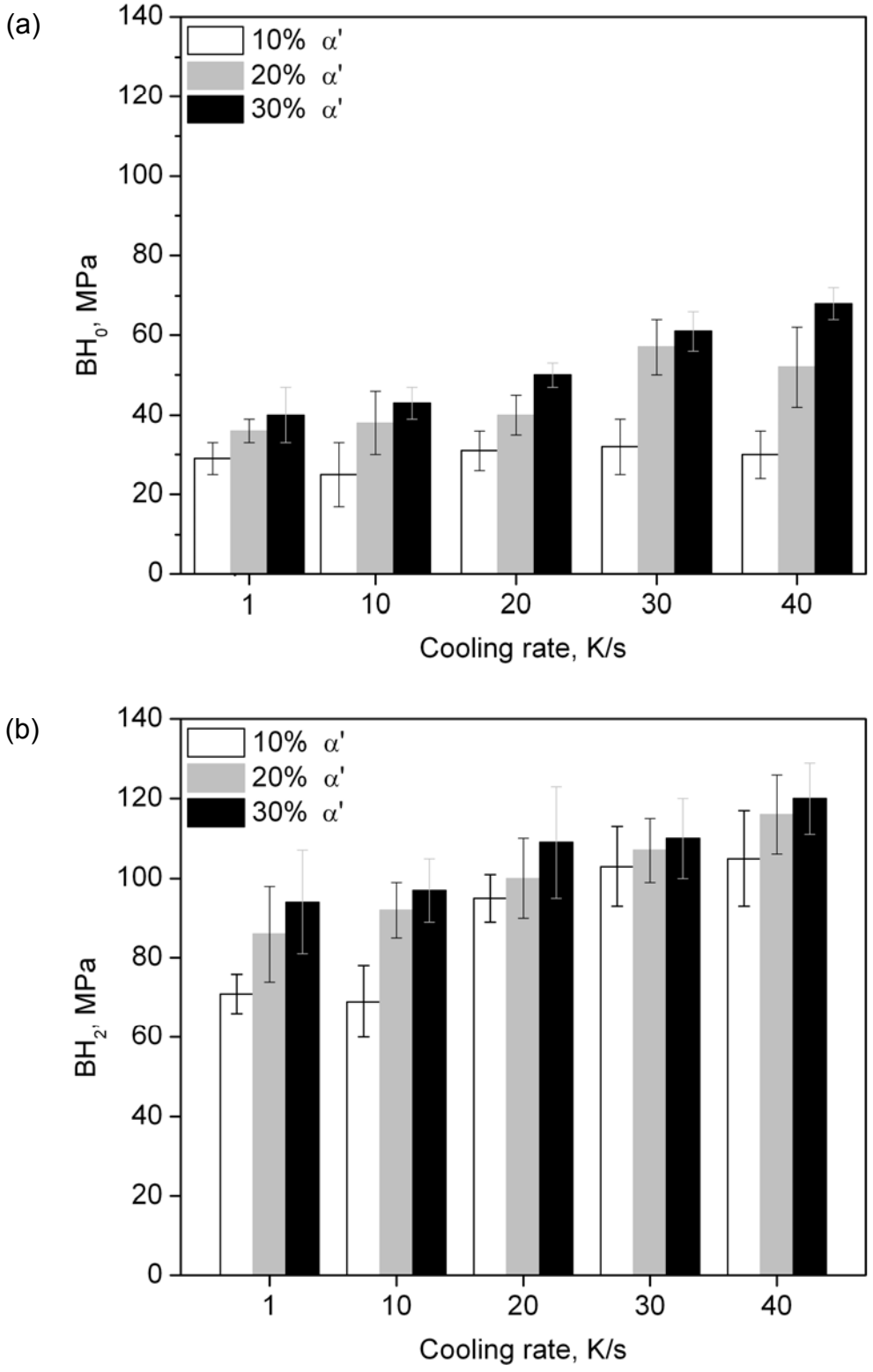

Fig. 5.7 (a) Dependence of BH_0 on the cooling rate and MVF, calculated from difference between $R_{P0.2}$ of the tensile sample and R_e of the respective BH sample and (b) dependence of BH_2 on the cooling rate and MVF.

5.4 Discussion

5.4.1 Influence of Cooling Rate on the Phase Transformation Behavior

The results of the dependence of transformation temperatures on the cooling rate are shown in Fig. 5.3. In general, the reproducibility of such phase transformation curve depends to a large extent on various factors: the achievable quenching speed to the respective holding temperature, uniform cooling of the test sample, compliance with isothermal temperature control, sensitivity of direct volume measurement and compliance with a defined austenitization condition. In addition, the actual chemical composition of all alloying elements must be taken into consideration for transferability to steels of the same designation.

Ar_1, Ar_3 and M_S temperatures obtained during the TMCP under different cooling conditions are listed in Tab. 5.3. These data indicate that the cooling rate exerts a stronger influence on the start temperature (Ar_3), when all the austenite phase is exhausted, than on the finishing temperature (Ar_1). It is observed from this table, that Ar_1 and Ar_3 increase with decreasing cooling rate. On the other hand, preliminary test showed that the dependence of transformation temperature on the cooling rate decreases as the cooling rate decreases. Slow cooling rates below 1 K/s could not effectively influence the Ar_1 and Ar_3 are independent on the cooling rate. This feature is associated with the transformation temperatures under the equilibrium Ae_1 and Ae_3 which depends only on the chemical composition, i.e. is independent on the heating or cooling rates [Sol07]. An inference is that at the cooling rate where the transformation temperatures start to be independent on the cooling rate, the Ar_1 and Ar_3 are close to the Ae_1 and Ae_3.

As discussed before, the increase in transformation temperatures is because of the greater density of nucleation sites, resulting from the fine grained structure. On the other hand, varying cooling rate shows no significant influence on the grain size (as mentioned in section 5.3.2). Thus, it can be deduced that grain size is not an operating mechanism. Therefore, this mechanism is ruled out.

Jun et al. [Jun06] pointed out that the influence of cooling rate on the transformation temperatures in ferrite formation region is due to a diffusion mechanism. They noted that low cooling rates influence transformation

temperatures by diffusion transformation because of the high diffusivity path produced by deformation. Therefore, increase in Ar_1 and Ar_3 temperatures could attribute to the diffusion mechanism of C atoms at low cooling rates. However, at higher cooling rates, change in transformation temperature is reported to be not controlled by diffusion [Jun06].

As can be seen from Tab. 5.3, M_S decreases by increasing cooling rates from 1 to 40 K/s. On the other hand, higher cooling rates lower the T^{FC} in the austenite and ferrite regime. Due to low T^{FC} temperatures at high cooling rates, the mechanical stability of austenite increases and, as a result, a higher driving force for martensitic transformation is needed [Nad08]. Higher driving forces are provided at lower M_S temperatures, i.e. M_S decreases by increasing cooling rate. This is confirmed for the given experimental conditions, since higher cooling rates shift M_S towards lower temperatures.

Another interpretation is the detraction of the M_S temperature. As described in previous chapter, the M_S temperature is mainly a function of C content, i.e. by increasing C content the M_S temperature is decreased. This can be explained as a consequence of ferrite formation in which C becomes enriched in the remaining austenite faster at higher cooling rates. Therefore, remaining austenite transforms into martensite at somewhat lower temperatures. Choi et al. [Cho04] noted that the lower MVF in the final DP steel causes a C enriched austenite at the onset of transformation. Hence, higher austenite C contents retard transformation to martensite.

5.4.2 Influence of Cooling Rate and Martensite Volume Fraction on the Microstructure

Results of microstructure evolution (Fig. 5.4) reveal an excellent correlation between the microstructure obtained after each TMCP and that predicted by dilatometric study. The microstructure is mostly ferrite and the rest is martensite. It was possible to set the volume fraction of martensite in DP structure during TMCP at different cooling rates by setting T^{FC}. By increasing T^{FC} at a given cooling rate the fraction of martensite within the microstructure is raised. From LOM observations it is obvious that in all conditions the morphology of martensite and the grain size of ferrite after the TMCP look similar. The only difference in the microstructure could be a change in the density and distribution

of dislocation in ferrite or at F/M interface due to the variation of the cooling rate and MVF.

Fig. 5.8 shows an example of HAADF STEM micrograph of a DP sample containing 30 % of MVF. This image allows distinguishing martensite clearly from the matrix as it exhibits higher lattice distortion. Each martensite block is surrounded by its neighboring ferrite grains. One could expect that larger blocks affect larger volume fractions of the adjacent ferrite grains, because the absolute volume increase is higher during transformation. However, even very small martensite blocks cause strong local plastic deformation [Moy75].

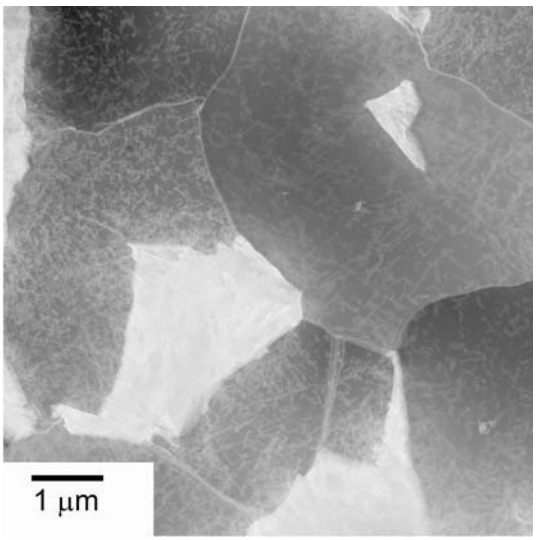

Fig. 5.8 HAADF STEM micrograph showing distribution of martensite and the dislocation density in the DP steel containing 30 % of MVF obtained after the TMCP.

Another aspect is the distribution of martensite around the ferrite grain. The more of the ferrite grain is surrounded by martensite, the higher is the resulting in dislocation density. It can be observed that the dislocation density in ferrite is increased with increasing martensite fraction (Fig. 5.8), i.e. a higher ferrite fraction experiences local plastic deformation due to the martensitic phase transformation. The introduction of additional dislocations decreases the average spacing between dislocations. The region affected by martensite is not necessarily distributed homogeneously around martensite blocks, as can be seen in this figure. In case of a high number of martensite neighbors, the ferrite grains are sometimes entirely affected by the shape accommodation, i.e. the whole grain is work-hardened after martensitic phase transformation. This steel contains a high density of non-uniformly distributed dislocations.

There were also some minor dislocation accumulations visible at the F/F and F/M grain boundaries of steel with a low MVF of 10 %. Yet, the dislocation density of this steel is scarce and less pronounced than of steels with higher MVFs (20 and 30 %).

5.4.3 Influence of Cooling Rate on the Mechanical Properties and Bake Hardening Behavior

For the DP steels discussed here, the cooling rate dependencies after TMCP as well as after PS and BH are plotted in Fig. 5.6. The increase in the dependency of strength with cooling rate indicates that there is an increase in the contribution of thermally activated dislocation processes, e.g. the formation of doublekink pairs, as dislocations move past Peierls barriers, to the overall stress required for dislocation movement such that at high cooling rates the properties are dominated by the stress for individual dislocation movement [Mat03]. Wu et al. [Wu08] have pointed out that the relaxation mechanism can be prevented during thermomechanical processing at higher cooling rates after the last deformation. This causes the generation of more dislocation in the final microstructure, which could increase the strength effect in DP steels.

For the prestrained and baked samples at higher cooling rates, the high strength and low ductility level suggest that the mechanisms responsible for strengthening are the same. If it is assumed that the process of aging produces a fully pinned dislocation structure, then on reloading the stress for deformation corresponds primarily to the stress to generate sufficient new dislocations as controlled by the long range stress fields associated with the dislocation structure and the stress required to operate dislocation sources [Bru03].

However, with an increase in cooling rate the inherent resistance to the movement of individual dislocations by the same processes operating for the not aged samples dominate and the effects of pinning due to aging are overshadowed by the inherent processes of dislocation movement over short range barriers, such as Peierls barriers. Therefore, DP steels containing a certain MVF exhibit a better strength level at high cooling rates.

The other influencing factor of the BH effect, which should be discussed here, is the solute C content. Marunouchi et al. [Mar87] reported that after hot rolling high cooling rate from a high temperature is effective to suppress carbide

precipitation. On the other hand, carbide formation can decrease the effective solute C content. Hence, suppression of carbide precipitation by higher cooling rates could increase the bake hardenability.

5.4.4 Influence of Martensite Volume Fraction on the Mechanical Properties and Bake Hardening Behavior

The TMCP and mechanisms involved during the production of DP steels using hot deformation simulation have been already presented in section 5.2. First of all it has to be stated that DP microstructures are successfully achieved through the TMCP schedules applied. The thermomechanical calculations predict that for the DP steel used the formation of martensite in given volume fraction is possible by varying fast cooling start temperature.

The main factor governing the mechanical properties of DP steels clearly is the amount of martensite [Che89b, Gup84]. The values of R_m, $R_{p0.2}$ and TEl after TMCP are plotted in Fig. 5.6 as a function of MVF. An increase of R_m is found for rising MVF. For $R_{p0.2}$ such a general relationship is found, too, but at smaller martensite levels the increase is less pronounced. TEl systematically decreases with an increase in strength, i.e. an increase in MVF which correlates with the increase of strength. The results show that for TMCP a direct influence of the phase composition in terms of the MVF on the mechanical properties of DP steels is given. In general, there are many factors affecting the magnitude of strength in DP steels, e.g. residual stresses, the mobile dislocation density at the F/M interfaces, plastic incompatibility of hard and soft phases, their amount and distribution and possibly the transformation of retained austenite to martensite [Spe81b]. As discussed earlier, the chemical strength and grain size of the ferrite are the same in all DP microstructures.

Lower elastic limit by increasing martensite fraction can be explained in terms of residual stresses [Pri84, Lie02]. As the fraction of F/M interfaces increases with increasing martensite fraction, a higher fraction of ferrite is affected by the martensitic phase transformation and hence, higher residual stresses are introduced into the matrix. This might be the reason why the elastic limit in ferrite is locally reached earlier during tensile deformation which is reflected by the lower initial slope of the curve with higher martensite fraction (30 % of MVF). As DP steels are stored at RT before tensile straining, dislocation locking by

segregation of solute C does not occur, and the reoccurrence of a yield point is suppressed. The higher strength levels are generally attributed to the higher phase fraction of the hard second phase and can be approximated by a volumetric linear rule of mixtures [Koo80].

On the other hand, overall dislocation density in ferrite is increased with increasing martensite fraction, i.e. a higher ferrite fraction experiences local plastic deformation due to the martensitic phase transformation. The introduction of additional dislocations decreases the average spacing between dislocations, which is linked to the yield strength of the material [Koc66].

The influence of the volume fraction of martensite as a hard phase was investigated by a number of authors [Ble04b, Cal10, Hwa05, Kim81, She84]. The growth of the volume fraction of martensite results in an increased yield point, tensile strength and impact strength of DP steels. According to [Bag99, Tav99], this effect was only observed for MVF of 55 %. At higher MVF, the authors observed a decrease of strength properties, which they explain by a decreased carbon concentration in martensite.

Similar behavior of mechanical properties can be observed for the samples after PS and BH treatment (Fig. 5.6). The strength values of samples after PS = 2 % and baking simulation at 170 °C for 20 min increase with increasing MVF. At the same time total elongation decreases. Clearly high BH_0 and BH_2 values are observed as the MVF increases (Fig. 5.7). Obviously, a large volume fraction of martensite favors large BH without and with 2 % prestrains. However, probably it is not only the MVF, which governs this process, but rather the state of martensite is likely to influence the BH behavior as well. It is reported [Kra01] that in martensite structures C atoms are trapped leading to a distorted bct lattice, i.e. supersaturation with C compared to the bcc ferrite. This leads to the high strength of martensite. In carbon steels with high M_S, tempering of martensite takes place already during cooling and also during storage and testing at RT. Thus, C may precipitate or diffuse towards dislocations and interfaces.

A possible explanation towards this behavior can be given by the specific microstructure. For DP steel having 30 % of MVF quite a large number of mobile dislocations at the F/M interfaces could be seen (Fig. 5.8). After deformation their number even increases. Together with the low volume fraction of ferrite it is

probable that the dislocations generated during prestraining can be blocked very effectively. Thus, the BH values are larger than those with lower MVF.

Waterschoot suggested that there should be an increase of BH levels with rising MVF [Wat03c]. This is explained by the higher level of residual stress to be relieved. In this study it was checked, whether such a correlation could be found for the DP steels. Comparing the samples with different MVFs it is obvious that in our study such a relation is valid, either for the BH_0 or for the BH_2. The results are presented in Fig. 5.9. A linear increase of BH_0 and BH_2 with MVF is found for the samples cooled at 10 K/s. This observation is valid for other cooling rates. However, a final answer, whether this dependence is solely attributable to the amount of martensite or to related changes in the microstructure affecting both R_m and solute C and hence BH_0 and BH_2, is yet to be given.

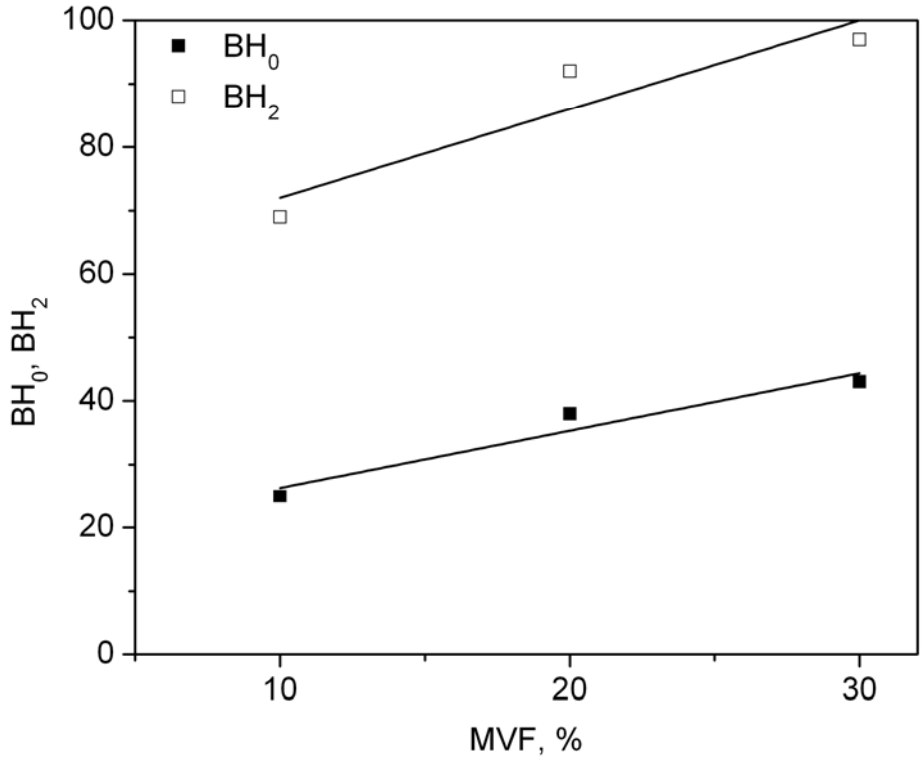

Fig. 5.9 Relationship between BH values and martensite volume fraction (MVF); Cooling rate during the $\gamma \rightarrow \alpha$ transformation was 10 K/s.

5.5 Conclusions

DP structure with different volume fractions of martensite and ferrite had been thermomechanically obtained by cooling the samples from the last deformation step to T^{FC} at different cooling rates and quenching samples from T^{FC} to RT. MVF in DP steels had been adjusted by setting T^{FC}. The influence of the cooling

rate in the first cooling stage as well as of MVF on the mechanical properties and BH behavior was studied. The major conclusions drawn from the present investigation are as follows:

1- Using the dilatometric analysis, a clear differentiation between $\gamma \rightarrow \alpha$ transformation temperatures depending on cooling rate after the last deformation step is found. This allows selecting the most appropriate fast cooling start temperature to obtain microstructures with defined volume fraction of martensite and ferrite. Increasing cooling rate shifts the Ar_3, Ar_1 and M_S towards lower temperatures.

2- The estimated MVF in the final microstructure based on dilatation curves is in good quantitative agreement. It is estimated that quenching of specimens from different T^{FC} temperatures results in different DP microstructures containing different MVFs at a given cooling rate. An assessment of the microstructures obtained in the thermomechanically processed samples with respect to MVF and cooling rate allows selection of processing parameters required to develop the specified DP microstructures.

3- By making use of the beneficial effect of the TMCP a variation in MVF and cooling rate does not influence the grain size of phases. The dislocation density in ferrite and at F/M interfaces increases with increasing MVF, resulting in a higher fraction of ferrite affected by the martensitic phase transformation and in higher residual stresses introduced into the matrix.

4- An increase in the cooling rate after the last deformation step to T^{FC} during the $\gamma \rightarrow \alpha$ transformation results in higher values of strength after TMCP as well as after PS and BH. This is due to an increase in the contribution of thermally activated dislocation processes.

5- The magnitude of mechanical properties after TMCP as well as after PS and BH is affected by the MVF. The increased number of dislocations in the ferrite grains and a higher amount of C atoms at the F/M interfaces is the most reasonable explanation for this observation, leading to a stronger dislocation pinning at large MVFs.

6 Chemical Composition: Results and Discussion

6.1 Introduction

The development of structural DP steels is characterized by a continuous search for higher strength and toughness combined with a good bake hardenability. During these two decades, development of DP steels has resulted in a wide variety of alloying combinations and processing technologies. The properties attained depend on the presence of small additions of alloying elements [Now10]. A knowledge of the precipitation strengthening effect in the steels with different additions is very important for development of optimal rolling schedules with the aim of improving as hot rolled mechanical properties and bake hardenability. DP steels alloyed with different elements are interesting variants to the already existing broad spectrum of AHSS steel for various applications. These can have favorable combinations of strength and toughness with fine-grained microstructures in the as thermomechanical controlled processing (TMCP)-rolled condition. Moreover, the variation of the chemical composition provides the possibility of changing the transformation temperatures and microstructure of the steel during TMCP which results in a wider window for designing mechanical properties and BH behavior.

Carbon is the main alloying element by which all transformations are noticeably affected and the final microstructure, the mechanical properties and BH effect can be controlled as could be shown in our actual investigations [Asa08a, Asa09c]. There are several studies that have dealt with the influence of C content and the influence of addition of solid solution strengthening elements (Mn, Si and P) on the mechanical properties and bake hardenability in low carbon steels [Han84, Miz94, Wat99]. Furthermore, niobium is known as a microalloying element by which austenitization, recrystallization, grain growth, phase transformation, and precipitation behavior can be controlled in a very efficient way and by which the mechanical properties can be varied in a wide range [Ble02]. Little investigations have been reported yet as to the study the influence of variation of alloying and microalloying elements on the mechanical properties and microstructure developing in combination with the BH effect in DP steels.

6.1.1 Aim of the Study

This chapter is concerned with a further investigation of the hot-rolled DP steel by variation their chemical composition. The study clarifies how the addition of alloying elements (C, Si, Mo and Nb) affects the microstructure, mechanical properties and BH behavior through the aforesaid metallurgical factors. The effect of both, alloying elements and TMCP, was studied in detail. Throughout the present work, the influence of alloying elements on phase transformation kinetic had been reviewed. Furthermore, the influence of reheating temperature (T_R) and Nb soulability during the simulation of roughing rolling process on the mechanical properties was investigated.

6.2 Investigated Materials and Alloying Concept

For this study the DP steel with chemical composition given in Tab. 3.1 was selected as the base steel which then was vacuum-melted in laboratory furnace and appropriately alloyed to obtain different chemical compositions. The selection of the compositions was based upon current researches under consideration of the industrial tolerance extent. Tab. 6.1 gives the chemical compositions of cast steels.

Tab. 6.1 Chemical composition of the steels (wt. %); D1 is the base steel

Steel	C	Si	Mo	Nb	Cr	N
D1	0.06	0.10	0.005	0.002	0.60	0.006
D2	**0.09**	0.10	0.005	0.002	0.60	0.006
D3	0.06	**0.25**	0.005	0.002	0.60	0.006
D4	0.06	0.10	**0.25**	0.002	0.60	0.006
D5	0.06	0.10	0.005	**0.04**	0.60	0.006
D6	**0.09**	**0.25**	**0.25**	**0.04**	0.60	0.006
D7	**0.09**	0.10	0.005	**0.04**	0.60	0.006
D8	**0.09**	**0.25**	**0.25**	0.002	0.60	0.006

Numerous alloying concepts have been developed for DP steels in order to adjust the desired microstructure and properties. The alloying elements change the thermodynamic stability of the phases and the kinetics of transformation whereby the transformation temperatures are shifted, the transformations are either promoted or hindered and the phase distribution is altered. Additionally, the elements might act as solid solution or precipitation hardeners and affect the grain size. As can be seen in Tab. 6.1, C ranges between 0.06 % to the

maximum of 0.09 % in the DP alloys. In this regards, all the investigated alloys are listed in the low carbon steel grades. C is the most important element which improves the mechanical properties and bake hardenability [Asa08a-b, Han84] of DP steels. Si is a solid solution strengthening element and increases the hardenability of DP steels [Lie96]. Nb in solid solution has been found to improve the mechanical properties of DP steels. Furthermore, the addition of Nb to DP steels not only provides noticeable grain refinement and thus improves mechanical behaviour but also renders an additional holding step in the temperature range of maximum ferrite formation unnecessary and enables continuous cooling to be applied after finish rolling. Ferrite formation involves C enrichment of the austenite thus retarding pearlite and bainite formation and facilitating martensite formation [Ble02]. Mo retards the precipitation of Nb(C, N), thus potentially improvement of the effectiveness of Nb [Bou98, Jia02]. Furthermore, Mo has the retardation effect on the austenite transformation to both ferrite and pearlite rendering the process control more manageable [Cap05].

6.3 Simulation of Roughing Rolling

The cast slabs were cut into blocks of 35 mm thickness, 50 mm width and 300 mm length. The simulation of roughing rolling took place at T_R of 1100 °C in four passes to a thickness of 10 mm and with a true strain value $\varphi = 0.27$ for each pass. During the final cooling of the hot rolled strips in air, the temperature was continually monitored using a pyrometer. It took up to 50 min to cool the strips from the final rolling temperature (about 1000 °C) to RT. The scale was removed from the plates using shot-blasting before being prepared for flat compression test, used for the simulation of the finishing rolling process.

In addition, alloys D5 and D7 having addition of Nb were reheated to 1200 °C in order to study the influence of T_R and Nb solution on the mechanical properties. This temperature was sufficient to dissolve the entire Nb in solution as it is clear from the relevant solubility versus temperature curve, which was calculated using Thermo-Calc (Fig. 6.1).

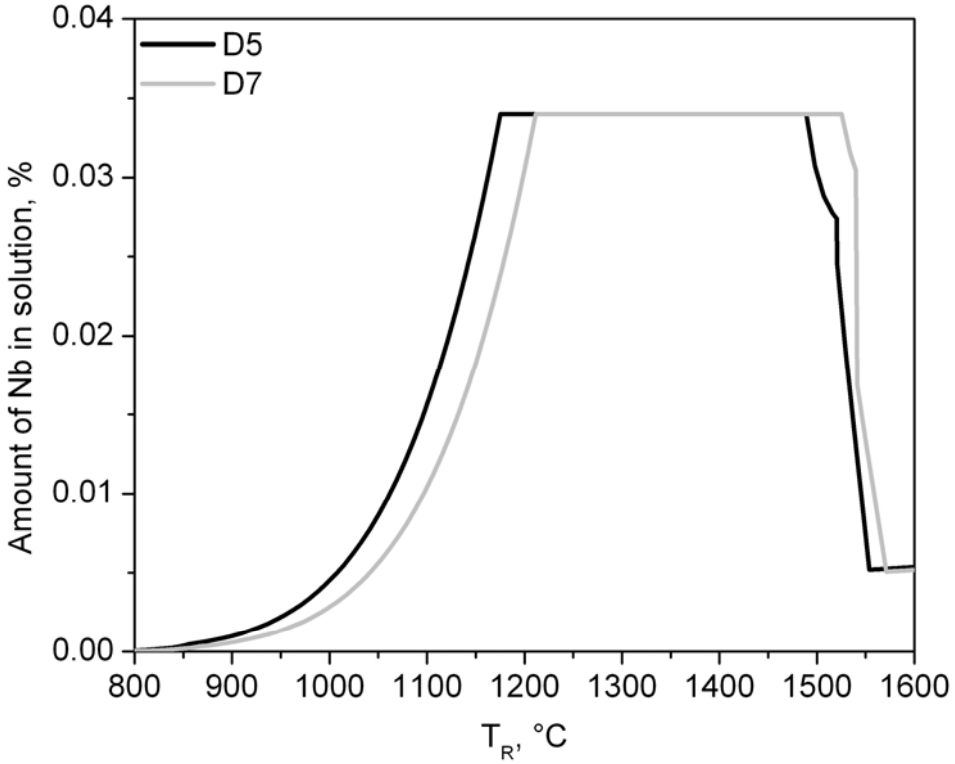

Fig. 6.1 Dependence of the amount of Nb, going under equilibrium into solution, on the reheating temperature (T_R).

6.4 Simulation of Finishing Rolling

The TMCP simulation of finishing rolling was applied using flat compression test in the same way as described in section 5.2. The hot deformation parameters of the last three deformation steps were the same as listed in Tab. 5.2. The cooling rate has been taken following industrial conditions. The flat compression specimens were cooled after the last deformation step to the fast cooling start temperature (T^{FC}) at a cooling rate of 10 K/s until required fraction of ferrite (80 %) and austenite (20 %) was obtained and then accelerated cooled down to RT at a cooling rate of ~100 K/s (Fig. 5.1). As well known, the alloying elements affect $\gamma \rightarrow \alpha$ transformation temperatures during cooling. Therefore, the T^{FC} temperature in γ and α region changes depending on the alloying elements. Defining T^{FC} is described in section 6.5.1.

6.5 Results

6.5.1 Phase Transformation Behavior and Defining T^{FC}

To define T^{FC} deformation / dilatometric measurements had been performed on different alloys, as described in section 4.3.1. Fig. 6.2(a) displays dilatation curves of different steels during cooling stage at a cooling rate of 10 K/s where the change in length as a function of temperature is plotted. This figure represents the effect of alloying elements on the $\gamma \rightarrow \alpha$ transformation behavior. Fig. 6.2(b) shows the fraction of austenite to ferrite during cooling for different alloys. The determination of the fraction of austenite to ferrite is described in chapter 4.3.1. From these curves the transformed volume fraction of austenite to ferrite at different temperatures can be found. In this study, the fraction of ferrite and martensite in the microstructure of different DP alloys was set to 80 % and 20 %, respectively. From the transformed volume fraction curves the appropriate T^{FC} for different alloys can be determined. This is shown in Fig. 6.2(b) by dashed line for 80 % of f_α and 20 % of f_γ. From this temperature the start of fast cooling during TMCP can be performed to obtain 80 % of ferrite and 20 % of martensite.

(a)

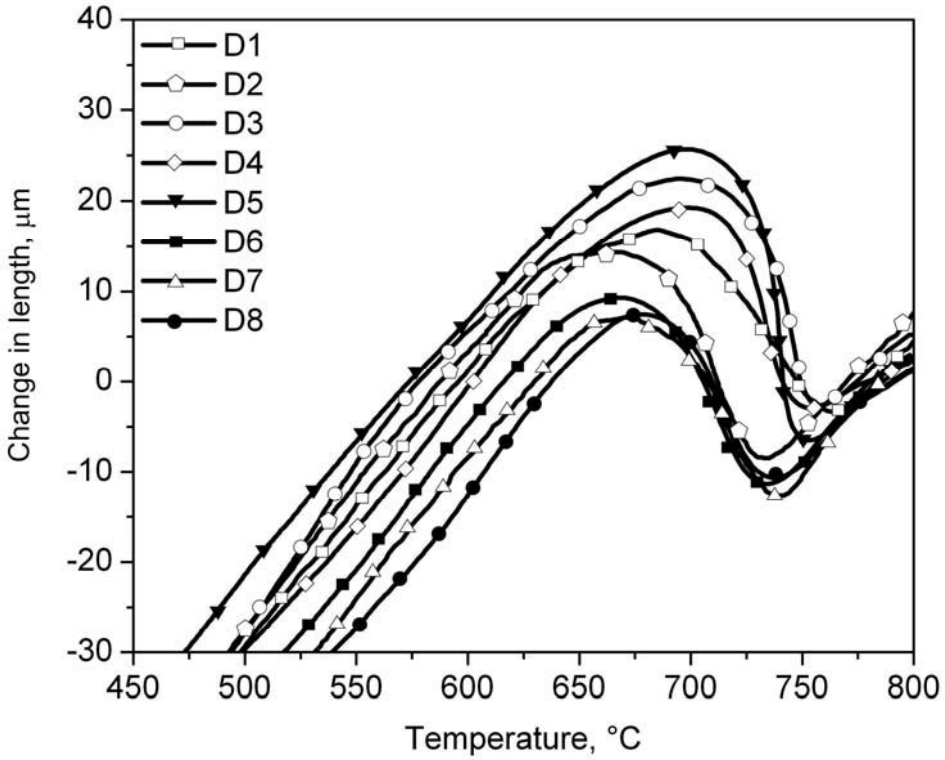

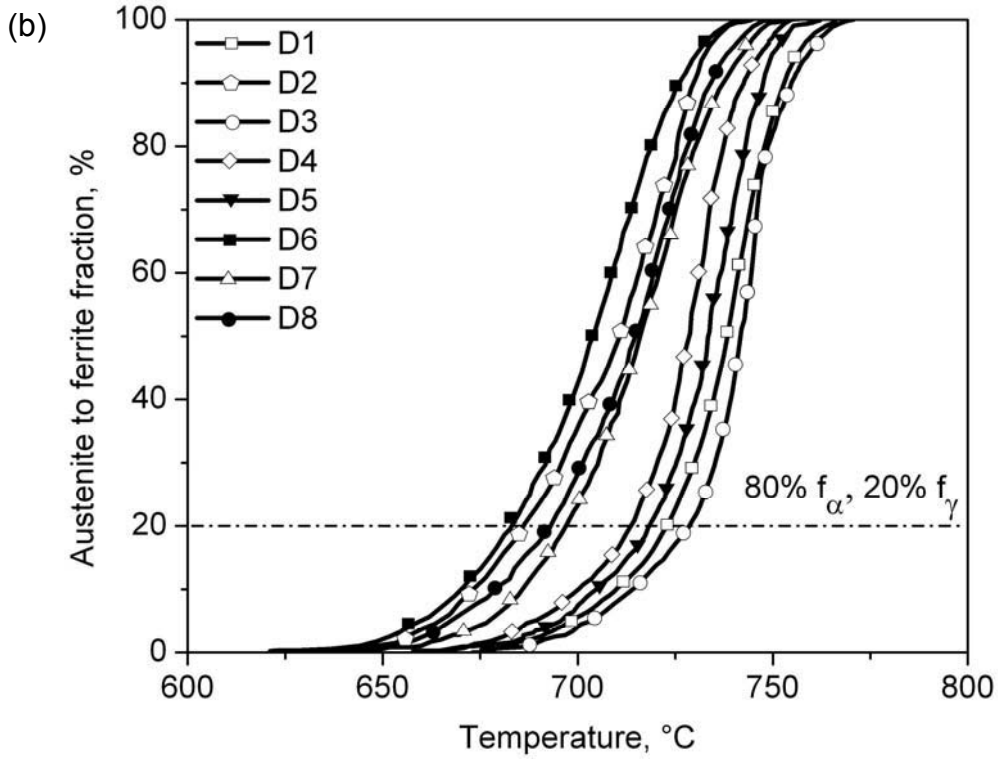

Fig. 6.2 Influence of the chemical composition on the phase transformation behavior; (a) dependences of the change in length on the temperature at $\gamma \rightarrow \alpha$ phase transformation during cooling stage at 10 K/s and (b) calculated fraction of $\gamma \rightarrow \alpha$ as a function of temperature for different alloys.

Tab. 6.2 lists Ar_3 and Ar_1 as well as determined T^{FC} temperatures. M_S temperatures of alloys obtained during accelerated cooling stage of TMCP can also be seen in this table. From Fig. 6.2 and Tab. 6.2 it can be noted that the variation of alloying elements influences Ar_3, Ar_1, M_S and T^{FC}. Alloy D6, containing the highest amount of elements reveals the lowest Ar_3 (721 °C), Ar_1 (639 °C), T^{FC} (683 °C) and M_S (395 °C), while alloy D3 with increased Si shows the highest Ar_3 (770 °C), Ar_1 (678 °C) and T^{FC} (729 °C). Increasing Si has a marginal decreasing effect on M_S (Tab. 6.2).

It is obvious that C has a strong influence on the phase transformation temperatures. Increasing C lowers these temperatures. It is also evident that Si and Nb have narrowed influence on the phase transformation temperatures. From steeply transformation slop of corresponding curve for alloy D5 (Fig. 6.2(a)) it is clear that Nb addition accelerates the $\gamma \rightarrow \alpha$ transformation. Increasing Mo lowers the Ar_3 and Ar_1 or correspondingly increases the austenite C content at the beginning of transformation with the effect to decrease M_S (discussed in section 4.4.1). One can state that alloying increments in DP steel,

which decrease the Ar_3 and Ar_1 temperatures, will in fact decrease the driving force for $\gamma \rightarrow \alpha$ transformation and for martensite formation in particular. Increasing Si from 0.1 to 0.25 % increases the Ar_3 and Ar_1 about 3 K, but has no influence on the M_S temperature. Comparing alloys D1 and D2 it is seen that the M_S decreases of about 20 K by C increasing from 0.06 to 0.09 %. The results are in a good agreement with other studies [And65, Nip03, Ouc82].

Tab. 6.2 Determined Ar_3, Ar_1, appropriate T^{FC} for f_α = 80 %, f_γ = 20 % and M_S obtained during accelerated cooling for different alloys

Steel	Ar_3 [°C]	Ar_1 [°C]	T^{FC} [°C]	M_S [°C]
D1	768	675	722	420
D2	742	638	685	398
D3	771	678	729	418
D4	757	665	715	415
D5	765	675	720	413
D6	739	635	682	395
D7	748	644	697	405
D8	745	640	693	401

Fig. 6.3 shows the change of length as a function of temperature (Fig. 6.3(a)) and corresponding curves of austenite to ferrite transformation with respect to temperature (Fig.6.3(b)) for alloys D5 and D7 which additionally were reheated at 1200 °C during the simulation of roughing rolling process. For better comparison the dilatation and austenite to ferrite transformation curves of these two alloys at the T_R of 1100 °C (Fig. 6.2) are also plotted in this figure. Tab. 6.3 presents Ar_3, Ar_1 as well as corresponding T^{FC} and M_S (obtained during accelerated cooling). For both alloys it is obvious that a higher T_R of 1200 °C lowers Ar_3, Ar_1 and the corresponding T^{FC}. M_S temperatures of both alloys reheated at 1200 °C during the roughing rolling simulation are lower than those reheated at 1100 °C.

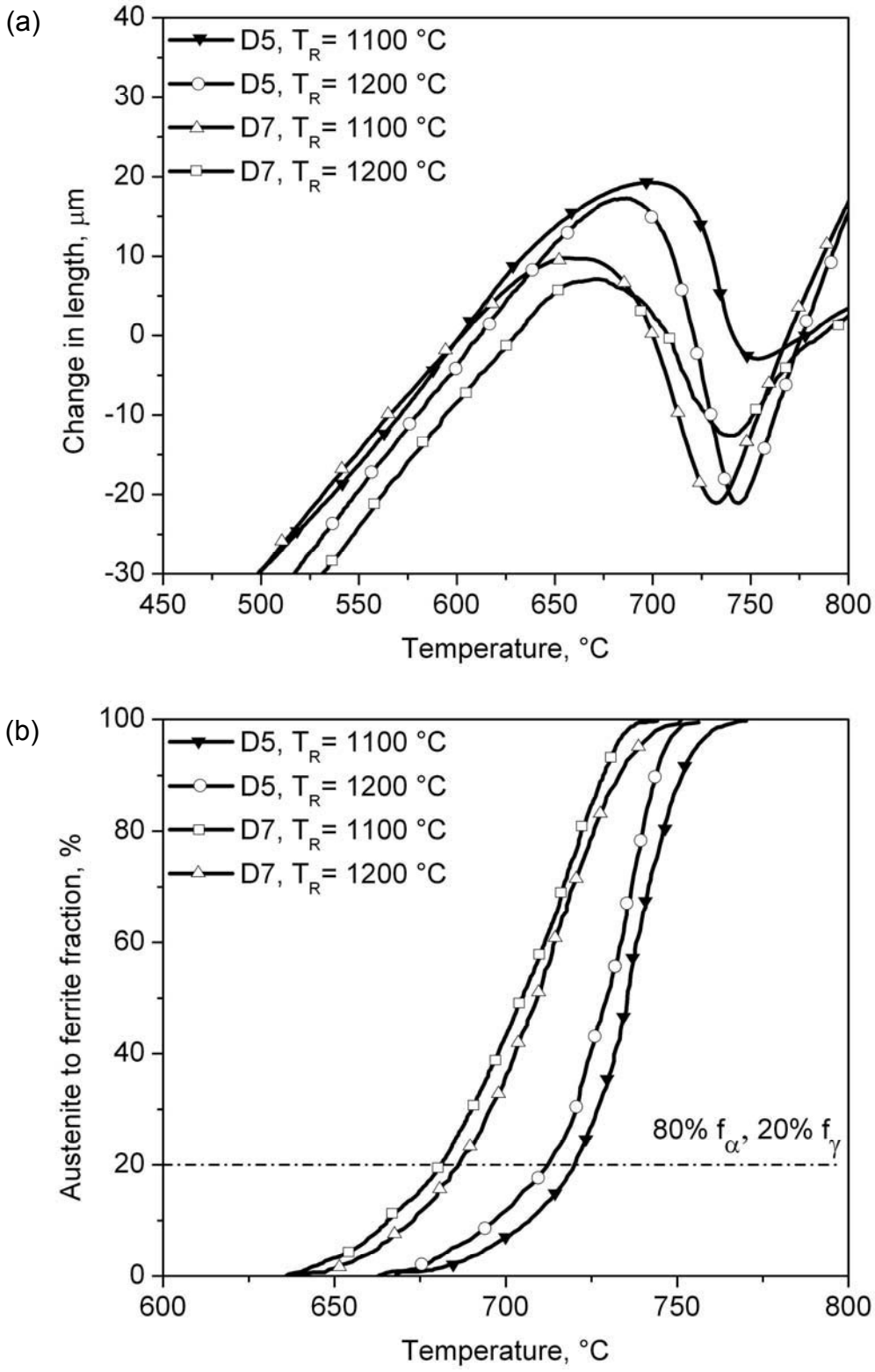

Fig 6.3 Influence of the T_R during simulation of roughing rolling on the phase transformation behavior; (a) dependences of the change in length on the temperature at $\gamma \rightarrow \alpha$ phase transformation during cooling stage at 10 K/s and (b) calculated fraction of $\gamma \rightarrow \alpha$ as a function of temperature for specimens reheated at different temperatures.

Tab. 6.3 Determined Ar_3, Ar_1 and the corresponding T^{FC} for obtaining 20 % MVF and M_S obtained during accelerated cooling for different alloys

Steel	Ar_3 [°C]		Ar_1[°C]		T^{FC} [°C]		M_S [°C]	
	$T_{R,\ 1200}$	$T_{R,\ 1100}$	$T_{R,\ 1200}$	$T_{R,\ 1100}$	$T_{R,\ 1200}$	$T_{R,\ 1100}$	$T_{R,\ 1200}$	$T_{R,\ 1100}$
D5	756	765	663	675	712	720	404	413
D7	741	748	641	644	691	695	396	405

6.5.2 Microstructure Evolution

Microstructure investigation of different alloys reveals that the grain refining effect of alloys D3 and D5 is demonstrative, whereas no refined grains are observed for other alloys. Fig. 6.4 shows exemplary the microstructure analyses of alloys D1 and D5 after TMCP. In general, the specific characteristics of the microstructural features reveal in the DP alloys with different alloying elements include:

a) The volume fraction of ferrite and martensite for all alloys is quite the same of 80 % and 20 %, respectively. The estimation of the MVF is in good agreement with the values calculated from dilatation curves.
b) Large martensite islands can be seen, but they often show dark substructures either within or in their immediate surroundings.
c) The average grain size of ferrite and martensite is finer in alloys containing low C content and addition of Nb or Si. For these alloys the grain refining effect of Nb is more visible than of Si.

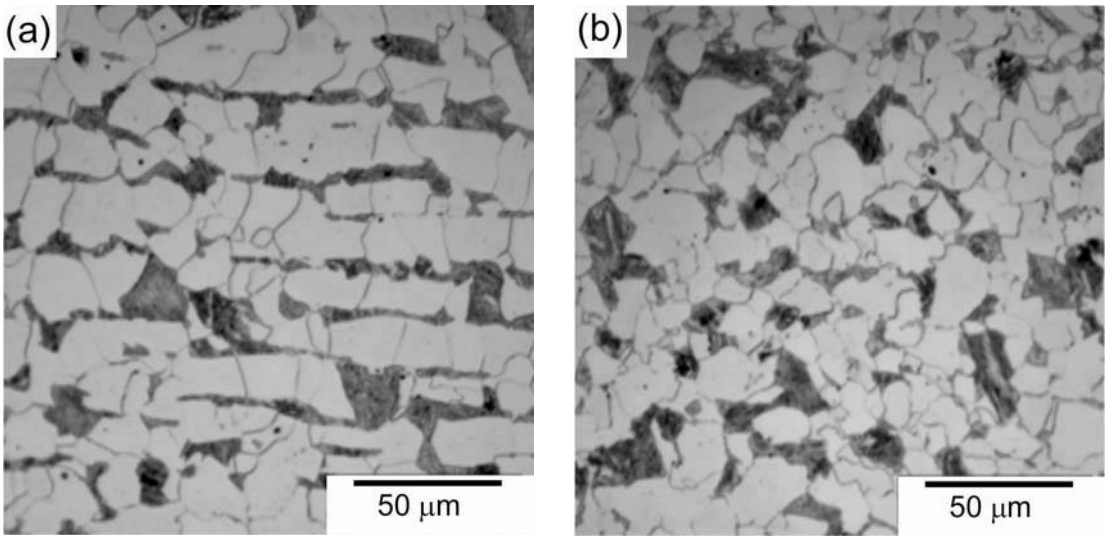

Fig. 6.4 Microstructure of DP steels showing different grains sizes obtained after TMCP: (a) alloy D1 (b) alloy D5; cooling rate of all samples in first cooling stage = 10 K/s and in second cooling stage = 100 K/s.

Tab. 6.4 compares the grain sizes of ferrite (d_α) and martensite block ($d_{\alpha'}$) being observed after TMCP for all alloys investigated. Evaluating this table fine d_α and $d_{\alpha'}$ are obtained for alloys D3 and D5, where grain refining of D5 is more noticeable. No grain refining could be found for other alloys. Whereas no differences of d_α are observed in alloys with high C content, these alloys exhibited finer $d_{\alpha'}$.

Tab. 6.4 Effect of variation of alloying elements on the grain size of ferrite (d_α) and martensite ($d_{\alpha'}$)

Steel	D1	D2	D3	D4	D5	D6	D7	D8
d_α [μm]	14.5 ± 3	13.9 ± 5	10.3 ± 6	14.2 ± 3	8.5 ± 5	14.3 ± 5	13.0 ± 4	13.5 ± 6
$d_{\alpha'}$ [μm]	11.8 ± 2	9.8 ± 5	9.5 ± 3	11.9 ± 3	6.0 ± 4	10.2 ± 2	9.1 ± 4	10.6 ± 4

Additionally, the microstructure of Nb microalloyed steels (D5 and D7) after roughing rolling simulation at different T_R temperatures was studied by thermal etching method in order to compare the influence of T_R and Nb solution on the prior austenite grain sizes (d_γ). Fig. 6.5 gives a comparison among the final structure grain sizes of prior austenite revealed by thermal etching in alloy D5. The comparison of Fig 6.5(a) and Fig. 6.5(b) suggests that d_γ decreases with increasing T_R. The same result is observed for D7. It should be noted that the samples are obtained after simulation of roughing rolling process and they are cooled after the last deformation step under air condition.

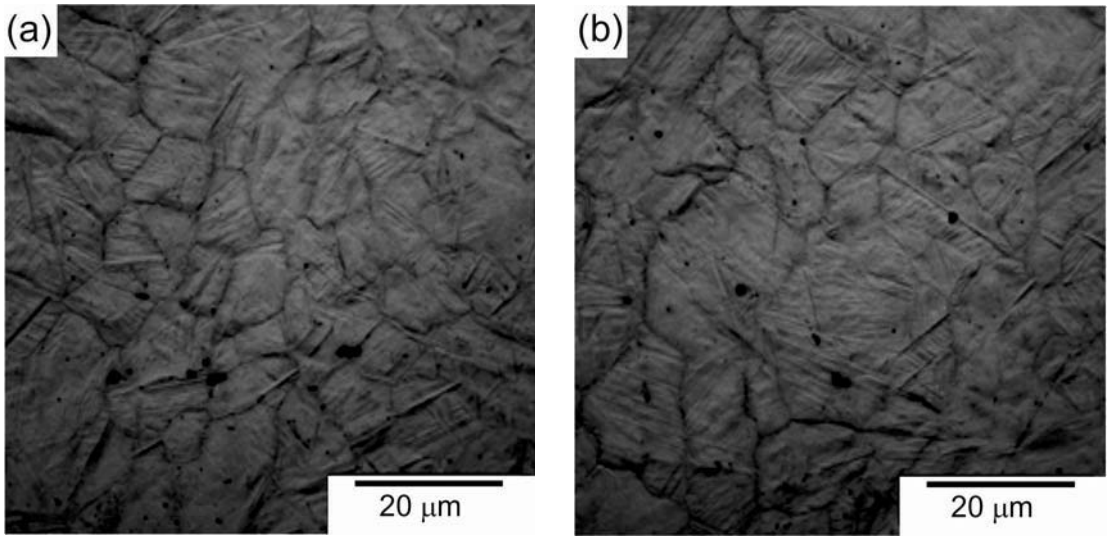

Fig. 6.5 LOM of the prior austenite grains at different temperatures revealed by thermal etching the Nb microalloyed steel D5; (a) T_R = 1200 °C (b) T_R = 1100 °C; both samples were austenitized at 950 °C and cooled at a rate of 1 K/s.

Further information about the microstructure of steel D1 after simulation of roughing rolling and finishing rolling were obtained from TEM. Fig. 6.6 represents a montage of 40 bright field TEM images from alloy D1 after TMCP providing an overview of the microstructure of ferrite and martensite phases. This figure clearly shows the F/F and F/M interfaces. The enhanced dislocation density around martensite can be visualized on this figure placing emphasis on F/M interfaces. The dominant martensite morphology of low carbon steel grades like DP steels is of lath type which is characterized by a high dislocation density [Gho06, Kim81]. The most affected areas of ferrite are in the vicinity of martensite crystals. However, the dislocation cells occasionally form with complex dislocation tangles into cell walls and free dislocations inside the cells. Dislocations inside the ferrite are distributed irregularly while in the interior of the grains a relatively low dislocation density is usually observed. At the F/M interfaces, a significantly higher dislocation density is present due to the volumetric expansion from austenite to martensite by accelerated cooling during TMCP [Jac01, Man93].

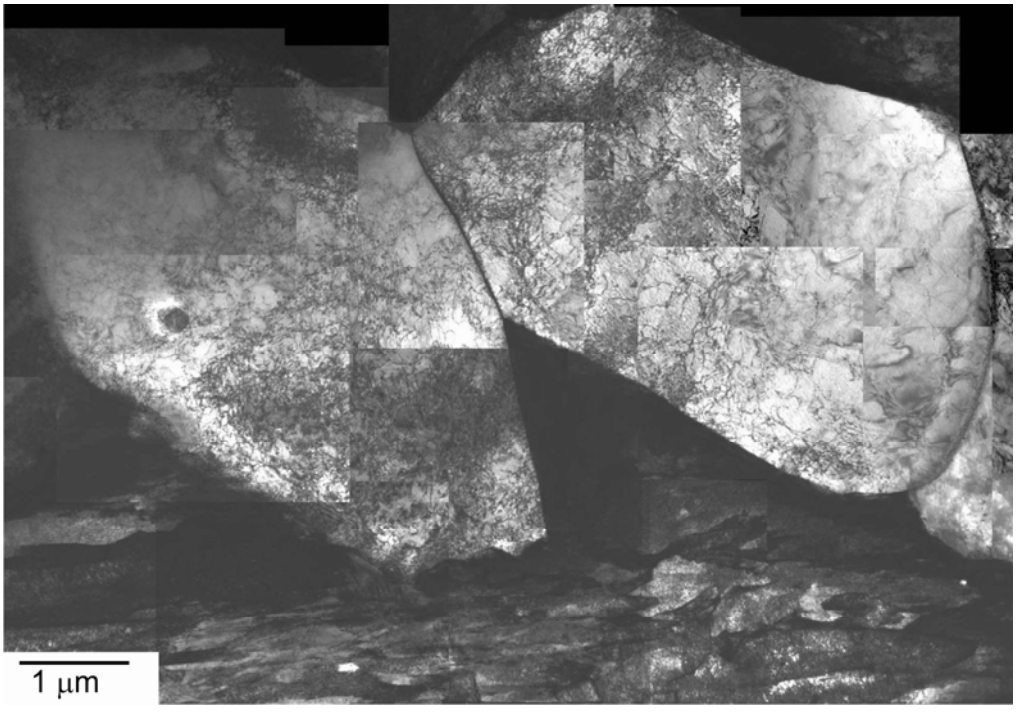

Fig. 6.6 Montage of 40 bright field TEM images from alloy D1 after TMCP showing microstructure of ferrite and martensite phases and dislocation distribution within ferrite and at F/F and F/M interfaces.

6.5.3 Mechanical properties

Mechanical properties corresponding to all of the investigated alloys after TMCP are displayed in Fig. 6.7. Stress vs. strain curves (Fig. 6.8) have been reproduced to show changes in the yielding behavior of different alloys. Evaluating the different alloys of DP steel, a pronounced influence of the chemical compositions on mechanical properties is obvious. It should be mentioned that the amount of martensite is kept the same for all alloys. Among the alloys with higher C content, D8 indicates the highest level of ultimate tensile strength (R_m) and yield strength ($R_{p0.2}$) combined with a narrowed total elongation (TEl) as compared to those of alloy D1. This alloy shows a R_m of (728 ± 18) MPa and $R_{p0.2}$ of (469 ± 14) MPa. The TEl value of this alloy is (14 ± 0.5) %. For alloy D1 (basic steel) R_m = (607 ± 15) MPa, $R_{p0.2}$ = (375 ± 12) MPa and Tel = (20.5 ± 1) % was found. Alloy D6 with the same alloying elements as D8 but more Nb content demonstrates nearly the same level of strength as alloy D8 but a slightly higher ductility. Alloys D2 (with higher C content) and D7 (with higher C and Nb content) show also high strength levels but lower than alloys D6 and D8. D2 and D7 reveal a higher ductility than alloys D6 and D8.

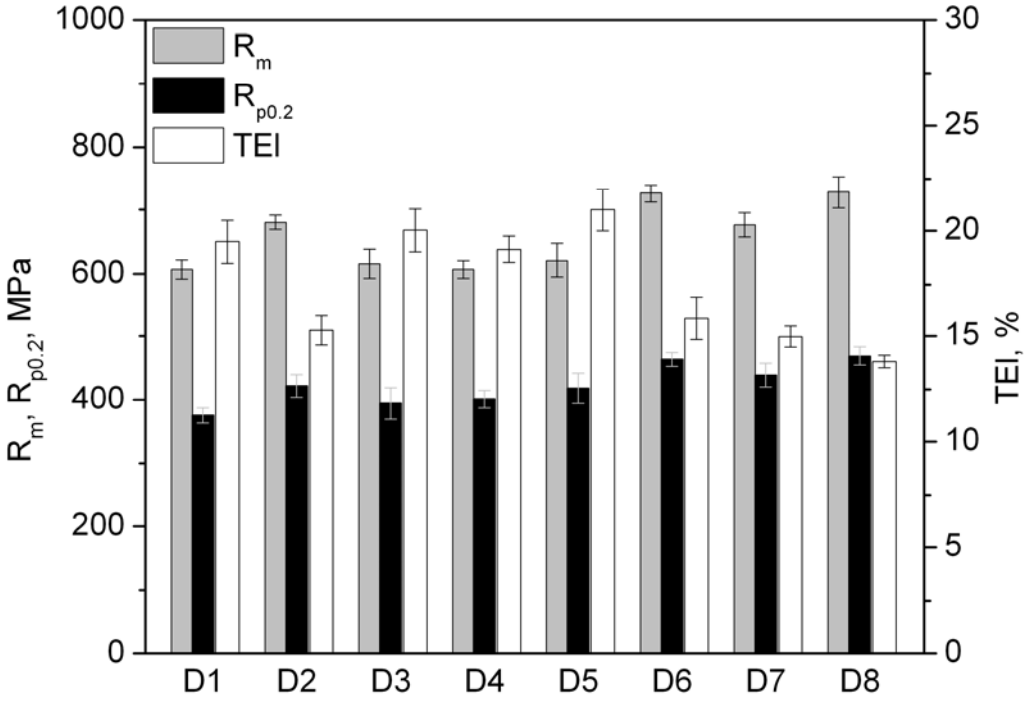

Fig. 6.7 Tensile strength (R_m), yield strength ($R_{p0.2}$) and total elongation (TEl) dependence on the chemical compositions of DP steel produced by TMCP way.

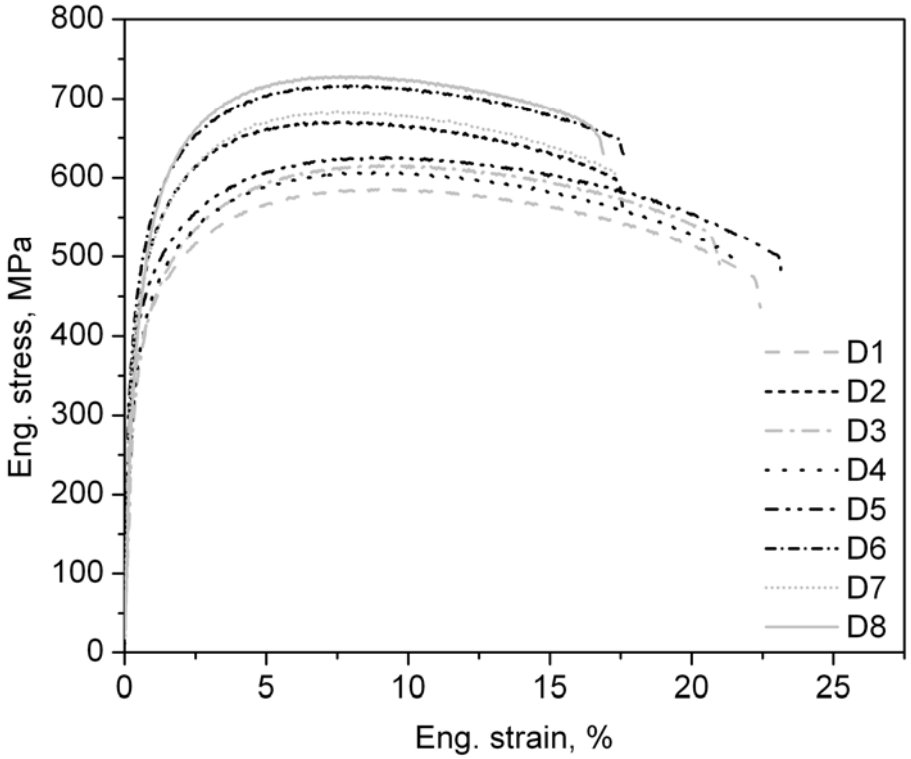

Fig. 6.8 Engineering stress-strain curves of DP steels containing different amount of alloying elements. The DP steels having 20 % of MVF are obtained by TMCP way.

In fact, the strengthening effect of DP steels generally increases with increasing C content. Thus, C is the most effective element in increasing strength of low carbon steels and reveals an essentially strong effect in DP steels together with increasing Si, Mo and Nb approaching to 0.25, 0.25 and 0.04 %, respectively.

Among alloys without C addition, D3 with the highest Si content indicates nearly the same strength and ductility level as D4 with the highest Mo content. The tensile curves of D3 and D4 show that very similar properties are achieved for these steels. R_m close to 620 MPa was found for both alloys. No significant differences were observed for the elongation properties. Among the alloys without any C addition, the highest values of R_m and $R_{p0.2}$ were observed in Nb microalloyed steel (D5). In all cases, addition of Nb seems to improve ductility.

Fig. 6.9 illustrates the stress-strain curves of two Nb microalloyed steels D5 and D7 and reheated at temperatures of 1100 and 1200 °C during simulation of roughing rolling process. Comparing these T_R temperatures a higher strength and simultaneously higher ductility after reheating at 1200 °C was observed for the both steels. For both T_R temperatures, alloy D7 having more C content is characterized by a larger $R_{p0.2}$ and R_m. The elongation properties of D7 are

lower than for D5. Under the same temperature conditions alloy D7 reached values of R_m = (676 ± 19) MPa and (703 ± 14) MPa, Tel = (17 ± 0.5) % and (18 ± 0.5) %, respectively. D5 reached R_m = (621 ± 23) MPa and (621 ± 17) MPa and Tel = (22 ± 1) % and (24 ± 1) %, respectively.

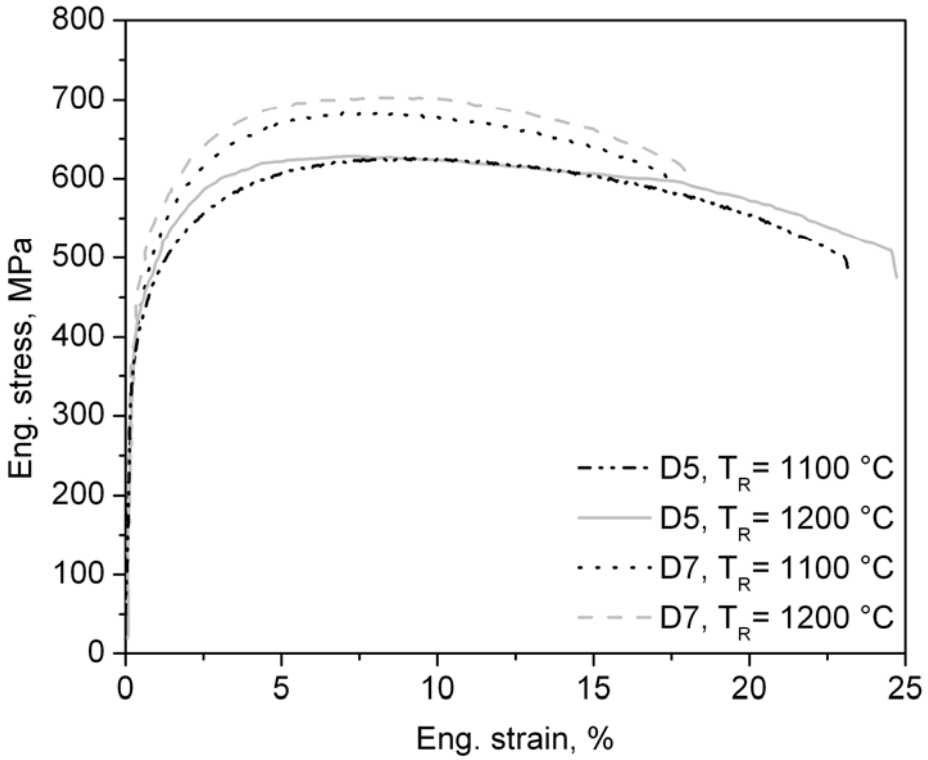

Fig. 6.9 Engineering stress-strain curves of alloys D5 and D7 containing Nb addition at different T_R temperatures.

6.5.4 Bake Hardening Behavior

This section considers the differences resulting from the different steel compositions after prestraining and baking condition. For these steels the two BH parameters - prestrain and baking temperature - were varied. The samples were prestrained at 0, 2 and 5 % and baked at 170 and 240 °C. The results of these experiments are presented a) in terms of changes in the ultimate tensile strength and b) in terms of BH values. Fig. 6.10 presents R_m values of all alloys with respect to prestraining at different baking temperatures. For better discrimination and illustration, some bar charts have been reproduced to show changes in the R_m behavior with respect to temperature of paint baking simulation at different prestrains (Fig. 6.11). Many interesting conclusions can be taken from these figures. In general, it can be noted that for all alloys R_m increases after PS and BH, as expected. The increase of R_m after PS and BH is more visible by increasing C content in the investigated alloys. Similar to the

condition before PS and BH, alloys with increasing C demonstrate larger strength level after PS and BH compared to alloys without increasing C.

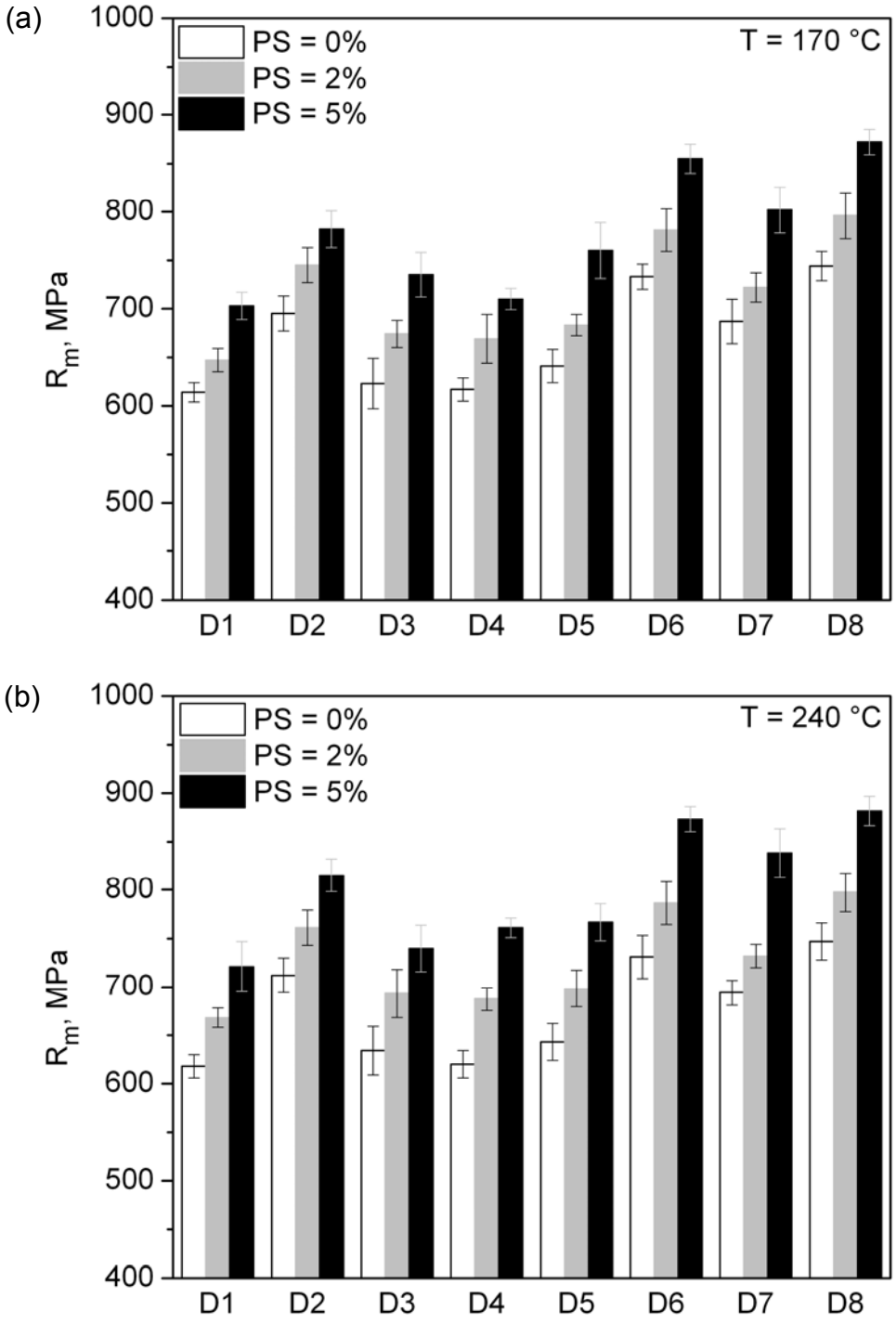

Fig. 6.10 Influence of prestraining on the tensile strength (R_m) of DP alloys; at PS = 0, 2 and 5 %; (a) T = 170 °C; (b) T = 240 °C; holding time for all conditions was t = 20 min.

The behavior of R_m with respect to prestrain can be described as follows (Fig. 6.10). While without any PS no distinct increase of R_m is found, R_m rises

steeply, when the PS is increased, reaching its maximum with the maximum amount of PS = 5 %. These observations are valid for all alloys.

The influence of baking temperature, been displayed in Fig. 6.11, can be described in general as a significant increase of R_m values at standard temperature of 170 °C, reaching the highest level by further increasing baking temperature up to 240 °C for all alloys at different prestrains.

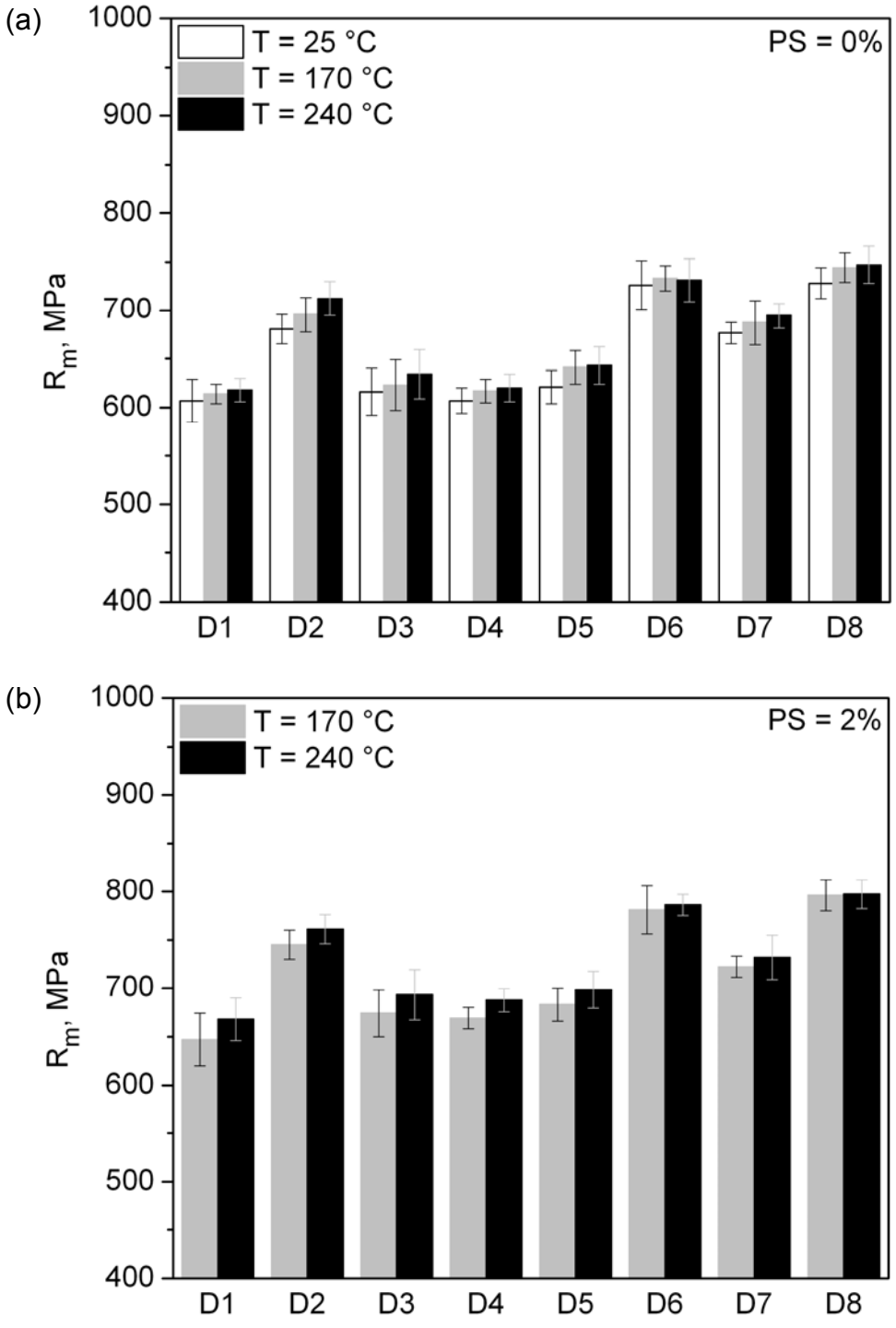

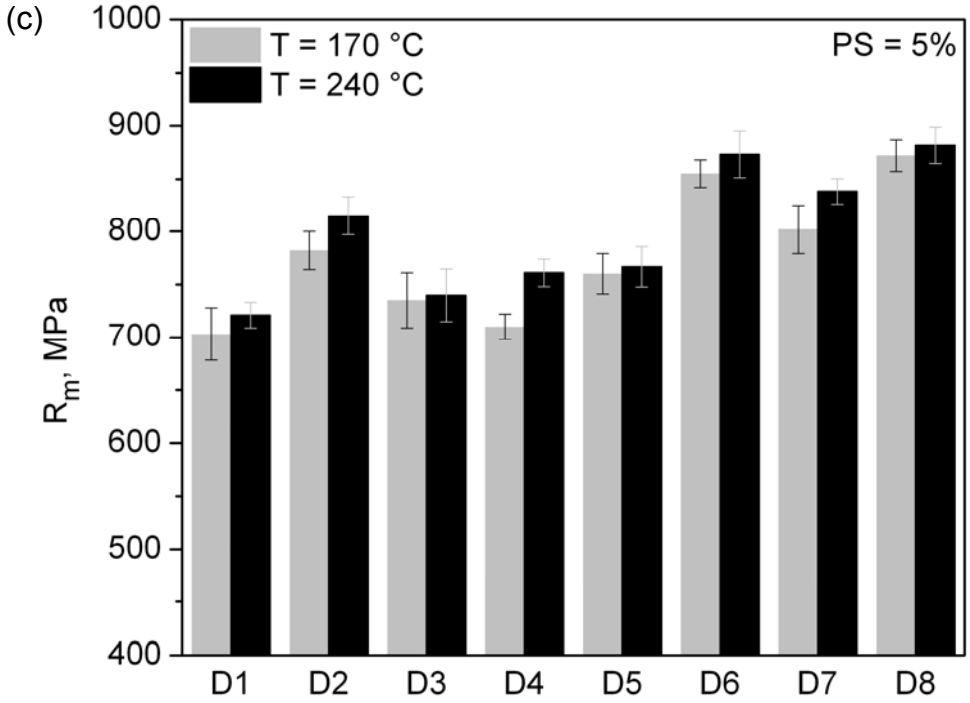

Fig. 6.11 Influence of baking temperature on the tensile strength (R_m) of DP alloys; (a) PS = 0 %, T = 25, 170, 240 °C; (b) PS = 2 %, T = 170, 240 °C; (c) PS = 5 %, T = 170, 240 °C; holding time for all conditions was t = 20 min.

In Fig. 6.12 the BH_0, BH_2 and BH_5 values of different alloys with respect to baking temperature are shown. These figures yield some clues about the possible mechanisms contributing to the BH behavior of DP steels. Considering the BH behavior under amounts of prestraining a higher BH level is found for prestrained steels (BH_2 and BH_5) than for non-prestrained ones (BH_0). The greatest level of BH is obvious for steels prestrained at 5 % (BH_5). Comparing the different baking temperatures (170 and 240 °C), clearly higher BH values are found for 240 °C. This difference between 170 and 240 °C is more demonstrative for BH_2 and BH_5 at prestrained condition. It is of less evidence for BH_0, when samples are not prestrained.

Evaluating the alloys with respect to their chemical composition the following results can be stated: Two main groups may be obtained from both the properties and the R_m balks: alloys containing the lowest and highest C content. Comparing the alloys with the highest C content, D2 and D7 show a high strength level but it is lower than that ones of the alloys D6 and D8 (Fig. 6.10 and Fig. 6.11). Among these alloys, D7 has the lowest R_m after PS and BH. Similar to the condition after TMCP (previous section), the highest R_m level is found for the alloys D6 and D8.

Comparing the alloys with respect to BH values, D2 and D8 demonstrate the highest BH values with a prestrain of 2 and 5 % (Fig. 6.12). For alloy D6 a high level of BH, but slightly lower than for D2 and D8, is found for these conditions, while D6 without prestraining shows a higher BH level than alloy D2 under comparable conditions. Among the steels with the highest C content, D8 exhibits the largest BH, while D7 reveals the smallest one.

In general, for alloys with a low C content a lower R_m level after PS and BH is found compared to alloys with higher C content (Fig. 6.10 and Fig. 6.11). Among these alloys, D5 demonstrates the highest strength level after PS and BH, whereas D1 (basic steel) indicates the lowest strength level.

Evaluating the low C content alloys with respect to BH behavior, a significantly higher BH level is obtained for Nb microalloyed steel D5 after PS and BH with different conditions (Fig. 6.12). D5 presents a comparable BH level to D7 with high C content. D3 shows also high BH values after PS and BH which are still lower than those of D5. For alloys D1 and D4 nearly the same BH level is observed in all conditions of prestraining and baking. However, D4 has a higher BH level than D1.

(a)

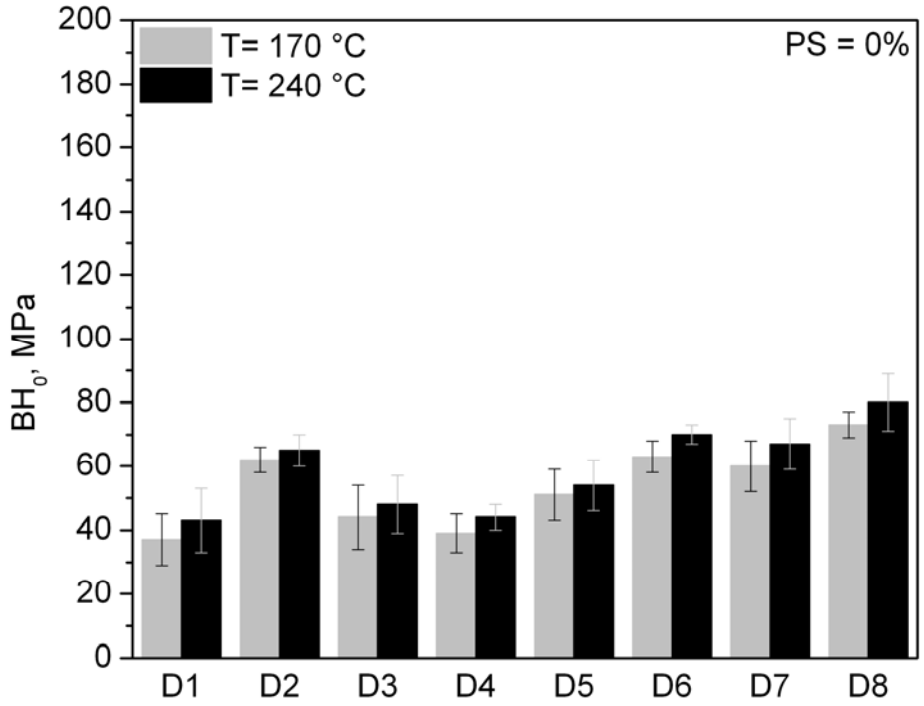

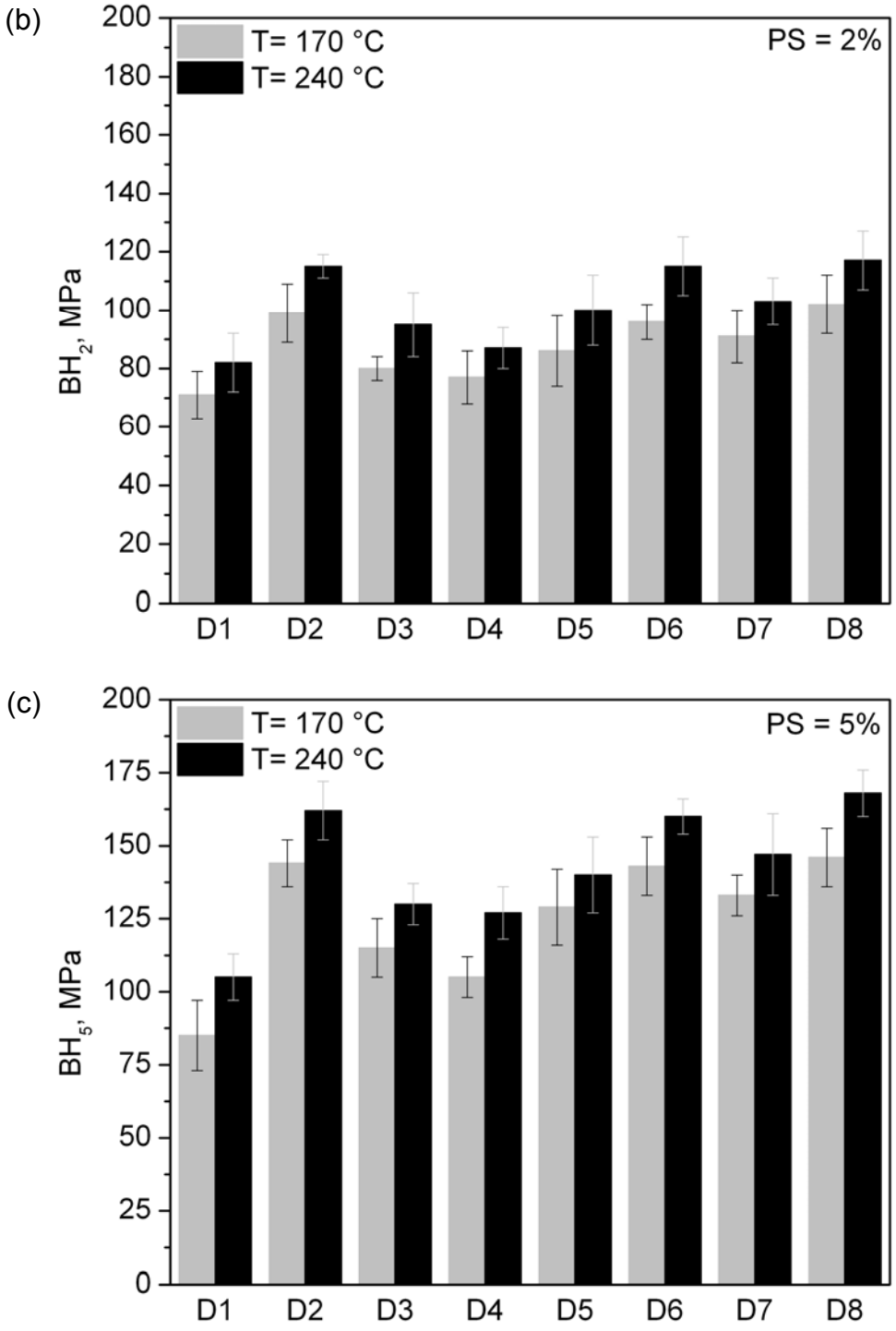

Fig. 6.12 Influence of variation the chemical composition in the DP steel on (a) BH_0, calculated from difference between $R_{p0.2}$ of the tensile sample and R_e of the respective BH sample; (b) BH_2 and (c) BH_5.

6.5.5 Microstructure Evolution after Prestraining and Baking Process

TEM analyses were conducted on alloy D1 after TMCP without any prestraining at RT and at T = 170 and 240 °C. Since no significant differences with regard to the morphology and dislocation distribution of ferrite were found in alloy D1 for

the given conditions, only TEM images of martensitic phases are evaluated in this section.

Fig. 6.13 provides overviews on martensite structure in different conditions. The martensite morphology, showing packets of laths with different orientations, can be seen more clearly from this figure. In addition to this, a number of very small particles, most probably carbides, within single laths can be observed in these figures. TEM experiments on sample baked at temperatures of 170 °C / 20 min (Fig. 6.13(b)) yielded no significant differences to the microstructure of basic steel (Fig. 6.13(a)). Clear changes in the martensite phase were observed after BH simulation at 240 °C / 20 min. In contrast to the martensite morphology of sample without baking treatment, strong tendencies for the martensite phase to decompose are found in heat baked state at T = 240 °C (Fig. 6.13(c)). Such decomposition does not necessary affect the whole structure all at once, but parts of the martensite may keep their initial structure. The formation of carbides can also be observed from Fig. 6.13(c) showing small carbide particles inside of lath martensite. Diffraction patterns confirmed that the carbides are of Fe_3C type (Fig. 6.13(d)). They indicate possible martensite aging as a result of the baking process.

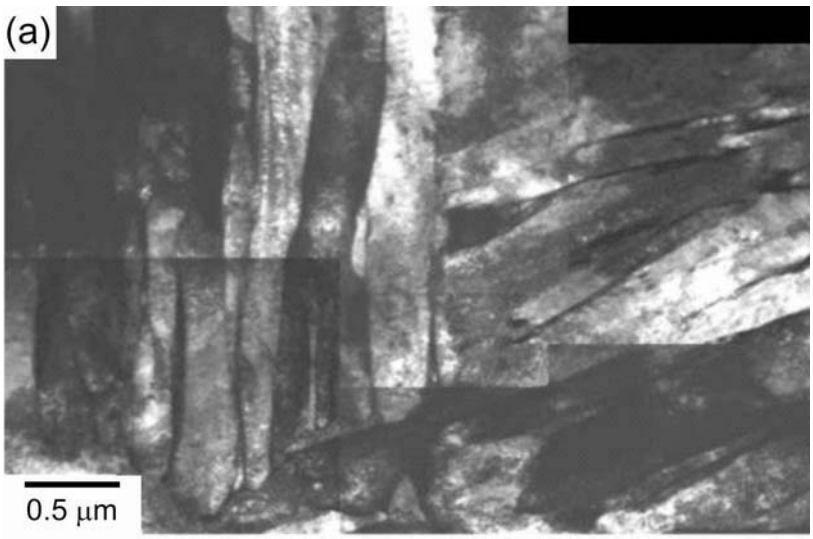

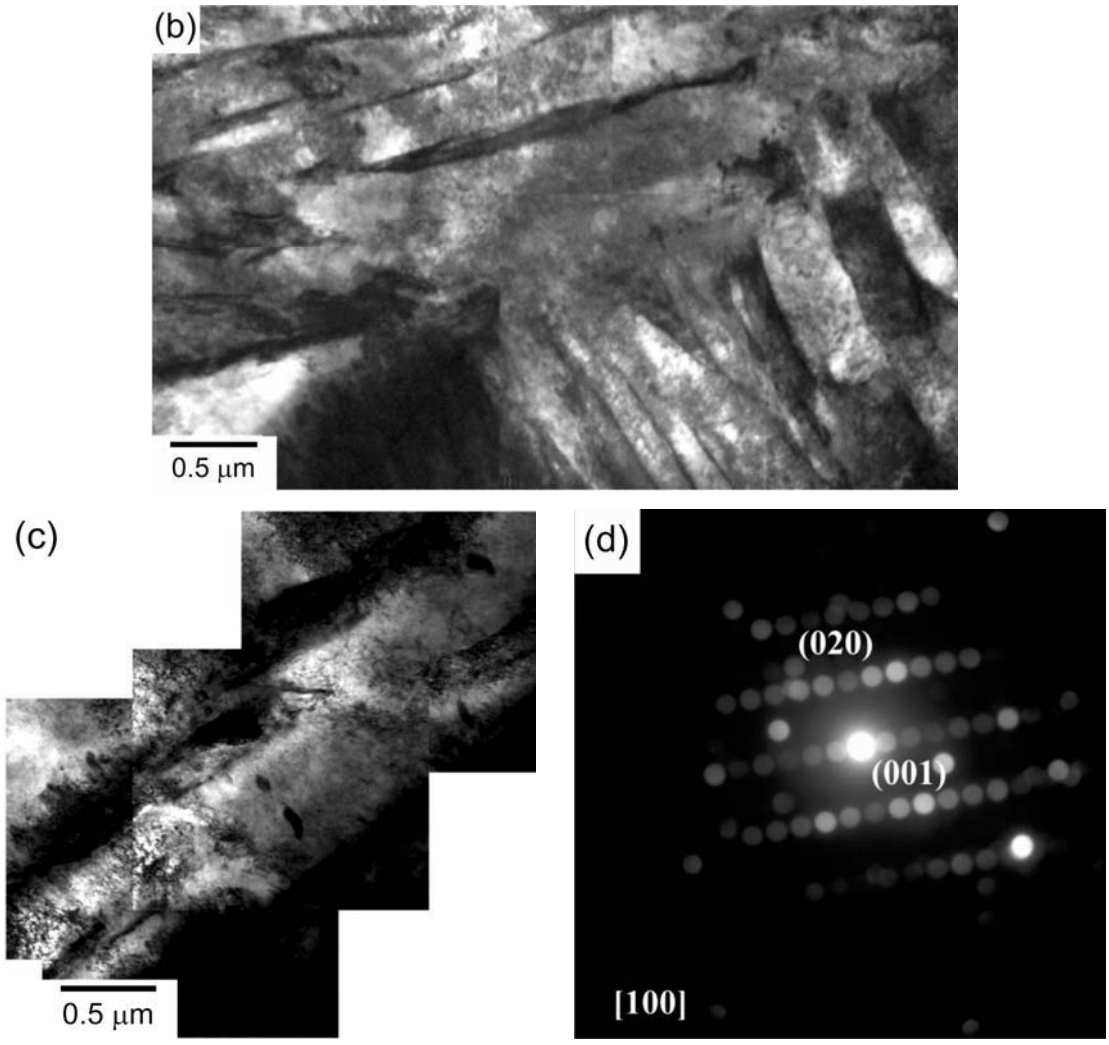

Fig. 6.13 TEM micrographs showing lath martensite, obtained from steel D1 after TMCP (a) without PS and BH; (b) after PS to 2 % and BH at 170 °C for 20 min; (c) after PS to 2 % and BH at 240 °C for 20 min and (d) diffraction pattern from cementite within single laths.

6.6 Discussion

6.6.1 Influence of Alloying Elements on the Phase Transformation Behavior

The results of transformation behavior (section 6.5.1) indicate that increasing C and Mo content lowers $\gamma \rightarrow \alpha$ and $\gamma \rightarrow \alpha$' transformation temperatures. Increasing these elements shifts Ar_3, Ar_1 and M_S towards lower temperatures. This effect is more significant for increasing C. Increasing Si has a negligible rising influence on the transformation temperatures.

As well known, the final mechanical properties depend upon the kinetics of the austenite to ferrite and martensite transformation, which is strictly related to phase stability, mostly dependent on C concentration in austenite [Lee02, Ryu02, Shi06], the size and arrangement of particles of this phase as well as its

strength and the present state of stress [Hai06, Tim03]. Thermodynamic stability of austenite is described by the temperature of ferrite start transformation Ar_3, expressed most often by Eq. 6.1 [Ouc82]:

$$Ar_3 = 910 - 310C - 80Mn - 20Cu - 15Cr - 80Mo - 55Ni \quad \text{(Eq. 6.1)}$$

where alloy contents are in wt. % and Ar_3 temperature is in °C. In agreement with our findings Mo decreases Ar_3 and is found to be an austenite stabilizer [Ble02]. Alloy D4 having increased Mo shows lower Ar_3 and Ar_1 than alloys D1 (Fig. 6.2). Furthermore, it is noted that Mo has the retardation effect on the austenite transformation to ferrite rendering the process control more manageable [Cap05]. On the basis of Eq. 6.1, the effect of γ phase stabilization obtained by Mo is substantially weaker compared to C. For this reason, determination of changes of C concentration in γ phase according to the conditions of TMCP has a fundamental significance for DP steels.

In the case of multiphase steels, taking into consideration Si is also very essential. The modification of Eq. 6.1 regarding Si is achieved by [Nip03], who modified the dependence (Eq. 6.1) into the following form:

$$Ar_3 = 879 - 516C - 66Mn + 38Si + 284P \quad \text{(Eq. 6.2)}$$

where alloy contents are in [wt. %] and Ar_3 temperature is in [°C]. On the basis of Eq. 6.2, it can be observed that Si has a small rising influence on the Ar_3 temperature, which is in good agreement with own investigations (alloy D3 in Fig. 6.2), as distinct from Mn, which has a stabilizing effect on retained austenite [Mur06, Soe04, Van02]. Mano et al. [Man82] showed that in a DP steel containing Si the ferrite starting temperature curve of the continuous cooling transformation diagram shifts towards the left. Elsewhere [Joa81] the same effect was reported. The formation of ferrite was found to accelerate the ferrite formation as a result of Si enhancement in Si-Cr-Mo DP steels. This may be attributed to the increased dislocation density which facilitates “pipe diffusion” thus, enabling partitioning of solute atoms from austenite to ferrite and resulting in more ferrite formation.

It can be seen from both equations that the influence of Nb on Ar_3 is not considered. From Fig. 6.2(a) it is also evident, that addition of Nb shows no significant influence on the Ar_3, Ar_1 temperatures but accelerates the $\gamma \rightarrow \alpha$ transformation (steeply slop of transformation curve for alloy D5). This is due to the grain refining effect (discussed elaborately in section 4.4.1) of Nb on

austenite, leading to the accelerated $\gamma \rightarrow \alpha$ transformation. In [Bau81] Nb has been classified as austenite stabiliser when added in amounts less than approximately 0.05 %.

From Tab. 6.2 it is obvious that M_S decreases by increasing C, Si, Mo and Nb content during accelerated cooling. The influence of C on M_S is more visible. It is reported that M_S is mainly a function of C content, i.e. by increasing C content M_S decreases [And65, Gra09]. Increasing C increases C content in the austenite. According to Fig. 4.14, C becomes enriched in the remaining austenite as a consequence of ferrite formation during the $\gamma \rightarrow \alpha$ transformation. Therefore, higher austenite C contents retard transformation to martensite upon cooling to RT [Goe87, Sug92, Wen05, Yue97]. The influence of increasing C on the M_S was reported by [Mey99]. He pointed out that the high C content results in the stabilization of austenite and decreasing M_S.

From Tab. 6.2 it can be seen that addition of Nb and Si lowers the M_S. It could be due to the effect of these elements on the d_γ. As mentioned in section 6.5.2, addition of Nb and Si results in decreasing prior austenite and thus ferrite grain size. Due to smaller austenite grain size the amount of strain (generated by austenite to martensite transformation) in the austenite phase region becomes sufficiently large. Therefore, the motion of glissile interfaces becomes impossible and causes the blockage of martensitic transformation [Nad08]. Consequently, a higher driving force for the martensitic transformation is required which can be provided at lower temperatures. Hence, the M_S temperature is decreased to lower temperatures. Takaki et al. [Tak93] examined the influence of austenite grain size in a Fe-Mn alloy and concluded that the amount of athermally transformed martensite becomes smaller with decreasing austenite grains. Finally, the dependence of the M_S temperature on austenite grain size in a Fe-Mn-Si-Cr alloy was investigated by Jiang et al. [Jia95], who stated that the start temperature of martensite is raised in larger austenite grains.

Furthermore, the lowering effect of Mo on M_S is in agreement with [And65]. As mentioned before, it can be stated that alloying increments in DP steel, which decrease the Ar_3 and Ar_1 temperatures, will in fact decrease the driving force for martensite formation and thus decrease the M_S temperature.

Additionally, dilatometric investigations show that varying T_R temperature during simulation of roughing rolling influences $\gamma \rightarrow \alpha$ transformation kinetics during

simulation of finishing rolling in a pronounced way (Fig. 6.3). From this figure it can be seen that the $\gamma \rightarrow \alpha$ transformation starts faster at lower T_R for both alloys. LOM observations (Fig. 6.5) show that the higher T_R results in finer prior austenite grains owing to dissolution of Nb in γ matrix, which is confirmed by ThermoCalc analysis (Fig. 6.1). Indeed, the decreasing prior austenite grains increases the nucleation sides at which the first ferrite subunits nucleate. Thus, the transformation starts faster due to an enhanced nucleation rate. The transformation then proceeds by nucleation and grow of new subunits from the tip of the previous ones towards the interior of the austenite grain. Furthermore, at lower T_R Nb possibly depletes C in γ matrix of both steels to form Nb(C, N). Thus, when the undissolved Nb(C, N) particles are increased the transformation proceeds in a slower rate [Hua01, Jac04, Mat04]. Therefore, it could be assumed that a lower C content is contained in γ matrix of both steels, leading to an increase of Ar_3.

6.6.2 Influence of Alloying Elements on the Microstructure

From the microstructural examination after TMCP it is obvious that alloying elements influence the ferrite and martensite grain size (section 6.5.2). Comparing the microstructure investigation of alloys (Fig. 6.4 and Tab. 6.4), the finest ferrite grain size can be obtained for the alloys D3 and D5 with increasing Si and Nb, respectively. It is reported that increasing Nb supersaturation in austenite is associated with increasing T_{nRX} [Pal96]. Zhu et al. [Zhu08] stated the same effect for Si. On the other hand, for a fixed rolling schedule which includes a specific number of roughing and finishing passes, the higher the T_{nRX}, the larger will be the amount of rolling strain imparted in the non-recrystallization region of austenite. This leads to a finer austenite grain size. Thus, increasing Nb and Si decreases the ferrite grain size due to increasing T_{nRX}.

For alloys having the highest addition of carbon (D2, D6-8) no noticeable difference in ferrite grain size but smaller martensite blocks were observed (Tab. 6.4). The observed refinement is a consequence mainly of the ability of high C content and low transformation temperature to enhance the strength of the austenite. It is expected that the martensite laths would become thinner as the yield strength of the austenite, from which they are formed, increases [Sin98]. As stated before, the high C content results in decreasing M_S.

Therefore, a lower fast cooling start temperature (T^{FC}) is required (Tab. 6.2) to expand the γ region and provide the same amount of martensite in the final microstructure of DP steels. Due to lower T^{FC} temperature, the mechanical stability of austenite increases and as a result, a higher driving force for martensitic transformation is needed [Nad08]. Thus, a high C content directly refines the martensite by strengthening the austenite and indirectly by lowering the M_S temperature and thus allowing performing the martensite transformation process at lower temperature.

Ankara et al. [Ank66] described that the lath shaped martensite transformation is often associated with grain boundaries. In contrast to the present observations, they found that the higher C content results in a coarser primary austenite grain size due to lower M_S temperature, i.e. larger martensite. Therefore, a nucleation argument would suggest that the finer grain sizes result in higher M_S temperatures, i.e. easier nucleation since grain boundary areas increase.

It has to be noted that a higher C content may lead to the existence of untransformed austenite in the microstructure, which is known to be detrimental to the mechanical properties. The incomplete transformation phenomenon, which limits the amount of martensite that can be formed at any temperature, is the reason for the existence of some regions of untransformed austenite [Aar06, Bha04].

6.6.3 Influence of Alloying Elements on the Mechanical Properties

Evaluating the results of mechanical properties for different alloys (section 6.5.3), a pronounced influence of alloying elements on the mechanical properties is obvious. In fact, multi phase steels rely on a combination of several strengthening mechanisms: structural refinement, precipitation strengthening and solid solution strengthening [Pal96]. Based on these mechanisms the influence of each element on the mechanical properties will be separately discussed as follows:

Influence of C: For alloys with the highest C amount a very high level of R_m and $R_{p0.2}$ combined with a narrowed TEl is obtained (Fig. 6.7 and Fig. 6.8). The high strength effect of these alloys is due to the effect of C which is the most hardenability enhancer and austenite stabiliser [Ble02]. C strengthens the martensite in DP steels as it is an effective solid solution strengthener. The

amount of martensite, which is the most effective phase in strengthening of DP steel, should be nearly the same for all steels investigated. From microstructure investigations it can be seen that increasing C has no influence on the ferrite grain size. Thus, the main factor governing the mechanical properties is the amount of solute C. The main part of this C is found in the C rich phases like martensite. Additionally, C is the most effective element in promoting ferrite strengthening. There are still reasons to assume that some C is dissolved in ferrite as well, resulting from the fast cooling after TMCP.

Influence of Si: The DP steel was investigated in two different Si contents of high and low level. The alloy D3 with higher Si contents results in somewhat higher $R_{p0.2}$, R_m and lower TEl than alloy D1 with lower Si contents (Fig. 6.7 and Fig. 6.8). As argued in previous section, the ferrite grain size becomes finer with increasing Si content. This leads to an increase in values of $R_{p0.2}$ and R_m through the Hall-Petch relationship (Eq. 4.4). Furthermore, Si as very effective substitutional solid solution strengthening element strengthens ferrite and thus can enhance the overall strength of DP steels [Ali63]. Si also strengthens the martensite by causing the partitioning of C to the austenite thus increasing its hardenability and the strength of the resulting martensite phase [Kot79]. Moreover, Si helps to retain C-enriched-austenite by suppressing cementite precipitation from austenite [Les78, Ray82]. However, little information is available as to the effect of this element upon the tensile ductility, especially at very fine grain sizes.

Influence of Mo: Increasing Mo in the alloy D4 indicates an enhanced effect on strength. The effect of Mo on the mechanical properties is similar to the effect of Si. As can be observed in Fig. 6.7 and Fig. 6.8, Mo raises the strength of DP steel. This can be due to a solid solution hardening effect of Mo. Moreover, Mo lowers the activity of C in austenite and promotes carbide formation from the thermodynamic point of view [Cap05]. It is noted that Mo is a strong carbide forming element and may lead to the formation of its carbides in addition to Fe_3C in the martensite and bainite regions [Ram79]. Although, Bleck has reported a contrary effect of Mo. Due to the strong solute drag effect, the carbide precipitation seems to be retarded in the presence of Mo [Ble02]. To achieve a significant increase in strength only small amounts of Mo are needed [Tra99].

Alloys D6 and D8 containing the highest amount of C, Si and Mo exhibit a quite high strength level. Probably, mutual effect of Mo together with other elements such as C and Si provides reasonable conditions to have higher strengthening by keeping the benefits of acceptable C content. The additions of Mo to Nb bearing steels were reported to bring about an improvement of the combination of strength and ductility and to constitute another possibility of lowering the silicon level [Ble02, Bou98].

Influence of Nb: The addition of Nb improves the strength and ductility of DP steel (alloy D5) as can be seen from Fig. 6.7 and Fig. 6.8. On the other hand, for this alloy finer ferrite grain sizes were observed (Fig. 6.4 and Tab. 6.4). It has been reported that Nb microalloying yields a significant grain refinement causing a clear increase in strength in hot rolled DP [Mon07]. The influence of austenite grain size on the transformation rate was already shown and modelled by Rees and Bhadeshia [Ree92]. Current practice has placed much emphasis on the study and application of Nb addition to HSLA steels, as it is deemed the most beneficial microalloying element, since it promotes austenite pancaking. The highly work hardened pancaked austenite provides numerous nucleation sites for the ferrite during the subsequent transformation which give very fine ferrite grains [Ouc77]. The high austenite contents are a result of the combination of the different mechanisms including grain refinement, C enrichment, and martensite nucleation inhibition [Ohl02]. Nb may also result in mechanical stabilisation of the small austenite particles [Han95b]. The improvement in ductility seems entirely to be due to microstructural refinement which is caused by the addition of Nb. It has been theoretically and experimentally shown that refinement of the microstructure in DP steel leads to a better work hardening rate and thus the ductility improves in agreement with the Considère criterion [Bal81, Mai88]. Accordingly, the optimum combination of strength and ductility can be achieved by homogeneously dispersing fine martensite islands in a fine grained ferrite matrix. Conglomerates of interconnected martensite should be avoided as much as possible. The basis of obtaining a fine grained and homogeneous microstructure in DP steel is the preparation of a suitable microstructure already in the hot band.

Comparing mechanical properties of the alloys D5 and D7 a greater strength level and lower ductility is obvious for D7 (Fig. 6.7 and Fig. 6.8). This is due to

the dominant effect of C content resulting in higher strengthening of D7. Moreover, higher C content provides a higher precipitate stability and binds more Nb in solution [Pic77]. Precipitation in multi phase microstructure must also be mentioned as an additional point. Yamamoto et al. [Yam82] found that LC steels with higher C content display more precipitation of Nb(C, N) particles which leads to slower softening behavior. In the case of hot rolled multi phase steels, a comparatively high C content accelerates the kinetics of Nb(C, N) precipitation [Tim01]. Furthermore, the re-dissolution of these carbides may become more difficult [Han95a].

Comparing alloys D2 and D7 with the same C content, the same level of mechanical properties was observed for both alloys (Fig. 6.7 and Fig. 6.8). On the other hand, no difference with regard to the grain size was found for both alloys. It can be concluded that under the chosen conditions the addition of Nb in combination with C doesn't influence the grain size and thus the mechanical properties of DP steels.

Finally, comparing alloy D7 with alloys of higher C content (D6 and D8), a lower strength level was found for D7. This might attribute to decrease the amount of C in solid solution by adding Nb which is accompanied with impairing strength effect. The same behavior was reported by Krizan [Kri05] for TRIP steels.

6.6.4 Influence of Reheating Temperature on the Microstructure and Mechanical Properties in Nb Microalloyed DP Steels

The effect of T_R on the microstructure and the mechanical properties of the alloys D5 and D7 (Nb addition) during roughing rolling has been investigated. An increase of the T_R results in higher strength for both alloys (Fig. 6.9) being attributed to two effects: a) grain refining of austenite and b) precipitation of finer Nb(C, N). In fact, the variation of T_R temperatures during hot rolling process result in pronounced differences in the hot rolled structure which is in correlation with the mechanical properties [Sol07]. From the images in Fig. 6.5 it can be seen that reheating alloy D5 at 1200 °C results in a marginal smaller d_γ. The same observation is valid for D7. This effect is due to solution of Nb at this temperature. From the ThermoCalc analyses (Fig. 6.1) it was found that Nb goes into solution at T_R of 1200 °C for both alloys. This occurs for D5 even at

lower temperature due to lower C content. The smaller d_γ at higher T_R was confirmed by dilatometric tests (Fig. 6.3), as already discussed in section 6.6.1.
Furthermore, the improvement of mechanical properties for both temperatures could also be due to Nb(C, N) precipitations. Whereas at low T_R the Nb(C, N) particles partially can be dissolved, a high T_R during simulation of roughing rolling process may lead to dissolution of initial coarse Nb(C, N) which is characterized by a lower precipitate density, a larger average distance between precipitates and a larger precipitate diameter [Kri05]. These coarse particles can be regenerated into a finer form during the deformation and cooling process. This improves the ability of Nb(C, N) precipitates to pin the austenite and ferrite grain boundaries during the processing of the Nb microalloyed steel [Kan97]. Therefore, the precipitation strengthening by fine Nb(C, N) particles will be increased. Hence, this effect may improve the mechanical properties of Nb microalloyed steels at higher T_R.

6.6.5 Influence of Alloying Elements on the Bake Hardening Behavior

As already mentioned in chapter 2, the main factors influencing the BH effect of DP steels are the solute C content, grain size and dislocation density. Based on these factors the influence of variation of alloying elements on BH behavior in DP steels will be discussed in this section.
It is observed that a higher C content results in a larger BH potential (section 6.5.4). Two main groups may be obtained from the results of mechanical properties after PS and BH process: Alloys containing low C content (D1, D3, D4 and D5) and alloys containing high C content (D2, D6, D7 and D8).
First, the BH behavior of low C content alloys is discussed. The results of BH clearly suggest that BH level of D3 and D5 steel is the highest among the four low C content alloys (Fig. 6.10 to Fig. 6.12). Alloy D3 with increasing Si content as a solid solution strengthening element shows intermediate values of strength increase after PS and BH. For D5 somewhat higher BH values are obtained. On the other hand, both alloys demonstrate the finest grain size (section 6.5.2). Therefore, the high BH level of alloys D3 and D5 could be due to finer grain sizes. Grain refining of ferrite by Nb addition in solid solution [Bou98, Jia02] and by increasing Si [Han84, Miz94] has been already reported.

Grain size is reported to be a long range barrier to the dislocation motion in bcc lattice and hence affects the BH [Asa08a, Han84]. The reason why bake hardenability depends on grain size is not clear, but it is inferred that the influence of dissolved C on bake hardenability differs depending on the location of C. Different effects of dissolved C were reported on the bake hardenability depending on its location, at grain boundary and inside grains [Kri07]. For a given C content, the bake hardenability increases with a decrease in grain size and the dependence on grain size increases with an increase in solute C. While the explanation of this effect is not complete, data suggests that free C located near grain boundaries has a more profound influence on the strength than free C located within the grain interior [Tak10].

The effect of ferrite grain refinement on the increase of bake hardenability is associated with the location of solute C. It is assumed that during cooling, the C atoms diffuse to the grain boundaries. Solute C positioned at the grain boundaries, so called “hidden” C atoms, can not be detected by internal friction measurement [Hua03], but it is supposed that this C makes a contribution to the BH effect [Mas04]. The smaller the grains are, the more C should be in the grain boundaries because of shorter diffusion paths. Thus, although the same overall solute C content can be measured, the “contributed” C content as well as bake hardenability can be higher in case of fine grains as the amount of “hidden” C is higher in finer grains [Kam61].

From Tab. 6.4 it is clear that the ferrite and martensite grain size in LC alloys D1 and D4 is nearly the same. It may therefore be inferred that a possible variation in the BH level of D4 will be due to a difference in the amount of solid solution additions others than C. Another reason could be the distribution of dislocation density as a result of variation of the chemical composition associated with influencing the recrystallization and $\gamma \rightarrow \alpha$ transformation behavior. Little or no information can be found in literature about the effect of Mo content on the BH behavior and mechanical properties of the DP steels. For hot rolled steels it is reported that recrystallization delay is induced by Mo [Her96]. The main consequences will be higher rolling loads in the rear stands of the finishing mill and the production of a strained microstructure before cooling and phase transformation. As discussed in chapter 4, the higher strains result in larger dislocation density, contributing to the BH effect.

Comparing D4 with D3 and D5, a lower bake hardenability is found for D4. As mentioned earlier, the presence of the stronger carbide forming elements like Mo in steel D4 may lead to the formation of its carbides (Mo_2C) in addition to Fe_3C. Therefore, the amount of solute C could decrease because it is tied up in the alloy by carbide particles [Ram79]. Compared to that of D3 and D5 this may cause the reduction of bake hardenability of D4.

Evaluating the BH behaviors of alloys with higher C content shows a significant higher BH level for these alloys compared to the alloys with low C content (Fig. 6.10 to Fig. 6.12). Higher C content in the alloys is associated with a larger magnitude of solute C. To maximize the strength increase associated with BH, it is necessary to have as much free C as possible. As outlined in chapter 2, the classical BH mechanism is related to pinning of mobile dislocations by C atoms. In multiphase steels the overall C content is larger than in the conventional BH steels (LC and ULC grades). The main part of this C is found in the C rich phases like martensite, retained austenite and bainite, of course. But there are still reasons to assume that some C is dissolved in ferrite as well, resulting from the fast cooling after intercritical annealing or after TMCP, when the solubility for C in ferrite is higher than at RT [Jeo85]. Thus, some excess C can be kept in solid solution. Nevertheless, significantly larger amounts of C in the ferrite phase are not likely for multiphase steels, since their alloying with manganese promotes the formation of austenite during $\gamma \rightarrow \alpha$ transformation, which in turn narrows the ferrite phase field [Kri07].

Evaluating the BH behavior of alloys D6 and D8, a comparable high BH level is obtained for both alloys. Both alloys contain the highest amounts of C, Si and Mo, while alloy D6 is additionally microalloyed by Nb. It has to be mentioned that Si is reported to increase solute C [Wat99]. As discussed before, the grain size becomes finer when Si [Miz94] and Nb [Mon07] contents are increased. On the other hand, no grain refining in high C content alloys is observed by increasing Si and Nb. Thus, the high BH behavior of high C alloys can be well explained in terms of the changes in solute C and formation of fine alloyed carbides and clusters like Nb-Si-Mo-Fe-C and Si-Mo-Fe-C by increasing alloying elements. Pereloma et al. [Per08a] have found the formation of fine alloy carbides and clusters as Nb-Mo-Fe-C in the alloyed TRIP steels. According to Cochardt et al. [Coc55] the binding energy of C atoms to dislocations is 0.75 eV, whereas

according to [Per08] the binding energy of C to such particles as Nb-Mo-Fe-C is 2.3 eV. Thus, the driving force for cluster / fine precipitate formation in alloyed steels would be higher than that for Cottrell atmosphere formation.
Among the alloys wit increased C content, D7 shows the lowest values of BH. This could be due to the formation of Nb(C, N) which could lead to reduction of solute C. As earlier mentioned, Nb forms Nb(C, N) which may tie up the solute C contributing to BH.

6.6.6 Influence of the Prestraining and Temperature on the Bake Hardening Behavior

The general relationships between baking conditions, i.e. prestrain and temperature, have been already shown in section 6.5.4. In this section the possible mechanisms related to the behavior observed will be discussed. Stress vs. strain curves (Fig. 6.14 to Fig. 6.21) therefore have been produced to show changes in the yielding behavior with respect to PS and temperature of paint baking simulation. This yields some clues about the possible mechanisms contributing to the BH behavior of DP steels.
As discussed before, generally, the same type of BH behavior was found for the alloys D1, D3, D4 and D5 having the lowest C content. They show quite similar tensile curves, too. Fig. 6.14 to Fig. 6.17 present the tensile curves of these four alloys with respect to the prestrain and baking temperature. Without PS no or just minimal deflection is visible, indicating aging effects. This is accompanied with very low BH_0 indices. The absence of a yield point elongation for 0 % prestrain in case of a DP steel has been found elsewhere, too [Han03]. A more distinct response to BH can be observed at 2 % and 5 % prestrains at which a real yield point phenomenon occurs. The occurrence of a yield point indicates that a dislocation pinning mechanism becomes involved.
Significant changes in the yielding characteristics of the tensile curves with increasing temperatures are found. For all four alloys distinct aging is observed at 170 °C. At the BH temperature of 240 °C the yielding characteristics become very pronounced showing strong yield drops up to yield point elongations. It is interesting to note that yielding is discontinuous at all imposed prestrains and temperatures exception at PS = 5 % and T = 170 °C. For this condition continuous yielding appears for all alloys. The yield point elongation becomes

more pronounced at a temperature of 240 °C. In general, the formation of Lüders bands is more pronounced at higher temperature and PS. In [Bal09a] it is noted that the gap between the aged and the classic behaviors during Lüders phenomenon increases with time and temperature of the aging treatment until a saturation. In the same literature, it is also argued that the difference between aged and classic behaviors depends on PS, i.e. an increase of PS leads to an increase of the gap.

The continuous increase of BH values at 240 °C can be attributed to the faster diffusion of C atoms towards the dislocation lines. The largest BH_2 and BH_5 values are observed for this high temperature. This indicates that additional processes start to become involved at elevated temperatures. Some authors reported tempering mechanism of martensite at temperatures between 200 and 250 °C in DP steels [Kri07, Tim07, Wat06]. In martensite structures C atoms are trapped leading to a distorted bct (body centered tetragonal) lattice, i.e. supersaturation with C compared to the bcc ferrite [Kra01]. In C steels with high amount of martensite, tempering of martensite takes place already during cooling and also during storage and testing at RT. Thus, C may precipitate or diffuse towards dislocations and interfaces. A volume decrease of about 0.5 % is reported, when freshly quenched martensite is tempered [Che88]. The additional aging process in martensite at high BH temperatures is discussed at the end of this section.

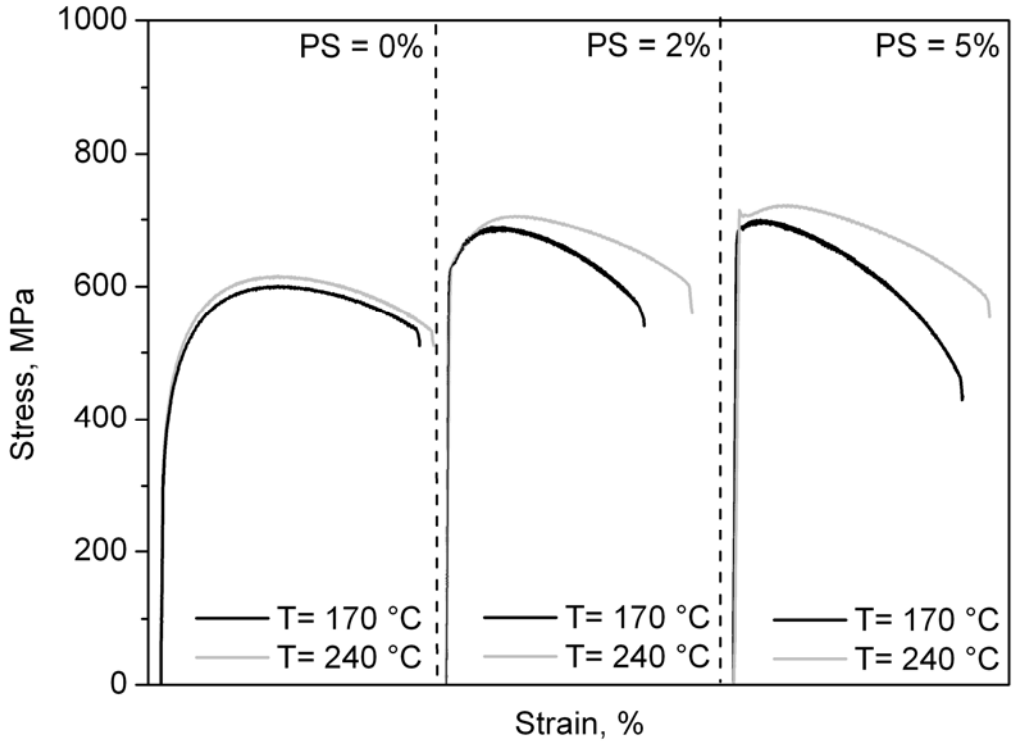

Fig. 6.14 Stress-strain curves for alloy D1 after PS and BH.

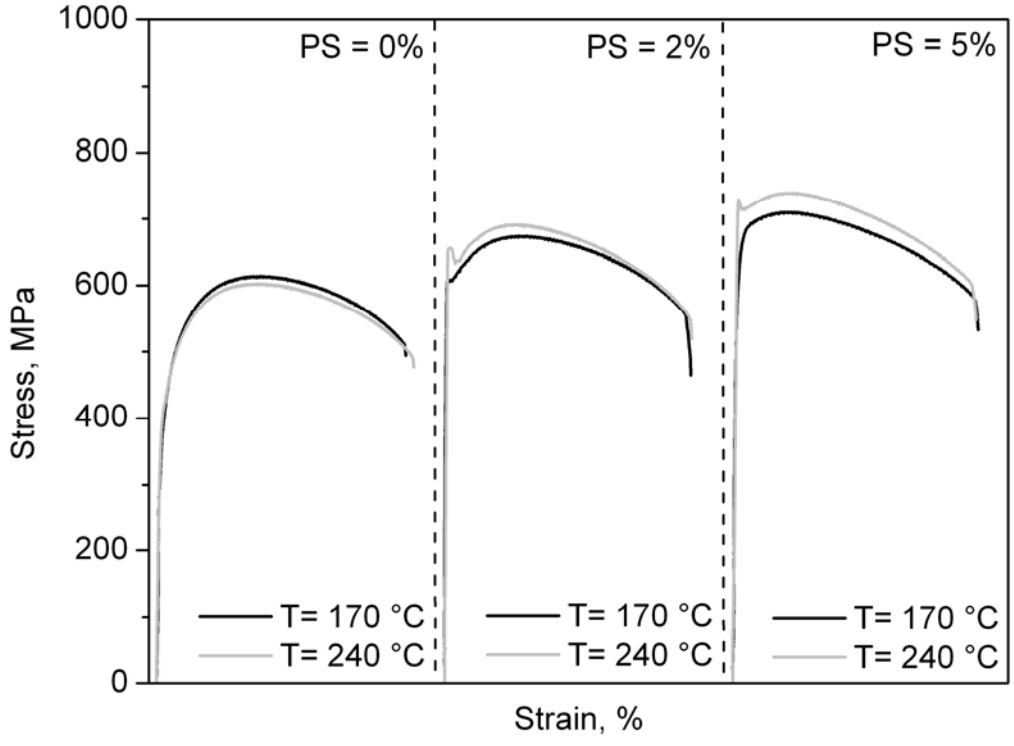

Fig. 6.15 Stress-strain curves for alloy D3 after PS and BH.

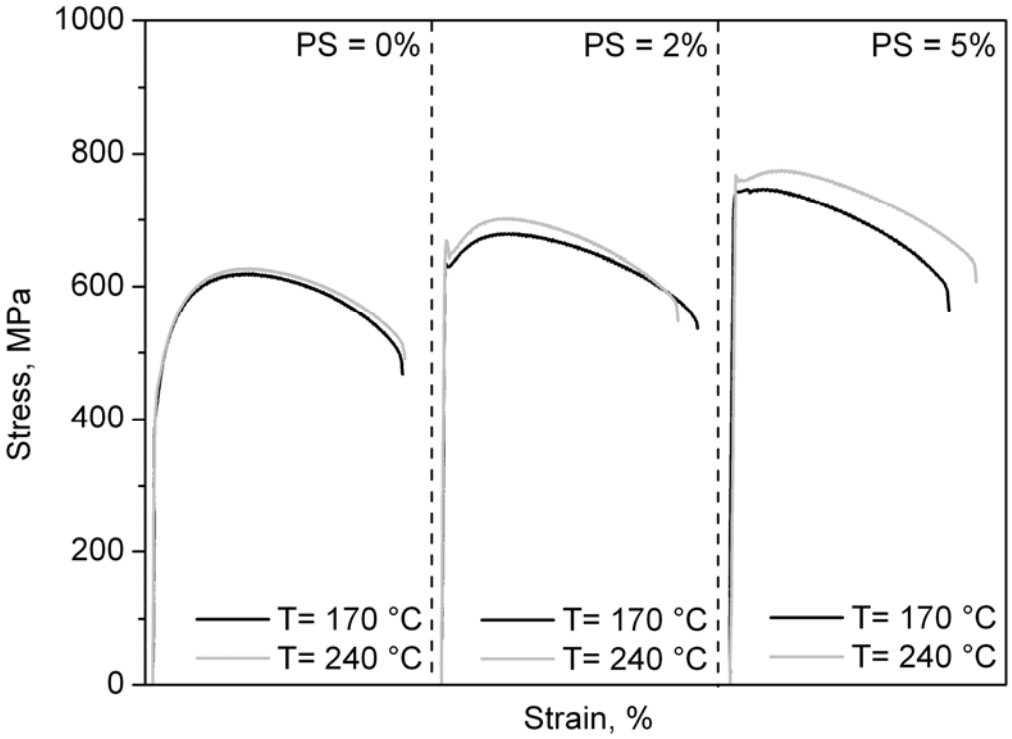

Fig. 6.16 Stress-strain curves for alloy D4 after PS and BH.

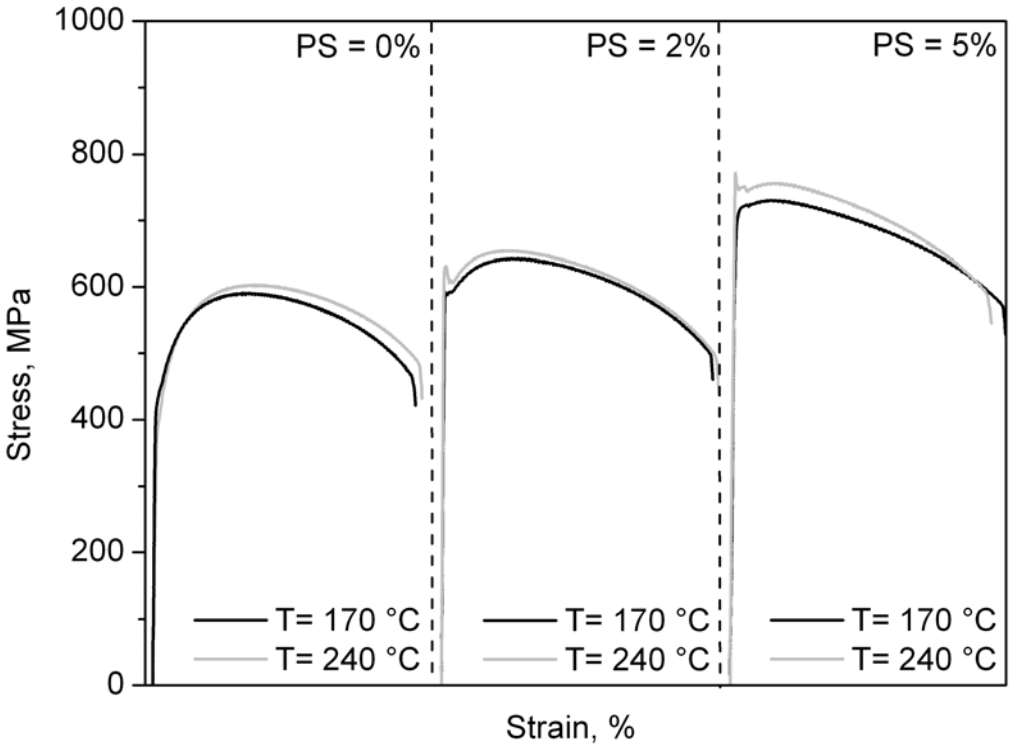

Fig. 6.17 Stress-strain curves for alloy D5 after PS and BH.

Fig. 6.18 to Fig. 6.21 present the general characteristics of the stress-strain curves of the alloys with higher C content. Along with the generally increasing R_m values after paint baking simulation, the main difference with the curves of high C content alloys is the larger value of R_e, leading to the large BH levels

calculated. This behavior is most likely attributable to initial tempering of freshly quenched martensite, leading to a relief of internal stresses [Wat06]. Thus, the onset of yielding is delayed and the stress-strain curves show linear behavior up to larger stresses than in the case of low C content alloys. It should be emphasised again that a very reliable calculation of the exact BH_0 indices is difficult due to the absence of a distinct yield point and the large WH of DP steels. It is interesting to note that the tensile curves are nearly as smoothly shaped and show a continuous yielding behavior after prestraining and baking.

Evaluating the tensile curves prestrained by 5 % and baked at 170 and 240 °C, a continuous decrease of stress after reaching the upper yield point is observed. Obviously, baking increases the R_e close to the R_m, i.e. after the onset of yielding the sample instantly starts to neck. This behavior is more pronounced for the alloy D6 at PS = 5 % PS and T = 170 °C. In this case the degree of PS approaches the uniform elongation of the particular alloy.

A first indication of aging can be seen in the curves after BH simulation at 240 °C. Especially for steel D8 this leads to BH as high as 120 MPa at PS = 2 %. The occurrence of a distinct yield point allows the conclusion that at 240 °C baking temperature a C-related mechanism has a distinct influence on the BH behavior. Such a mechanism is probably present at lower temperatures as well, since cooling of alloys after last deformation step during TMCP and accelerated cooling from fast cooling start temperature (T^{FC}) should provide a certain amount of C in solid solution, but it might be overshadowed by a strong tempering phenomena taking place in these alloys. It is reported that such C is present at sites where it is hindered to contribute to baking at low temperatures [Kri07]. Possible sites where C resides are regions in the vicinity of the ferrite and martensite interfaces with a high density of geometrically necessary dislocations [Tim07].

It should be noted that these alloys show higher yield point after PS and BH than those of alloys containing low C content. It can be conjectured that this effect is attributable to a large amount of solute C present in such steels due to higher C content. It is probable that the dislocations generated during prestraining can be blocked very effectively.

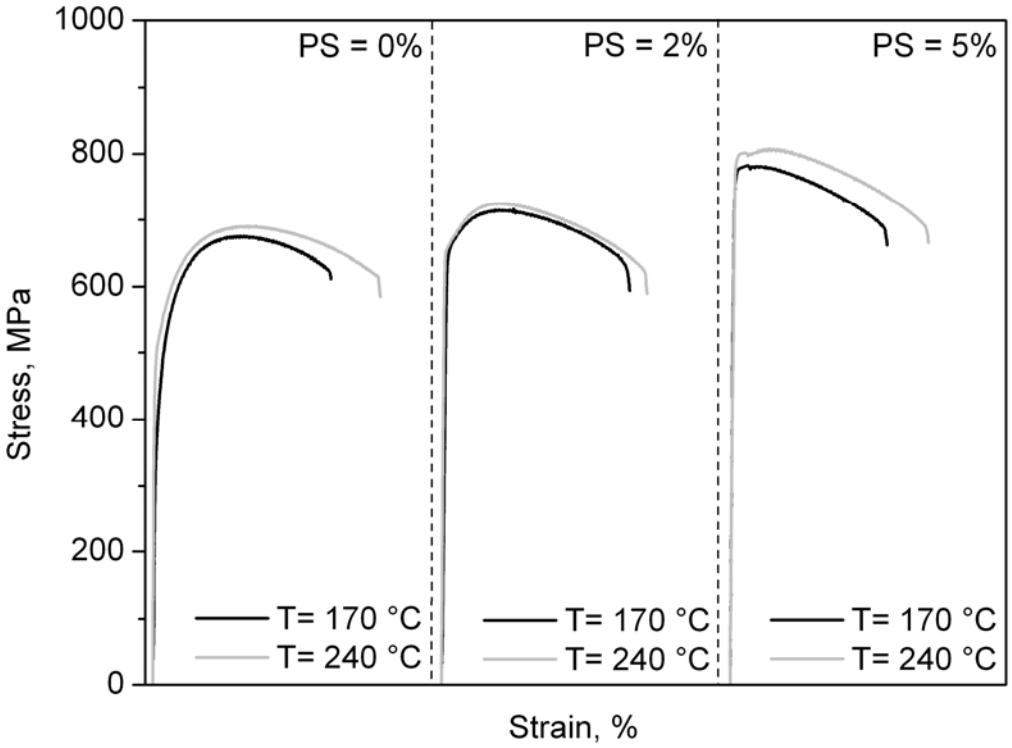

Fig. 6.18 Stress-strain curves for alloy D2 after PS and BH.

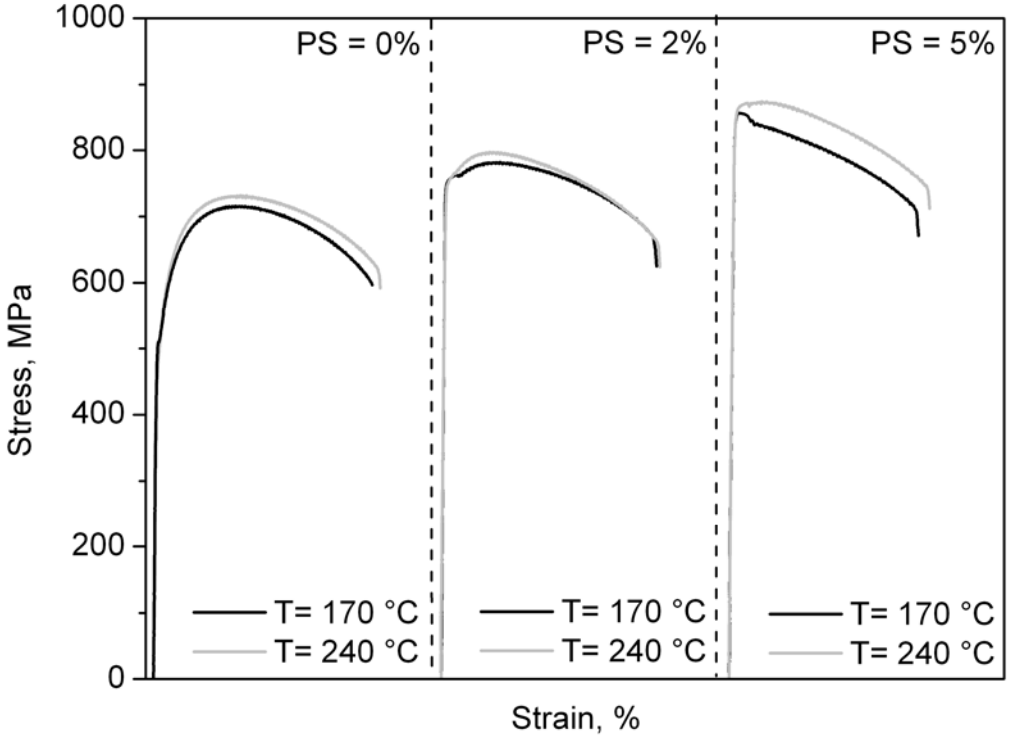

Fig. 6.19 Stress-strain curves for alloy D6 after PS and BH.

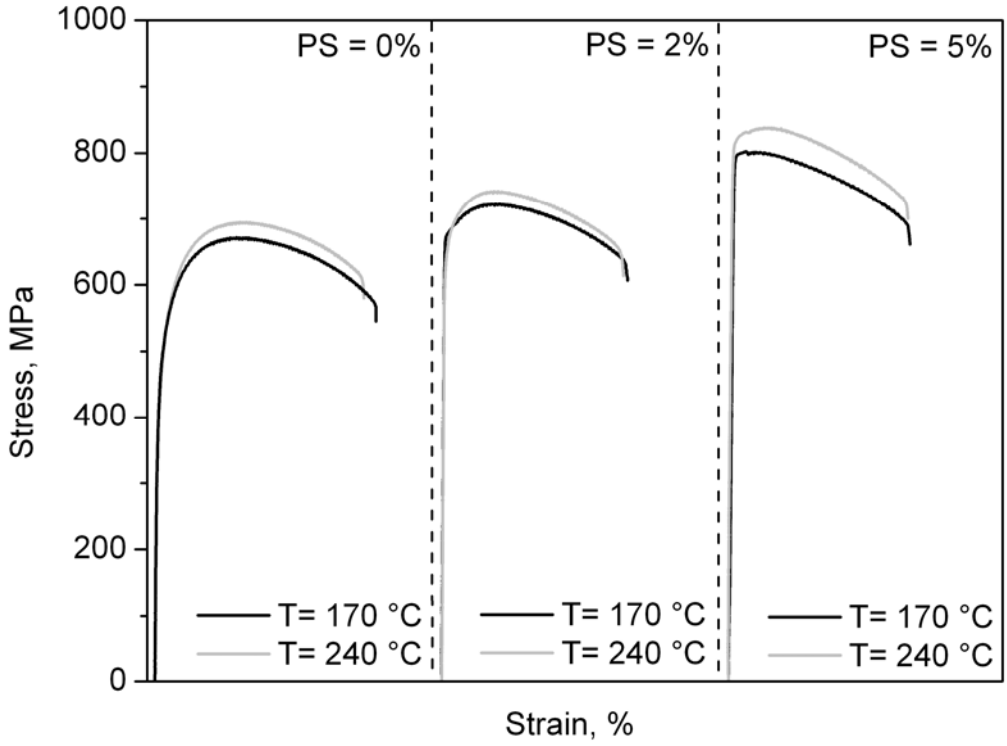

Fig. 6.20 Stress-strain curves for alloy D7 after PS and BH.

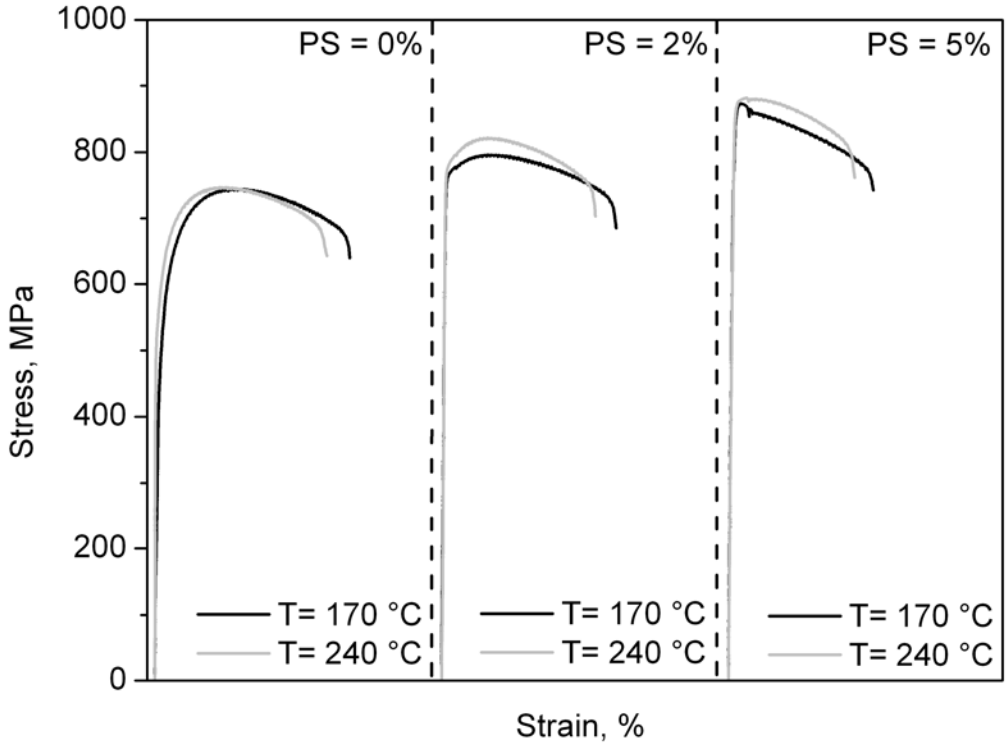

Fig. 6.21 Stress-strain curves for alloy D8 after PS and BH.

Two major observations from these data on the response to BH are: a) the contribution of BH increases with an increase in prestrain and (b) the BH sensitivity of the baked alloys at 240 °C is much higher than that at 170 °C.

As can be well recognised in TEM image (Fig. 6.6), the transformation of austenite to martensite leads to a volume increase which has to be compensated by the generation of dislocations in the surrounding ferrite. This observation coincides with a number of other investigations [Lie02, Tim07, Tim08, Wat03]. During the ferrite to martensite transformation process compressive stresses are introduced in the surrounding ferrite causing an increase of yield strength. As mentioned earlier, TEM experiments on the alloy D1 prestrained to 2 % and without baking yield a negligible higher dislocation density compared to the condition before prestraining. Moreover, no significant differences are observed after BH at 170 °C with 20 min baking time to the microstructure (martensite phase) of the basic alloy (Fig. 6.13 (a)-(b)). A distinct tempering of martensite takes place after BH simulation at 240 °C for 20 min, showing a clear decomposition of martensite structures and the formation of carbides (Fig. 6.13(c)). Diffraction pattern confirms the Fe_3C carbides (Fig. 6.13(d)). This can lead to a high BH level at this temperature. This observation was reported elsewhere [Bar02, Brü10, kri07, Nag83, Wat06].

Fig. 6.22 shows an example of HAADF STEM images used to detect the dislocation densities and Fe_3C precipitations in martensite. These precipitations appear bright in martensite structure. The micrographs are obtained from the DP sample after TMCP without PS and baked at T = 240 °C for t = 20 min. Between the martensite laths a localized dislocation density is clearly observed (Fig. 6.22(a)). Moreover, the formation of fine, nano-scaled Fe_3C carbides is detected in the martensite after BH at 240 °C (Fig. 6.22(a)). The most advanced formation of carbides can be observed from Fig. 6.22(b), showing regularly oriented carbides of around 50 nm. This structure is identified as tempered martensite, i.e. Fe_3C particles surrounded by ferrite at places originally occupied by lath martensite [Bha92a, Bra90].

At temperatures about 250 °C, decomposition of retained austenite into χ-carbides (Fe_2C_5) and ferrite, transformation of transition carbides into Hägg-carbides and finally the formation of θ-carbides (Fe_3C) take place. The last process is associated with bcc lattice formation [Wat06, Van97]. Cheng et al. [Che88] found the precipitation of small orthorhombic ε-carbides (Fe_2C) and/or hexagonal η-carbides ($Fe_{2,4}C$) at about 200 °C.

It should be noted, that for martensite structures in low alloyed steels these stages are likely to overlap [Wat06]. The strongest changes in microstructures usually are attributed to temperatures above 200 °C. Experiments show that the processes, which are associated with significant changes of mechanical properties, are completed at about 300 °C [Brü10].

Samek et al. [Sam06] reported Fe_3C precipitation at 170 °C already, but only for very long aging times ($\geq$ 5000 min). Similar observations using SEM experiments were reported by Speich et al. [Spe83], yielding distinct substructures compared to the smooth surfaces in the as-quenched martensite. Changes caused by martensite tempering can be observed in the mechanical and BH properties, too. For all alloys and conditions an increase of yield strength and re-occurrence of a distinct yield point is observed at BH temperature of 240 °C.

Due to the number of possible mechanisms involved in the BH of DP steels it is thus not surprising that a very broad range of BH levels may be found, depending on various factors: chemical composition (including content of dissolved C), microstructure (e.g. MVF, grain sizes, distribution of phases), parameters of paint baking simulation: prestrain, time and temperature. Especially the baking temperature was found to have a big influence on the BH behavior of these DP steels. This is different to common BH steels, for which no influence of temperature on the general BH level is found [Ste04].

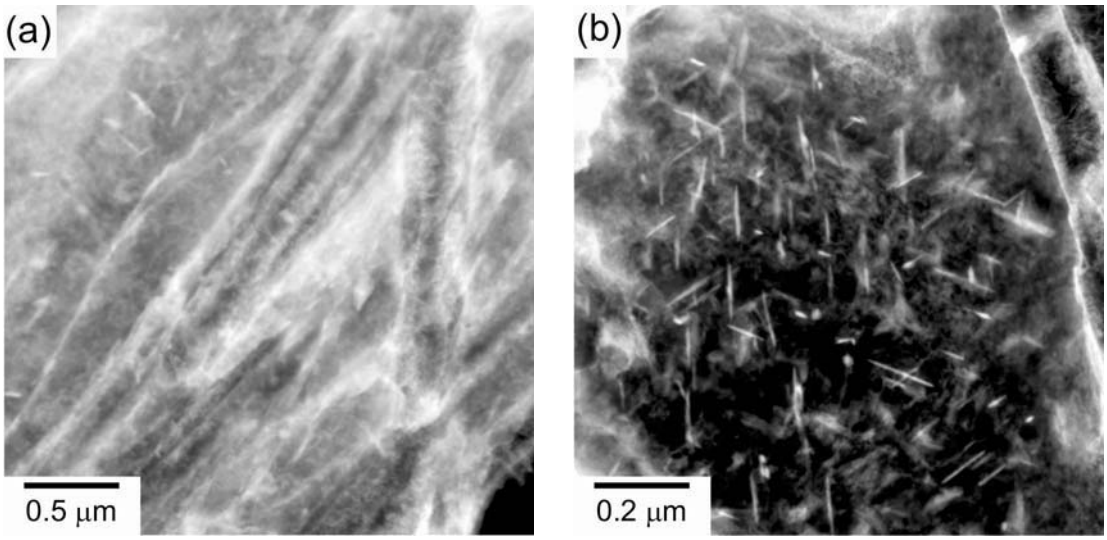

Fig. 6.22 HAADF STEM micrographs showing distribution of Fe_3C precipitations for steel D1 applied TMCP after prestaining at PS = 0 % and baking at T = 240 °C for t = 20 min; (a) martensite structure containing Fe_3C precipitations and dislocation densities and (b) tempered martensite (Fe_3C in different orientations).

6.7 Conclusions

The major conclusions drawn from the present investigation are as follows:

1- Increasing alloying elements can exert a significant influence on the transformation behavior allowing promoting or retarding the formation of individual phases. This can be exploited to exert better process control and optimize properties during producing of DP steels. In general, increasing C, Mo and Nb shifts the Ar_3, Ar_1 and M_S towards lower temperatures, while increasing Si raises the Ar_3, Ar_1 and decreases the M_S.

2- Among the four alloying elements, increasing C and Mo does not influence the ferrite and martensite grain sizes. Increasing Nb and Si refines the final microstructure of DP steel when they are added into steels individually. The effect is more pronounced for the addition of Nb. No grain refining effect is observed for the steel by addition of Nb together with increasing C. Moreover, TEM studies of basic alloy show localized increased density of dislocations in the ferrite regions adjacent to the pre-existing martensite.

3- Increasing all alloying elements increases the strength of DP steels. C is the most important element influencing the mechanical properties of DP steels. Nb is more effective than Mo and Si in increasing strength without deteriorating ductility in alloys without C increasing. Since much of the Nb effectiveness in steels with high C content results from complex two-, three-

and four-way alloy interactions, Nb alloying does not cause an increase in the strength of steels unless Mo and Si were also added. It thus allows working with an alloying concept to reach a specified strength level.

4- Increasing T_R during roughing rolling process leads to improvement of mechanical properties of two Nb microalloyed steels. This could be attributed to the grain refining effect of Nb solution and dissolution of initial coarse Nb(C, N) particles at the higher T_R and partially reformation of fine Nb(C, N) particles during TMCP.

5- Variation of alloying elements as well as prestrains and baking temperatures indicates a pronounced influence on BH behavior of DP steels as follows:

(a) C is the most important element affecting BH behavior. The steels investigated having high C content exhibit a high BH potential.

(b) Increasing Si and Nb improves BH behavior in steels without rising C where Nb is more effective than Si in increasing BH behavior. This is due to grain refining effect of both elements. Increasing C content of DP steels from (0.06 - 0.09) % strongly reduces the effectiveness of Nb alloying on bake hardenability. The formation of Nb(C, N) precipitations is used to scavenge solute C from the ferrite matrix in DP steel. Partial re-dissolution of Nb(C, N) during the roughing rolling can be used to liberate C for the BH effect.

(c) For Mo increasing in steels without C rising a slightly improving in BH behavior is observed. Increasing Mo together with other alloying elements shows a rising effect on BH.

(d) For all alloys a strength increment is observed without PS and with prestrains at 2 % and 5 % after baking simulation. This increment is significantly high for the alloys prestrained at 5 % and baked at 170 and 240 °C for 20 min where for the baking temperature of 240 °C a slightly higher BH level is found. TEM and HAADF STEM observations reveal the formation of Fe_3C carbides corresponding martensite tempering at 240 °C.

7 Summary

Dual phase (DP) steels offer a combination of tensile properties such as a low yield strength and a high tensile strength, which make them unique among high strength low alloy (HSLA) steels. They also exhibit high work hardening rates in the early stage of plastic deformation and good ductility during forming relative to strength in the deformed conditions. The correct distribution of the two phases allows a low yielding stress, a high elongation value and a smooth flow-stress curve. In order to produce DP steel, different methods can be employed such as heat treatment and hot rolling. The utilization of thermomechanical controlled processing (TMCP) by hot rolling is an industrial method for manufacturing DP steels. In this technique, the control of the rolling parameters and chemical compositions has a significant role on the final microstructure and mechanical behavior.

This work provided a detailed study of replication of hot rolling mill by TMCP aimed at further development of new categories of DP steels in terms of mechanical properties and bake hardenability via affordable addition of alloying elements together with optimisation of the processing conditions.

In this study, the influence of hot rolling parameters (deformation temperatures and amounts of strain), cooling conditions during $\gamma \rightarrow \alpha$ transformation, amount of martensite as well as variation of alloying elements (C, Si, Mo and Nb) on the phase transformation behavior, microstructure development, mechanical properties and BH behavior of DP steels was investigated. The TMCP simulation of the three last finishing rolling steps was conducted on a deformation simulator using flat compression test. The specimens were cooled after the last deformation step to T^{FC} temperatures to obtain prescribed amount of ferrite and retained austenite and subsequently accelerated cooled below M_S to obtain martensite from retained austenite. Dilatation tests under similar conditions to that of hot deformation were conducted to determine T^{FC} temperatures and to the study the transformation behavior.

For the simulation of changing process conditions within the final hot rolling the specimens were hot deformed using different schedules with different reductions and temperatures which were selected according to the non-recrystallization temperature. It was possible to refine the DP steel structure by controlling the deformation temperature and the amount of strain below non-recrystallization

during the TMCP. This structure refinement resulted in improvement of the strength and BH behavior. A wide spectrum of mechanical properties was obtained mainly as a result of employing different hot deformation schedules. The best strength and BH levels were recorded for the materials applied deformation below T_{nRX} at the highest amount of strain. It was also found that applying hot deformation steps below T_{nRX} at high strains accelerates the $\gamma \rightarrow \alpha$ transformation and increases the Ar_3 and Ar_1 as a result of grain refining.

In chapter 5, specimens were hot deformed using a hot deformation schedule according to the industrial conditions combined from deformations above and below non-recrystallization. Different cooling rates were applied after the last deformation step to T^{FC} temperatures during the $\gamma \rightarrow \alpha$ transformation. Different MVFs from 10 to 30 % were obtained by varying T^{FC}. DP-like properties were obtained for all conditions. It was found that an increase of the cooling rate and MVF resulted in improving both, strength and BH behaviors together with a decreased ductility. The highest cooling rate during the $\gamma \rightarrow \alpha$ transformation together with the largest amount of martensite led to highest strength and lowest ductility either after TMCP or after prestraining and baking. No noticeable changes in microstructure in terms of ferrite and martensite morphology and grain size were observed for all conditions. Furthermore, increasing cooling rate shifted the Ar_3, Ar_1 and M_S towards lower temperatures.

To achieve an improvement in mechanical and BH behavior of hot rolled DP steels the alloying concept was successfully used in the present work (chapter 6). For this purpose, eight alloys had been cast, rolled down in four passes, simulating roughing rolling and followed by three deformation steps in the deformation simulator, simulating last steps of the finishing rolling process. In order to investigate the influence of reheating temperature on the mechanical properties of Nb microalloyed steels, these alloys were additionally rolled at higher T_R during simulation of roughing rolling process. All specimens were deformed using the same deformation schedule as in chapter 5.

It has been shown that the addition of a small amount of alloying elements to this steel grade caused a significant change in mechanical properties and bake hardenability due to content of solute C, precipitation strengthening and refinement of the final microstructure. Increasing C yielded increased C in solution resulting in improved strength and BH levels. Finer grain sizes achieved

by increasing Nb and Si without C enhancement are expected to have a beneficial influence on both, strength and bake hardening, too. Furthermore, Ar_3, Ar_1 shifted towards lower temperatures by increasing C, Mo and Nb, while increasing Si shifts Ar_3, Ar_1 towards higher temperatures. The influence of C is more pronounced than for other elements. Moreover, increasing T_R during the roughing rolling led to decreasing Ar_3, Ar_1 and M_S as well as improvement of strength and ductility.

Principally, the BH properties of DP steels investigated were characterised by low values when no prestrain was applied before the paint baking simulation, while the BH values were rising very steeply as soon as a prestrain of 2 % was introduced. It could be explained by a more effective dislocation pinning, jointly resulting from the migration of dislocations from the F/M interfaces to the interior of the ferrite grains, where they were blocked by solute C atoms, which are released from the trapping sites near F/M interfaces at the same time. Further increase in prestrain caused an increased number of dislocations leading to an increase of BH. With respect to the baking temperature a nearly continuous increase of the BH values was found towards larger temperatures. A distinct change of yield point behavior with increasing temperature was observed, pointing to additional dislocation pinning due to the faster diffusion of carbon at higher temperatures. At temperatures above 200 °C additional tempering of martensite was recognised, indicated by a regular orientation of Fe_3C particles.

Generally, it can be summarized that for hot rolled DP steels through optimizing composition and processing schedules, a spectrum of mechanical behaviors was observed, outperforming many commercially available steel grades.

References

[Aar06] Aaronson, H.I.; Reynolds, W.T. and Pury, G.R.: The Incomplete Transformation Phenomenon in Steel. Metallurgical and Materials Transactions A, 37A (2006) 6, 1731-1745.

[Abe84] Abe, H.; Suzuki, T. and Okada, S.: Decomposition of Mn-C Dipoles During Quench-Aging in Low-Carbon Aluminum-Killed Steels. Transactions of the Japan Institute of Metals, 25 (1984) 4, 215-225.

[Agh09] Aghajani, A.; Somsen, C. and Eggeler, G.: On the effect of long-term creep on the microstructure of a 12 % chromium tempered martensite ferritic steel. Acta Materialia, 57 (2009) 17, 5093-5106.

[Ahm08] Ahmad, E.; Manzoor, T.; Hussain, N. and Qazi, N.K.: Effect of thermomechanical processing on hardenability and tensile fracture of dual-phase steel. Materials & Design, 29 (2008) 2, 450-457.

[Ajm09] Ajmal, M.; Tindyala, M.A. and Priestner, R.: Effect of controlled rolling on the martensitic hardenability of dual phase steel. International Journal of Minerals Metallurgy and Materials, 16 (2009) 2, 165-169.

[Ali63] Alien, N. P.: Iron and Its Dilute Solid Solutions. Eds. Spencer, C.W. and Werner, F.E., Interscience, New York, (1963), 271-308.

[And65] Andrews, K.W.: Empirical Formulae for Calculation of Some Transformation Temperatures. Journal of the Iron and Steel Institute, 203 (1965), 721.

[Ang06] Angeli, J.; Fuereder, E.; Panholzer, M. and Kneissl, A.C.: Etching techniques for characterizing the phases of low-alloy dual-phase and TRIP steels. Praktische Metallographie-Practical Metallography, 43 (2006) 10, 489-504.

[Ank05] Anke, T.: Bake Hardening von warmgewalzten Mehrphastenstählen. Ph.D. Thesis, Clausthal University of Technology, (2005).

[Ank66] Ankara, O.A.; Sastri, A.S. and West, D.R.F.: Some Effects of Austenitizing Conditions on Martensite Formation in An Iron-20 Percent Nickel Alloy. Journal of the Iron and Steel Institute, 204 (1966), 509.

[Asa08a] Asadi, M. and Palkowski, H.: Untersuchung zur Auswirkung von Legierungsschwankungen auf den BH-Effekt in Dualphasen- und Martensit-Stählen bei der Warmbanderzeugung. VFWH Abschlussbericht zum Projekt AW141, (2008).

[Asa08b] Asadi, M. and Palkowski, H.: Thermo-mechanical Processing Parameters and Chemical Composition on Bake Hardening ability of Hot Rolled Multiphase Steels. 1st International Conference on “IAS”, Pohang, South Korea, (2008), 137-145.

[Asa09a] Asadi, M. and Palkowski, H.: Influence Local Use of Ageing Effects in Multiphase Steels for Designing Local Properties of Constructional Elements. TMS-AIME, San Francisco, (2009).

[Asa09b] Asadi, M.; Schulze, N. and Palkowski, H.: Nutzung des Alterungseffektes zur lokalen Eigenschaftsänderung von Strukturbauteilen. 7. Industriekolloquium Hochfeste Strukturen, Clausthal-Zellerfeld, (2009), 49-55.

[Asa09c] Asadi, M. and Palkowski, H.: Thermo-mechanical Processing Parameters and Chemical Composition on Bake Hardening ability of Hot Rolled Martensitic Steels. Steel Research International, 80 (2009) 7, 499-506.

[Asa10a] Asadi, M.; N. Schulze and Palkowski, H.: Use of the aging effect to change the local properties of structure components. Advanced Materials Research, 137 (2010), 35-79.

[Asa10b] Asadi, M. and Palkowski, H.: Designing Local Properties of Constructional Elements by Local Use of Ageing Effects in Multiphase Steels. Materials Science Forum, 638-642, (2010), 3062-3067.

[Ash71] Ashby, M.E.: Strengthening Methods in Crystals. Applied Science, Eds. Kelly, A. and Nicholson, R.B., London, (1971), 137-192.

[AST04] ASTM Standards 1033-04 2: Practice for Quantitative Measurement and Reporting of Hypoeutectoid Carbon and Low-Alloy Steel Phase Transformations. ASTM International, American Society for Testing and Materials, USA, (2004).

[Ast80] Astie, P.; Peyrade, J.P. and Groh, P.: Relaxation Peaks of Dislocations in Iron after Low-Temperature Deformation. Scripta Metallurgica, 14 (1980) 6, 611-616.

[Bäc09] Bäcke, L.: Modeling the Microstructural Evolution during Hot Deformation of Microalloyed Steels. Ph.D. Thesis, Royal Institute of Technology, Stockholm, (2009).

[Bag01] Bagramov, R.; Mari, D. and Benoit, W.: Internal friction in a martensitic high-carbon steel. Philosophical Magazine A, 81 (2001) 12, 2797-2808.

[Bag99] Bag, A.; Ray, K.K. and Dwarakadasa, E.S.: Influence of martensite content and morphology on tensile and impact properties of high-martensite dual-phase steels. Metallurgical and Materials Transactions A, 30 (1999) 5, 1193-1202.

[Bai93] Bai, D.Q.; Yue, S.; Sun, W.P. and Jonas, J.J.: Effect of Deformation Parameters on the No-Recrystallization Temperature in Nb-Bearing Steels. Metallurgical Transactions A, 24 (1993) 10, 2151-2159.

[Bai94] Bailey, F.D.: Effects of mill processing and pre-strain mode on the aging behavior of a commercially produced bake hardenable steels. M.S.Thesis, (1994).

[Bak02a] Baker, L.J.; Daniel, S.R. and Parker, J.D.: Metallurgy and processing of ultralow carbon bake hardening steels. Materials Science and Technology, 18 (2002) 4, 355-368.

[Bak02b] Baker, L.J.; Parker, J.D. and Daniel, S.R.: Mechanism of bake hardening in ultralow carbon steel containing niobium and titanium additions. Materials Science and Technology, 18 (2002) 5, 541-547.

[Bal09a] Ballarin, V.; Soler, M.; Perlade, A.; Lemoine, X. and Forest, S.: Mechanisms and Modeling of Bake-Hardening Steels: Part I. Uniaxial Tension. Metallurgical and Materials Transactions A, 40A (2009) 6, 1367-1374.

[Bal09b] Ballarin, V.; Perlade, A.; Lemoine, X.; Bouaziz, O. and Forest, S.: Mechanisms and Modeling of Bake-Hardening Steels: Part II. Complex Loading Paths. Metallurgical and Materials Transactions A, 40A (2009) 6, 1375-1382.

[Bal81] Balliger, N.K. and Gladman, T.: Work-Hardening of Dual-Phase Steels. Metal Science, 15 (1981) 3, 95-108.

[Bar02] Barbe, L.; Conlon, K. and De Cooman, B.C.: Characterization of the metastable austenite in low-alloy FeCMnSi TRIP-aided steel by neutron diffraction. Zeitschrift für Metallkunde, 93 (2002) 12, 1217-1227.

[Bau81] Baumgart, H.; Boer, H.F. and Heisterkamp, F.: Proceedings of the International Symposium on Niobium, ed.: Stuart, H., TMS-AIME, Warrendale, (1981), 883-915.

[Bel98] Belyakov, A.; Kaibyshev, R. and Sakai, T.: New grain formation during warm deformation of ferritic stainless steel. Metallurgical and Materials Transactions A, 29 (1998) 1, 161-167.

[Bel03] Belyakov, A.; Tsuzaki, K.; Miura, H. and Sakai, T.: Effect of initial microstructures on grain refinement in a stainless steel by large strain deformation. Acta Materialia, 51 (2003) 3, 847-861.

[Ber04] Berbenni, S.; Favier, V.; Lemoine, X. and Berveiller, M.: A micromechanical approach to model the bake hardening effect for low carbon steels. Scripta Materialia, 51 (2004) 4, 303-308.

[Ber83] Bergström, Y.: The plastic deformation of metals - a dislocation model and its applicability. Reviwes on powder metallurgy and ceramic, Royal Institute of Technology, Stockholm, 2 (1983) 84.

[Bha92a] Bhadeshia, H. K. D. H.: Bainite in Steels. Institute of Materials, London, (1992), 1-458.

[Bha92b] Bhadeshia, H. K. D. H.: High strength steels. Eds. Charles, J.A.; Greenwood, G.W. and Smith, G.C., Institute of Materials, London, (1992), 25-74.

[Bha93] Bhattacharyya, A.; Sakaki, T. and Weng, G.J.: The Influence of Martensite Shape, Concentration, and Phase-Transformation Strain on the Deformation-Behavior of Stable Dual-Phase Steels. Metallurgical Transactions A, 24 (1993) 2, 301-314.

[Bha04] Bhadeshia, H.K.D.H.: Developments in martensitic and bainitic steels: role of the shape deformation. Materials Science and Engineering A, 378 (2004) 1-2, 34-39.

[Bir05] Birol, Y. and Karlik, M.: Bake hardening of twin roll cast Al-Mg-Si sheet. Materials Science and Technology, 21 (2005) 2, 153-158.

[Ble02] Bleck, W.: Using the TRIP Effect - The Dawn of a Promising New Group of Cold Formable Sheets. International Conference on TRIP-Aided High Strength Ferrous Alloys, ed.: De Cooman, B.C., GRIPS, Ghent, (2002), 13-23.

[Ble04a] Bleck, W.; Frehn, A.; Ohlert, J.; Sonne, H.M. and Steinbeck, G.: Influence of temperature and prestraining on the plastic material behaviour of modern sheet steels for autobody applications. Materialwissenschaft und Werkstofftechnik, 35 (2004) 8, 495-504.

[Ble04b] Bleck, W.; Papaefthymiou, S. and Frehn, A.: Microstructure and tensile properties in dual phase and TRIP steels. Steel Research International, 11 (2004), 704-710.

[Ble07] Bleck, W.; Brühl, S.; Gerber, T.; Katsamas, A.; Ottaviani, R.; Samek, L. and Traint, S.: Control and exploitation of the bake-hardening effect in multi-phase high-strength steels. EU-Report 22448, Luxembourg, (2007).

[Bou98] Bouet, M.; Root, J.; Es-Sadiqi, E. and Yue, S.: The effect of Mo in Si-Mn Nb bearing TRIP steels. Proceedings of the International Conference on Microalloying in Steels, 284-286 (1998), 319-326.

[Bou06] Bouvier, S.; Gardey, B.; Haddadi, H. and Teodosiu, C.: Characterization of the strain-induced plastic anisotropy of rolled sheets by using sequences of simple shear and uniaxial tensile tests. Journal of Materials Processing Technology, 174 (2006) 1-3, 115-126.

[Bra77] Bradley, J.R.; Rigsbee, J.M. and Aaronson, H.I.: Growth Kinetics of Grain-Boundary Ferrite Allotriomorphs in Fe-C Alloys. Metallurgical Transactions A, 8 (1977) 2, 323-333.

[Bra90] Bramfitt, B.L. and Speer, J.G.: A perspective on the morphology of bainite. Metallurgical Transactions A, 21 (1990) 4, 817-829.

[Bro93] Browning, N.D.; Chisholm, M.F. and S.J. Pennycook: Atomic-Resolution Chemical-Analysis Using A Scanning-Transmission Electron-Microscope. Nature, (1993) 366, 143-146.

[Bru03] Bruce, D.M.: Dynamic Tensile Testing of Sheet Steels and Influence of Strain Rate on Strengthening Mechanisms in Sheet Steels, Ph.D. Thesis, Colorado School of Mines, Golden, Colorado, MT-SRC-003-018 (2003).

[Brü05] Brühl, S.; Bleck, W.: Bake-Hardening Verhalten von mehrphasigen Stählen (DP / TRIP). 20 Aachener Stahlkolloquium, Aachen, Germany, (2005), 91-10.

[Brü10] Brühl, S.: Einfluss der Martensitephase auf das Bake-Hardening-Verhalten von Dualphasen-Stählen. Ph.D. Thesis, RWTH Aachen, Germany, (2010).

[But62] Butler, J.F.: Luders Front Propagation in Low Carbon Steels. Journal of the Mechanics and Physics of Solids, 10 (1962) 4, 313-334.

[But63] Butler, R.D. and Wilson, D.V.: Mechanical Behavior of Temper Rolled Steel Sheets. Journal of the Iron and Steel Institute, 201 (1963) 1, 16.

[Cal08] Calcagnotto, M.; Ponge, D. and Raabe, D.: Ultrafine grained ferrite/martensite dual phase steel fabricated by large strain warm deformation and subsequent intercritical annealing. ISIJ International, 48 (2008) 8, 1096-1101.

[Cal10] Calcagnotto, M.; Ponge, D.; Demir, E. and Raabe, D.: Orientation gradients and geometrically necessary dislocations in ultrafine grained dual-phase steels studied by 2D and 3D EBSD. Materials Science and Engineering A, 527 (2010) 10-11, 2738-2746.

[Cap05] Capdevila, C.; Caballero, F.G. and de Andres, C.G.: Neural network model for isothermal pearlite transformation. Part II: Growth rate, ISIJ International, 45 (2005) 2, 238-247.

[Cha02] Chan Hong, S. and Sub Lee, K.: Influence of deformation induced ferrite transformation on grain refinement of dual phase steel. Materials Science and Engineering A, 323 (2002) 1-2, 148-159.

[Cha84] Chang, P.H.: Effects of Prior Cold-Rolling and Post Temper Rolling on the Properties of Continuously Annealed Low-Carbon Dual Phase Steel. Metallurgical Transactions A, 15 (1984) 4, 671-678.

[Cha86] Chang, L.; Smith, G.D.W. and Olson, G.B.: Aging and Tempering of Ferrous Martensites. Journal de Physique, 47 (1986) C-2, 265-275.

[Che85] Chen, Q.A.; Kaspar, R. and Pawelski, O.: Contribution to the Deformation Characteristics of Dual-Phase Steels. Zeitschrift für Metallkunde, 76 (1985) 5, 348-352.

[Che89a] Chen, H.C.; Era, H. and Shimizu, M.: Effect of Phosphorus on the Formation of Retained Austenite and Mechanical-Properties in Si-Containing Low-Carbon Steel Sheet. Metallurgical Transactions A, 20 (1989) 3, 437-445.

[Che89b] Chen, H.C. and Cheng, G.H.: Effect of Martensite Strength on the Tensile-Strength of Dual Phase Steels. Journal of Materials Science, 24 (1989) 6, 1991-1994.

[Che98] Chen, X. and Foley R.P.: Effects of cold rolling reductions, solute carbon content and strain rate on the tensile properties of a 0.04wt. % carbon AKDQ steel. 40th MWSP Conference Proceedings, ISS, (1998) 35, 889-898.

[Che88] Cheng, L.; Brakman, C.M.; Korevaar, B.M. and Mittemeijer, E.J.: The Tempering of Iron-Carbon Martensite - Dilatometric and Calorimetric Analysis. Metallurgical Transactions A, 19 (1988) 10, 2415-2426.

[Cho04] Choi, I.D.; Kim S.J.; Bruce D.; Matlock, D.K. and Speer J.G.: The Effect of Retained Austenite Stability on High Speed Deformation Behavior of TRIP Steels. Proceedings of ICASS 2004, Chinese Society for Metals, Shanghai, China, (2004), 703-706.

[Chr98] Christen, J., Rubianes, J.M.: The bake hardenable steels for automotive outer body panels: Correlation between the BH measurement and the dent resistance. 40th MWSP Conference Proceedings, ISS, (1998), 77-81.

[Coc55] Conchardt, A.W.; Schoek, G. and Wiedersich, H.: Interaction between Dislocations and interstitial atoms in body-centered cubic metals. Acta Metallurgica, 3 (1955) 6, 533-537.

[Col09] Colla, V.; De Sanctis, M.; Dimatteo, A.; Lovicu, G.; Solina, A. and Valentini, R.: Strain Hardening Behavior of Dual-Phase Steels. Metallurgical and Materials Transactions A, 40A (2009) 11, 2557-2567.

[Cot49a] Cottrell, A.H. and Bilby, B.A.: Dislocation Theory of Yielding and Strain Ageing of Iron. Proceedings of the Physical Society of London Section A, 62 (1949) 349, 49-62.

[Cot49b] Cottrell, A. H.; Jawson M. A.: Distribution of Solute Atoms Round a Slow Dislocation. Proceeding the Royal Society A, 199 [1056] (1949), 104-114.

[Cud82] Cuddy, L.J.: The Effect of Microalloy Concentration on the Recrystallization of Austenite During Hot Deformation. TMS-AIME, (1982), 129-140.

[Dan68] Dantonio, C.R.; Maciag, R.J.; Mukherje, K and Fischer, G.J.: Effect of Strain Rate and Temperature on Flow Stress of 7075 Aluminum. TMS-AIME, 242 (1968) 11, 2295.

[Das09] Das, D. and Chattopadhyay, P.P.: Influence of martensite morphology on the work-hardening behavior of high strength ferrite-martensite dual-phase steel. Journal of Materials Science, 44 (2009) 11, 2957-2965.

[Dav78a] Davies, R.G.: Influence of Martensite Composition and Content on Properties of Dual Phase Steels. Metallurgical Transactions A, 9 (1978) 5, 671-679.

[Dav78b] Davies, R.G.: Deformation-Behavior of a Vanadium-Strengthened Dual Phase Steel. Metallurgical Transactions A, 9 (1978) 1, 41-52.

[Dav79] Davies, R.G.: Early Stages of Yielding and Strain Aging of a Vanadium-Containing Dual-Phase Steel. Metallurgical Transactions A, 10 (1979) 10, 1549-1555.

[De99] De, A.K.; Vandeputte, S. and De Cooman, B.C.: Static strain aging behavior of ultra low carbon bake hardening steel. Scripta Materialia, 41 (1999) 8, 831-837.

[De00] De, A.K.; De Blauwe, K.; Vandeputte, S. and De Cooman, B.C.: Effect of dislocation density on the low temperature aging behavior of an ultra low carbon bake hardening steel. Journal of Alloys and Compounds, 310 (2000), 405-410.

[De01] De, A.K.: Static strain aging in ultra low carbon steels: Effect of interstitial content, dislocation density and grain boundaries. Ph.D. Thesis, University of Ghent, (2001).

[De03] De, A.K.; Speer, J.G. and Matlock, D.K.: Color Tint-Etching for Multiphase Steels. Advanced Materials and Processes, (2003) 161, 27-30.

[De04] De, A.K.; Vandeputte, S.; Soenen, B. and De Cooman, B.C.: Effect of grain size on the static strain aging of a ULC-bake hardening steel. Zeitschrift für Metallkunde, 95 (2004) 8, 713-717.

[DeA84] DeArdo, A.J.; Gray, J.M. and Meyer, L.: Fundamental Metallurgy of Niobium in Steel. San Francisco, California, (1984), 685-759.

[DeA88] DeArdo, A.J.: Fundamental Aspects of the Physical Metallurgy of Thermomechanical Processing of Steel. International Conference on Physical Metallurgy of Thermomechanical Processing of Steels and Other Metals, Tokyo, (1988), 20-29.

[Dec78] Decristofaro, N.; Kaplow, R. and Owen, W.S.: Kinetics of Carbon Clustering in Martensite. Metallurgical Transactions A, 9 (1978) 6, 821-825.

[DeC04] De Cooman, B.C.: Structure-properties relationship in TRIP steels containing carbide-free bainite. Current Opinion in Solid State & Materials Science, 8 (2004) 3-4, 285-303.

[DIN85] DIN 50601: Metallografische Prüfverfahren. Ermittlung der Ferrit - oder Austenitkorngröße von Stahl und Eisenwerkstoffen. Deutsches Institut für Normung, Berlin, (1985).

[Dja72] Djaic, R.A.P. and Jonas, J.J.: Static Recrystallization of Austenite Between Intervals of Hot Working. Journal of the Iron and Steel Institute, 210 (1972), 256.

[Doe07] Doernberg, E.: Ermittelung des freien Kohlenstoffgehaltes mit verschiedenen Methoden und seine Auswirkungen auf das Bake-Hardening-Verhalten von Stählen. Diploma Thesis, Clausthal University of Technology, (2007).

[Dre90] Drewes, E.J. and Engl, B.: Neuere Entwicklungen auf dem Gebiet der Feinblechwerkstoffe. Ingenieur-Werkstoffe im technischen Fortschritt, VDI-Gesellschaft Werkstofftechnik, VDI- Verlag, Düsseldorf, 797 (1990), 601-608.

[Dre99] Drewes, E.-J.; Engl, B.; Kruse, J.: Höherfeste Stähle - heute und morgen, Stahl und Eisen. 119 (1999) 5, 115-122

[Edm90] Edmonds, D.V. and Cochrane, R.C.: Structure-Property Relationships in Bainitic Steels. Metallurgical Transactions A, 21 (1990) 6, 1527-1540.

[Egh06] Eghbali, B. and Abdollah-Zadeh, A.: Influence of deformation temperature on the ferrite grain refinement in a low carbon Nb-Ti microalloyed steel. Journal of Materials Processing Technology, 180 (2006) 1-3, 44-48.

[Egh07a] Eghbali, B. and Abdollah-Zadeh, A.: Deformation-induced ferrite transformation in a low carbon Nb-Ti microalloyed steel. Materials & Design, 28 (2007) 3, 1021-1026.

[Egh07b] Eghbali, B.: Effect of Warm Deformation on Ferrite Microstructure Evolution in a Ti-Microalloyed Steel. Materials Science Forum, 558-559 (2007), 497-504.

[Els93] Elsen, P. and Hougardy, H.P.: On the Mechanism of Bake-Hardening. Steel Research International, 64 (1993) 8-9, 431-436.

[Emb66] Embury, J.D.; Keh, A.S. and Fisher, R.M.: Substructural Strengthening in Materials Subject to Large Plastic Strains. TMS-AIME, 236 (1966) 9, 1252.

[Eng96] Engl, B. and Gerber, T.: Microalloyed, vacuum degassed high-strength steels with special emphasis on IF steels. Steel Research International, 67 (1996) 10, 430-437.

[Eur06] European standard EN 10325: Steel – Determination of yield strength increase by the effect of heat treatment (bake-hardening-index). European Committee for Standardization, Bruxelles, (2006).

[Exe01] Exebio J.J.M.: Metallurgical phenomena governing the bake hardening response of bake hardenable steels, Literature Review, (2001).

[Fan94] Fan, Z.; Tsakiropoulos, P. and Miodownik, A.P.: A Generalized Law of Mixtures. Journal of Materials Science, 29 (1994) 1, 141-150.

[Fan02] Fang, X.; Fan, Z.; Ralph, B.; Evans, P. and Underhill, R.: Effect of temper rolling on tensile properties of C-Mn steels. Materials Science and Technology, 18 (2002) 3, 285-288.

[Far06] Farías,D.: Bake Hardening Response of DP800 and the Influence on the "In Service Performance". M.S. Thesis, Eindhoven University of Technology, (2006).

[Fau01] Fausto, D.M.M.; New approaches to higher strength in interstitial free steels. M.S. Thesis, University of Pittsburgh, (2001).

[Fu09] Fu, R.Y.; Su, Y.; Ye, P.; Wei, X.C.; Li, L. and Zhang, J.C.: Internal Friction on the Bake-Hardening Behavior of 0.11C-1.67Mn-1.19Si TRIP Steel. Journal of Materials Science & Technology, 25 (2009) 1, 141-144.

[Fuj78] Fujita, H. and Miyazaki, S.: Luders Deformation in Polycrystalline Iron. Acta Metallurgica, 26 (1978) 8, 1273-1281.

[Fuj98] Fujiwara, K. and Okaguchi, S.: Morphology and mechanical properties of bainitic steels deformed in unrecrystallized austenite region. Proceedings of the International Conference on Microalloying in Steels, 284-286 (1998), 271-277.

[Fur84] Furukawa, T.; Tanino, M.; Morikawa, H. and Endo, M.: Effects of Composition and Processing Factors on the Mechanical-Properties of As-Hot-Rolled Dual-Phase Steels. Transactions of the Iron and Steel Institute of Japan, 24 (1984) 2, 113-121.

[Gar81] Garcia, C.I. and Deardo, A.J.: Formation of Austenite in 1.5 Pct Mn Steels. Metallurgical Transactions A, 12 (1981) 3, 521-530.

[Gar02] Garcia de Andrés, C.; Caballero, F.G.; Capdevila, C.; and San Martin, D.: Revealing austenite grain boundaries by thermal etching: advantages and disadvantages, Materials Characterization. 49 (2002) 2, 121-127.

[Gho94] Ghosh, G. and Olson, G.B.: Kinetics of Fcc-Bcc Heterogeneous Martensitic Nucleation, Part I: the Critical Driving-Force for Athermal Nucleation. Acta Metallurgica et Materialia, 42 (1994) 10, 3361-3370.

[Gho06] Ghosh, A.; Shukla, R.; Das, S. and Chatterjee, S.: The structure and properties of a thermo-mechanically processed low carbon high strength steel. Steel Research International, 77 (2006) 4, 276-283.

[Gle82] Gleiter, H.: On the Structure of Grain-Boundaries in Metals. Materials Science and Engineering, 52 (1982) 2, 91-131.

[God02] Godet, S.; Harlet, P.; Delannay, F. and Jacques, P.J.: Effect of hot-rolling conditions on the tensile properties of multiphase steels exhibiting a TRIP effect. Steel Research International, 73 (2002) 6-7, 280-286.

[Goe87] Goel, N.C.; Chakravarty, J.P. and Tangri, K.: The Influence of Starting Microstructure on the Retention and Mechanical Stability of Austenite in An Intercritically Annealed Low-Alloy Dual-Phase Steel. Metallurgical Transactions A, 18 (1987) 1, 5-9.

[Gou03] Gourdet, S. and Montheillet, F.: A model of continuous dynamic recrystallization. Acta Materialia, 51 (2003) 9, 2685-2699.

[Gra09] Grajcar, A. and Krztoń, H.: Effect of isothermal bainitic transformation temperature on retained austenite fraction in C-Mn-Si-Al-Nb-Ti TRIP-type steel. Journal of Achievements in Materials and Manufacturing Engineering, 35 (2009) 2, 169-175.

[Gün08] Gündüz, S. and Tosun, A: Influence of straining and ageing on the room temperature mechanical properties of dual phase steel. Materials & Design, 29 (2008), 1914-1918.

[Gup84] Gupta, I. and Chang, P.H.: Effect of Composition and Processing on the Variability of the Tensile-Strength of Water Quenched Dual Phase Steels. Journal of Metals, 36 (1984) 7, 34-41.

[Hai06] Haidemenopoulos, G.N.; Katsamas, A.I. and Aravas, N.: Stability and constitutive modelling in multiphase TRIP steels. Steel Research International, 77 (2006) 9-10, 720-726.

[Han01] Han, K.; van Genderen, M.J.; Bottger, A.; Zandbergen, H.W. and Mittemeijer, E.J.: Initial stages of Fe-C martensite decomposition. Philosophical Magazine A, 81 (2001) 3, 741-757.

[Han01] Hanlon, D.N.; Sietsma, J. and Van der Zwaag, S.: The effect of plastic deformation of austenite on the kinetics of subsequent ferrite formation. ISIJ International, 41 (2001) 9, 1028-1036.

[Han03] Hance, B.M.; Link, T.M. and Hoydick, D.P.: Bake hardening of multiphase high strength sheet steels. 45th Mechanical Working and Steel Processing Conference, Chicago, USA, XLI (2003), 195-206.

[Han84] Hanai, S.; Takemoto, N.; Tokunaga, Y. and Mizuyama, Y.: Effect of Grain-Size and Solid-Solution Strengthening Elements on the Bake Hardenability of Low-Carbon Aluminum-Killed Steel. Transactions of the Iron and Steel Institute of Japan, 24 (1984) 1, 17-23.

[Han95a] Hanzaki, A.Z.; Hodgson, P.D. and Yue, S.: Hot Deformation Characteristics of Si-Mn TRIP Steels with and Without Nb Microalloy Additions. ISIJ International, 35 (1995) 3, 324-331.

[Han95b] Hanzaki, A.Z.; Hodgson, P.D. and Yue, S.: The Influence of Bainite on Retained Austenite Characteristics in Si-Mn TRIP Steels. ISIJ International, 35 (1995) 1, 79-85.

[Han97] Hanzaki, A.Z.; Hodgson, P.D. and Yue, S.: Retained austenite characteristics in thermomechanically processed Si-Mn transformation-induced plasticity steels. Metallurgical and Materials Transactions A, 28 (1997) 11, 2405-2414.

[Har66] Hartley, S.: Strain-Ageing in Tantalum. Acta Metallurgica, 14 (1966) 10, 1237.

[Hel05] Heller, T. and Nuss, A.: Effect of alloying elements on microstructure and mechanical properties of hot rolled multiphase steels. Ironmaking & Steelmaking, 32 (2005) 4, 303-308.

[Her96] Herman, J.C. and Leroy, V.: Influence of Residual Elements on Steel Processing and Mechanical Properties. Metal Working and Steel Processing, Cleveland, (1996), 1-15.

[Hil09] Hilditch, T.; Timokhina, I.; Robertson, L.; Pereloma, E. and Hodgson, P.: Cyclic Deformation of Advanced High-Strength Steels: Mechanical Behavior and Microstructural Analysis. Metallurgical and Materials Transactions A, 40A (2009) 2, 342-353.

[Hod97] Hodgson, P.D.; Collison, D.C. and Perret, B.: The Use of Hot Torsion to Simulate the Thermomechanical Processing of Steel Proceedings, 7th International Symposium. on Physical Simulation of Casting, Hot Rolling and Welding, Japan, (1997) 21-23, 219-229.

[Hol45] Hollomon, J.M. and L.D. Jaffe: Time-Temperature Relations in Tempering of Steel. TMS-AIME, (1945) 162, 223-249.

[Hua01] Huang, C.; Hawbolt, E.B.; Chen, X.; Meadowcroft, T.R. and Matlock, D.K.: Flow stress modeling and warm rolling simulation behavior of two Ti-Nb interstitial-free steels in the ferrite region. Acta Materialia, 49 (2001) 8, 1445-1452.

[Hua03] Huang,J.; Poole, W.J. and Militzer, M.: Study of ferrite recrystallization in a TRIP steel. Internat. Symposium on Transformation and Deformation Mechanisms in Advanced High-Strength Steels, Vancouver, Canada, (2003), 37-50.

[Hua04] Huang, J.; Poole, W.J. and Militzer, M.: Austenite formation during intercritical annealing. Metallurgical and Materials Transactions A, 35A (2004) 11, 3363-3375.

[Hul84] Hull, D. and Bacon, D.J.: Introduction to Dislocations. Third Edition, Pergamon Press Ltd, Oxford, (1984), 230.

[Hum04] Humphreys, F.J. and Hatherly, M.: Recrystallization and related annealing phenomena. Elsevier Science Ltd , Oxford, (2004).

[Hup99] Huper, T.; Endo, S.; Ishikawa, N. and Osawa, K.: Effect of volume fraction of constituent phases on the stress-strain relationship of dual phase steels. ISIJ International, 39 (1999) 3, 288-294.

[Haw79] Hawkins, D.N. and Shuttleworth, A.A.: The effect of warm rolling on the structure and properties of a low-carbon steel. Journal of Mechanical Working Technology, 4 (1979) 2, 333-345.

[Hwa05] Hwang, B.C.; Cao, T.Y.; Shin, S.Y.; Kim, S.H.; Lee, S.H. and Kim, S.J.: Effects of ferrite grain size and martensite volume fraction on dynamic deformation behaviour of 0 center dot 15C-2 center dot 0Mn-0 center dot 2Si dual phase steels. Materials Science and Technology, 21 (2005) 8, 967-975.

[Ino78] Inoue, T.; Haraguchi, K. and Kimura, S.: Analysis of Stresses Due to Quenching and Tempering of Steel. Transactions of the Iron and Steel Institute of Japan, 18 (1978) 1, 11-15.

[Jac01] Jacques, P.J.; Ladriere, J. and Delannay, F.: On the influence of interactions between phases on the mechanical stability of retained austenite in transformation-induced plasticity multiphase steels. Metallurgical and Materials Transactions A, 32 (2001) 11, 2759-2768.

[Jac04] Jacques, P.J.: Transformation-induced Plasticity for High Strength Formable Steels. Current Opinion in Solid State and Materials Science, 8 (2004), 259-265.

[Jeo85] Jeong, W.C. and Kim, C.H.: Ferrite Growth on Cooling After Intercritical Annealing in a Dual Phase Steel. Scripta Metallurgica, 19 (1985) 1, 37-42.

[Jeo98] Jeong, W.C.: Effect of prestrain on aging and bake hardening of cold-rolled, continuously annealed steel sheets. Metallurgical and Materials Transactions A, 29 (1998) 2, 463-467.

[Jia95] Jiang, B.H.; Sun, L.M.; Li, R.C. and Hsu, T.Y.: Influence of Austenite Grain-Size on Gamma-Epsilon Martensitic-Transformation Temperature in Fe-Mn-Si-Cr Alloys. Scripta Metallurgica et Materialia, 33 (1995) 1, 63-68.

[Jia01] Jiao, S.; Hassani, F.; Donaberger, R.L., Essadiqi, E. and Yue, S.: The Effect of Prior Heat Treated Structure on a Cold Rolled and Annealed Mo-Nb Microalloyed TRIP Steel, 43rd MWSP Conference Proceedings, ISS, (2001) 39, 385-395.

[Jia02] Jiao, S.; Hassani, F.; Donaberger, R.L.; Essadiqi, E. and Yue, S.: The effect of processing history on a cold rolled and annealed Mo-Nb microalloyed TRIP steel. ISIJ International, 42 (2002) 3, 299-303.

[Joa81] Jonas, J.J.; Do Nascimanto, R.A.; Weiss, I. and Rothwell, A.B.: Effect of Deformation on the γ→ α Transformation in Two High Silicon Dual-Phase Steels. Proceeding International Conference on Fundamentals of dual phase steels. TMS-AIME, Warrendale, (1981), 95.

[Jun06] Jun, H.J.; Kang, J.S.; Seo, D.H.; Kang, K.B. and Park, C.G.: Effects of deformation and boron on microstructure and continuous cooling transformation in low carbon HSLA steels. Materials Science and Engineering A, 422 (2006) 1-2, 157-162.

[Kam61] Kamber, K.; Keefer, D. and Wert, C.: Interactions of Interstitials with Dislocations in Iron. Acta Metallurgica, 9 (1961) 5, 403-414.

[Kan97] Kang, K.B.; Kwon, O.; Lee, W.B. and Park, C.G.: Effect of precipitation on the recrystallization behavior of a Nb containing steel. Scripta Materialia, 36 (1997) 11, 1303-1308.

[Kar74] Karlsson, B. and Sundstro, B.: Inhomogeneity in Plastic-Deformation of 2-Phase Steels. Materials Science and Engineering, 16 (1974) 1-2, 161-168.

[Keh63] Keh, A.S. and Leslie, W.C.: Recent Observations on Quench-Aging and Strain-Aging of Iron and Steel. Material Science Research, Plenum Press, New York, (1963) 1, 208-250.

[Kem90] Kemp, I.P.; Pollard, G. and Bramley, A.N.: Static Strain Aging in High-Carbon Steel Wire. Materials Science and Technology, 6 (1990) 4, 331-337.

[Kim81] Kim, N.J. and Thomas, G.: Effects of Morphology on the Mechanical-Behavior of a Dual Phase Fe-2Si-0.1C Steel. Metallurgical Transactions A, 12 (1981) 3, 483-489.

[Kim87] Kim, I.S.; Reichel, U. and Dahl, W.: Effect of Bainite on the Mechanical-Properties of Dual-Phase Steels. Steel Research International, 58 (1987) 4, 186-190.

[Kim00] Kim, S.J.; Lee, C.G.; Lee, T.H. and Lee, S.: Effects of coiling temperature on microstructure and mechanical properties of high-strength hot-rolled steel plates containing Cu, Cr and Ni. ISIJ International, 40 (2000) 7, 692-698.

[Koc66] Kocks, U.F.: A Statistical Theory of Flow Stress and Work-Hardening, Philosophical Magazine. 13 (1966) 123, 541.

[Koo80] Koo, J.Y.; Young, M.J. and Thomas, G.: On the Law of Mixtures in Dual-Phase Steels. Metallurgical Transactions A, 11 (1980) 5, 852-854.

[Kor80] Korzekwa, D.A.; Lawson, R.D.; Matlock, D.K. and Krauss, G.: A Consideration of Models Describing the Strength and Ductility of Dual-Phase Steels. Scripta Metallurgica, 14 (1980) 9, 1023-1028.

[Kor84] Korzekwa, D.A.; Matlock D.K. and Krauss, G.: Dislocation substructure as a function of strain in a dual-phase steel. Metallurgical and Materials Transactions A, (1984) 15, 1221-1228.

[Kot79] Kot, R.A.; Morris, J.W. (Eds.): Structure and properties of dual-phase steels. TMS-AIME, Warrendale, 1979.

[Koz75] Kozasu, I.; Ouchi, C.; Sampe,T.i. and Okita, T.: Hot rolling as a high temperature thermo-mechanical process, Proceedings of the International Symposium on Microalloying, Union Carbide Corporation, Washington DC, (1975), 120.

[Koz77] Kozasu, I.; Ouchi, C.; Sampei, T. and Okita, T.: Hot Rolling as a High-Temperature Thermo-Mechanical Process. Proceedings of Microalloying 75, ed.: Korchynsky, M., Union Carbide Corporation, Washington DC, New York, (1977), 120-135.

[Koz97] Kozeschnik, E. and Buchmayr, B.: A contribution to the increase in yield strength during the bake hardening process. Steel Research International, 68 (1997) 5, 224-230.

[Kra01] Krauss, G.: Deformation and fracture in martensitic carbon steels tempered at low temperatures. Metallurgical and Materials Transactions A, 32 (2001) 4, 861-877.

[Kri05] Krizan, D.: Structure-Properties Relationship in I GPa Micro-Alloyed TRIP Steel. Ph.D. Thesis, University of Ghent, Ghent, Belgium, (2005).

[Kri03] Krieger, M.: Bake-Hardening bei kaltgewalzten Mehrphasenstählen. Diploma Thesis, Clausthal University of Technology, (2003).

[Kri06] Krieger, M.; Estrin, Y.; Janecek, M.; Niemeyer, M. and Paul, S.: Mechanical properties and bake hardening behaviour of two cold rolled multiphase sheet steels subjected to CGL heat treatment simulation. Steel Research International, 77 (2006) 9-10, 668-674.

[Kri07] Krieger, M.: Mechanical properties and bake hardening behaviour of cold rolled dual phase steels subjected to advanced galvanising process routes. Ph.D. Thesis, Clausthal University of Technology, (2007).

[Kwo03] Kwon, O.; Lee, K.Y. and Hong, M.H.: Interstitial-Free Steels for Automotive Applications in Korea. International Forum for the Properties and Applications of IF Steels, Tokyo, (2003), 39-46.

[Kya98] Kvackaj, T. and Mamuzic, I.: A quantitative characterization of austenite microstructure after deformation in nonrecrystallization region and its influence on ferrite microstructure after transformation. ISIJ International, 38 (1998) 11, 1270-1276.

[Lan82] Lanzillotto, C.A.N. and Pickering, F.B.: Structure Property Relationships in Dual-Phase Steels. Metal Science, 16 (1982) 8, 371-382.

[Law81] Lawson, R.D.; Matlock, D.K. and Krauss, G.: Fundamentals of Dual-Phase Steel. Eds. Kot, R.A. and Bramfitt, B.L., TMS-AIME, Warrendale, (1981).

[Lee02] Lee, Y.K.; Shin, H.C.; Jang, Y.C.; Kim, S.H. and Choi, C.S.: Effect of isothermal transformation temperature on amount of retained austenite and its thermal stability in a bainitic Fe-3 %Si-0.45 %C-X steel. Scripta Materialia, 47 (2002) 12, 805-809.

[Les78] Leslie, W.C. and Rauch, G.C.: Precipitation of Carbides in Low-Carbon Fe-Al-C Alloys. Metallurgical Transactions A, 9 (1978) 3, 343-349.

[Les81] Leslie, W.C.: The physical metallurgy of steels. New York, McGraw-Hill, (1981).

[Li07] Li, Z. and WU D.: Effects of finishing rolling temperatures and reduction on the mechanical properties of hot rolled multiphase steel. Journal of Zhejiang University Science A, 8 (2007) 5, 797-804.

[Lid01] Liedl, U.; Werner, E.A.; Pichler, A.; Stiaszny, P.: Initial flow behavior of dual-phase steels. 43rd Mechanical Working and Steel Processing Conference, Charlotte, USA, XXXIX (2001), 175-184.

[Lie02] Liedl, U.; Traint, S. and Werner, E.A.: An unexpected feature of the stress-strain diagram of dual-phase steel. Computational Materials Science, 25 (2002) 1-2, 122-128.

[Lie03] Liedl, U.: Anfangsverformungs- und Alterungsverhalten von Dual Phasen Stahl. Ph.D. Thesis, Technische Universität München, (2003).

[Lie96] Liewellyn, D.T. and Hillis, D.J.: Dual phase steels – review. Ironmaking & Steelmaking, 23 (1996) 6, 471-478.

[Lou56] Louat, N.: The Effect of Temperature on Cottrell Atmospheres. Proceedings of the Physical Society of London Section B, 69 (1956) 4, 459-467.

[Lui09] Luis, C.; Gaspérini, M.; Bouvier, S. and Li, J.J.: Effect of Temper Rolling on the Mechanical Behaviour of Thin Steel Sheets Under Monotonous and Reverse Simple Shear Tests. International Journal of Material Forming, 2 (2009) 1, 471-474.

[Mah02] Mahieu, J.; De Cooman, B.C.; Maki, J. and Claessens, S.: Hot - Dip Galvanizing of Al Alloyed TRIP Steels. Ironmaking & Steelmaking, (2002) 29, 29-34.

[Mai86] Maid, O.: Einfluß der Gefügeparameter auf die mechanischen Eigenschaften von warm- und kaltgewalztem Flachzeug aus Dualphasen-Stahl. Ph.D. Thesis, RWTH Aachen, (1986).

[Mai88] Maid, O.; Dahl, W.; Strassburger, C. and Müschenborn, W.: Einfluss der Gefügeparameter auf die mechanischen Eigenschaften von Dualphasen-Stahl. Stahl und Eisen, (1988), 355-364.

[Man82] Mano, J.; Saeki, M.; Morita, M.; Nishida, M.; Tanaka, T.; Kato, T.; Aoyagi, N. and Yamada, N.: Production of As Hot Rolled Dual Phase Steel Sheet - Formation of Dual Phase-Structure During Cooling of Hot Strip. Transactions of the Iron and Steel Institute of Japan, 22 (1982) 6, 177.

[Man93] Mandziej, S.T.: Low-Energy Dislocations and Ductility of Ferritic Steels. Materials Science and Engineering A, 164 (1993) 1-2, 275-280.

[Man96] Manohar, P.A.; Dunne, D.P.; Chandra, T. and Killmore, C.R.: Grain growth predictions in microalloyed steels. ISIJ International, 36 (1996) 2, 194-200.

[Man98] Manohar, P.A. and Chandra, T.: Continuous cooling transformation behaviour of high strength microalloyed steels for linepipe applications. ISIJ International, 38 (1998) 7, 766-774.

[Mar69] Marder, A.R. and Krauss, G.: Formation of Low-Carbon Martensite in Fe-C Alloys. Asm Transactions Quarterly, 62 (1969) 4, 957.

[Mar81] Marder, A.R.: The Effect of Heat-Treatment on the Properties and Structure of Molybdenum and Vanadium Dual-Phase Steels. Metallurgical Transactions A, 12 (1981) 9, 1569-1579.

[Mar82a] Marder, A.R.: Deformation Characteristics of Dual-Phase Steels. Metallurgical Transactions A, 13 (1982) 1, 85-92.

[Mar82b] Marder, A.R. and Benscoter, A.O.: Quantitative Microanalysis of Dual-Phase Steels. Metallography, 15 (1982) 1, 73-85.

[Mar87] Marunouchi, K.K.: Thermomechanical Control Process for High Strength Austenitic Stainless Steel Plates. ISIJ International, 27 (1987) 9, 757-757.

[Mas04] Massardier, V.; Lavaire, N.; Soler, M. and Merlin, J.: Comparison of the evaluation of the carbon content in solid solution in extra-mild steels by thermoelectric power and by internal friction. Scripta Materialia, 50 (2004) 12, 1435-1439.

[Mat79] Matlock, D.K.; Krauss, G.; Ramos, L. F. and Huppi, G.S.: A Correlation of Processing Variables with Deformation Behaviour of Dual Phase Steels. In [Kot79]. (1979), 62-90.

[Mat98] Matlock, D.K.; Allen, B.J. and Speer, J.: Aging behavior and properties of ultra low carbon bake hardenable steels. International Symposium-Conference Book, 1 (1998), 265-276.

[Mat03] Matlock, D.K.; Bruce, D.M. and Speer, J.G.: Strengthening Mechanisms and their Applications in Extremely Low C Steels. International Forum for the Properties and Applications of IF Steels, (2003), 118-127.

[Mat04] Matsuda, H. and Bhadeshia H.K.D.H.: Kinetics of the Bainite Transformation. Proceedings of the Royal Society of London, 460A (2004), 1707-1722.

[Mat84] Matsumura, N. and Tokizane, M.: Microstructure and Mechanical-Properties of Dual-Phase Steel Produced by Intercritical Annealing of Lath Martensite. Transactions of the Iron and Steel Institute of Japan, 24 (1984) 8, 648-654.

[Mat87] Matsumura, O.; Sakuma, Y. and Takechi, H.: Trip and Its Kinetic Aspects in Austempered 0.4C-1.5Si-0.8Mn Steel. Scripta Metallurgica, 21 (1987) 10, 1301-1306.

[Mei67] Meisel, L.V.: Stress-Assisted Diffusion to Dislocations and Its Role in Strain Aging. Journal of Applied Physics, 38 (1967) 12, 4780.

[Mes89] Messien, P. and Leroy, V.: Scavenging Additions of Boron in Low-C - Low Al Steels. Steel Research International, 60 (1989) 7, 320-328.

[Met09] Metals Knowledge : Effect of Phosphorus on the Properties of Carbon Steels. Part 1, (2009).

[Mey94] Meyer, L.; Bleck, W. and Müschenborn, W.: Product-oriented IF-steel design. International Forum for Physical Metallurgy of IF-Steels, Tokyo, (1994), 203-222.

[Mey99] Meyer, M.D.; Vanderschueren, D. and De Cooman, B.C.: The Influence of Al on the Properties of Cold Rolled C-Mn-Si TRIP Steels. 41st MWSP Conference Proceedings, ISS, XXXVII (1999), 265-276.

[Mil69] Mileiko, S.T.: Tensile Strength and Ductility of Continuous Fibre Composites. Journal of Materials Science, 4 (1969) 11, 974.

[Mil85] Mills, K.: Metalography and Microstructures. American Society for Metals. ASM International, Handbook Committee, Ohio, (1985), 670.

[Min96] Minote, T.; Torizuka, S.; Ogawa, A. and Niikura, M.: Modeling of transformation behavior and compositional partitioning in TRIP steel. ISIJ International, 36 (1996) 2, 201-207.

[Min01] Mintz, B.: Hot Dip Galvanizing of Transformation Induced Plasticity and Other Intercritically Annealed Steels. International Materials Reviews, 46 (2001), 169-197.

[Mit91] Mittemeijer, E.J. and Wierszyllowski, I.A.: The Isothermal and Nonisothermal Kinetics of Tempering Iron-Carbon and Iron-Nitrogen Martensites and Austenites. Zeitschrift für Metallkunde, 82 (1991) 6, 419-429.

[Miz90] Mizui, N. and Okamoto, A.: Recent development in bakehardenable sheet steels for automotive body panels. Steel in Motor Vehicle Manufacture, International Conference, Würzburg, (1990), 85-94.

[Miz94] Mizui, N. and Kojima, N.: Effect of Si on the Mechanical Property of Ultra-Low Carbon Ti-Added Cold-Rolled Sheet Steels with Various Content of Mn or P, Coiled at 500-Degrees-C in Hot-Rolling Process. ISIJ International, 34 (1994) 1, 123-131.

[Miz98] Mizui, N.: Precipitation control and related mechanical property in ultra-low carbon sheet steel. Modern LC and ULC Sheet Steels for Cold Forming. Processing and Properties International Symposium, Aachen, (1998), 169-178.

[Mon07] Mohrbacher, H. and Klinkenberg, Ch.: The Role of Niobium in Lightweight Vehicle Construction. Materials Science Forum, 537-538 (2007), 679-686.

[Mor03] Morito, S.; Tanaka, H.; Konishi, R.; Furuhara, T. and Maki, T.: The morphology and crystallography of lath martensite in Fe-C alloys. Acta Materialia, 51 (2003) 6, 1789-1799.

[Moy75] Moyer, J.M. and Ansell, G.S.: Volume Expansion Accompanying Martensite-Transformation in Iron-Carbon Alloys. Metallurgical Transactions A, 6 (1975) 9, 1785-1791.

[Muk96] Mukunthan, K. and Hawbolt, E.B.: Modeling recovery and recrystallization kinetics in cold-rolled Ti-Nb stabilized interstitial-free steel. Metallurgical and Materials Transactions A, 27 (1996) 11, 3410-3423.

[Mül07] Müller, T.: Bake-Hardening-Effekts im mehrachsigen Spannungszustand. Ph.D. Thesis, Stuttgart University (2007).

[Mur06] Murugaiyan, A.; Podder, A.S.; Pandit, A.; Chandra, S.; Bhattacharjee, D. and Ray, R.K.: Phase transformations in two C-Mn-Si-Cr dual phase steels. ISIJ International, 46 (2006) 10, 1489-1494.

[Nab05] Nabarro, F.R.N.: Distribution of solute atoms round a moving dislocation, Materials Science and Engineering A, 400 (2005), 22-24.

[Nad08] Naderi, M.; Saeed-Akbari, A. and Bleck, W.: The effects of non-isothermal deformation on martensitic transformation in 22MnB5 steel. Materials Science and Engineering A, 487 (2008) 1-2, 445-455.

[Nag83] Nagakura, S.; Hirotsu, Y.; Kusunoki, M.; Suzuki, T. and Nakamura, Y.: Crystallographic Study of the Tempering of Martensitic Carbon-Steel by Electron-Microscopy and Diffraction. Metallurgical Transactions A, 14 (1983) 6, 1025-1031.

[Naj92] Najafizadeh, A.; Jonas, J.J. and Yue, S.: Grain-Refinement by Dynamic Recrystallization During the Simulated Warm-Rolling of Interstitial Free Steels. Metallurgical Transactions A, 23 (1992) 9, 2607-2617.

[Nei94] Neife, S.I.; Pink, E. and Stuwe, H.P.: The Isothermal Precipitation Behavior in A Low-Carbon Steel at Low-Temperatures Investigated by Internal-Friction. Scripta Metallurgica et Materialia, 30 (1994) 3, 361-366.

[Nip03] Nippon Steel: R&D Team of the kimitsu steelworks of Nippon steel, (2003).

[Now72] Nowick, A.S. and Berry, B.S.: Anelastic relaxation in crystalline solids. Academic Press, New York, (1972).

[Now10] Nowotnik, A. and Siwecki, T.: The effect of TMCP parameters on the microstructure and mechanical properties of Ti-Nb microalloyed steel. Journal of Microscopy-Oxford, 237 (2010) 3, 258-262.

[Oga10] Ogawa, T.; Maruyama, N.; Sugiura, N. and Yoshinaga, N.: Incomplete Recrystallization and Subsequent Microstructural Evolution during Intercritical Annealing in Cold-rolled Low Carbon Steels. ISIJ International, 50 (2010) 3, 469-475.

[Ohl02] Ohlert, J.; Bleck, W. and Hulka, K.: Control of Microstructure in TRIP Steels by Niobium. Proceeding International Conference on TRIP-Aided High Strength Ferrous Alloys, Gent, (2002), 199-206.

[Ohm92] Ohmori, Y. and Tamura, I.: Epsilon Carbide Precipitation During Tempering of Plain Carbon Martensite. Metallurgical Transactions A, 23 (1992) 10, 2737-2751.

[Oka89] Okamoto, A.; Takeuchi, K. and Takagi, M.: A mechanism of paint bake-hardening. The Sumitomo Search, 39 (1989) 9, 183-194.

[Ols83] Olson, G.B. and Cohen, M.: Early Stages of Aging and Tempering of Ferrous Martensites. Metallurgical Transactions A, 14 (1983) 6, 1057-1065.

[Ouc77] Ouchi, C.; Sanpei, T.; Okita, T. and Kozasu, I.: Microstructural Changes of Austenite During Hot Rolling and Their Effects on Transformation Kinetics. TMS-AIME, New York, (1977), 316-340.

[Ouc82] Ouchi, C.; Sampei, T. and Kozasu, I.: The Effect of Hot-Rolling Condition and Chemical-Composition on the Onset Temperature of Gamma-Alpha-Transformation After Hot-Rolling. Transactions of the Iron and Steel Institute of Japan, 22 (1982) 3, 214-222.

[Pal06] Palkowski, H. and Anke, T.: Bake hardening of hot rolled multiphase steels under biaxial pre-strained conditions. Steel Research International, 77 (2006) 9-10, 675-679.

[Pal08a] Palkowski, H.; Kugler, G. and Asadi, M.: Influence of Chemical Composition on Bake Hardening Effect for Hot Rolled Multiphase Steels. TMS-AIME, New Orleans, Louisiana, (2008), 225- 235.

[Pal08b] Palkowski, H. and Bruck, A.: Local use of ageing effects in multiphase steels for designing local properties of constructional elements. Steel Research International, 79 (2008) 3, 172-177.

[Pal96] Palmiere, E.J.; Garcia, C.I. and Deardo, A.J.: The influence of niobium supersaturation in austenite on the static recrystallization behavior of low carbon microalloyed steels. Metallurgical and Materials Transactions A, 27 (1996) 4, 951-960.

[Pan09] Panda, S.K.; Hernandez, V.H.B.; Kuntz, M.L. and Zhou, Y.: Formability Analysis of Diode-Laser-Welded Tailored Blanks of Advanced High-Strength Steel Sheets. Metallurgical and Materials Transactions A, 40A (2009) 8, 1955-1967.

[Par05] Park, K.T.; Lee, Y.K. and Shin, D.H.: Fabrication of ultrafine grained ferrite/martensite dual phase steel by severe plastic deformation. ISIJ International, 45 (2005) 5, 750-755.

[Pep07] Pepelnjak, T. and Barisic, B.: Analysis and elimination of the stretcher strains on TH415 tinplate rings in the stamping process. Journal of Materials Processing Technology, 186 (2007) 1-3, 111-119.

[Per08a] Pereloma, E.V.; Miller, M.K. and Timokhina, I.B.: On the Decomposition of Martensite during Bake Hardening of Thermomechanically Processed Transformation-Induced Plasticity Steels. Metallurgical and Materials Transactions A, 39A (2008) 13, 3210-3216.

[Per08b] Pereloma, E.V.; Russell, K.F.; Miller, M.K. and Timokhina, I.B.: Effect of pre-straining and bake hardening on the microstructure of thermomechanically processed CMnSi TRIP steels with and without Nb and Mo additions. Scripta Materialia, 58 (2008) 12, 1078-1081.

[Pic01] Pichler, A.; Traint, S.; Pauli, H.; Mildner, H.; Szinyur, J.; Blaimschein, M.; Stiaszny, P. and Werner, E.: Processing and Properties of Cold-Rolled TRIP Steels. 43rd MWSP Conference Proceedings, ISS, (2001), 411-434.

[Pic77] Pickering, F.B.: High-Strength, Low-Alloyed Steels - A Decade of Progress. Proceedings of Microalloying 75, ed. Korchynsky, M., Union Carbide Corporation, Washington DC, New York, (1977), 9-31.

[Pic78] Pickering, F.B.: Physical Metallurgy and the Design of Steels. Applied Science Publishers LTD, London, (1978), 64.

[Pic99a] Pichler, A. and Stiaszny, P.: TRIP Steel with Reduced silicon Content. Steel Research International, (1999) 70, 459-465.

[Pic99b] Pichler, A.; Hribernig, G.; Tragl, E.; Angerer, R.; Radlmayr, K. Szinyur, J.; Traint, S.; Werner, E. and Stiaszny, P.: Aspects of the production of dual phase and multiphase steel strips. 41st Mechanical Working and Steel Processing Conference, Baltimore, USA, XXXVII (1999), 37-60.

[Pra90] Pradhan, R.: Metallurgic aspects of batched-annealed bake-hardening steel. Metallurgy of Vacuum-Degassed Steel Products, The Minerials. Metals & Material Society, (1990), 309-325.

[Pri84] Priestner, R. and Aw, C.L.: On Initial Yielding in Dual-Phase Steel. Scripta Metallurgica, 18 (1984) 2, 133-136.

[Qu02] Qu, J.B.; Shan, Y.Y.; Zhao, M.C. and Yang, H.: Effects of hot deformation and accelerated cooling on microstructural evolution of low carbon microalloyed steels. Materials Science and Technology, 18 (2002) 2, 145-150.

[Ram79] Ramos, L.F.; Matlock, D.K. and Krauss, G.: Deformation-Behavior of Dual-Phase Steels. Metallurgical Transactions A, 10 (1979) 2, 259-261.

[Rat00] Rathbun, R.W.; Matlock, D.K. and Speer, J.G.: Strain aging behavior of austenitic stainless steels containing strain induced martensite. Scripta Materialia, 42 (2000) 9, 887-891.

[Rau89] Rauch, E.F. and Schmitt, J.H.: Dislocation Substructures in Mild-Steel Deformed in Simple Shear. Materials Science and Engineering A, 113 (1989), 441-448.

[Ray81] Ray, S.K.; Mishra, S. and Mohanty, O.N.: Magnetic Aging Characteristics of A Phosphorous-Bearing Low-Carbon Steel. Scripta Metallurgica, 15 (1981) 9, 971-973.

[Ray82] Ray, S.K.; Mishra, S. and Mohanty, O.N.: Tem Study of Carbide Precipitation in A Phosphorus-Bearing Low-Carbon Steel. Scripta Metallurgica, 16 (1982) 1, 43-47.

[Ree92] Rees, G.I. and H.K.D.H. Bhadeshia: Bainite Transformation Kinetics. Part I Modified Model, Material Science Technology, 8 (1992), 985-993.

[Rig79] Rigsbee, J.M.; Abraham, J.K.; Davenport, A.T.; Franklin J.E. and Pickens, J.W.: Structure and Properties of Dual-phase Steels. Eds. Kot, R.A. and Morris, J.W. TMS-AIME, New York, (1979), 304-329.

[Rob78] Roberts, W. and Ahlblom, B.: Nucleation Criterion for Dynamic Recrystallization During Hot Working. Acta Metallurgica, 26 (1978) 5, 801-813.

[Roc05] Rocha, R.O.; Melo, T.M.F.; Pereloma, E. and Santos, D.B.: Microstructural evolution at the initial stages of continuous annealing of cold rolled dual-phase steel. Materials Science and Engineering A, 391 (2005) 1-2, 296-304.

[Ryu02] Ryu, H.B.; Speer, J.G. and Wise, J.P.: Effect of thermomechanical processing on the retained austenite content in a Si-Mn transformation-induced plasticity steel. Metallurgical and Materials Transactions A, 33 (2002) 9, 2811-2816.

[Sai89] Saitoh, H. and Ushioda, K.: Influences of Manganese on Internal-Friction and Carbon Solubility Determined by Combination of Infrared-Absorption in Ferrite of Low-Carbon Steels. ISIJ International, 29 (1989) 11, 960-965.

[Sai91] Saitoh, H. and Ushioda, K.: Influence of P on Solubility of C and on Snoek Peak in Low-Carbon Steels. Journal of the Japan Institute of Metals, 55 (1991) 6, 639-645.

[Sak83] Sakaki, T.; Sugimoto, K. and Fukuzato, T.: Role of Internal-Stress for Continuous Yielding of Dual-Phase Steels. Acta Metallurgica, 31 (1983) 10, 1737-1746.

[Sak89] Sakamoto, M.: Diffusion Equation and Cottrell Atmosphere Dragging of Edge Dislocation in High-Concentration Solid-Solutions. Materials Transactions Jim, 30 (1989) 5, 337-344.

[Sak91] Sakuma, Y.; Matsumura, O. and Takechi, H.: Mechanical-Properties and Retained Austenite in Intercritically Heat-Treated Bainite-Transformed Steel and Their Variation with Si and Mn Additions. Metallurgical Transactions A, 22 (1991) 2, 489-498.

[Sal06] Salehi, A.R.; Serajzadeh, S. and Taheri, A.K.: A study on the microstructural changes in hot rolling of dual-phase steels. Journal of Materials Science, 41 (2006) 7, 1917-1925.

[Sam06] Samek, L.; De Moor, E.; De Cooman, B.C.; Speer, J.G. and Houbaert, Y.: Bakehardening behavior of low-alloyed multi-phase high-strength steels. ICASS 2006, 3rd International Conference on Advanced Structural Steels, Gyeongju, Republic of Korea, (2006), 835-840.

[Sam88] Samuel F.H.; Barbosa R.; Boratto F.; Yue, S. and Jonas J.J.: Laboratory Simulation of Flow Stresses During Strip Rolling Using High Strain Rate Torsion Testing. THERMEC 88, Tokyo, (1988), 721-728.

[Sam08] Samek, L.; De Moor, E.; Penning, J.; Speer, J.G. and De Cooman, B.C.: Static strain aging of microstructural constituents in transformation-induced-plasticity steel. Metallurgical and Materials Transactions A, 39A (2008) 11, 2542-2554.

[Sea03] Seal, R.K.: New Ultra- Low Carbon High Strength Steels with Improved Bake Hardenability for Enhanced Stretch Formability and Dent Resistance. M.S. Thesis, University of Pittsburgh, (2003).

[Sha01] Shalfan, W.: Bake hardenability of microalloyed ULC steels. Ph.D. Thesis, Colorado School of Mines, (2001).

[She83] Sherman, A.M.; Eldis, G.T. and Cohen, M.: The Aging and Tempering of Iron-Nickel-Carbon Martensites. Metallurgical Transactions A, 14 (1983) 6, 995-1005.

[She84] Shen, H.P. and Lei, T.C.: Shear Lag Analysis of Strength of Dual Phase Steels. Metal Science, 18 (1984) 5, 257-264.

[Shi06] Shi, W.; Li, L.; Yang, C.X.; Fu, R.Y.; Wang, L. and Wollants, P.: Strain-induced transformation of retained austenite in low-carbon low-silicon TRIP steel containing aluminum and vanadium. Materials Science and Engineering A, 429 (2006) 1-2, 247-251.

[Sic96] Siciliano, Jr. F.; Minami, K.; MacCagno, T.M. and Jonas, J.J.: Mathematical Modeling of the Mean Flow Stress, Fractional Softening and Grain Size during the Hot Strip Rolling of C-Mn Steels. ISIJ International, 36 (1996) 12, 1500-1506.

[Sic00] Siciliano, F. and Jonas, J.J.: Mathematical modeling of the hot strip rolling of microalloyed Nb, multiply-alloyed Cr-Mo, and plain C-Mn steels. Metallurgical and Materials Transactions A, 31 (2000) 2, 511-530.

[Sin98] Singh, S.B. and Bhadeshia, H.K.D.H.: Estimation of Bainite Plate-Thickness in Low-Alloy Steels. Material Science Engineering A, 245 (1998) 1, 72-79.

[Siw97] Siwecki, T. and Engberg, G.: Recrystallization controlled rolling of steels, Thermo - Mechanical Processing in Theory. Modelling & Practice, Stockholm, (1997), 121-144.

[Smi93] Smith, W.F.: Structure and Properties of Engineering Alloys. 2nd edition, McGraw-Hill, (1993), 119-123.

[Sno39] Snoek, J.L.: Mechanical after effect and chemical constitution. Physica, 6 (1939), 591-592.

[Sno41] Snoek, J.L.: Effect of small quantities of carbon and nitrogen on the elastic and plastic properties of iron. Physica, 8 (1941) 7, 711-733.

[Soe04] Soenen, B.; De, A.K.; Vandeputte, S. and De Cooman, B.C.: Competition between grain boundary segregation and Cottrell atmosphere formation during static strain aging in ultra low carbon bake hardening steels. Acta Materialia, 52 (2004) 12, 3483-3492.

[Sol07] Soliman, M.: Phase Transformation and Mechanical Properties of New Austenite-Stabilised Bainite Steels. Ph.D. Thesis, Clausthal University of Technology, (2007).

[Sol10] Soliman, M.; Asadi, M. and Palkowski, H.: Role of Dilatometer in Designing new Bainitic Steels. Advanced Materials Research, 89-91 (2010), 35-40.

[Son05] Son, Y.I.; Lee, Y.K.; Park, K.T.; Lee, C.S. and Shin, D.H.: Ultrafine grained ferrite-martensite dual phase steels fabricated via equal channel angular pressing: Microstructure and tensile properties. Acta Materialia, 53 (2005) 11, 3125-3134.

[Son05] Song, R.; Ponge, D. and Raabe, D.: Mechanical properties of an ultrafine grained C-Mn steel processed by warm deformation and annealing. Acta Materialia, 53 (2005) 18, 4881-4892.

[Spe02] Speer, J.G. and Matlock, D.K.: Recent developments in low-carbon sheet steels. Jom-Journal of the Minerals Metals & Materials Society, 54 (2002) 7, 19-24.

[Spe03] Speer, J.; Matlock, D.K.; De Cooman, B.C. and Schroth, J.G.: Carbon partitioning into austenite after martensite transformation. Acta Materialia, 51 (2003) 9, 2611-2622.

[Spe65] Speich, G.R. and Swann, P.R.: Yield Strength and Transformation Substructure of Quenched Iron-Nickel Alloys. Journal of the Iron and Steel Institute, 203 (1965), 480.

[Spe72] Speich, G.R. and Leslie, W.C.: Tempering of Steel. Metallurgical Transactions, 3 (1972) 5, 1043.

[Spe81a] Speich, G.R.; Demarest, V.A. and Miller, R.L.: Formation of Austenite During Intercritical Annealing of Dual-Phase Steels. Metallurgical Transactions A, 12 (1981) 8, 1419-1428.

[Spe81b] Speich, G.R. and Miller, R.L.: Tempering of ferrite-martensite steels. Eds. Kot, R.A.; Bramfitt, B.L.: Fundamentals of dual-phase steels. TMS-AIME, Warrendale, (1981), 279-303.

[Spe83] Speich, G.R.; Schwoeble, A.J. and Huffman, G.P.: Tempering of Mn and Mn-Si-V Dual-Phase Steels. Metallurgical Transactions A, 14 (1983) 6, 1079-1087.

[Sre07] Sreekala, S. and Haataja, M.: Recrystallization kinetics: A coupled coarse-grained dislocation density and phase-field approach. Physical Review B, 76 (2007) 9.

[Sta87] Stahl-Eisen-Werkstoffblatt (SEW) 094: Kaltgewalztes Band und Blech mit höherer Streckgrenze zum Kaltumformen aus phosphorlegierten Stählen sowie aus Stähle mit zusätzlicher Verfestigung nach Wärmeeinwirkung (Bake-Hardening) - Technische Lieferbedingungen, Verlag Stahleisen, Düsseldorf, (1987).

[Ste04] Steinhäusler, M.: Bake-hardening behaviour of multiphase steels. Diploma Thesis, University of Leoben, (2004).

[Sti90] Stiaszny, P.; Ponschab, H.; Mildner, H.; Radlmaye, K.; Giedenbacher, G. and Schwarz, W.: Neuere Entwicklung bei höherfesten kaltgewalzten Feinblechen - Werkstofffragen, Formgebung und Gebrauchseigenschaften. Stahl im Automobilbau, Düsseldorf, Verlag Stahleisen mbH, (1990), 489-490.

[Sti98] Stiaszny, P. and Pichler, A.: Influence of annealing technology on the material properties of LC and ULC-steel grades. Modern LC and ULC Sheet Steels for Cold Forming, Processing and Properties. International Symposium, Aachen, (1998), 225-236.

[Sto00] Storojeva, L.; Escher, C.; Bode, R.; Hulka, K. and Burko, D.: Effect of Nb/C ratio and processing conditions on aging behavior and BH-effect of ULC sheet steels. IF Steels 2000 Proceeding, International Conference, Pittsburgh, (2000), 201–213.

[Sto01] Storozheva, L.M.: Ultralow carbon steels for the automotive industry with the effect of hardening due to drying of finished parts. Metal Science and Heat Treatment, 43 (2001) 9-10, 336-344.

[Sug92] Sugimoto, K.; Kobayashi, M. and Hashimoto, S.: Ductility and Strain-Induced Transformation in A High-Strength Transformation-Induced Plasticity-Aided Dual-Phase Steel. Metallurgical Transactions A, 23 (1992) 11, 3085-3091.

[Tak10] Takaki, S.: Review on the Hall-Petch Relation in Ferritic Steel. Materials Science Forum, 654-656 (2010), 11-16.

[Tak93] Takaki, S.; Nakatsu, H. and Tokunaga, Y.: Effects of Austenite Grain-Size on Epsilon-Martensitic Transformation in Fe-15Mass-Percent-Mn Alloy. Materials Transactions Jim, 34 (1993) 6, 489-495.

[Tav99] Tavares, S.S.M.; Pedroza, P.D.; Teodosio, J.R. and Gurova, T.: Mechanical properties of a quenched and tempered dual phase steel. Scripta Materialia, 40 (1999) 8, 887-892.

[Tim01] Timokhina, I.B.; Pereloma, E.V. and Hodgson, P.D.: Microstructure and mechanical properties of C-Si-Mn(-Nb) TRIP steels after simulated thermomechanical processing. Materials Science and Technology, 17 (2001) 2, 135-140.

[Tim03] Timokhina, I.B.; Hodgson, P.D. and Pereloma, E.V.: Effect of deformation schedule on the microstructure and mechanical properties of a thermomechanically processed C-Mn-Si transformation-induced plasticity steel. Metallurgical and Materials Transactions A, 34A (2003) 8, 1599-1609.

[Tim04] Timokhina, I.B.; Hodgson, P.D. and Pereloma, E.V.: Effect of microstructure on the stability of retained austenite in transformation-induced-plasticity steels. Metallurgical and Materials Transactions A, 35A (2004) 8, 2331-2341.

[Tim07] Timokhina, I.B.; Hodgson, P.D. and Pereloma, E.V.: Transmission electron microscopy characterization of the bake-hardening behavior of transformation-induced plasticity and dual-phase steels. Metallurgical and Materials Transactions A, 38A (2007) 10, 2442-2454.

[Tim08] Timokhina, I.B.; Hodgson, P.D.; Ringer, S.P.; Zheng, R.K. and Pereloma, E.V.: Understanding Bake-Hardening in Modern High Strength Steels for the Automotive Industry Using Advanced Analytical Techniques. Proceeding International Conference New Developments on Metallurgy and Applications of High Strength Steels, (2008), 104-113.

[Tim09] Timokhina, I.B.; Hodgson, P.D.; Ringer, S.P.; Zheng, R.K. and Pereloma, E.V.: Effect of Bake-Hardening on the Structure-Property Relationship of Multiphase Steels for the Automotive Industry. Steel Research International, 80 (2009) 7, 507-514.

[Tom76] Tomota, Y.; Kuroki, K.; Mori, T. and Tamura, I.: Tensile Deformation of 2-Ductile-Phase Alloys - Flow Curves of Alpha-Gamma Fe-Cr-Ni Alloys. Materials Science and Engineering, 24 (1976) 1, 85-94.

[Tor03] Toroghinejad, M.R.; Humphreys, A.O.; Ashrafizadeh, F.; Najafizadeh, A. and Jonas, J.J.: Effect of rolling temperature on the recrystallization texture of warm rolled steels. THERMEC 2003, Spain, 426-428 (2003), 3691-3696.

[Tra99] Traint, S.; Werner, E.A.; Pichler, A.; Stiaszny, P.: Microstructure-property relationships for dual-phase and multiphase steel strip. 41st Mechanical Working and Steel Processing Conference, Baltimore, USA, XXXVII, (1999), 25-36.

[Tra02] Traint, S.; Pehler, A. and Hauzenberger, K.: Influence of Silicon, Aluminum, Phosphorus, and Copper on Phase Transformation of Low Alloyed TRIP-Steels. International Conference on TRIP-Aided High Strength Ferrous Alloys, ed.: De Cooman, B.C., Ghent: GRIPS, (2002), 121-128.

[Tsi06] Tsipouridis, P.; Werner, E.; Krempaszky, C. and Tragl, E.: Formability of high strength dual-phase steels. Steel Research International, 77 (2006) 9-10, 654-667.

[Ume00] Umemoto, M.; Liu, Z.G.; Sugimoto, S. and Tsuchiya, K.: Tensile stress-strain analysis of single-structure steels. Metallurgical and Materials Transactions A, 31 (2000) 7, 1785-1794.

[Val91] Valiev, R.Z.; Krasilnikov, N.A. and Tsenev, N.K.: Plastic-Deformation of Alloys with Submicron-Grained Structure. Materials Science and Engineering A, 137 (1991), 35-40.

[Van02] Van der Zwaag, S.; Zhao, L.; Kruijver, S.O. and Sietsma, J.: Thermal and mechanical stability of retained austenite in aluminum-containing multiphase TRIP steels. ISIJ International, 42 (2002) 12, 1565-1570.

[Van97] Van Genderen, M.J.; Isac, M.; Bottger, A. and Mittemeijer, E.J.: Aging and tempering behavior of iron-nickel-carbon and iron-carbon martensite. Metallurgical and Materials Transactions A, 28 (1997) 3, 545-561.

[Van98] Van Snick, A.; Lips, K.; Vandeputte, S.; De Cooman, B. C. and Dilewijns, J.: Effect of carbon content, dislocation density and carbon mobility on bake hardening. Modern LC and ULC sheet steels for cold forming. Processing and Properties Conference Book, RWTH Aachen, 2 (1998), 413-424.

[Wan00] Wang, J.J.; Van der Wolk, P.J. and Van der Zwaag, S.: Determination of martensite start temperature in engineering steels part I. Empirical relations describing the effect of steel chemistry. Materials Transactions Jim, 41 (2000) 7, 761-768.

[Wan03] Wang, X.T.; Siwecki, T. and Engberg, G.: A physical model for prediction of microstructure evolution during thermo mechanical processing. THERMEC 2003, Spain, 426-428 (2003), 3801-3806.

[Wat77] Watanabe, H.; Smith, Y.E. and Pehlke, R.D.: Precipitation Kinetics of Niobium Carbonitride in Austenite of High-Strength Low-Alloy Steels, The Hot Deformation of Austenite. TMS-AIME, New York, (1977), 140-168.

[Wat99] Waterschoot, T.; Vandeputte, S.; De Cooman, B.C. and Houbaert, Y.: The influence of P, Si and Mn on the mechanical properties and bake-hardening of Ti-ULC steels. 41st Mechanical Working and Steel Processing Conference, XXXVII (1999), 425-433.

[Wat03a] Waterschoot, T.; De, A.K.; Vandeputte, S. and De Cooman, B.C.: Static strain aging phenomena in cold-rolled dual-phase steels. Metallurgical and Materials Transactions A, 34A (2003) 3, 781-791.

[Wat03b] Waterschoot, T.; De Cooman, B.C.; Vandeputte, S. and Conlon, K.: Neutron diffraction study of the low-temperature ageing of martensite in dual-phase steel. Zeitschrift für Metallkunde, 94 (2003) 4, 424-435.

[Wat03c] Waterschoot, T.: Fundamentals of aging in multiphase steels: static strain aging and tempering in dual phase steels. Ph.D. Thesis, University of Ghent, Ghent, Belgium, (2003).

[Wat06] Waterschoot, T.; Verbeken, K. and De Cooman, B.C.: Tempering kinetics of the martensitic phase in DP steel. ISIJ International, 46 (2006) 1, 138-146.

[Wat96] Watte, P.; VanHumbeeck, J.; Aernoudt, E. and Lefever, I.: Strain ageing in heavily drawn eutectoid steel wires. Scripta Materialia, 34 (1996) 1, 89-95.

[Wei79] Weiss, I. and Jonas, J.J.: Interaction Between Recrystallization and Precipitation During the High-Temperature Deformation of Hsla Steels. Metallurgical Transactions A, 10 (1979) 7, 831-840.

[Wen05] Weng, Y.Q.; Sun, X.J. and Dong, H.: Overview on the Theory of Deformation Induced Ferrite Transformation. Iron and Steel Supplement, 40 (2005), 9-15.

[Wil68] Wilson, D.V.: Grain-Size Dependence of Discontinuous Yielding in Strain-Aged Steels. Acta Metallurgica, 16 (1968) 5, 743.

[Wil94] Wilson, D.V.: Influences of Cell-Walls and Grain-Boundaries on Transient Responses of an IF Steel to Changes in Strain Path. Acta Metallurgica et Materialia, 42 (1994) 4, 1099-1111.

[Wu08] Wu, D.; Li, Z. and Lue, H.S.: Effect of controlled cooling after hot rolling on mechanical properties of hot rolled TRIP steel. Steel Research International, 15 (2008) 2, 65-70.

[Yam76] Yamada, Y.: Static Strain Aging of Eutectoid Carbon-Steel Wires. Transactions of the Iron and Steel Institute of Japan, 16 (1976) 8, 417-426.

[Yam82] Yamamoto, S.; Ouchi, C. and Osuka, T.: The Effect of Microalloying Elements on the Recovery and Recrystallization in Deformed Austenite. Thermomechanical Processing of Microalloyed Austenite, Pittsburgh, Pennsylvania, (1982), 613-639.

[Yam88] Yamazaki, K.; Horita, T.; Umehara, Y. and Morishita, T.: Manufacturing condition and automotive use of bake hardenable steel sheets. Nippon Steel and Toyota Motor Corporation, (1988), 327-337.

[Ye02] Ye, W.P.; Le Gall, R. and Saindrenan, G.: A study of the recrystallization of an IF steel by kinetics models. Materials Science and Engineering A, 332 (2002) 1-2, 41-46.

[Yue97] Yue, S.; DiChiro, A. and Hanzaki, A.Z.: Thermomechanical processing effects on C-Mn-Si TRIP steels. Jom-Journal of the Minerals Metals & Materials Society, 49 (1997) 9, 59-61.

[Zha00] Zhao, J.Z.; De, A.K. and De Cooman, B.C.: Kinetics of Cottrell atmosphere formation during strain aging of ultra-low carbon steels. Materials Letters, 44 (2000) 6, 374-378.

[Zha01] Zhao, J.Z.; De, A.K. and De Cooman, B.C.: Formation of the Cottrell atmosphere during strain aging of bake-hardenable steels. Metallurgical and Materials Transactions A, 32 (2001) 2, 417-423.

[Zha03] Zhao, M.C.; Shan, Y.Y.; Xiao, F.R. and Yang, K.: Acicular ferrite formation during hot plate rolling for pipeline steels. Materials Science and Technology, 19 (2003) 3, 355-359.

[Zhu96] Zhu, A.W.; Neife, S.I. and Pink, E.: Characterization of medium- and low-temperature carbides in a low-carbon steel by internal friction. Steel Research International, 67 (1996) 11, 507-512.

Eidesstattliche Erklärung

Hiermit erkläre ich an Eides statt, dass ich die vorliegende Arbeit selbständig ohne unerlaubte Hilfe verfasst und die benutzten Hilfsmittel vollständig angegeben habe und noch keine früheren Promotionsversuche unternommen habe.

Mehdi Asadi

Lebenslauf

Persönliche Daten

Name:	Mehdi Asadi
Geburtstag:	21.09.1977
Geburtsort:	Teheran
Familienstand:	verheiratet

Ausbildung

02.2007 – 10.2010	Technische Universität Clausthal Fachrichtung: Werkstoffumformung, Abschluss: Promotion
10.2005 – 02.2007	Technische Universität Clausthal Fachrichtung: Werkstofftechnik, Abschluss: Master
09.1996 – 11.2001	Technische Universität Poly Technik, Teheran / Iran Fachrichtung: Materialwissenschaft, Abschluss: Bachelor
09.1988 – 06.1995	Beheshti Oberschule, Teheran / Iran Schwerpunkte: Mathematik und Physik, Abschluss: Abitur

Beruflicher Werdegang

seit 02.2007	Technische Universität Clausthal Wissenschaftlicher Mitarbeiter, Institut für Metallurgie, Werkstoffumformung
10.2005 – 02.2007	Technische Universität Clausthal Studentische Hilfskraft, Institut für Metallurgie
09.2002 – 05.2004	Yaragh Avaran Pouya Co. (Y.A.P. Co.), Teheran / Iran Projektbearbeiter, Abteilung für technische Kundenberatung
11.2001 – 08.2002	Rooy Sazan Co, Zanjan / Iran Produktionsleiter, Produktionsabteilung
04.1998 – 03.2001	Iran-Aluminium-Forschungszentrum, Teheran / Iran Projektbearbeiter, Forschungsabteilung

Zusatzkenntnisse und –aufgaben, Fachliche Ehrenämter

seit 05.2007	Mitglied Fachausschuss „Mikrostruktur, Gefüge- und Werkstoffmikroanalytik“ bei VDEh, Umformdilatometrie und Grenzformänderungsanalyse
seit 07.2007	Gastmitglied VFWH „Verein zur Förderung von Forschungsarbeiten auf dem Gebiet der Walzwerkstechnik in der Hüttenindustrie“

Patent

01.2009	Entwicklung von Al-Si-Zylinderkopflegierungen mit geringem Silizium- und erhöhtem Eisengehalt, Nr.: WO 2009/010264

Weitere Fähigkeiten und Qualifikationen

Sprache:	Persisch als Muttersprache, Deutsch und Englisch
EDV-Kenntnisse:	MS-Office, MS-Projekt
Systemkenntnisse:	MatCalc HYBREX, Firma Siemens, Erlangen Statistische Versuchsplanung, Firma Umetrix Grenzformänderungsanalyse (ARGUS / ARAMIS) Umformdilatometer, Firma Bähr

Veröffentlichungsliste

Zeitschriften

1) Asadi, M.; Schulze, N.; Palkowski, H.: Use of the Aging Effect to Change the Local Properties of Structure Components. Advanced Materials Research, Vol. 137 (2010), 35-79.

2) Asadi, M.; Frommeyer, G.; Timokhina, I.; Palkowski, H.: Local Laser Heat Treatment in Dual Phase Steels, accepted in Metallurgical Material Transaction A, Feb. (2011)

3) Asadi, M.; Palkowski, H.: Designing Local Properties of Constructional Elements by Local Use of Ageing Effects in Multiphase Steels. Materials Science Forum, Vol. 638-642 (2010), 3062-67

4) Palkowski, H.; Asadi, M.; Soliman, M.: Role of Dilatometer in Designing new Bainitic Steels. Advanced Materials Research, Vol. 89-91 (2010), 35-40

5) Asadi, M.; Palkowski, H.: Thermo-Mechanical Processing Parameters and Chemical Composition on Bake Hardening Ability of Hot Rolled Multiphase Steels, Steel research international, Vol. 7 (2009), 499-506

Konferenzen

6) Asadi, M.; Palkowski, H.: Influence of the Hot Rolling Process on the Mechanical Behavior in Martensitic Steels, accepted in Thermec Conference, Quebeck, Canada, Aug. 1-5 (2011)

7) Asadi, M.; Schlosser, N.; Palkowski, H.: Locally Influencing the Properties by Local deformation and Bake Hardening in Hot rolled Multi Phase Steels, accepted in 3rd International Conference on Steels in Cars and Trucks, SCT, Salzburg, Austria, June 5-9 (2011)

8) Asadi, M.; Schlosser, N.; Palkowski, H.: Study of Bake Hardening Effect on Laser Welded Hot-rolled Bainitic Steel, Proc. TMS Annual Meeting & Exhibition, San Diego, California, USA, 27 Feb. - 03 Mar. (2011)

9) Asadi, M.; Palkowski, H.: Investigation on Local Mechanical Properties in Multiphase Steels for Designing Local Properties of Constructional Elements, 2nd International Conference on Super-High Strength Steels, Peschiera del Garda, Italy, Oct.17-20 (2010)

10) Asadi, M.; Palkowski, H.: Influence Local Use of Ageing Effects in Multiphase Steels for Designing Local Properties of Constructional Elements, Proc. TMS Annual Meeting & Exhibition, San Francisco, USA, (2009)

11) Asadi, M.; Palkowski, H.: Use of Ageing Effects in Multiphase Steels, Thermec Conference, Berlin, Germany, Aug. (2009)

12) Asadi, M.; Schulze, N.; Palkowski, H.: Nutzung des Alterungseffektes zur lokalen Eigenschaftsänderung von Strukturbauteilen. 7. Industriekolloquium Hochfeste Strukturen, Clausthal-Zellerfeld, Nov. 25-26 (2009), 49-55

13) Palkowski, H.; Brück, A.; Asadi, M.: Thermo-Mechanical processing by Laser in multiphase steels. 10th Annual Conf. Yucomat, Montenegro, (2008)

14) Asadi, M.; Palkowski, H.: Thermo-mechanical Processing Parameters and Chemical Composition on Bake Hardening ability of Hot Rolled Multiphase Steels. 1st International Conference on "IAS". Pohang , South Korea, (2008), 137-145

15) Asadi, M.; Kugler, G.; Soliman, M.; Palkowski, H.: Effect of Thermo-Mechanical Processing Parameters and Chemical Composition on Bake Hardening ability of Hot Rolled Martensite Steel. 3rd International Conference Thermo-mechanical Process. Padova, Italy, (2008)

16) Palkowski, H.; Kugler, G.; Asadi, M.: Influence of Chemical Composition on Bake Hardening Effect for Hot Rolled Multiphase Steels. Proc. TMS Annual Meeting & Exhibition, New Orleans, Louisiana, USA, (2008)

17) Palkowski, H.; Brück, A.; Asadi, M.: Nutzung des Bake Hardening Effektes zur lokalen Festigkeitssteigerung in Mehrphasenstählen. 15. Sächsische Fachtagung Umformtechnik. Dresden, Germany, (2008)

Abschlussberichte

18) Asadi, M.; Schlosser, N.; Palkowski, H.: Untersuchungen zur Veränderung der Festigkeit von Bauteilen aus Mehrphasenstählen mit Bake-Hardening-Effekt durch den Fügeprozess, Abschlussbericht SFB362, Transferbereich, folgt bei DFG, Mär. (2011)

19) Asadi, M.; Palkowski, H.: Einfluss der Gefügeausbildung und Prozessparameter auf die mechanische Eigenschaften und den Bake-Hardening-Effekt in Mehrphasen-Stählen, Abschlussbericht AW142, eingereicht bei VFWH, Feb. (2011)

20) Asadi, M.; Schulze, N.; Palkowski, H.: Use of the Aging Effect to Change the Local Properties of Structure Components. Abschlussbericht SFB675, eingereicht bei DFG, Feb. (2010)

21) Asadi, M.; Palkowski, H.: Untersuchung zur Auswirkung von Legierungsschwankungen auf den BH-Effekt in Dualphasen- und Martensit-Stählen bei der Warmbanderzeugung, Abschlussbericht AW141, eingereicht bei VFWH, Juni (2008)

22) Asadi, M.; Kugler, G.; Palkowski, H.: Untersuchung zur Auswirkung der Warmumformung von hochfesten Stählen auf den BH-Effekt bei der Warmbanderzeugung. Abschlussbericht AW139, eingereicht beiVFWH, Mai (2007)